

**Au-Sn-W-Cu-Mineralization in the Astaneh-Sarband Area,  
West Central Iran**

**including a comparison of the ores with ancient bronze artifacts from Western Asia**

**DISSERTATION**

zur Erlangung des Grades eines Doktors der Naturwissenschaften

der Geowissenschaftlichen Fakultät  
der Eberhard-Karls-Universität Tübingen

vorgelegt von

**NIMA NEZAFATI**  
aus ABADAN, dem IRAN

2006

**Tag der mündlichen Prüfung:**

**3. November 2006**

**Dekan:**

**Professor Dr. Klaus-Georg Nickel**

**1. Berichterstatter:**

**Professor Dr. Gregor Markl**

**2. Berichterstatter:**

**Professor Dr. Ernst Pernicka**



بسم الله الرحمن الرحيم  
*In the name of God, the compassionate, the merciful*

دل گرچه در این بادیه بسیار شتافت  
یک موی ندانست ولی موی شکافت  
اندر دل من هزار خورشید بتافت  
آخر به کمال ذره ای راه نیافت

پور سینا

*Although my soul delved far into the wilderness  
It could split the hair but failed to know a hair breadth  
It raised thousands of suns into my heart  
But yet failed to fathom a trace*

Avicenna (980-1037 CE)

*To my Parents*

## Table of Contents

Acknowledgments.....	III
Abstract.....	IV
Zusammenfassung (Abstract in German).....	VI
Chekideh (Abstract in Persian).....	VIII
<b>Chapter 1: Introduction.....</b>	<b>1-6</b>
1.1 Problem definition.....	1
1.2 Objectives and aims.....	3
1.2.1 Genetic model.....	3
1.2.2 Archaeometric investigations.....	3
1.3 Geographic setting and exploration history.....	4
1.4 Background to the research.....	4
1.4.1. Economic geological aspects.....	4
1.4.2 Archaeometrical aspects.....	6
1.5 Methodology.....	6
<b>Chapter 2: Stratigraphy and geologic setting of the study area.....</b>	<b>7-15</b>
2.1 Introduction.....	7
2.2 The Sanandaj-Sirjan zone.....	9
2.3 Stratigraphy of the study area.....	11
2.4 Magmatism in the study area.....	13
2.5 Structure and tectonism.....	14
<b>Chapter 3: Petrography, mineralogy and geochemistry of the Deh Hosein occurrence.....</b>	<b>16-32</b>
3.1 Introduction.....	16
3.2 Methods.....	16
3.3 Geology of the prospect and petrography of the host rocks.....	17
3.4 Alteration.....	19
3.5 Mineralization.....	21
3.6 Paragenetic sequence.....	27
3.7 Metal associations and distribution at Deh Hosein.....	28
<b>Chapter 4: Petrography, mineralogy and geochemistry of the Astaneh gold occurrence.....</b>	<b>33-43</b>
4.1 Introduction.....	33
4.2 Geology of the prospect and petrography of the host rocks.....	34
4.3 Alteration.....	38
4.4 Mineralization.....	38
4.5 Paragenetic sequence.....	41
4.6 Metal associations and distributions at Astaneh.....	42
<b>Chapter 5: Petrography, mineralogy and geochemistry of the Nezam Abad occurrence.....</b>	<b>44-57</b>
5.1 Introduction.....	44
5.2 Geology of the prospect and petrography of the host rocks.....	44
5.3 Alteration.....	46
5.4 Mineralization.....	48
5.4.1 Ancient mining relics.....	48

5.4.2 Modern mining and exploration activities.....	48
5.4.3 Geophysical investigations.....	49
5.4.4 Ore minerals.....	50
5.5 Paragenetic sequence.....	52
5.6 Metal associations and distributions at Nezam Abad.....	54
5.7 Mineralization in pegmatite.....	57
<b>Chapter 6: Isotope studies and geothermometry.....</b>	<b>58-75</b>
6.1 Introduction.....	58
6.2 Sulfur isotope analyses.....	58
6.2.1 Method.....	59
6.2.2 Results.....	59
6.3 Oxygen isotope analyses.....	60
6.3.1 Methods.....	61
6.3.2 Results.....	61
6.4 Lead isotope studies.....	63
6.4.1 Methodology and analytical procedure.....	64
6.4.2 Results.....	64
6.5 Age determination studies.....	70
6.5.1 Rb-Sr method.....	70
6.5.1.1 Results.....	70
6.5.2 Single zircon evaporation method.....	71
6.5.2.1 Sample preparation, zircon morphology and methodology.....	72
6.5.2.2 Results.....	72
6.6 Arsenopyrite geothermometry.....	74
6.6.1 Method.....	74
6.6.2 Results.....	74
<b>Chapter 7: Archaeometrical investigations on the Deh Hosein ore and the ancient bronze artefacts.....</b>	<b>76-94</b>
7.1 Introduction.....	76
7.2 Review of the riddle of tin in antiquity.....	76
7.3 Early tin bronzes.....	76
7.4 Archaeological evidence.....	77
7.5 Texts referring to the Bronze Age tin trade.....	79
7.6 Geological aspects.....	80
7.7 The Luristan Bronzes.....	82
7.8 Ancient workings and relics at Deh Hosein ancient mine.....	85
7.9 Compositional analyses from Luristan Bronzes.....	87
7.10 Lead Isotope analysis.....	89
7.11 Summary and conclusions.....	93
<b>Chapter 8: Conclusions and recommendations.....</b>	<b>95-101</b>
Comparison of the prospects in the Astanceh-Sarband area with each other.....	96
Comparison of the occurrences with known deposits.....	98
Recommended future researches.....	99
<b>References.....</b>	<b>102</b>
<b>Curriculum vita.....</b>	<b>115</b>

## Acknowledgments

First of all, I would like to thank God for giving me the opportunity to successfully fulfill my thesis and granting me the ability to study a very small part of His wonderful and astonishing masterwork of nature.

This thesis presents the results of four years of scientific research at the universities of Freiberg and Tübingen including field work in Iran. This work is a continuation of the project that was initiated by the joint Iranian-German geological, archaeological and archaeometallurgical collaboration in the Arisman Project in 1999. I would like to take the opportunity to thank all individuals and friends who supported me during the course of my doctoral project and stay in Germany.

I am greatly obliged to my supervisors Professors Dr. Gregor Markl, Dr. Ernst Pernicka, Dr. Peter Michael Herzig and Dr. Morteza Momenzadeh for their full assistance during the performance of my project. Without their sound supervision, motivation, kindness and continual support this work would not have materialized.

I am greatly indebted to Professor Dr. Pernicka for offering me the PhD position, for his aboveboard and great support and for his valuable scientific discussions and technical assistance.

I am really grateful to Professor Dr. Momenzadeh for offering the subject of my PhD project, his scientific guidance and his support during field work in Iran.

Great thanks must be extended to Professor Dr. Herzig who kindly received me as his student, for his invaluable scientific support and financial matters related to this research.

I would like to sincerely thank Professor Dr. Gregor Markl for accepting me as his student after my move to the University of Tübingen following professor Pernicka and for his practical and intellectual input into several areas of the work. His comments, valuable scientific discussions and critical ideas are highlights of various aspects of this research.

I wish to thank Klaus-Peter Becker for providing technical assistance as regards the use of the electron microprobe equipment. I would like to express my sincere thanks to Bernd Höppner and Jörg Adam for their effort to measure the lead isotope ratios of the Astaneh-Sarband samples and the bronze artifacts. I also thank Susann Rabe for her assistance in EDXRF analyses of the Luristan bronze artifacts. I am grateful to Dr. Marion Tichomirowa and her colleagues who performed the stable-isotope and Rb/Sr analyses and single zircon evaporation measurements. I also appreciate her scientific guidance to my work.

I am very grateful to the DAAD (German academic exchange service), the Curt-Engelhorn-Zentrum Archäometrie in Mannheim, the Volkswagen Foundation, and Professor Dr. Pernicka for providing me with scholarships for study in Germany. I would also like to acknowledge the financial support for analyses and field work from the PHD-Program, and the Leibniz Laboratory for Applied Marine Research at the TU Bergakademie Freiberg, and Zaryaban Exploration. I express my gratitude to Thomas Stöllner for providing the radiocarbon date and Professor Dr. Friedrich Begemann for his helpful discussions and permission to use unpublished data about Luristan and Mesopotamian artifacts.

I wish to express my gratitude to Ms. Manuela Wagner, Ms. Kerstin Adam-Staron, Ms. Cornelia Hanzlik-Rudolph, Dr. Corina Dunger and Ms. Edda Paul for their administrative support, and for facilitating me a pleasant stay in Germany.

I would particularly like to thank the staff of the National Museum of Iran, particularly Mr. Mohammad-Reza Kargar (director) and his deputy Mr. Vakili, Ms. Mahnaz Gorji (the head of conservation) and Ms. Soury Ayazi (head keeper, historic and Luristan department) for allowing me access to Luristan Bronze artifacts.

I wish to acknowledge Dr. Sadegh Malek-Shahmirzadi, Dr. Thomas Seifert, Mr. Bahram Ojaghi, Dr. Zahra Hezarkhani, Dr. Thomas Wagner, Dr. Sven Petersen, Mr. Mohammad Hashem Ataii, Ms. Gesa Graser, Mr. Gabriel Nokandeh and Mr. Mohammad Reza Izadi-Motlagh for their encouragement and cooperation.

I would also like to thank all my friends, PhD colleagues and other staff members of the TU Bergakademie Freiberg and the University of Tübingen for their encouragement and moral support during the entire duration of my work.

Last but not least, I am indebted to my parents and my brothers for their love, support and patience during my long absence from home.

## Abstract

The present study deals with two primary aims; (1) geological, mineralogical, and geochemical investigations of the Deh Hosein, Astaneh, and Nezam Abad mineralizations in the Astaneh-Sarband area, west central Iran, with the aim to understand the characteristics of the occurrences and their conditions of formation, and (2) geochemical investigations on ancient bronze artifacts from Iran and Western Asia in order to compare their characteristics with the high-tin copper ore of Deh Hosein and examine their possible relationship.

The Astaneh-Sarband area is located in the northern part of the NW-SE aligned Sanandaj-Sirjan metamorphic belt and consists mainly of Mesozoic schists, Middle Jurassic to Middle Tertiary intrusive rocks and related contact metamorphic aureoles, and pegmatites. Regional metamorphism in the area has reached a peak of greenschist facies, but further metamorphism has occurred locally, associated with granitoid emplacement. Magmatism has produced large felsic to intermediate intrusive bodies along a general northwest trend. The main trend of the faults, fractures and other structural features of the area is NW-SE.

The Deh Hosein prospect is mainly hosted by Jurassic meta-sedimentary rocks, which have been intruded by the Astaneh complex. Mineralization continues into the southern part of the Astaneh intrusion. The meta-sedimentary rocks consist of alternating meta-sandstone, phyllite, schist, spotted slate and hornfels. The main faults and other structural features, with NW and NE trends, have controlled the mineralization, which occurs in the form of quartz, quartz-sulfide and quartz-gossan veins and veinlets, partly sheeted in structure. These veins are up to 1.5 m wide and several to tens of meters long. Mineralization also occurs as disseminations and impregnations, especially in the vein selvages. Adjacent to and within zones of intense quartz veining, the predominant alteration assemblage is quartz + sericite + tourmaline + monazite. Some 35 metalliferous minerals have been detected at Deh Hosein. Arsenopyrite is the dominant sulfide mineral, with lesser amounts of chalcopyrite > pyrite > pyrrotite. Cassiterite and ferberite are the rather abundant oxide minerals. The sulfide content in the ore is generally less than two volume percent. Arsenopyrite associated with early alteration and veining typically contains 1-150 $\mu$ m large inclusions of native bismuth, bismite and bismuthinite. Gold occurs in "invisible" form in the arsenopyrite and bismuth-bearing minerals of Deh Hosein. Bulk gold contents determined by NAA in the ore ranged from 0.05 to 13.3 ppm, while the Cu, Sn, W, and Bi concentrations of veins range up to 10%, 6.7%, 2420ppm, and 1800ppm, respectively.

At Astaneh, gold mineralization is confined to the NW-SE trending Astaneh intrusion that is composed mainly of biotite granite ( $98.9 \pm 1.0$  Ma; Masoudi 1997), which is locally accompanied by granodiorite, tourmaline granite and quartz diorite. The northeastern part of the Astaneh intrusion has been cut by the Shirmazd granodiorite. This stock is about 400 m in diameter and Eocene in age (Rb/Sr and single zircon evaporation methods, this study). The Shirmazd granodiorite has been cut by NE-trending microgranodiorite dykes. Gold mineralization occurs mainly as NE-trending quartz- and quartz-sulfide veins and veinlets, as well as in disseminations in the Shirmazd stock and the intersecting microgranodiorite dykes, and in some nearby, smaller, altered granitic stocks. Alteration minerals include sericite, chlorite, quartz, calcite and in some cases kaolinite. At Astaneh chalcopyrite and arsenopyrite are the major sulfide minerals, of which the latter contains 1-50  $\mu$ m sized inclusions of native bismuth and bismite. Gold occurs in both visible and invisible forms at Astaneh. Visible gold has been reported in the form of very fine grained particles (<15  $\mu$ m) either in goethite produced from the oxidation of chalcopyrite or in sericitized plagioclase (Hashemi 2002), while invisible gold occurs in arsenopyrite and bismuth-bearing minerals. Bulk gold contents determined by NAA ranged from 0.05 to 9.5 ppm, while the Cu, Sn, W, and Bi concentrations of veins range up to 1%, 0.05%, 100 ppm and 138ppm, respectively.

The Nezam Abad mineralization is hosted by a Lower-Mid Eocene quartz diorite unit. This rock unit has been cut by several aplitic and quartz or quartz-tourmaline veins; the latter host the mineralization. The faults of the area are NW-, NE- and N-trending. Associated alteration minerals include quartz, chlorite, sericite, and tourmaline. At Nezam Abad, chalcopyrite, arsenopyrite and scheelite are the most abundant ore minerals. Gold occurs as "invisible" form predominantly in arsenopyrite with bismuth inclusions at Nezam Abad. Bulk gold contents determined by NAA ranged from 0.05 to 36.2 ppm while the Cu, Sn, W, and Bi concentrations of veins range up to %10, %0.87, %3.37 and 548ppm, respectively (Farhadian 1999).

In all three occurrences, gold shows positive correlations with arsenic, bismuth, selenium, silver, tellurium and antimony. Microprobe investigations revealed that the arsenopyrites from Deh Hosein, Astaneh and Nezam Abad contain 32.3 to 34.3, 30.7 to 31.4, and 33.6 to 35.6 atomic percent of arsenic. Average compositions lead to the conclusion that the mineralization formed at temperatures of 460°C, 410° to 380°C and 565° to 510 °C, respectively. Oxygen isotope ratios for gold-bearing quartz veins in the area range from

13.6 to 19.2‰ for Deh Hosein, from 11.5 to 13.7‰ for Astaneh and from 11.6 to 15‰ (V-SMOW) for Nezam Abad. The oxygen isotope data suggest a metamorphic or a mixed magmatic-metamorphic source for the quartz veins. Measured sulfur isotope values for pyrite, chalcopyrite, galena and arsenopyrite in quartz veins of the Deh Hosein, Astaneh and Nezam Abad range from -5.6 to 0‰, -0.5 to 1.8‰ and 1.2 to 4‰ (CDT), respectively. The sulfur-isotope values of all these occurrences are compatible with a magmatic sulfur source. Pb isotope ratios from the sulfide and host rock samples of the prospects indicate a good agreement between the lead ratios of the ore of Deh Hosein and the hosting meta-sandstone, the ore of Astaneh and the Shirmazd Stock and the ore of Nezam Abad and the hosting quartz diorite. The Pb isotope signatures of the ore from the three occurrences show also rather close ratios. According to the plumbotectonics model of Zartman and Doe (1981) the lead in the ores has a lower crustal Pb component.

The studied occurrences share several similarities in terms of their mineralogy, geochemistry, formation temperatures, isotope ratios, alteration and occurrence of gold. They also indicate many similar features with the “intrusion-related gold systems” that have been described from Alaska, the Yukon and other parts of the world (e.g., Lang et al. 1997, 2000; McCoy et al. 1997; Thompson et al. 1999). According to the present data, it appears that a fertile magmatic source (probably of lower crustal origin) has affected the already present metamorphic rocks of the area (by remobilizing some of their elements) and caused a rather intensive gold mineralization in the area during the Pyrenean Orogeny.

The extensive ancient mining relics at Deh Hosein, the simultaneous occurrence of tin and copper in it, together with frequent archaeological and ancient textual references which refer to the Iranian plateau as supplier of the raw material for the ancient Mesopotamia and southwestern Iran (Susa and Luristan) encouraged me to examine the possible relationship between the ore of this ancient mine and the ancient bronze artifacts. For this purpose, several bronze artifacts of typical Luristan style which date most probably to the Iranian Iron Age (from about 1300-1250 to 650 BCE) were investigated. The results were compared to the analyses of the Deh Hosein ore and other bronze artifacts previously published. Examination of 29 bronze artifacts from Luristan by energy-dispersive X-ray fluorescence analysis revealed that the Luristan bronzes show variable concentrations of As, Pb, Zn and Fe in addition to high concentrations of tin (0.48-15.4%). The ore composition of Deh Hosein is matched by several bronze artifacts from Luristan analyzed in this study as well as in previous investigations (Fleming et al. 2005). Even more noteworthy is the observation that the lead isotope ratios of the ore samples from Deh Hosein are in very good agreement with 25 samples of metal artifacts from Luristan and other bronze artifacts dated to the third millennium BCE from the southern Persian Gulf (Weeks 1999), the Aegean (Begemann et al. 1992), as well as from third millennium BCE sites in Luristan and Mesopotamia (Begemann & Schmitt-Strecker in preparation).

At Deh Hosein, which is located at the western rim of the Luristan area and is close to ancient civilization centers of Susa and Mesopotamia, the ancient workings appear as numerous big ellipsoidal open depressions in two rows along the mineralized horizons. The old workings are up to 70 by 50m in size and up to 15m deep and are aligned over some 500m. Several hammer stones of silicified phyllite and granite, pottery shards and grinding stones have been found in the open-cast mines and adjacent ancient settlements. The pottery shards can be dated to the early first millennium BCE. Pieces of charcoal found in one of the diggings yielded a radiocarbon date of  $3380 \pm 55$ , which on calibration ( $2\sigma$ ) results in an age range of 1775-1522 BCE.

Several indications attest that Deh Hosein has been a major supplier of tin for ancient civilizations of Iran and Mesopotamia and perhaps even further west beginning in the third millennium BCE.

In summary: i) The lead isotope compatibility of ores from Deh Hosein with many bronze artifacts from Bronze and Iron Age sites distributed from the southern Persian Gulf to the Aegean is good. ii) This is combined with a good match for trace element patterns of ores and artifacts. iii) Copper and tin occur within one mineralization. iv) Ancient textual references mention tin and bronze supply from regions east of Mesopotamia. v) The dating of surface finds of pottery and charcoal finally supports these findings. At present Deh Hosein is the only known copper-tin occurrence close to Luristan and Mesopotamia.

The northern part of the Sanandaj-Sirjan zone which is characterized by intrusion of several intrusive bodies in metamorphic terranes favors the occurrence of similar deposits as in the Astaneh-Sarband area. Thus, the prospects are good for further exploration in the region which may also reveal some other ancient mines.

# **Mineralisationen von Au, Sn, W und Cu im Sarband-Astaneh-Gebiet, westlicher Zentraliran**

## **und ein Vergleich der Erze mit antiken Bronzeartefakten aus Westasien**

### **Kurzfassung**

Diese Arbeit befasst sich mit zwei Zielsetzungen; (1) geologische, mineralogische und geochemische Untersuchungen an den Deh Hossein, Astaneh und Nesam Abad Mineralisationen im Astaneh-Sarband-Gebiet, westlicher Zentraliran, um die Zusammensetzungen der Mineralisationen und ihre Bildungsbedingungen zu erfassen, und (2) geochemische Untersuchungen an antiken Bronzeartefakten aus dem Iran und Westasien, um ihre Eigenschaften mit dem zinn- und kupferreichen Erz von Deh Hossein zu vergleichen und mögliche Zusammenhänge zu beurteilen.

Das Astaneh-Sarband-Gebiet befindet sich im nördlichen Teil der NW-SE ausgerichteten Sanandasch-Sirschan Metamorphosezone, die hauptsächlich aus mesozoischen Schiefen, mitteljurassischen bis tertiären Intrusivgesteinen mit Kontaktaureolen und Pegmatiten besteht. Die Regionalmetamorphose erreicht die Grünschieferfazies, aber manche granitoiden Intrusionen zeigen örtlich Kontaktmetamorphe Phänomene. Durch Magmatismus entstanden großflächige, felsisch bis intermediäre Intrusiva entlang eines generellen NW-Trends. Die Hauptausrichtung von Störungen, Brüchen und anderen Strukturmerkmalen ist NW-SE.

Die Nebengesteine der Mineralisationen bei Deh Hossein sind jurassische Metasedimente, in die der Astaneh-Komplex intrudierte. Die Mineralisation setzt sich auch im südlichen Teil der Astaneh-Intrusion fort. Die metamorphen Gesteine bestehen aus alternierenden Meta-Sandsteinen, Phylliten, Schiefen und Hornfelsen. Die Hauptstörungen und die anderen geologischen Strukturen mit NW- und NE-Trend haben die Ausrichtung der Mineralisation gesteuert. Die Mineralisationen treten in Form von Quarz und Quarz-Sulfid Gängen und Adern auf, teilweise in parallelen Schwärmen. Die Gänge sind bis zu 1.5m breit und mehrere zehner Meter mächtig. Die Vererzung kommt auch als Dissemination und Impregnation vor, insbesondere an den Salbändern. Die vorherrschenden Alterationsprodukte, die neben und innerhalb intensiver Quarz-Äderungszonen vorkommen, sind Quarz, Serizit, Turmalin und Monazit. Etwa 35 Erzminerale wurden bei Deh Hossein aufgefunden. Arsenopyrit ist das dominante Sulfidmineral. In geringeren Mengen sind Kupferkies > Pyrit > Pyrrhotin vorhanden. Kassiterit und Ferberit treten seltener auf. Der Sulfidgehalt des Erzes ist generell geringer als zwei Volumenprozent. Arsenopyrit enthält üblicherweise 1-150µm große Einschlüsse aus gediegen Wismut, Bismut und Bismuthinit. Gold kommt nicht sichtbar im Arsenopyrit und in wismuthaltigen Mineralen bei Deh Hossein vor. Der Goldgehalt des Erzes, analysiert mit NAA, reicht von 0.05 bis 13.3ppm, während die Cu-, Sn-, W- und Bi-Konzentration der Gänge jeweils bis zu 10%, 6.7%, 2420 ppm und 1800 ppm ausmacht.

Bei Astaneh ist die Goldvererzung begrenzt auf die NW-SE ausgerichtete Astaneh-Intrusion, die hauptsächlich aus Biotit-Granit ( $98.9 \pm 1.0$  Ma; Masoudi 1997) neben geringeren Anteilen an Granodiorit, Turmalin-Granit und Quarz-Diorit besteht. Der nordöstliche Teil der Astaneh-Intrusion wird vom Schirmazd Granodiorit durchschnitten. Der Schirmazd Stock, mit 400 m Durchmesser, hat Eozänes Alter (Rb/Sr- und Zirkon-Alter, diese Studie). Der Schirmazd Granodiorit wird selbst von NE-streichenden Mikrogranodiorit-Gängen durchschnitten. Goldvererzungen kommen hauptsächlich als NE-verlaufende Quarz- und Quarz-Sulfid-Gänge und Adern und auch als Dissemination im Schirmazd Stock, in den Mikrogranodiorit-Gängen und in einigen kleineren benachbarten alterierten Granit-Stöcken vor. Alterationsminerale sind Serizit, Chlorit, Quarz, Calcit und in einige Fällen Kaolinit. Kupferkies und Arsenopyrit sind die vorherrschenden Sulfidminerale, von denen letzterer 1-50 µm große Einschlüsse aus gediegen Wismut und Bismut enthält. Gold kommt in sichtbarer und unsichtbarer Form vor. Sichtbares Gold ist in Form sehr feinkörniger Partikel (<15µm) entweder im Goethit (oxidiert aus Kupferkies) oder in serizitisierendem Plagioklas vorhanden (Hashemi 2002), unsichtbares Gold hingegen in Arsenopyrit und bismuthaltigen Mineralen. Die Goldgehalte (NAA) reichen von 0.05 bis 9.5 ppm, während die Cu-, Sn-, W- und Bi-Konzentrationen der Gänge bis jeweils 1%, 0.05%, 100 ppm and 138 ppm reichen.

Die Nesam Abad Mineralisation bildete sich in einem unter- bis mitteleozänen Gesteinsverband. Dieser Gesteinsverband wird von mehreren aplitischen bzw. Quarz- oder Quarz-Turmalin-Gängen durchschnitten. Die Quarz- und Quarz-Turmalin-Gänge enthalten die Mineralisation. Die Störungen des Gebietes streichen NW-, NE-, und N. Durch hydrothermale Prozesse entstandene Minerale sind Quarz, Chlorit, Serizit und Turmalin. Die häufigsten Erze bei Nesam Abad sind Kupferkies, Arsenopyrit und Scheelit. Gold kommt unsichtbar vor, überwiegend im Arsenopyrit mit Wismut-Einschlüssen. Der Goldgehalt des Erzes reicht von 0.05 bis 36.2 ppm (NAA). Der Gehalt an Cu, Sn, W, und Bi in den Gängen reicht jeweils bis 10%, 0.87%, 3.37% and 548 ppm (Farhadian 1999).

Die Goldkonzentration korreliert positiv mit Arsen, Wismuth, Selen, Silber, Tellur und Antimon in allen drei Lagerstätten. Mikrosondenuntersuchungen zeigen, daß der Arsenopyrit von Deh Hossein, Astaneh und

Nesam Abad jeweils 32.3 bis 34.3, 30.7 bis 31.4, and 33.6 bis 35.6 Atom% Arsen enthält. Aus den Durchschnittszusammensetzungen wurde Bildungstemperaturen von 460°C, 410° bis 380°C und 565° bis 510 °C errechnet. Die Sauerstoffisotopenverhältnisse für goldhaltige Quarzgänge in dem Gebiet reichen von 13.6 bis 19.2‰ (V-SMOW) für Deh Hossein, von 11.5 bis 13.7‰ für Astaneh und von 11.6 bis 15‰ für Nesam Abad. Die Sauerstoffisotopendaten deuten eine metamorphe oder eine gemischte magmatisch-metamorphe Quelle für die Quarzgänge an. Die gemessenen Schwefelisotopenwerte für Pyrit, Kupferkies, Bleiglanz und Arsenopyrit in Quarzgängen bei Deh Hossein, Astaneh und Nasam Abad reichen jeweils von -5.6 bis 0‰, -0.5 bis 1.8‰ und 1.2 bis 4‰ (CDT). Die Schwefelisotopendaten aller Vorkommen deuten auf eine magmatische Schwefelquelle hin. Die Bleiisotopenverhältnisse von Sulfid- und Nebengesteinsproben der Lagerstätten zeigen eine gute Übereinstimmung des Erzes von Deh Hossein mit dem Metasandstein, des Erzes von Astaneh mit dem Schirmazd-Stock und des Erzes von Nesam Abad mit dem Quarzdiorit. Die Bleiisotopensignaturen der Erze aller drei Vorkommen sind auch untereinander relativ ähnlich. Nach dem Plumbotectonics-Model von Zartman and Doe (1981) hat das Blei einen unterkrustalen Ursprung.

Die untersuchten Vererzungen zeigen vielfältige Ähnlichkeiten bezüglich ihrer Mineralogie, Geochemie, Bildungstemperaturen, Isotopenverhältnisse, Alterationen und Goldvorkommen. Sie weisen auch viele Ähnlichkeiten mit den „Intrusion-Related Gold Systems“ auf, die von Alaska, aus dem Yukon-Gebiet und anderen Teilen der Welt beschrieben wurden (z.B. Lang et al. 1997, 2000; McCoy et al. 1997; Thompson et al. 1999). In Anbetracht der vorliegenden Daten scheint eine ergiebige magmatische Quelle (wahrscheinlich von unterkrustaler Herkunft), die schon vorhandene metamorphe Gesteine beeinflusst hat (durch Remobilisierung einiger ihrer Elemente), zu einer relativ intensiven Goldvererzung in dem Gebiet während der Pyrenäischen Orogenese geführt zu haben.

Die umfangreichen Relikte von antikem Bergbau bei Deh Hossein, das gleichzeitige Vorkommen von Zinn und Kupfer, nebst zahlreichen archäologischen und schriftlichen Quellen, die auf die iranische Hochebene als Liefergebiet für die Rohstoffe Mesopotamiens und Südwestirans (Susa und Luristan) verweisen, brachten mich dazu, eine mögliche Beziehung zwischen Deh Hossein und antiken Bronzeartefakten zu untersuchen. Für diesen Zweck wurden mehrere typische Luristanbronzen, die höchstwahrscheinlich in die iranische Eisenzeit zu datieren sind (von circa 1300-1250 bis 650 v.Chr.) analysiert und mit der Zusammensetzung der Erze von Deh Hossein und mit Literaturdaten von anderen Bronzeartefakten verglichen. Die Untersuchung von 29 Luristanbronzen mittels energie-dispersiver Röntgenfluoreszenzanalyse ergab variable Konzentrationen von As, Pb, Zn und Fe und hohe Konzentrationen an Zinn (0.48-15.4%).

In vielen Fällen stimmt die Zusammensetzung der in dieser Arbeit untersuchten Luristanbronzen ebenso wie die aus früheren Untersuchungen (Fleming et al. 2005) mit der Zusammensetzung der Erze von Deh Hossein überein. Noch bemerkenswerter ist die sehr gute Übereinstimmung der Bleiisotopenverhältnisse von Deh Hossein mit 25 prähistorischen Metallartefakten aus dem 3. Jahrtausend v.Chr. von Luristan und anderen Regionen, wie dem südlichen Persischen Golf (Weeks 1999), der Ägäis (Begemann et al. 1992) und Mesopotamien (Begemann & Schmitt-Strecker in Vorbereitung).

Bei Deh Hossein, am westlicher Rand des Luristangebietes, nahe den antiken Zentren von Susa und Mesopotamien, ist alter Bergbau anhand zahlreicher großer, elliptischer Pinggen zu erkennen, die in zwei Reihen entlang der Vererzungshorizonte verlaufen. Diese Pinggen messen bis zu 70 m im Durchmesser, sind bis zu 15 m tief und erstrecken sich über eine Länge von 500 m. Zahlreiche Schlagsteine aus silifiziertem Phyllit und Granit, Keramik und Mahlsteine wurden im Bereich der Pinggen und den nahe liegenden Siedlungen gefunden. Die Keramik wurde auf das frühe 1. Jahrtausend v.Chr. datiert. Stücke von Holzkohle, die in einem Abbau gefunden wurden, ergaben ein Radiokarbonalter von  $3380 \pm 55$  a, das nach Kalibration ( $2\sigma$ ) eine Altersspanne von 1775-1522 v.Chr. ergibt.

Viele Indizien weisen darauf hin, dass Deh Hossein am Anfang des 3. Jahrtausend v. Chr. eine bedeutende Quelle von Zinn und Kupfer für den westlichen Iran und Mesopotamien und vielleicht sogar für weiter westlich gelegene Regionen war.

Zusammenfassend ergaben die Untersuchungen: i) Die Bleiisotopenverhältnisse von Deh Hossein ähneln denen vieler Bronzeartefakte aus der Bronze- und Eisenzeit vom südlichen Persischen Golf bis zur Ägäis. ii) Ebenso besteht eine gute Übereinstimmung in Bezug auf das Spurenelementmuster zwischen Erzen und Artefakten. iii) Kupfer und Zinn treten zusammen im gleichen Vorkommen auf. iv) Antike Texte erwähnen Zinn- und Bronzelieferungen aus Regionen östlich Mesopotamiens. v) Letztendlich unterstützen die Datierungen von Keramik und Holzkohle diese Ergebnisse. Zur Zeit ist Deh Hossein das einzige bekannte Kupfer-Zinn-Vorkommen, das in der Nähe von Luristan und Mesopotamien liegt.

Der gesamte nördliche Teil der Sanandadsch-Sirdschan Zone ist durch mehrere Intrusivkörper charakterisiert, ähnlich wie im Astaneh-Sarband-Gebiet. Deshalb ist es denkbar, dass eine geologische und archäometallurgische Exploration in dieser Region zur Entdeckung weiterer alter Bergwerke führen könnte.



## بررسی کانی سازی طلا، قلع، تنگستن و مس در منطقه آستانه - سربند، غرب ایران مرکزی

### شامل مقایسه کانسنگ مربوطه با اشیاء مفرغی باستانی ایران و آسیای غربی

#### توسط: نیما نظافتی

#### چکیده

در نوشتار پیش رو دو موضوع اصلی مورد پژوهش و بررسی قرار گرفته اند؛ نخست، زمین شناسی، کانی شناسی و ژئوشیمی کانسارهای ده حسین، آستانه و نظام آباد واقع در منطقه آستانه - سربند به منظور درک خصوصیات آنها و چگونگی شکل گیریشان و دوم، ژئوشیمی اشیاء مفرغی باستانی ایران و آسیای غربی به منظور مقایسه آنها با کانسنگ غنی از مس - قلع ده حسین و بررسی ارتباط احتمالی آنها.

منطقه آستانه - سربند که در بخش شمالی کمربند دگرگونی سندانج - سیرجان واقع شده عمدتاً شامل شیست های مزوزوئیک، سنگ های نفوذی ژوراسیک میانی - ترسیر میانی، هاله های دگرگونی آنها و پگماتیت می باشد. دگرگونی ناحیه ای به حد رخساره شیست سبز می رسد اما در حاشیه گرانیتوئیدهای منطقه دگرگونی مجاورتی نیز مشاهده می گردد. ماگماتیسیم توده های بزرگی از سنگ های نفوذی با ترکیب فلسیک تا حدواسط را با روند عمومی شمال باختر - جنوب خاور در منطقه ایجاد نموده است. روند اصلی گسل ها، درزه ها و سایر ساختارهای منطقه شمال باختر - جنوب خاور می باشد.

کانسار ده حسین عمدتاً در سنگ های دگرگونی ژوراسیک که توده آستانه در آنها نفوذ کرده رخ داده است. کانی سازی علاوه بر سنگ های دگرگونی در بخش جنوبی توده آستانه نیز ادامه می یابد. سنگ های دگرگونی کانسار شامل تناوبی است از ماسه سنگ دگرگون شده، فیلیت، شیست، اسلیت لکه دار و هورنفلس. گسل ها و درزه های کانسار با روند عمومی شمال باختری و شمال خاوری جهت جایگیری کانی سازی را مشخص نموده اند. کانی سازی عمدتاً به صورت رگه - رگچه های کوارتز، کوارتز - سولفیدی و کوارتز - گوسانی با شیب قائم رخ داده است که گاهی به شکل صفحاتی موازی هم هستند. رگه ها تا 1.5 متر پهنا و چندین ده متر درازا دارند. کانی سازی همچنین به صورت افشان و آغشتگی بخصوص در حاشیه رگه ها مشاهده می گردد. دگرسانی اصلی در درون و مجاورت بخش های کانی سازی شده شامل سیلیسی شدن، سربیسیتی شدن، تورمالینی شدن و دگرسانی مونازینی می باشد. حدود 35 کانی فلزی طی پژوهش حاضر در کانسار ده حسین شناسایی شده اند. ارسنوپیریت کانه سولفیدی غالب است که با مقادیر کمتری از کالکوپیریت، پیریت و پیروتیت همراهی می شود. کاسیت و فریریت نیز کانه های نسبتاً فراوان اکسیدی هستند. محتوی سولفید کانسنگ عموماً کمتر از دو درصد حجمی آنست. کانی ارسنوپیریت حاوی ادخال های 1 تا 150 میکرومتری از بیسموت فلزی، بیسمیت و بیسموتینیت می باشد. در کانسار ده حسین طلا به صورت نامرئی در ارسنوپیریت و کانی های بیسموت دار رخ می دهد. تجزیه عنصری به روش فعال سازی نوترونی نشانگر وجود 0.05 تا 13.3 گرم در تن طلا، تا 10% مس، تا 6.7% قلع، تا 2420 گرم در تن تنگستن و تا 1800 گرم در تن بیسموت در کانسنگ ده حسین می باشد.

در کانسار آستانه کانی سازی طلا محدود است به توده نفوذی آستانه که عمدتاً از بیوتیت گرانیت و به مقدار کمتر از گرانودیوریت، تورمالین گرانیت و کوارتز دیوریت تشکیل شده است. استوک گرانودیوریتی شیرمزد در بخش شمال خاوری توده آستانه نفوذ نموده است. بر اساس مطالعات سن سنجی به روش های روبیدیوم - استرانسیوم و تبخیر تک کانی زیرکون (انجام گرفته طی پژوهش حاضر) استوک شیرمزد با فطری حدود 400 متر سنی معادل ائوسن دارد. خود این استوک توسط دایک های میکروگرانودیوریتی با روند شمال خاوری قطع شده است. کانی سازی طلا عمدتاً به صورت رگه - رگچه های کوارتز، کوارتز - سولفید و افشان در استوک شیرمزد، دایک های میکروگرانودیوریتی قطع کننده آن و چند استوک دگرسان شده کوچک واقع در نزدیکی آنها رخ می دهد. کانی های دگرسانی شامل سربیسیت، کلریت، کوارتز، کلسیت و تا حدودی کائولین می باشند. در کانسار آستانه کالکوپیریت و ارسنوپیریت کانی های اصلی سولفیدی هستند که ارسنوپیریت حاوی ادخال های 1 تا 50 میکرونی از بیسموت فلزی و بیسمیت است. طلا به هردو شکل مرئی و نامرئی در کانسار آستانه رخ داده است. طلای مرئی به صورت ذرات بسیار ریز (<15 میکرون) در گوتیت حاصل از اکسیدشدگی کالکوپیریت و نیز در پلاژیوکلاز سربیسیتی شده دیده می شود (هاشمی 1380)، در حالیکه طلای نامرئی در ارسنوپیریت و کانی های بیسموت دار رخ داده است. تجزیه عنصری به روش فعال سازی نوترونی نشانگر حضور 0.05-9.5 گرم در تن طلا، تا 1% مس، تا 0.05% قلع، تا 100 گرم در تن تنگستن و تا 138 گرم در تن بیسموت می باشد.

کانی سازی نظام آباد در یک واحد سنگی کوارتز دیوریتی به سن ائوسن پائینی - میانی رخ داده است. این واحد سنگی توسط دایک های آپلیتی و رگه های کوارتز و کوارتز - تورمالین قطع شده است که دو مورد آخری میزبان کانی سازی هستند. گسل های منطقه روندهای شمال باختری، شمال خاوری و شمالی دارند. کانی های دگرسانی مرتبط با کانی سازی شامل کوارتز، کلریت، سربیسیت و تورمالین هستند. طلا به صورت نامرئی عمدتاً در ارسنوپیریت حاوی ادخال های بیسموت در نظام آباد رخ می دهد. تجزیه عنصری به روش فعال سازی نوترونی نشانگر وجود 0.05 تا 36.2 گرم در تن طلا، تا 10% مس، تا 0.87% قلع، تا 3.37% گرم در تن تنگستن (فرهادیان 1378) و تا 548 گرم در تن بیسموت در کانسنگ نظام آباد می باشد.

در هر سه کانسار، طلا همبستگی مثبتی را با ارسنیک، بیسموت، آنتیموان، نقره، سلنیوم و تلوریوم نشان می دهد. بررسی های مایکروپروب بر روی ارسنوپیریت نشاندهنده درصد اتمی ارسنیک معادل 32.3 تا 34.3 در کانسار ده حسین، 30.7 تا 31.4 در آستانه و 33.6 تا 35.6 در نظام آباد می باشد. میانگین مقادیر فوق نمایانگر درجه حرارت های سیال اولیه کانه داری حدود 460 درجه سانتیگراد برای کانسار ده حسین، 380 تا 410 درجه سانتیگراد برای کانسار آستانه و 510 تا 565 درجه

سانتیگراد برای کانسار نظام آباد می باشد. نسبت های ایزوتوپ اکسیژن برای رگه های کوارتز طلا دار در منطقه از 13.6 تا 19.2 در هزار برای ده حسین، 11.5 تا 13.7 در هزار برای آستانه و 11.6 تا 15 در هزار برای نظام آباد تغییر می کنند. نتایج مطالعات ایزوتوپی اکسیژن، منشائی دگرگونی یا یک منشأ دگرگونی - ماگماتیک را برای رگه های کوارتز پیشنهاد می کند. مقادیر اندازه گیری شده ایزوتوپ گوگرد برای پیریت، کالکوپیریت، گالن و ارسنوپیریت در رگه های کوارتز - سولفیدی مقادیر 5.6 تا 0 در هزار برای ده حسین، 1.8 تا 0.5- در هزار برای آستانه، و 1.2 تا 4 در هزار برای نظام آباد را نشان می دهند که نمایانگر یک منشأ ماگمایی برای گوگرد می باشند. نسبت های ایزوتوپی سرب در کانیهای سولفیدی و سنگ درونگیر کانسارهای مورد مطالعه نشانگر همخوانی خوبی میان این نسبت های ایزوتوپی بین کانسنگ ده حسین و ماسه سنگ دگرگونی، کانسنگ آستانه و گرانودیوریت شیرمزد و نیز کانسنگ نظام آباد و سنگ درونگیر کوارتز دیوریتی آن می باشد. نسبت های ایزوتوپی سرب کانسنگ هر سه کانسار مورد مطالعه نیز مقادیری نزدیک به یکدیگر را به نمایش می گذارند. بر اساس مدل پلومیوتکتونیکس ارائه شده توسط Zartman and Doe (1981) نسبت های ایزوتوپی سرب در کانسنگ ها نشانگر منشائی از پوسته زیرین برای آنهاست.

کانسارهای مورد بررسی شباهت های فراوانی را از نظر کانی شناسی، ژئوشیمی، دمای تشکیل، نسبت های ایزوتوپی، دگرسانی و نحوه رخداد طلا با یکدیگر نشان می دهند. علاوه بر این، کانسارهای منطقه خصوصیات مشابه فراوانی را با "سیستم های طلای مرتبط با توده های آذرین نفوذی" به نمایش می گذارند. چنین سیستم هایی از آلاسکا، منطقه یوکون و نقاط دیگری از جهان گزارش شده اند (Lang et al. 1997, 2000; McCoy et al. 1997; Thompson et al. 1999).

بر اساس اطلاعات موجود چنین به نظر می رسد که یک ماگمای بارور (احتمالاً با خاستگاه پوسته زیرین) با تحت تاثیر قرار دادن سنگ های دگرگونی منطقه (و جنبایش بعضی عناصر موجود در آنها) منشأ کانی سازی بوده و موجب کانی زایی نسبتاً وسیعی از طلا طی دوره کوهزایی پیرنه در منطقه شده است.

آثار فراوان معدنکاری باستانی در کانسار ده حسین، حضور توأمان قلع و مس در آن و نیز وجود شواهد بسیار باستان شناسی و منابع نوشتاری باستانی فراوان که فلات ایران را به عنوان تأمین کننده مواد خام میانرودان باستان و تمدن های جنوب باختر ایران (شوش و لرستان) معرفی می نمایند، مشوقی بودند برای مقایسه کانسنگ ده حسین و اشیاء مفرغی باستانی جهت بررسی ارتباط احتمالی آنها. بدین منظور چندین شیء مفرغی نمادین لرستان که به احتمال قوی متعلق به عصر آهن ایران می باشند (حدود 3300 تا 2650 سال پیش) مورد بررسی قرار گرفتند. نتایج به دست آمده با نتایج حاصل از کانسنگ ده حسین و آزمایشات منتشر شده قبلی مقایسه گردیدند. تجزیه 29 شیء مفرغی لرستان به روش پراکنش انرژی فلورسانس اشعه ایکس نشاندهنده تمرکزهای متفاوتی از آرسنیک، سرب، روی و آهن و نیز درصد بالای قلع (0.48 تا 15.4%) در آنها می باشد. کانسنگ ده حسین نیز شباهت قابل توجهی را از نظر ترکیب شیمیایی با اشیاء فوق الذکر و نیز اشیاء مطالعه شده توسط دیگران (Fleming et al. 2005) نشان می دهد. نکته قابل توجه تر همخوانی بسیار خوب نسبت های ایزوتوپی سرب کانسنگ ده حسین با نسبت های سرب اشیاء مفرغی بررسی شده طی این مطالعه و نیز اشیاء مفرغی متعلق به هزاره سوم پیش از میلاد گزارش شده از جنوب خلیج فارس (Weeks 1999)، منطقه اژه (Begemann et al. 1992) و منطقه لرستان و میانرودان (Begemann & Schmitt-Strecker, in preparation) می باشد.

در معدن باستانی ده حسین که در حاشیه باختری منطقه لرستان و در نزدیکی تمدن های باستانی شوش و میانرودان واقع شده، کنده کاری های باستانی به صورت فرورفتگی های بیضوی فراوانی در دو ردیف در طول افق های کانی سازی دیده می شوند. کنده کاری های باستانی 50 تا 70 متر قطر و تا 15 متر ژرفا دارند و گاه تا 500 متر در کنار یکدیگر چیده شده اند. چندین چکش سنگی از جنس فیلیت سیلیسی شده و گرانیت، قطعات سفال و سنگ ساب درون کنده کاری ها و محوطه های باستانی مجاور آنها یافت شدند. قطعات سفالی سنی حدود اوایل هزاره نخست پیش از میلاد را نشان می دهند. تکه های ذغال چوب پیدا شده در یکی از کنده کاری ها سنی معادل 1522 تا 1775 پیش از میلاد را بر اساس مطالعات رادیوکربن نشان می دهند.

شواهد فراوانی گواه بر این ادعا هستند که معدن باستانی ده حسین از تأمین کنندگان عمده قلع برای تمدن های باستانی ایران و میانرودان و حتی شاید مناطق واقع در باختر آنها طی هزاره سوم پیش از میلاد می باشد. رویهمرفته این شواهد شامل موارد زیرند؛ الف) همخوانی خوب نسبت های ایزوتوپی سرب میان کانسنگ ده حسین و تعداد فراوانی از اشیاء مفرغی عصرهای آهن و مفرغ از جنوب خلیج فارس تا منطقه اژه. ب) همخوانی خوب الگوی عناصر جزئی کانسنگ و اشیاء مفرغی. پ) حضور همزمان قلع و مس در کانسار ده حسین. ت) منابع نوشتاری باستانی که به تأمین قلع و مفرغ از مناطق شرقی میانرودان اشاره می کنند و ث) نتایج سن سنجی یافته های سطحی که شواهد فوق را تأیید می نمایند. در حال حاضر ده حسین تنها معدن باستانی شناخته شده حاوی قلع و مس در نزدیکی لرستان و میانرودان است.

بخش شمالی زون سنندج - سیرجان که میزبان تعداد زیادی توده های آذرین نفوذی در گستره سنگ های دگرگونی است، مکان مناسبی برای رخداد و در نتیجه پی جویی کانسارهای مشابه منطقه آستانه - سرپند می باشد. این مطلب معیار مناسبی را برای اکتشاف در این منطقه ارائه می دهد که همچنین می تواند منجر به کشف معادن باستانی دیگری گردد.

# *Chapter 1*

## **Introduction**

### **1.1 Problem definition**

The central part of the Alpine-Himalayan orogenic-metallogenic belt in Iran hosts various mineral deposits in a diverse geology. This along with the emergence of the earliest known civilizations of the world in southwestern Iran and Mesopotamia has made this country one of the first places in which the human being has exploited different metals and extracted them via smelting from ores.

The recent discovery of an ancient copper-tin-gold mine at Deh Hosein, in the previously known Astaneh-Sarband tungsten-gold area has inspired a comprehensive economic geological and archaeometallurgical study on those deposits in the frame of a PhD project. The assessment of the gold, tin and tungsten potentials of the area as well as the relationship between the ancient mining activities and the ancient bronze production in Western Asia were the aims of this work.

The Astaneh-Sarband area is located in the northern part of the Sanandaj-Sirjan tectonic unit (Figure 1.1) and has long been recognized to host gold and tungsten occurrences of hydrothermal origin. There are five tungsten, gold and tungsten-gold occurrences in the area from which the three occurrences of Deh Hosein, Astaneh, and Nezam Abad have been investigated as part of this thesis.

Two individual problems are addressed in this work; (1) The development of a conceptual/genetic model for the mineralizations and consequently the presentation of an exploration model for the Astaneh-Sarband area. (2) The investigation of a possible relationship between Deh Hosein and the ancient bronze production and the consequent development of an ancient trade route.

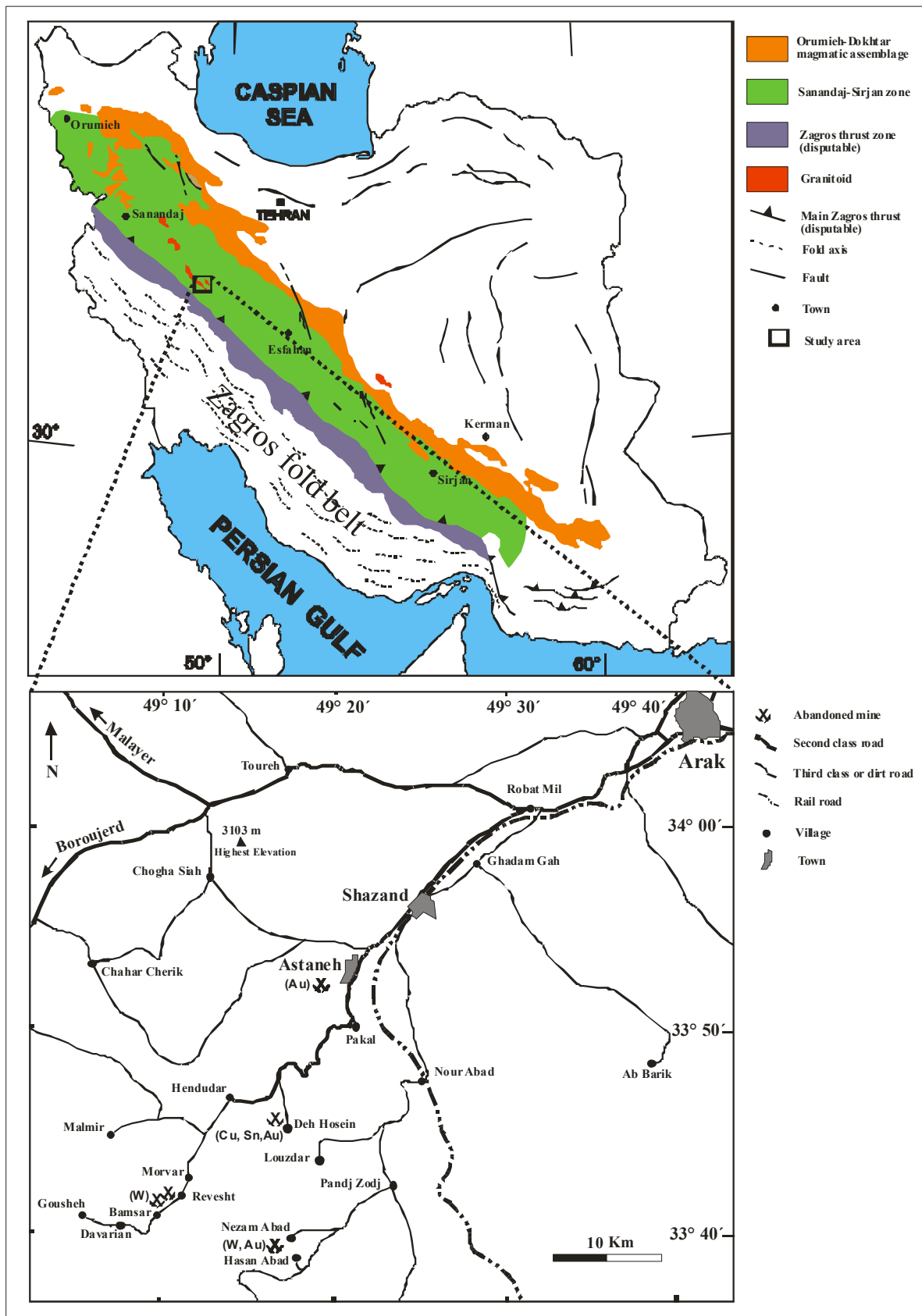


Figure 1.1 Location of the study area, with its access roads, in the geological context of Iran.

This is probably the first time that economic geological and archaeometric studies are tied together in the frame of a PhD project in Iran. Such a work is important because the majority of modern base and precious metal mines in Iran were discovered by tracing relics of ancient mining activities which have a long tradition in Iran. Such studies may help both to reduce the dependence on a single-product economy based on petroleum and to understand the ancient history of technology and its trade patterns.

This subject was suggested by Morteza Momenzadeh for accomplishing a PhD project which started at the Freiberg University of Mining and Technology under the direction of Professors Peter M. Herzig and Ernst Pernicka and was completed at the University of Tübingen under the supervision of Professors Gregor Markl and Ernst Pernicka.

## **1.2 Objectives and aims**

The research has the following objectives:

1. to develop a genetic model of gold mineralization at the Astaneh-Sarband area and to show how the application of these models can be used to recognize the presence of similar mineralizations in the surrounding regions; and
2. to investigate the relationship between Deh Hosein and the ancient bronze production and consequently development of ancient trade.

### **1.2.1 Genetic model**

The following items are the main issues which are investigated in order to understand the genesis of the occurrences in the Astaneh-Sarband area:

- Litho-structural controls on mineralization
- Petrography of host formations and their role in gold precipitation
- The alteration assemblages
- Fabric (texture, structure and orientation) of the ore
- Composition of the ore and associated minerals
- Paragenesis of the ore and associated minerals
- Modes of occurrence of gold in the ore minerals
- Temperature of mineralization
- Source of the mineralizing hydrothermal fluids
- Heat source driving their circulation
- Source of gold and associated metals
- Age of the host rocks and the mineralization
- Role of magmatism and metamorphism in the mineralization

The above mentioned data would help in reconstructing the geologic conditions and events during the mineralization in the Astaneh-Sarband area. This could be implemented as an exploration guide to discover similar mineralizations in the surrounding regions.

### **1.2.2 Archaeometric investigations**

- Comparison of the trace element patterns of ancient bronze artifacts with the ores of Deh Hosein

- Comparison of the lead isotope signature of some ancient bronze artifacts from different localities in southwestern Asia with the ores from Deh Hosein
- Comparison of the archaeological and ancient textual evidence with the locality of Deh Hosein

This would reveal the role of the ancient Deh Hosein mine as a copper-tin source in the region.

### **1.3 Geographic setting and exploration history**

The Astaneh-Sarband area, west-southwest of the town Astaneh in west-central Iran (33°40′-33°50′ N, 49°08′-49°20′ W), is located in the north of the Sanandaj-Sirjan metamorphic belt (Figure 1.1).

The area is generally mountainous. The climate of the area is arid to semi-arid cold with 350-800 annual rate of precipitation which is often in form of snow in cold seasons. The climate is moderate in summer (June to October with maximum 32-36°C) and very cold during the winter (with minimum -20°C and average of -5°C).

The outcrops are mostly open but in elevations have been covered by grass and heather. In valleys, fruit and grape gardens have been planted. Wheat, barley and other crops are cultivated in lower elevations.

There are five known tungsten gold occurrences in the area, including the Astaneh gold occurrence, the Deh Hosein polymetallic mineralization, and the Nezam Abad, and Revesht and Bamsar tungsten-(gold) occurrences from which the first three were investigated. All these deposits were recognized by traces of old or ancient mining of copper, tin and/or gold. During the last two decades, the Nezam Abad and Astaneh occurrences were explored for gold and tungsten by the Geological Survey of Iran and Samim resources, while the Deh Hosein has been discovered in 2000 during a survey (Momenzadeh et al. 2002). Some MSc theses (Azizpour 2000; Ben Yaghoub 1999; Farhadian 1991; Hashemi 2002; Radfar 1987) and a PhD project (Masoudi 1997) were conducted in the area.

### **1.4 Background to the research**

#### **1.4.1. Economic geological aspects**

The northern part of the Zagros orogenic belt of Iran, which itself comprises the middle part of the Alpine-Himalayan orogenic-metallogenic belt, hosts diverse types of base-metal, gold and tungsten mineralizations of hydrothermal origin. Several deposits in this region have been proven to be economic and are already in operation or in the exploration phase.

The Zagros orogenic belt embraces the Sanandaj-Sirjan zone in its northern part. The Sanandaj-Sirjan zone has experienced both the Cimmerian and Late Cretaceous orogenies and younger Alpine phases and is in its northern part composed of Mesozoic low grade metamorphic rocks which have been intruded by Jurassic to Mid-Tertiary intrusive bodies and granitoids. The intrusives have caused contact metamorphism in their aureoles.

The discovery of the new polymetallic occurrence of Deh Hosein in 2000 has encouraged more investigations in the already known metallogenic area of Astaneh-Sarband. According to the present study, the gold mineralization in the Astaneh-Sarband area shares several characteristics with intrusion-related gold systems, a specific class of gold deposits recently defined. The definition is based largely on deposits in the Fairbanks district, Alaska, and similar deposits in the Yukon Territory (McCoy et al. 1997; Lang et al. 2001; Baker and Lang 2001; Maloof et al. 2001). Several deposits in other parts of the world have been proposed as

further examples of this class (Thompson et al. 1999; Lang and Baker 2001; Baker 2002) (Figure 1.2).

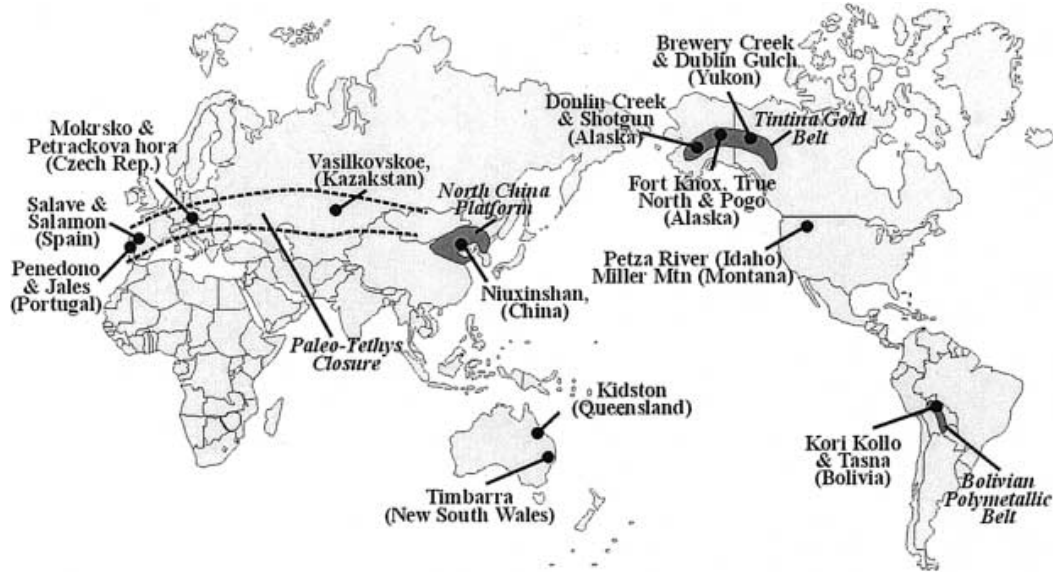


**Figure 1.2** Location of major recognized intrusion-related gold systems and related plutonic provinces. Diagram after Thompson et al. (1999) and Lang et al. (2001).

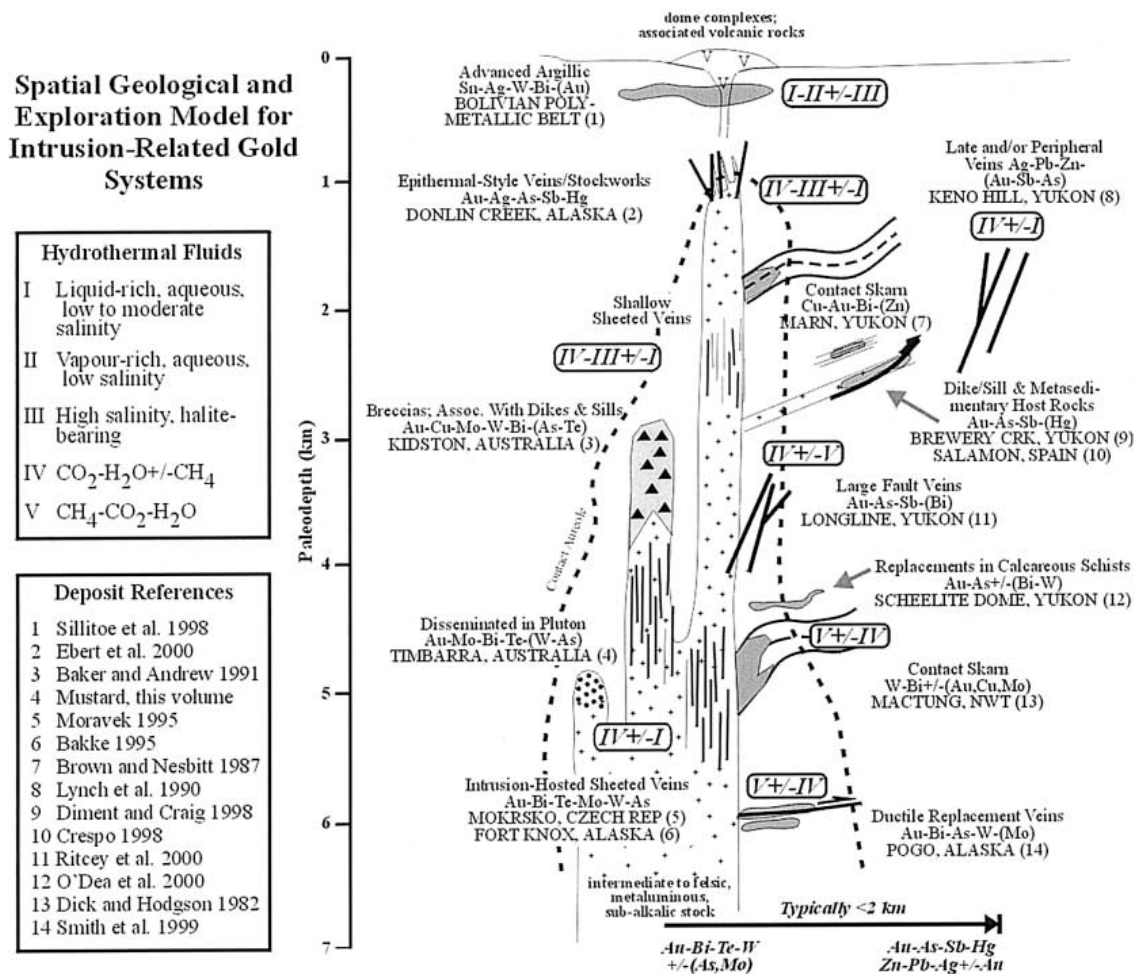


**Figure 1.3** Schematic geological and exploration model for intrusion-related systems emphasizing the vertical and lateral variation in deposit style, fluid characteristics, and metal signatures (After Lang and Baker 2001).

In these deposits, which are mainly of Phanerozoic age and located mainly in magmatic provinces, best or formerly known for tungsten and/or tin deposits, granitic to granodioritic intrusions are emplaced into metasedimentary rocks in continental settings well inboard of convergent plate margins. These intrusions are moderately reduced and of dominantly crustal origin. The deposits are characterized by a reduced (pyrrhotite-stable with no magnetite or hematite), low-sulfide (<5 vol. %) ore assemblage and geochemical enrichment in gold, bismuth, arsenic, tungsten, molybdenum, tellurium, and/or antimony with usually strong correlation of gold and bismuth. Gold commonly occurs in sheeted quartz veins (McCoy et al. 1997; Thompson et al. 1999; Lang et al. 2001; Baker 2002) (Figure 1.3). This research therefore investigates whether, and in what ways, the occurrences of the Astaneh-Sarband area fit the model of intrusion-related gold systems.

#### **1.4.2 Archaeometric aspects**

Although tin bronzes emerge in the late fourth millennium BCE in Mesopotamia, Khuzestan and Luristan, the main production and consumption of this alloy begins at the second half of third millennium BCE, first in the aforementioned areas and later in all of Western Asia. This lasts till the end of the Iron Age in these areas. In spite of rather extensive archaeological and geological investigations in Western Asia during the past decades, the source of tin for the huge bronze production in the ancient Near- and Middle-East has long remained enigmatic. In the last two decades three ancient tin mining sites were reported in Anatolia (Kestel) and Middle Asia (Karnab and Mushiston). However, the role of Kestel in the early production of tin is in dispute. The remaining sites are rather far away from the regions that first apply tin bronze so that their relevance is also not clear.

The recent discovery of the ancient tin-copper mine at Deh Hosein in the Astaneh-Sarband area, at the eastern rim of the Zagros mountains that resulted from the identification of traces of tin in early studies, encourages further investigations on this issue. It will be shown that much geological, analytical, archaeological, textual, chronological and geographical evidence supports the hypothesis that Deh Hosein has been a major source for tin and copper in the Bronze and Iron Ages.

#### **1.5 Methodology**

The research is divided into two parts; economic geology and archaeometry. The economic geologic part is based on surface mapping and sampling as well as on previously accomplished data in the Astaneh-Sarband area. Neutron activation analyses (NAA), conventional microscopy, electron probe microanalyses, Rb/Sr and Pb-Pb age determination analyses, oxygen, sulfur and lead isotope ratios were employed in order to determine features that characterize the morphology and genesis of the occurrences.

The second part (chapter 7) involves the investigation of ancient bronze artifacts by means of trace element (EDXRF) and lead isotope analyses in order to compare them to the results obtained from Deh Hosein. Since this is the only ancient mine known so far in the vicinity of developed ancient cultures which contains copper and tin together, the investigation would reveal (part of) the trade pattern in ancient southwestern Asia.



## *Chapter 2*

### **Stratigraphy and geologic setting of the study area**

This chapter presents a brief overview of the Iranian geology with a focus on the regional geology of west central Iran and the study area. Magmatic, metamorphic, and structural events in the study area are described.

#### **2.1 Introduction**

According to Stöcklin (1968, 1977) and Nabavi (1976), Iran can be divided into ten major lithotectonic domains; Makran, the Lut Block, Eastern Iran, Kopet Dagh, the Alborz Mountains, the Central Iran Block, the Urumieh-Dokhtar zone, the Sanandaj-Sirjan zone, the Zagros fold belt, and the Khuzestan plain. The boundaries of these units are usually marked by faults or in some cases (mainly tectonic) depressions (Nabavi, 1976).

The three tectonically related parallel zones of the Urumieh-Dokhtar magmatic assemblage, the Sanandaj-Sirjan zone, and the Zagros simply folded belt which extend from northeast to southwest of Iran form the Zagros orogenic belt (Alavi 1994), which as part of the Alpine-Himalayan orogenic and metallogenic belt, extends for about 2000 km in a NW-SE direction from the East Anatolian Fault of eastern Turkey to the Oman Line in southern Iran (Alavi 1994). Figure 2.1 shows the main geologic subdivisions of Iran (a) along with a cross section across the Zagros Orogenic Belt (b). A brief explanation of the characteristics of the major Iranian geologic subdivisions and the metallic resources they contain has been presented in the Table 2.1.

There are two major hypotheses concerning the tectonic setting and formation of the Zagros Orogenic Belt; the subduction and the continental rifting hypothesis.

The subduction hypothesis which is widely accepted, assumes that the neo-Tethys oceanic crust, generated in the early Mesozoic, was subducted below the Iranian plate (Central Iran Block), until the closure of the Tethys ocean led to collision of the Afro-Arabian and Iranian Plates in the Late Cretaceous (Alavi 1994) or Miocene (Mohajjel et al. 2003) (Figure 2.1,b).

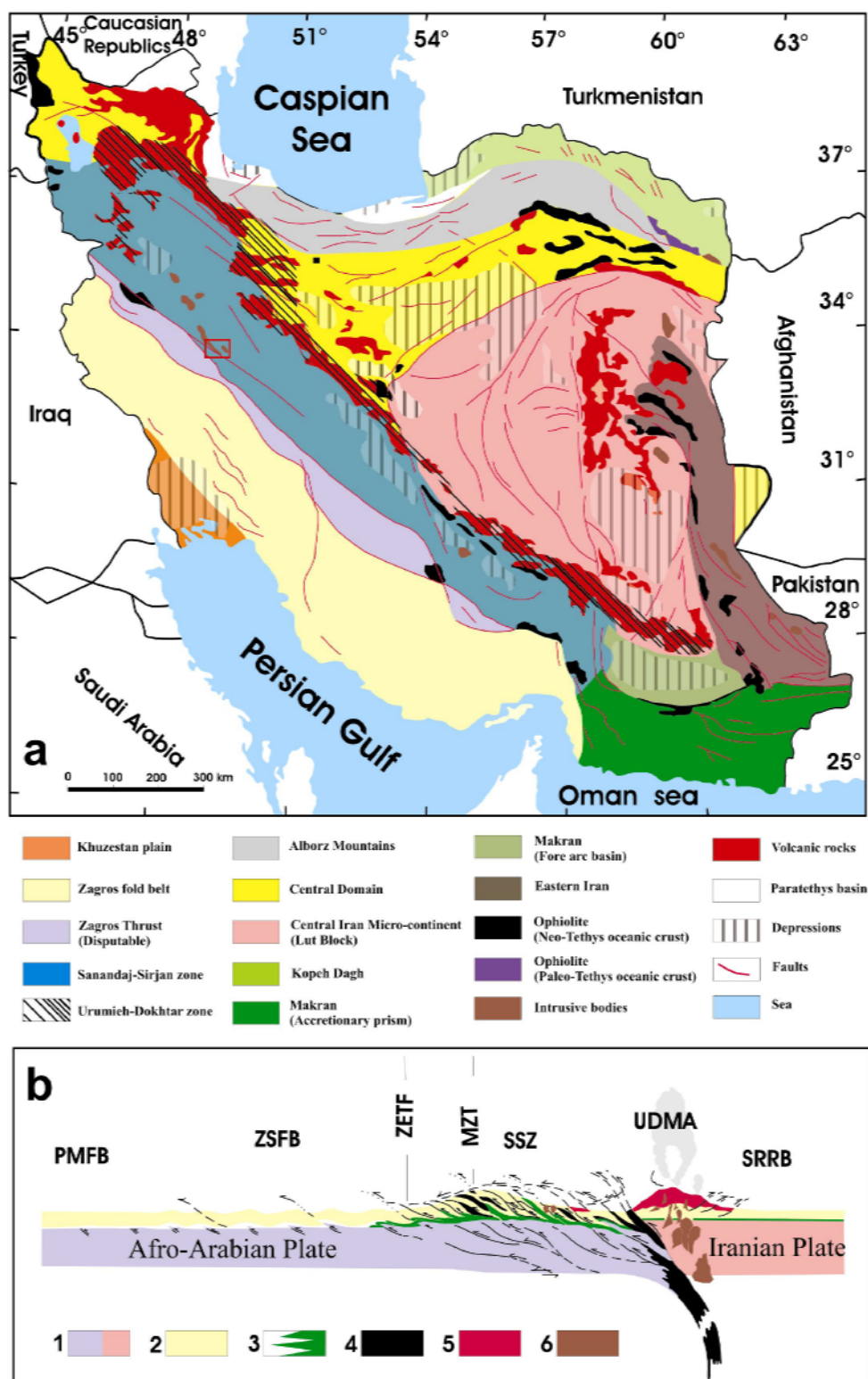


**Figure 2.1 a)** Major geological subdivisions of Iran modified after Stöcklin 1968, 1977; Nabavi 1976 and publications of the Geological Survey of Iran. **b)** Schematic cross-section of the Zagros Orogenic Belt, 1= continental crust; 2= Phanerozoic sedimentary cover; 3= evaporates (blank) and dolomites (green) at the base of the sedimentary cover; 4= oceanic crust; 5= extrusive rocks; 6= intrusive rocks. Modified after Alavi (1994), and Asadi (2000). The red square shows the approximate location of the study area.

The precise location of the suture zone of this collision is much debated amongst the scientists (Alavi 1980, 1994; Takin 1972; Cherven 1986; Berberian and King 1980). A large number of earth scientists have adopted the so-called "Main Zagros Thrust line" as the suture between the Afro-Arabian and Iranian plates (see, for example, Wells 1969; Takin 1972; Crawford 1972; Dewey et al. 1973; Haynes and McQuillan 1974; Stoneley 1975; M. Berberian and King 1981; F. Berberian et al. 1982; Dercourt et al. 1986; Sengör 1990), which was first suggested by Stöcklin (1968), while Alavi (1980, 1994), according to recent investigations, believes that the entire Sanandaj-Sirjan Zone consists of numerous overlapping nappes which have transported various rock sequences from a suture zone that is located along the northeastern boundary of the Sanandaj-Sirjan Zone and not along the so-called "Main Zagros Thrust line".

The continental rift theory proposed by Sabzehie (1974) and discussed by Amidi (1975) and Luscuyer and Rio (1976) assumes the presence of a continental rift zone during the Eocene generating the volcanic rocks of the Urumieh-Dokhtar Zone.

## 2.2 The Sanandaj-Sirjan Zone

The Sanandaj-Sirjan Zone is one of the most dynamic structural zones of Iran and possesses complex structural and stratigraphic features (Darvishzadeh 1991; Alavi 1994). This zone, which was first recognized as a separate linear structural element by Stöcklin (1968), lies - with a width of 150-250 km - between the main Zagros Thrust in the southwest and the Urumieh-Dokhtar volcanic belt in the northeast. It joins the Taurus orogenic belt in Turkey. The ranges occupy a NW-trending 1500 km belt (parallel to the rest of the Zagros orogenic elements) in which the Zagros structural grain is overprinted on the typical Central Iran structural framework (Davoudzadeh 1997). The northeastern part of the zone contains a series of elongated depressions that are well developed parallel to the southwestern boundary of the Urumieh-Dokhtar magmatic assemblage (Alavi 1994).

As a whole the Sanandaj-Sirjan Zone is characterized by the consistent Zagros trend of the zone, the nearly complete lack of Tertiary volcanics, the poor development of Tertiary formations in general, mostly Mesozoic age of the rocks except the Palaeozoic rocks exposed in the southeast, and metamorphic and complexly deformed rocks associated with abundant deformed and undeformed plutons in addition to widespread Mesozoic volcanic rocks (Davoudzadeh 1997; Mohajjel et al. 2003).

The Sanandaj-Sirjan Zone is divided into five sub-zones of radiolarite, Bisotun (Behistun), ophiolite, marginal, and complexly deformed, among which the latter is composed of Late Mesozoic rocks, Hamadan phyllite, Paleozoic-Early Mesozoic rocks, and Late Precambrian-Early Paleozoic rocks (Mohajjel et al. 2003).

Mohajjel et al. (2003) have summarized the formation of the major structures in the Sanandaj-Sirjan Zone in three separate events (1) subduction along the active margin of Central Iran at the northeastern margin of Tethys in Late Jurassic-Early Cretaceous, (2) ophiolite obduction along the northeastern margin of Tethys in the Late Cretaceous, and (3) continental collision of Arabia and Central Iran in the Miocene.

The igneous activity of the zone is consistent with the initiation of subduction in the Late Jurassic. This activity in the Jurassic-Quaternary interval within and adjacent to the northeastern Sanandaj-Sirjan Zone included; (1) Late Jurassic plutonic activity (Berberian and Berberian, 1981), (2) Jurassic and less abundant Cretaceous intermediate to silicic volcanic activity of the marginal sub-zone, (3) Paleocene gabbroic to granodioritic intrusions in the complexly deformed sub-zone, and (4) widespread Eocene-Quaternary magmatism of the Urumieh-Dokhtar Magmatic Arc (Mohajjel et al. 2003).

Subdivision	Geologic Feature	Geologic time	Metallic Resources	Instance
<b>Alborz Mountains</b>	Volcanic and volcanoclastic rocks	Tertiary	Lead-zinc, copper ( $\pm$ gold), iron	Duna (Pb-Zn-Ag)
<b>Central Iran</b>	Horsts of Precambrian crystalline basement, Paleozoic platform sediments, Cambrian to Triassic cover rocks, and magmatic rocks	Precambrian, Paleozoic, Triassic, Tertiary	Copper ( $\pm$ nickel-cobalt), lead-zinc, iron ( $\pm$ manganese), gold, tungsten-copper ( $\pm$ tin)-gold, manganese, antimony	Deposits of Anarak area (e.g. Talmesi, Meskani)
<b>Eastern Iran</b>	Flysh-molasse sediments	Post-Cretaceous	Tungsten-gold, copper-gold, copper (+ lead-zinc), chromite-manganese	Qaleh Zari (Au-Cu-Bi)
<b>Khuzestan plain</b>	Covered by alluvia	Quaternary, (Neogene)	No metallic source but numerous oil fields	-----
<b>Kopet Dagh</b>	Sediments (mostly carbonates)	Mesozoic-Tertiary	Few metallic resources	-----
<b>Lut Block</b>	Old stable platform covered by thick Mesozoic sediments and Eocene volcanics	Mesozoic-Eocene	Copper, lead-zinc ( $\pm$ copper-antimony), Tungsten ( $\pm$ tin)-copper, iron	Seh Changi (Pb-Zn-Cu)
<b>Makran</b>	Colored melange + thick flysh-molasse sediments	Upper Cretaceous-Paleocene for melanges, post-Cretaceous for flysh sediments	Placer Ti, Cr-Mn, Cu-Zn, Cu-Au	Giravan (Cu)
<b>Orumieh-Dokhtar Zone</b>	Mainly volcanic (basalt to dacite), pyroclastic (i.g. tuff and ignimbrite) and plutonic (diorite to granite) rocks sporadically with numulitic limestone	Post-Upper Jurassic to Quaternary, Peak of magmatic activities: Eocene	Vast collection of deposits of different types of various metals including porphyry, VMS, MS, skarn, hydro- and epithermal deposits of Fe, Cu (-Mo-Au), Au, Pb, Zn, Mn	Veshnaveh (Cu), Sar Cheshmeh (Cu, Mo)
<b>Sanandaj-Sirjan Zone</b>	Mainly metamorphic rocks along with intrusive bodies	Phanerozoic (mainly Mesozoic)	Tungsten ( $\pm$ tin)-copper-gold, iron, iron-manganese, gold, lead-zinc, chromite	Deh Hosein (Cu-Sn-Au),
<b>Zagros fold belt</b>	Mainly fold thick sediments (carbonate rocks and carbonates) overlying a high-grade metamorphic Precambrian basement, salt diapirs in the south	Late-Precambrian-Early Cambrian, Carboniferous to late Cretaceous, Cretaceous to Recent	Rare metallic sources including Pb, Fe and chromite	Surmeh (Pb-Zn), Hormoz (Fe)
<b>Zagros thrust</b>	The same as Zagros fold belt plus ophiolite melanges	Mesozoic	Chromite	-----

**Table 2.1** The major Iranian geologic subdivisions and their metallic resources.

Some of the Paleozoic and Mesozoic rock successions in this zone are metamorphosed under low-and medium-grade greenschist conditions during Late Cretaceous times (Alavi 1994), although Middle to Late Triassic medium to high-grade greenschist metamorphism has been reported in some places as well (e.g. Sabzehi 1992).

## 2.3 Stratigraphy of the study area

The study area of Astaneh-Sarband is located in the northern part of the Sanandaj-Sirjan Zone, within the Khorramabad quadrangle, Markazi and Luristan provinces, west central Iran (Figure 2.2). The Khorramabad quadrangle covers 15,000 km<sup>2</sup> between latitudes 33° N to 34° N and longitudes 48°E to 49° 30' E. Much of the southeast and center of the quadrangle is covered by sedimentary rocks of the Zagros Mountains which normally lack metallic resources. The northeastern corner of the quadrangle hosts many intrusive bodies intruded into metamorphic rocks (the so-called Hamadan phyllite) of the Sanandaj-Sirjan Zone.

The study area consists mainly of Mesozoic schist, middle Jurassic to Paleogene intrusive rocks and their contact metamorphic aureoles and pegmatites (Figure 2.2). The oldest known exposed rocks are Precambrian in age while the youngest are the Paleogene intrusive bodies. In the following, major characteristics of the exposed rocks of the area are presented.

### *Precambrian*

The oldest rock units exposed in the area are Precambrian in age. Their outcrops are exposed to the south of the area, between Malmir and Tavandasht, and are separated from other units by faults. These rocks are predominantly composed of metarhyolite and amphibolite, together with marmorized dolomite. The colors of the Precambrian rocks, red rhyolites, white to light gray dolomite and dark amphibolite, as well as systematic fractures of rhyolite and amphibolite demarcate this unit among the surrounding rocks (Masoudi 1997).

### *Triassic*

The Triassic units are exposed in the southwest of the area and are mainly comprised of metavolcanics and tuff with other volcano-sedimentary (mainly sandstone) rocks near the base, followed by volcano-sedimentary rocks with some marble and meta-quartzite. Metavolcanics and tuffs are broadly of andesitic composition and have been regionally metamorphosed up to greenschist facies.

### *Jurassic*

The Jurassic series with its low topography occurs widely in the region. It is composed of an alternation of pelitic schist and metamorphosed graywacke sandstone layers of which the latter is dominant in the upper parts. This implies that the original rocks of Jurassic (mainly shale and sandstone) have experienced a low grade regional metamorphism (greenschist facies). However, in the lowermost parts, up to 10 meters of marble are exposed (Masoudi 1997). The Jurassic schist, phyllite and slate in the region are mostly black-gray to dark greenish gray in color. The original bedding planes of the original rocks are generally disturbed and the schistosity is mostly discordant to the bedding (Masoudi 1997). A rather large amount of quartz veins of different width and northwest-southeast trending cut the Jurassic series.

Because of the scarcity of the fossils in the above-mentioned rocks, the age determination of the rocks has been controversial. The presently agreed age is based on studies outside the Astaneh-Sarband region, mostly to the north and southeast. These studies considered botanic fossils as well as ammonites, orbitolina and gastropods in the surrounding areas (Bellon and Braud 1975; Emami 1981; Va,ezi Pour and Eghlimi 1984). Other studies suggested that some of the metamorphic rocks belong to upper Triassic-lower Jurassic or even older periods (Thiele et al. 1968; Razavi et al. 1983; Hajian 1977).

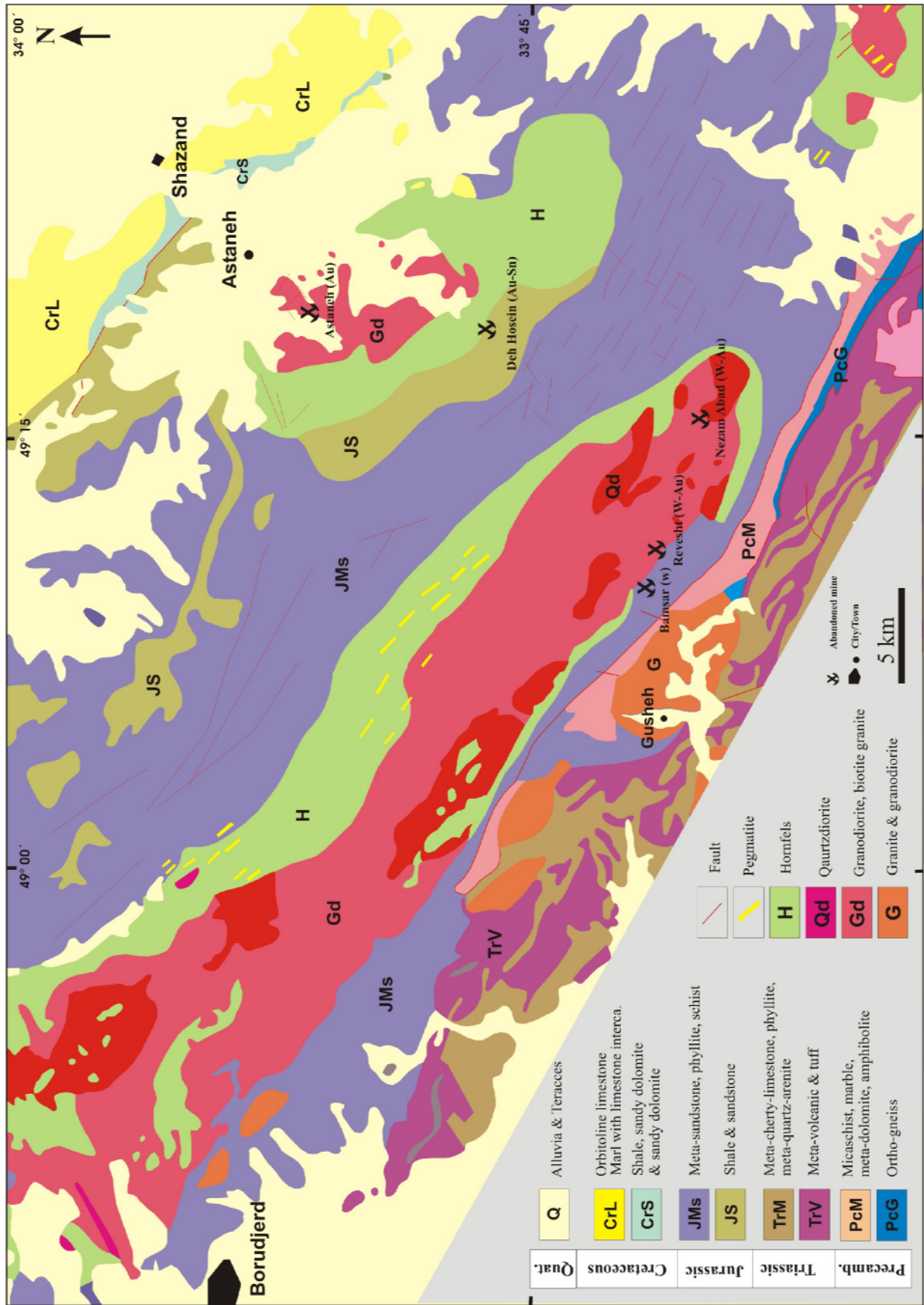


Figure 2.1 Simplified geological map of the Astaneh-Sarband-Borudjerd area. Modified after Soheili et al. 1992.

### ***Cretaceous***

Cretaceous rocks have formed a mountain range with northwest-southeast trend to the northeast of the region. According to Radfar (1987) these rocks have the following sequence (from the lowermost part to the uppermost): a) Sandy-conglomerate horizon, b) Volcanic and tuff horizon, c) Sandy dolomite and sandy limestone, d) Orbitolina limestone, e) Marl and limestone.

### ***Quaternary sediments***

Quaternary sediments in the area consist of young sediments and alluvia as well as fluvial alluvia. The young sediments are mostly a product of granite weathering. The fluvial alluvia are mainly composed of granitic arenites and are usually gold-bearing, in particular in the valleys of the rivers of Haj Ali Akbari and Parmeh (surrounding valleys of the Astaneh gold occurrence). After each rainfall in the area, the amount of gold in these sediments increases and gold panning is more rewarding.

## **2.4 Magmatism in the study area**

Magmatism in the study area is revealed by the exposure of huge amounts of intrusive rocks which with general trend of northwest-southeast are part of the west Iranian granitoids (Vali Zadeh 1992) in the Sanandaj-Sirjan zone. These intrusive rocks have intruded to Jurassic and partly Triassic formations of the area and have normally caused a contact metamorphism in their direct aureoles. Based on the geo-chronological studies carried out as part of this thesis, Masoudi (1997) and Farhadian (1991) the magmatism of the area has been continued from middle Jurassic to Paleogene. The majority of the plutonic rocks are granodiorites and granites and show typical calc-alkaline trends (Masoudi 1997). Such magmas are normally associated with subduction and collision zones. The alkalinity values (e.g. molar  $Al_2O_3/(Na_2O+K_2O-CaO)$ ) suggest a peraluminous composition for all the intrusives and imply their formation during collision (Masoudi 1997). The rocks of the area have been altered by extensive hydrothermal fluids, although the fluids have not been mineralogically fertile in many cases.

There are the three major intrusive bodies of Astaneh, Borudjerd and Tavandasht-Gousheh in the area (Figure 2.1), whose general characteristics, based on the current research and Masoudi's (1997), are described in the following:

### ***Astaneh intrusion***

The Astaneh intrusive body with general NW-SE trend and some 30 km<sup>2</sup> area is located south-southwest of Astaneh. Although biotite granite comprises the main rock type of the Astaneh intrusion, granodiorite, granite, quartz diorite and tourmaline granite are common as well. Abundant veins of aplite and quartz have intersected the above-mentioned rock types. There are different xenolite types of various sizes (up to 1m) in the Astaneh intrusion. These are usually round pieces of andalusite schist, hornfels and quartz diorite, granodiorite and diorite. The granodiorite of the Astaneh has been dated at 99 Ma (Masoudi 1997), while the Shirmazd granodiorite stock, which intruded the main body of intrusion in the north and hosts the gold mineralization, shows Eocene age ( $35.05 \pm 0.92$  Ma Rb/Sr age, and  $44 \pm 13$  Ma single zircon evaporation age, this study). The tourmaline granite exposed in the southern part of the intrusion dates to middle Jurassic ( $177 \pm 8$  Ma single zircon age, this study).

### ***Borujerd complex***

The large Borudjerd intrusive complex extends NW-SE-ward from Nezam Abad village to the southeast (Borudjerd in the Middle) to Nahavand town to the northwest. This complex contains a wide range of intrusions from granite to diorite, although granodiorite and quartz diorite are

the most common rock types. According to dating results (Rb/Sr), Masoudi (1997) has classified the rocks of this complex to two older and younger granites with Lower Cretaceous and Late Cretaceous-Early Paleocene age, respectively. Farhadian and Hasani Pak (1991) have dated the mineralized quartz diorite of Nezam Abad at 52 to 40 Ma (Lower-Mid Eocene). Ghaderi et al. (2004) suggest a 169-172 Ma age for the rocks of the Borudjerd complex, according to U-Pb zircon chronologic data.

### ***Tavandasht-Gousheh intrusions***

In the south of the Borudjerd complex in the area of Tavandasht-Gousheh there are three granite bodies which according to Soheili et al. (1992) and Masoudi (1997) show alkali granitic to granitic compositions, predominantly leucogranite. According to Masoudi (1997) all plutons of the area have both I-type and S-type characteristics, although the Borudjerd older granites are in most respect I-type.

The intrusive rocks of the area have caused thermal metamorphism in their surrounding Paleozoic and Mesozoic sediments – in the Astaneh and Borudjerd case the schists, phyllites and sandstones of Jurassic, in the Tavandasht-Gousheh case the surrounding meta-volcanic and meta-limestones/dolomites of Paleozoic and Triassic age.

Apart from intrusive bodies there is an extensive amount of pegmatites and quartz veins in the area which are related to magmatic activities. The quartz veins occur mainly in the Jurassic rocks around the intrusions and their general trend is NW-SE.

Pegmatites are abundant in the area and especially widespread in the northern part of the Borudjerd igneous complex aureole. Pegmatites occur generally as linear bodies or veins with general NW-SE trend. They are a few to hundred meters in length and up to tens of meters thick. Pegmatites are of simple mineralogy, characteristically composed of quartz, feldspar, muscovite with minor amounts of tourmaline, apatite, garnet, andalusite, xenotime and arsenopyrite. The arsenopyrite does not show high contents of gold (this study, see chapter 5).

Based on geochronologic studies (Masoudi 1997), the pegmatites belong to two generations: an older one, mainly intruded into hornfels (Early Cretaceous), and a younger ones are hosted by younger granites (Early Eocene). Only some of the older Pegmatite bodies are zoned.

## **2.5 Structure and tectonism**

The main structural features of the Astaneh-Sarband area are consistent with the Zagros and Sanandaj-Sirjan Zone NW-SE trend.

The Hercynian Orogeny (Late Paleozoic) is the oldest recognized movement in the area (Thiele et al. 1968) whose NE-trending traces have been recognized in the Precambrian formations of the southern part of the area (Masoudi 1997). Nevertheless, the Alpine Orogeny (Mid-Mesozoic to mid-Quaternary) is the main cause of formation of the rather simple tectonic elements of the area namely foliation, schistosity, lamination and faults. According to Masoudi (1997), the Alpine movement has occurred in two stages; Upper Jurassic and Lower Cretaceous, and Middle-Upper Cretaceous. The earlier phase of the movement in Upper Jurassic and Lower Cretaceous has caused the deformation and regional metamorphism in the area which has resulted in the development of an S1 schistosity in Jurassic and older rocks. This has been followed by the intrusion of older generations of granites and pegmatites in the area.

The second stage of the Alpine Orogeny has occurred in the Middle and Upper Cretaceous. This has caused a second S2 schistosity in Mesozoic rocks along with a deformation in Cretaceous rocks. This phase has been accompanied by a syntectonic intrusive activity



(Astaneh intrusion), followed by a post-tectonic intrusive activity (Shirmazd and Nezam Abad intrusion). A summary of the most important known events have presented in Table 2.1.

<i>Era (Period)</i>	<i>Sedimentation</i>	<i>Metamorphism</i>	<i>Magmatism</i>	<i>Tectonic movement</i>
<i>Quaternary</i>	Alluvium			
~~~~~				
<i>Paleogene</i>			Post tectonic granite	(Laramide, Pyrenean)
<i>Cretaceous</i>	Marl & shale Orbitolina limestone, shale, sandy dolomite & limestone	(S2)  Hornfels (S1) phyllite	Syntectonic granite (Astaneh)  Granite & pegmatite	
<i>Jurassic</i>	Sandstone & shale		Tourmaline granite	(Late Cimmerian)
<i>Triassic</i>	Limestone & phyllite		Volcanic & tuff	?
<i>Paleozoic</i>		Metamorphism of Pre-Cambrian units up to amphibolite facies		Hercynian Orogenic movement
~~~~~				
<i>Pre-Cambrian</i>	Clastic & carbonate sediments		Basalt & rhyolite	

**Table 2.1** List and chronology of geological events in the study area (modified after Masoudi 1997).

## *Chapter 3*

# **Petrography, mineralogy and geochemistry of the Deh Hosein occurrence**

The newly discovered Deh Hosein occurrence shows high contents of gold, copper and tin. This chapter introduces the Deh Hosein prospect based on surface mapping and sampling along with extensive petrographic observations, geochemical analyses and mineralogical investigations.

### **3.1 Introduction**

The Deh Hosein occurrence is located 13 km south of the town of Astaneh and north, northeast of the village Deh Hosein ( $33^{\circ} 45' - 33^{\circ} 47' \text{ N}$ ,  $49^{\circ} 17' - 49^{\circ} 20' \text{ W}$ ), in west central Iran (Figure 3.1). The mineralization is mainly hosted by Mesozoic schists and phyllites along the southern contact of the Astaneh intrusive body. The Deh Hosein occurrence was worked in antiquity (see chapter 7) and therefore most of the rich mineralized sections and veins at the surface have been removed by ancient miners. Consequently, our information of shape, form and type of mineralization is based on the shape of ancient diggings, and the ore found in ancient waste dumps and the rather weak mineralization left by ancient miners at the selvage of the veins. The description of ancient diggings and ancient mining traces is presented in chapter 7.

A suite of 50 representative ore and rock samples (each sample approx. 1 kg) was collected from the occurrence by the author in the course of 2001 to 2003. The results of geochemical, mineralogical and petrographic investigations on the samples are presented in the current chapter and chapter 6.

### **3.2 Methods**

42 polished thin sections and 12 polished sections were prepared from ore and rock samples from ancient diggings, ancient waste dumps and outcrops (including unaltered host rocks, mineralized and altered zones) at Deh Hosein. Descriptions of the hand specimens from which

these sections were prepared along with analytical results are given in Table 3.1. Petrographic and mineralogical examinations were carried out at the Department of Mineralogy of Freiberg University of Mining and Technology, Germany.

The petrographic examination of the thin sections and polished thin sections was by optical microscopy using reflected and transmitted light. The compositions of selected minerals were determined on carbon-coated polished sections using a JEOL electron probe microanalyser (JXA-8900RL) in qualitative, quantitative and X-ray scanning modes. The instrument is equipped with three wavelength dispersive spectrometers with sets of LDE1/TAP and PET/LIF analyzing crystals. Standards used for instrument calibration included native gold, iodargyrite for silver, galena for lead and sulfur, sphalerite for zinc, marcasite for iron, cinnabar for mercury, a synthetic GaAs (gallium arsenide) compound for arsenic and  $Sb_2Te_3$  for antimony and tellurium. Counting times for major elements were 20 to 50 seconds using an accelerating voltage of 20 kV and a beam current of  $20 \times 10^{-8}$  A. Analyses for gold was made with a counting time of 300 seconds on peak and background using an accelerating voltage of 40 kV and a beam current of  $4 \times 10^{-8}$  A, yielding a detection limit of about 40 ppm. Atomic concentrations of elements and the number of atoms in the mineral formula were used to determine mineral compositions.

43 samples, mostly studied by electron microprobe analyses, were analyzed for gold and other trace elements by neutron activation at the Act Labs, Canada (Table 3.1).

### 3.3 Geology of the prospect and petrography of the host rocks

The mineralization at Deh Hosein is located in Jurassic meta-sedimentary rocks, which have experienced a greenschist facies metamorphic overprint and were intruded by the Astaneh complex in the north (Figure 3.1). The mineralization continues in the southern part of the Astaneh intrusion at its contact with the metamorphic country rocks. The meta-sedimentary rocks consist of alternating meta-sandstone, phyllite, schist, spotted slate and hornfels at the contact with the Astaneh intrusion. Although the mineralization is not restricted to any specific rock unit, it shows an obvious connection with intercalations of meta-sandstone present in phyllite, schist and spotted slate. In the following, a brief description of the major rock units of the area, based on field and petrographic observations, is given.

*Meta-Sandstone* is the most mineralized unit of the area. It has its greatest expansion in the eastern and northern part of the study area, in Luzdar Mount (Figure 3.1). In addition, intercalations of meta-sandstone which reach up to 30 m width and 1 km length and with a general NW-SE trend are present in the other metamorphic rocks of the area. In fact the mineralization in the other rock units is usually accompanied by meta-sandstone intercalations (Figure 3.3c). To the east, close to the contact of the Astaneh complex, there is no sharp contact between the meta-sandstone and the hornfels units. The meta-sandstone, which in some cases shows laminate structure (N110-130, 50S), consists of up to 80% 1000 $\mu$ m quartz, 20% micaceous minerals, and <7% accessory and opaque minerals, mainly monazite, zircon, apatite, and pyrite (Figure 3.2a). In some places, this rock can also be named meta-greywacke. Especially close to the mineralized areas, the meta-sandstone contains quartz veinlets with granoblastic texture and veinlets of oxidized sulfides. In the northeastern part of the prospect (on Luzdar Mount, out of the extensive zone of mineralization and ancient mining) this unit contains patches of rich copper mineralization which is seen as extensive impregnation of malachite in the rock (sample 51, Table 3.1).

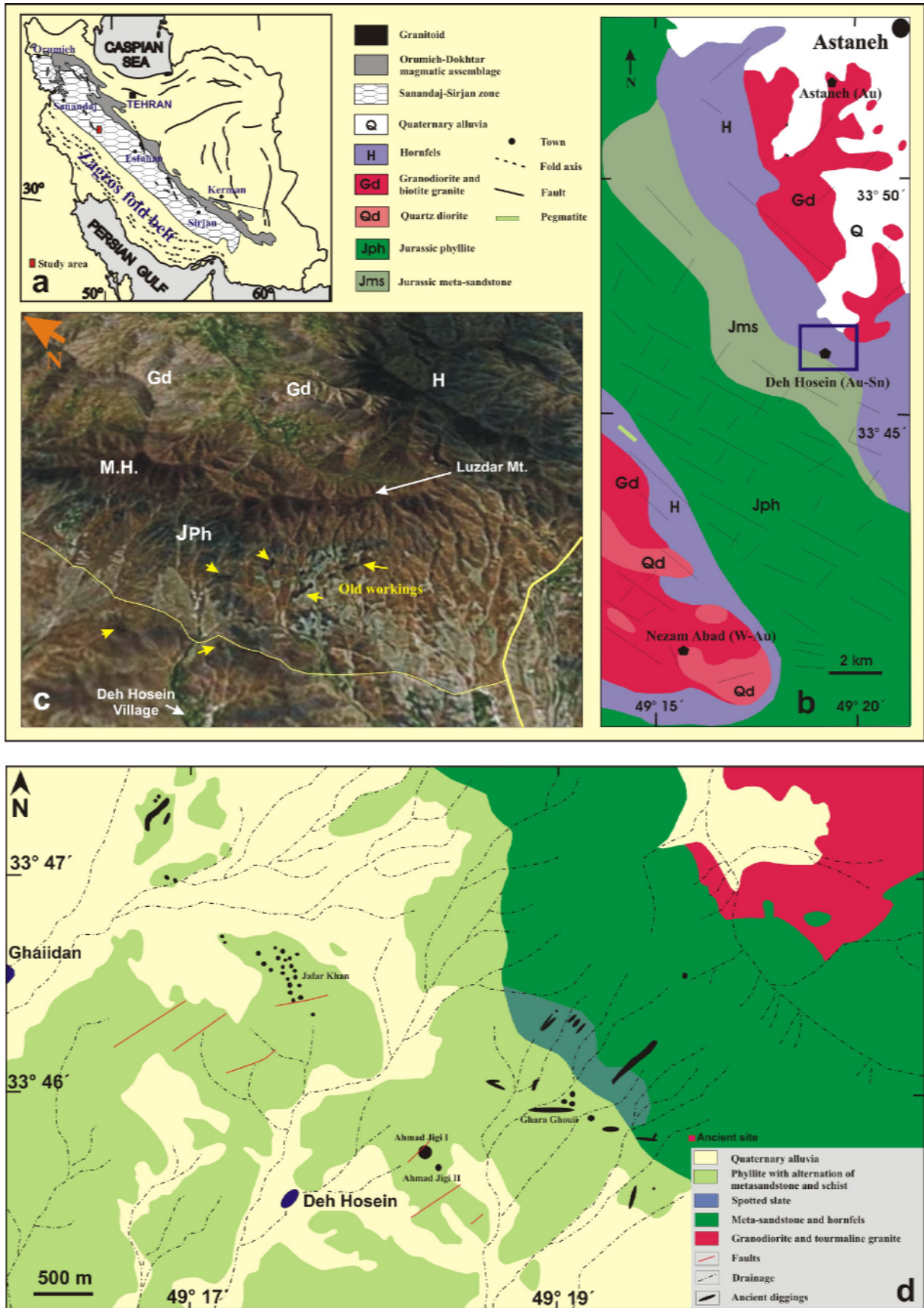


**Figure 3.1** a) Location of the study area in Iran, b) General geology of the Astaneh-Sarband area, c) Satellite map of the Deh Hosein occurrence, d) Geology of the Deh Hosein occurrence (modified after Ojaghi et al. 2001).

An alternation of *schist, phyllite and spotted slate* cover a vast portion of the area, especially to the east of the Astaneh intrusion. Because of their alternating nature and their similar appearance, it is not always easy to sort out these rocks in the field, although the spotted slate is distinctive due to its darker color. Under the microscope the rocks are recognizable by their grain sizes (schist: >1mm, phyllite: 0.1-1mm, and slate <0.1mm). Round to ellipsoid spots of fine grained minerals are visible in all of the above mentioned rocks, although they are considerably more abundant in the spotted slate.

The spotted slate has a fine lamination with NW-SE trend and 45-80 SW dip. It contains numerous round to ellipsoid spots (<200µm) which are composed of accumulation of fine grains of andalusite and cordierite (Figure 3.2b). The spots are sporadically surrounded by dark rims which are of iron oxides or fine grained opaque minerals. The spotted slate is comprised of up to 60% quartz, 30% micaceous minerals, up to 20% spots and less than 7% accessory minerals, mainly monazite, zircon, apatite, and pyrite. The micaceous minerals of the rock have been highly altered into sericite, especially at the periphery of mineralized areas.

Schist and phyllite indicate a general NW-SE (N120-140) schistosity with 50-80SW dip and their colors differ from light gray to dark green. It seems that the schistosity and primary layering of these rocks are of the same trend. Fine foliation textures are frequently observed under the microscope especially in phyllite (Figure 3.2c).

The *hornfels* unit covers the western and southern rim of the Astaneh intrusion and normally comprises higher elevations in the area. In the study area, hornfels does not show a sharp contact with the meta-sandstone unit. In hand specimen it appears as a dark hard rock which in some cases still shows the primary stratification. There are a few ancient workings (mineralization) in this unit in which the traces of mineralization can rarely be seen. Patches of highly altered granitoids are seen in the hornfels close to its contact with Astaneh intrusion.

*Granodiorite and tourmaline granite* are exposed in the northeastern part of the Luzdar Mount and Darreh Gapeh valley. The tourmaline granite is characterized by numerous round and ellipsoidal grains of tourmaline which reach up to 10cm diameter.

The granodiorite shows granular texture and consists of quartz (25-35%), plagioclase (35-40%), orthoclase (about 20-25%), and biotite (15-20%). Zircon, apatite, rutile, esphene and opaque minerals (including chalcopyrite, pyrite and Fe-oxides) are among accessory minerals. Plagioclase has been altered into sericite and sporadically chlorite and clay minerals. Both granite and tourmaline granite host mineralized quartz veins and veinlets. Close to mineralized veins silicification and tourmalinization are visible in the rocks. Scattered grains of sulfide minerals have been observed in the granodiorite.

### 3.4 Alteration

Hydrothermal alteration at Deh Hosein is not extensive and is mainly vein- and fracture-controlled. It extends as far as some meters beyond the mineralized zones. Four major types of alterations have been observed at Deh Hosein which are associated with mineralization; sericitization, silicification, tourmalinization and monazite alteration. Except the monazite alteration which has only been observed in meta-sedimentary rocks, the other alterations can be seen in both meta-sedimentary and granitoid host rocks. There has also been a late oxidation and acid leaching event.

*Sericitization* is the most widespread alteration at Deh Hosein (Figure 3.2d and e). The fine-grained micaceous minerals have been largely replaced by fine-grained white mica (sericite). Also small patches of sericite accumulations are visible beside the veins and veinlets. This alteration implies low pH (acidic) conditions of the mineralized fluid (Faulkner 1992).



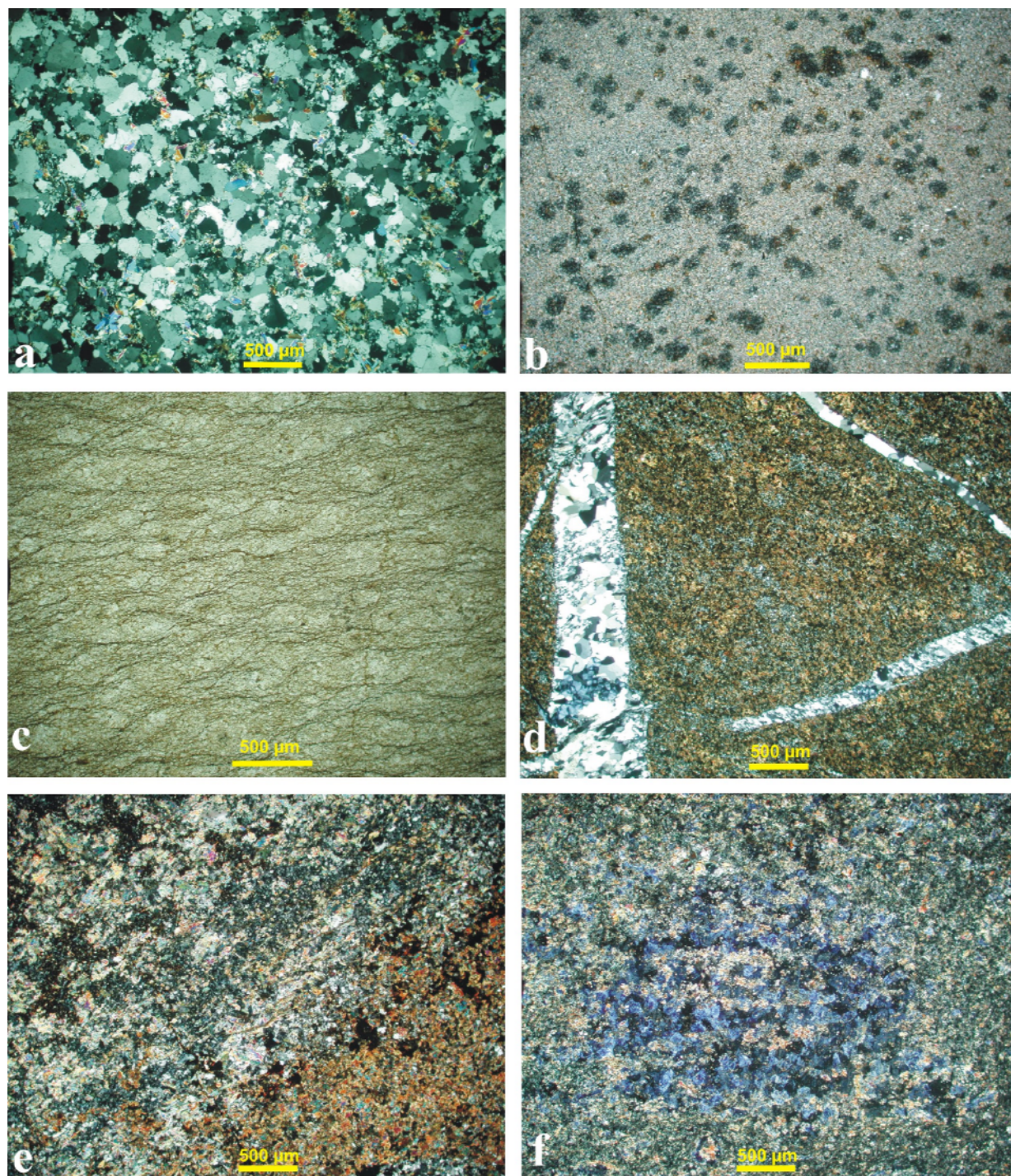


**Figure 3.2** a) Photograph of meta-sandstone, b) Spotted slate, c) Phyllite with foliation, d) Altered phyllite with sericitic alteration and quartz veinlets, e) strongly sericitized rock (left) beside a partly oxidized sulfide veinlet (right), f) Tourmaline (blue) and sericite (pink) alteration in phyllite.

The intensity of *silicification* varies from weak to the intensive replacement of the original rock by quartz. The rocks are normally silicified along faults and fractures. Massive cryptocrystalline quartz and hydrothermal quartz with euhedral crystals (1 to 500µm) are the

main components of siliceous alteration and are visible in most of the thin sections from silicified zones of the host rocks. Veinlets of quartz are common features along with silicification (Figure 3.2 d).

*Tourmalinization* in the host rocks occurs as small patches and veinlets and is mainly associated with sericitic alteration (Figure 3.2f). Some of the accessory minerals in the meta-sedimentary rocks at Deh Hosein are found in association with hydrothermal alteration and mineralization. *Monazite* and *xenotime* are found in altered metasandstone, phyllite, schist and spotted slate. Monazite is seen as disseminated grains (up to 100  $\mu\text{m}$ ) in the host rocks, although its abundance rises greatly in the vein selvages. Xenotime is much less abundant than monazite.

Weak *argillization* has been observed in the granodiorite which is due to replacement of plagioclase and feldspar by clay minerals. Oxidation of pyrite, chalcopyrite and other sulfide minerals of the quartz-sulfide veins and veinlets has produced gossan patches on the surface.

### 3.5 Mineralization

Mineralization at Deh Hosein has occurred in the form of quartz, quartz-sulfide and quartz-gossan veins and veinlets in an area of 4.5 x 6 km<sup>2</sup>. The area has a moderate topography and is covered with many farm fields that in some cases have covered the ancient diggings (Figure 3.3 a). The mineralized veins which are partly sheeted in structure (in different scales, Figure 3.3b) are fracture-controlled and show mainly NW-SE, NE-SW and sporadically E-W trends. These trends correspond with the trends of the main faults and other structural features in the area. The veins are subvertical and high angle, up to 1.5 m wide and up to 500m long. In addition to quartz and quartz-sulfide veins, the mineralization is present in the form of disseminations and impregnations, especially in the vein selvages. Quartz veins hosting the sulfide mineralization is the dominant ore-related feature of mineralization. Although the mineralization is mainly hosted by meta-sedimentary rocks, but it continues into the contact granite and tourmaline-granite where it is much less intense and occurs as small veins with disseminated selvages.

Some 35 types of ore minerals were detected at Deh Hosein through this study. The mineralization on the surface has been highly altered by weathering and many sulfide minerals have been thoroughly oxidized. Sulfide content in the ore is generally less than two volume percent, although it is higher in arsenopyrite veins. In the following, the description of the detected minerals is given.

*Arsenopyrite* is the most abundant sulfide at Deh Hosein. It is present almost in all small veins, veinlets and fracture fillings but it is most abundant in the localities Ahmad Jigi I and II, where it occurs as small massive veins (Figure 3.3h). Arsenopyrite occurs as massive patches in the arsenopyrite veins (Ahmad Jigi I and II) and as single grains, veinlets and disseminations in quartz, quartz-sulfide, and gossan veins and vein selvages. The grains are euhedral (rhombic) to subhedral crystals which are from 5 $\mu\text{m}$  to 1000 $\mu\text{m}$  in size. Massive arsenopyrite contains inclusions of pyrite, chalcopyrite, bismuth, bismuthinite and bismuth oxides (Figure 3.4a). No gold grains have been observed in the arsenopyrite. According to electron microprobe analyses, the arsenopyrite typically contains up to 1900 ppm gold, 1% bismuth, 1.61% antimony and 0.5% selenium. The arsenopyrite at Deh Hosein is directly associated with gold mineralization and many of the other gold bearing ore minerals are commonly associated with it. The arsenopyrite is altered into scorodite and Fe-oxide minerals during weathering (Figure 3.4b). In the case of massive patches it has a cataclastic texture.



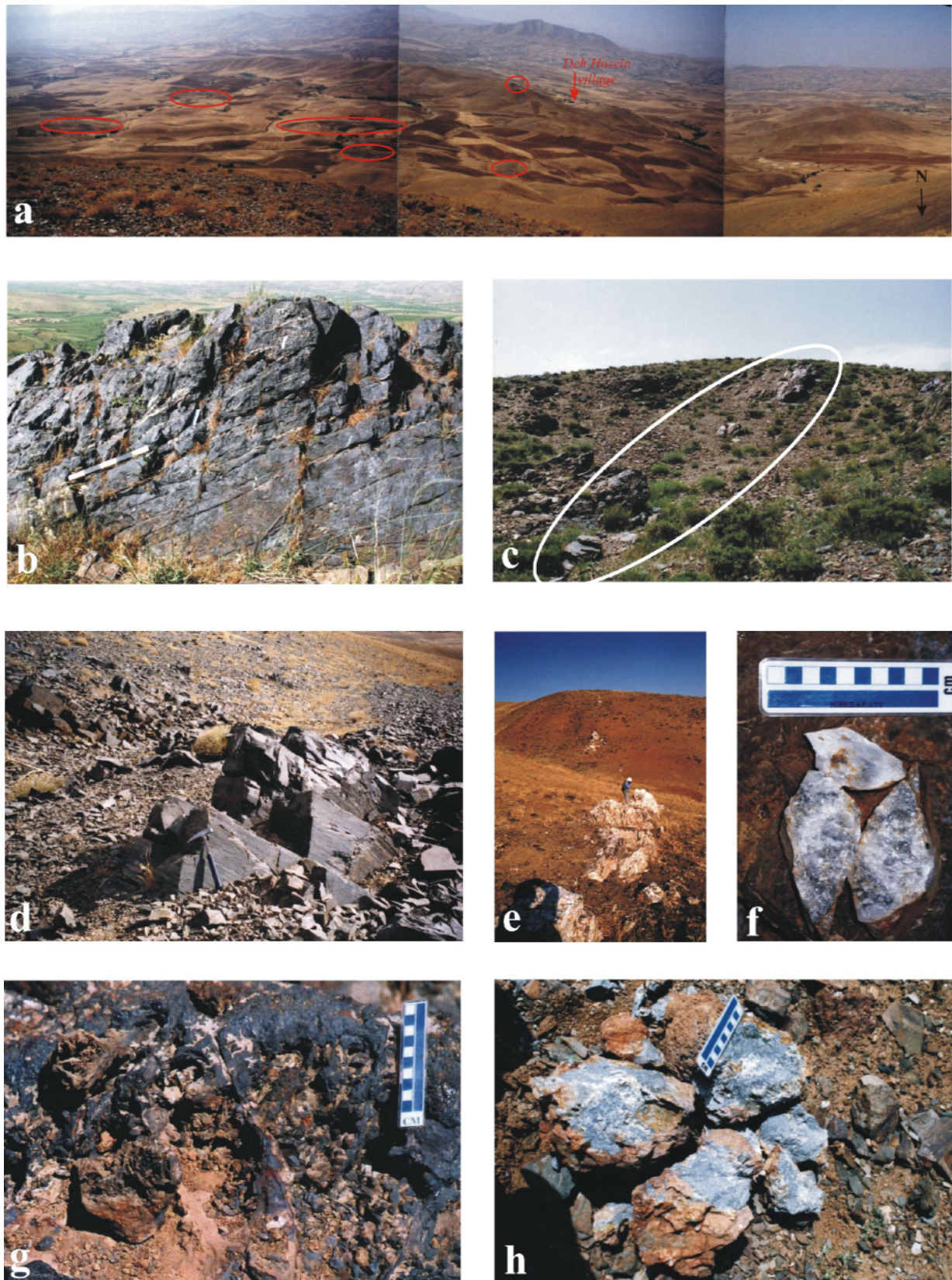


**Figure 3.3** a) An overview of the eastern part of the mineralization area, some of the ancient workings have been marked by red, b) Sheeted quartz veins in meta-sandstone, scale 50 cm, c) A mineralized meta-sandstone vein in phyllite which has been worked by ancient miners, d) Outcrop of hornfels at the contact with tourmaline granite, e) A weakly mineralized quartz vein in the eastern part of the study area, f) Pieces of a quartz vein with arsenopyrite and kobellite, g) Part of a gossan vein at the Jafar Khan locality, h) Part of an arsenopyrite vein at Ahmad Jigi II.



*Pyrite* is the most widespread and one of the most abundant sulfide minerals at Deh Hosein. It occurs as euhedral to subhedral crystals up to 500 $\mu\text{m}$  in size which in many cases are altered into Fe-oxides (Figure 3.4c, d, and e). Pyrite is visible in almost all mineralized zones as scattered and single crystals. Inclusions of chalcopyrite, galena and minute grains of stannite (<5 $\mu\text{m}$ ) have been observed in pyrite. It also occurs as single grains in quartz. Although most of the pyrite is primary, in some cases it is observed as veinlets which intersect the other minerals and host rocks. In one case, inclusions of pyrite have been found in apatite. Pyrite-I has formed prior to chalcopyrite.

*Chalcopyrite* is widespread in the mineralization. It occurs as euhedral to pseudomorphic crystals as well as small veinlets (Figure 3.4f). The massive chalcopyrite has a cataclastic texture. The crystals are up to 500 $\mu\text{m}$  in size and have been replaced by covellite, malachite and Fe-oxides. Inclusions of chalcopyrite are observed in pyrite and sphalerite. Chalcopyrite occurs in close association with pyrite and its veinlets intersect pyrite.

*Gold* in its native form is rare in the occurrence. Examination of 42 thin polished and 12 polished sections of the ore samples by means of high-resolution optical microscopy and electron microprobe failed to reveal any native gold with the exception of one case. The only micron-size (about 5  $\mu\text{m}$ ) gold grain was observed in a quartz vein in the granodiorite which is located at the northern border of the main mineralization (Figure 3.6a). Qualitative microprobe analysis of this gold grain showed no indication of other metals commonly found with gold e.g. Ag, Te, and Se.

The scarcity of visible gold, coupled with the high concentrations of gold in the mineralized samples at Deh Hosein, suggests the occurrence of “invisible gold”. The term “invisible” arises when conventional microscopy cannot distinguish between gold chemically bound in the mineral and submicroscopic inclusions (Cabri et al. 2000). This invisible gold owes its origin either to submicroscopic metallic particles or to incorporation as “chemically bound” gold (Maddox et al 1998).

*Marcasite* occurs in minor quantities as euhedral to subhedral grains which are up to 400 $\mu\text{m}$  in size (Figure 3.4g). It has been observed in diggings at the east and center of the prospect (samples 1A, 70). In some cases it has been totally replaced by Fe-oxides. Inclusions of Bi-oxides up to 30 $\mu\text{m}$  long are present in the marcasite. Marcasite is in a good association with chalcopyrite and pyrite and its occurrence precedes the chalcopyrite. According to Oberthur et al. (1997), marcasite is a primary constituent of ores precipitated during the waning stages of hydrothermal mineralization.

*Pyrrhotite* occurs as a minor mineral (Figure 3.4h). Only at locality Ghara Ghouii it has been observed as rather big euhedral to subhedral grains (up to 400 microns) which are altered into Fe-oxides and only tiny grains of them have remained.

*Löllingite* is a very rare and minute mineral which has only been detected in the samples from Ahmad Jigi I by means of microprobe analyses. It occurs in close association with arsenopyrite and bismuth-bearing minerals.

*Cassiterite* is a rather abundant ore mineral and has been observed in both meta-sedimentary and granitic host rocks. It has been observed in quartz-sulfide (gossan) veins at Ghara Ghouii, Ahmad Jigi II, and at the east and center of the occurrence (samples 7A, 14, 40, 42, 43, 47, 65, and 68, Table 3.1). Cassiterite occurs in the form of grains up to 250 $\mu\text{m}$  in size and is in association with oxidized copper minerals and gossan (Figure 3.5a). No zonation has been observed in the cassiterite.

*Ferberite* ( $\text{FeWO}_4$ ) is rare but has been seen in both granitic and metamorphic host rocks, at Ghara Ghouii and at the northern granodiorite of the occurrence (samples 65 and 47). It shows a close association with cassiterite and copper minerals and occurs as up to 1000 $\mu\text{m}$  grains (Figure 3.5b).

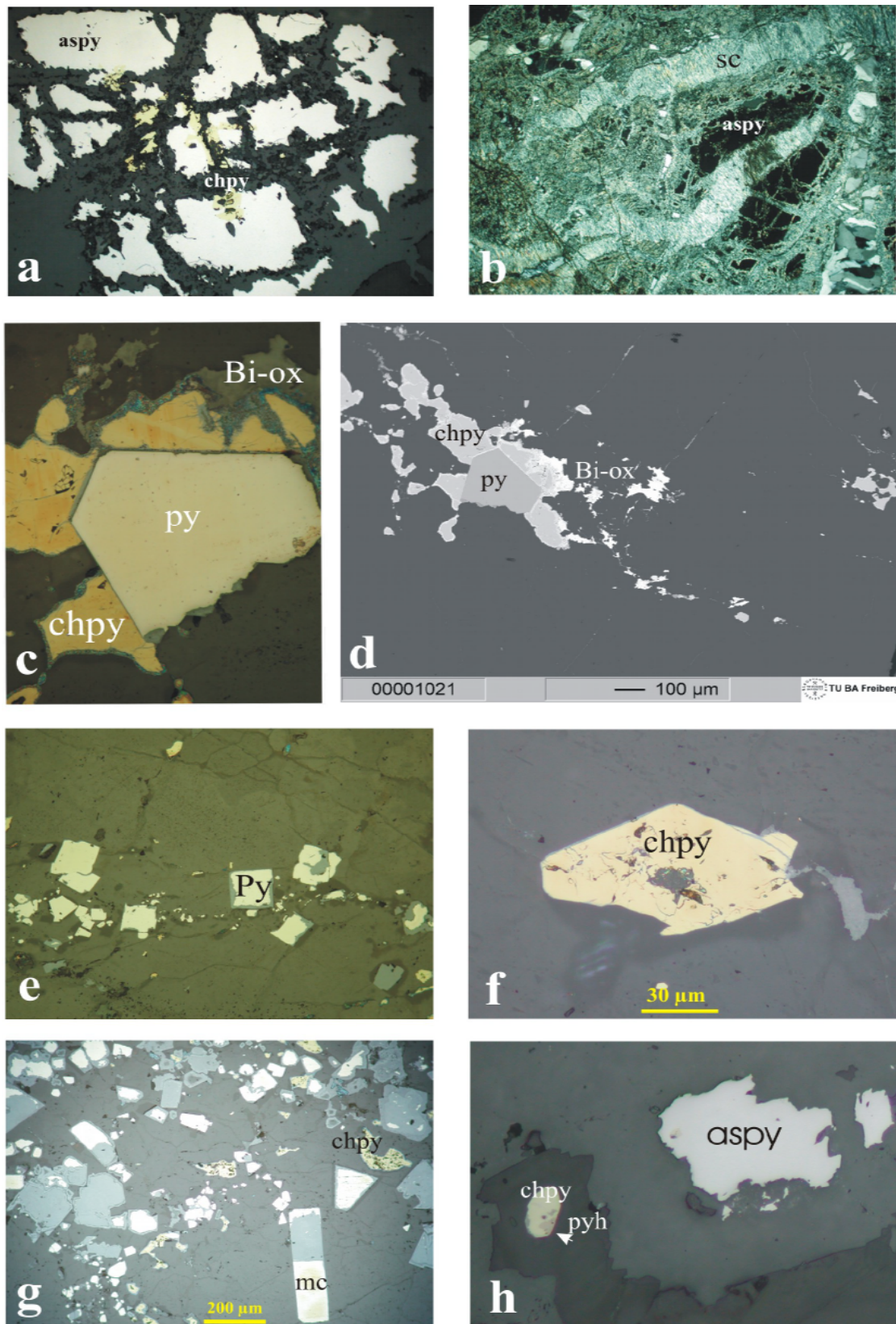


**Figure 3.4** a) Arsenopyrite with inclusions of chalcopyrite, b) Arsenopyrite partly altered into scorodite, c) An assemblage of chalcopyrite, pyrite and bismuth oxides, d) Back scattered electron micrograph of the photo (c), e) Euhedral pyrite grains in quartz, f) Euhedral chalcopyrite grain in quartz, g) Euhedral marcasite with chalcopyrite in quartz, h) An assemblage of arsenopyrite, chalcopyrite and pyrrhotite.

*Native copper* is rare and has been only observed at Ahmad Jigi I, where it is also visible in hand specimen size. It occurs as small veinlets which have partly been replaced by cuprite and tenorite (Figure 3.5c).

*Galena* has been mainly observed in quartz and gossan veins at Ghara Ghouii and the diggings at the east and center of the prospect (samples 1B, 2, 7B, and 9). It occurs as small patches in quartz or as subhedral to anhedral grains (up to 350 $\mu$ m). It is in most cases partly or completely replaced by cerussite. Minute grains of galena are present as inclusions in pyrite, arsenopyrite and sphalerite. Galena is closely associated with sphalerite but no close association has been seen between galena and Pb-sulfosalts.

*Sphalerite* is not very abundant at Deh Hosein and is closely associated with galena. It has been observed as up to 100 $\mu$ m grains in quartz and gossan veins at Ghara Ghouii and northern and eastern part of the occurrence (samples 43, 58, 60, and 64, Figure 3.5e).

*Pyrolusite* ( $MnO_2$ ) is observed in gossan-quartz veins at Cheshmeh Jafar Khan and Ghara Ghouii Localities, where it occurs as patches in close association with goethite, secondary hematite and limonite. It contains small inclusions of native bismuth at Ghara Ghouii (Figure 3.5d).

*Monazite* ( $CePO_4$ ) is a widespread and abundant mineral closely associated with mineralized and altered zones. It occurs as disseminated subhedral to euhedral grains in the mineralized selvages of the veins and also in gossan and Fe- and Cu-As-oxides, where it comprises up to 7 volume percent of the sections (Figure 3.5f). The general size of the grains is 5 $\mu$ m but they can reach up to 100 $\mu$ m. Schandl and Gorton (2004) have reported that hydrothermal (secondary) monazites that crystallize from aqueous fluids occur generally in clusters consisting of 5 to 20 (or more) grains in a small area while primary monazite is more sparsely distributed. Euhedral to anhedral grains occasionally intergrown with sulfides and oxides are another criterion to distinguish hydrothermal monazite from the primary ones. Close association of monazite with the mineralization at Deh Hosein, its subhedral to euhedral form and its abundance match the characteristics of hydrothermal monazite described by Schandl and Gorton (2004) and attest that this monazite has a hydrothermal source.

*Xenotim* ( $YPO_4$ ) is not as abundant as monazite, but it occurs together with it.

*Kobellite* ( $Pb_{22}Cu_4(Bi, Sb)_{30}S_{69}$ ) is rare and closely associated with quartz, arsenopyrite, sulphotsumoite, and sztrokayite. Kobellite has been observed as a 1000 $\mu$ m crystal in a quartz vein at Ahmad Jigi II (Figure 3.5g). It is partly altered to oxide minerals from its rims. Since it has occurred as a single mineral floating in quartz, its exact association with the other minerals is not clear.

*Krupkaite* ( $PbCuBi_3S_6$ ) is also rare and associated with pyrite and chalcopyrite. It has been observed at a digging east of the prospect (sample 1A) as a 250 $\mu$ m lamellar subhedral grain beside pyrite and chalcopyrite in quartz (Figure 3.5h). It is replacing by oxide minerals from its rims.

*Sulphotsumoite* ( $Bi_3Te_2S$ ), and *Szrokayite* ( $Bi_3TeS_2$ ) have both been observed as single and rather small grains (100 $\mu$ m) at Ahmad Jigi II together with kobellite in a quartz vein.

*Bismuth minerals* occur as native bismuth, bismuthinite ( $Bi_2S_3$ ), bismite ( $Bi_2O_3$ ), arsenobismite ( $Bi_2(AsO_4)(OH)_3$ ), rooseveltite ( $BiAsO_4$ ), ingodite ( $Bi(S,Te)$ ), and some Bi-As- and Bi-oxides. These minerals are in close association with arsenopyrite and bismuth-bearing sulfosalts and have been observed at Ahmad Jigi I and II and a digging at the east of the prospect (sample 1A). Bismuth minerals and especially native bismuth occur as numerous 1-150 $\mu$ m inclusions in arsenopyrite and are closely associated with the increase in gold content (Figures 3.6c and d). Bismite has been observed as a rim around chalcopyrite grains at a digging at the east of the prospect (sample 1A). Native bismuth and bismite occur also as individual grains in quartz veins (Figure 3.6d).



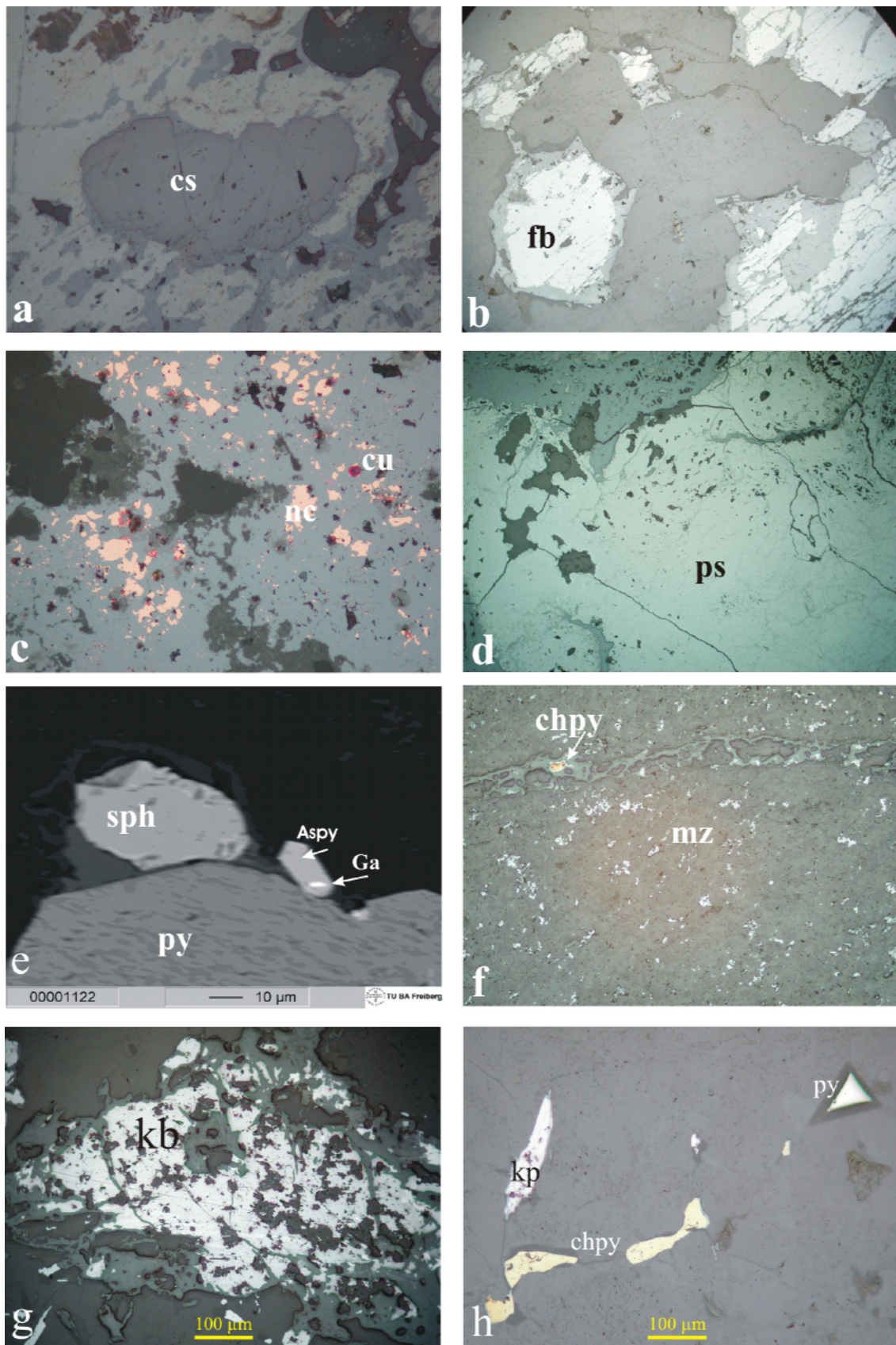


**Figure 3.5** a) Cassiterite in Fe-oxides, b) Ferberite in quartz and Fe-oxide, c) Native copper converting into cuprite and tenorite, d) Massive pyrolusite, e) Back-scattered electron micrograph of an assemblage of pyrite, sphalerite, euhedral arsenopyrite with inclusions of galena in arsenopyrite, f) Disseminated monazite around an altered veinlet of chalcopyrite, g) Kobellite grain in quartz, h) Krupkaite, chalcopyrite and pyrite in quartz.

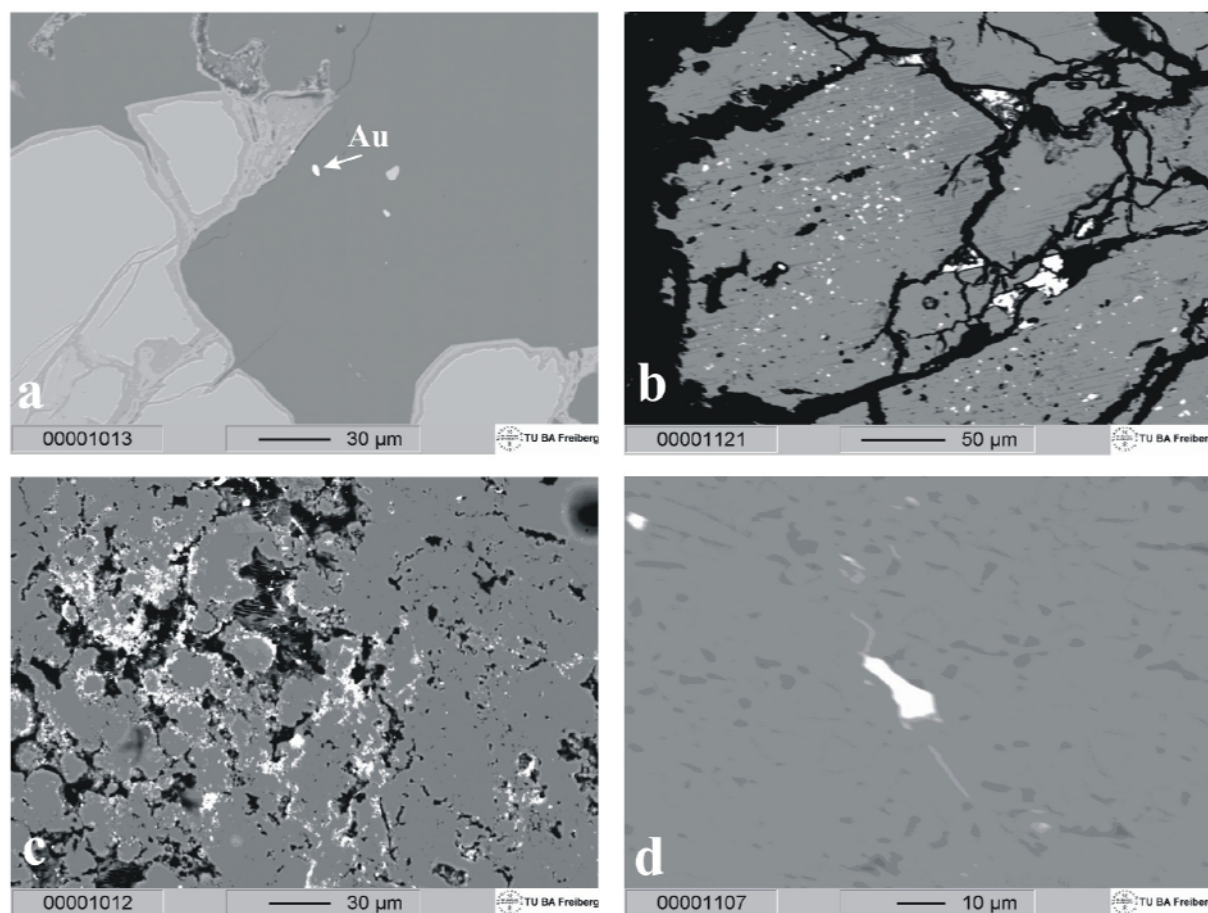


**Figure 3.6** Back scattered electron micrographs of **a)** The only observed gold grain in quartz, **b)** Inclusions of native bismuth in arsenopyrite, **c)** Bismuth oxides (light) in arsenopyrite, **d)** Native bismuth grain in quartz-mica.

*Rutile* and *apatite* are present as single small grains (<100μm) in the host rocks and the mineralized sections of the area.

Some other minerals which are present in minor amounts or as alteration products are listed below: Anglesite, beaverite  $[\text{PbCu}^{++}(\text{Fe}^{+++}, \text{Al})_2(\text{SO}_4)_2(\text{OH})_6]$ , plumbojarosite  $[\text{PbFe}^{+++}_6(\text{SO}_4)_4(\text{OH})_{12}]$ , native sulfur, delafossite, malachite, bornite, covellite, ilmenite, limonite, goethite, cerussite, scorodite, stannite, cuprite, and tenorite.

Microprobe investigations also determined some rare compositions of Fe-Cu-sulfate, Sb-Pb-sulfide, Mn-Fe-Pb-Zn and Ti-Fe-W-oxide from Ghara Ghouii and the mineralized meta-sandstone of Luzdar Mount which proved impossible to attribute a mineral name to them.

### 3.6 Paragenetic sequence

Several characteristics of the Deh Hosein prospect make it difficult to deduce the real paragenetic sequence; extensive ancient mining activities which have exploited almost all rich mineralization on the surface and subsurface, limited subsurface information and sparse mineralization in the remnant inhibit conventional paragenetic interpretation.

It is difficult to sort out separate events at a given locality into a definitive time sequence and even more difficult to correlate events between different localities in the ore deposit, because so many of the alteration processes were intermittent and overlapping. Therefore, it is only

possible to establish an overall paragenetic sequence. The main features are described in the following:

#### Early hydrothermal assemblage

This assemblage is characterized by very low sulfur content and is comprised of quartz, sericite, tourmaline, and monazite. It seems that at first very low-mineralized veins of quartz were accompanied with sericite, tourmaline and monazite alteration. This phase contains no gold in its minerals.

#### Intermediate hydrothermal assemblage

In this assemblage the metallic ions have been introduced into the pioneer hydrothermal fluids under a low fugacity of sulfur. Cassiterite, ferberite, pyrolusite and then native metals (bismuth and copper) were probably the first minerals of the assemblage. With the introduction of some sulfur to the system the early sulfide minerals including arsenopyrite have accompanied the above mentioned minerals. The deposition of gold, which especially can be seen in native bismuth grains, has started in this stage.

#### Main hydrothermal assemblage

This assemblage which has occurred after the intermediate assemblage is marked by increase of the sulfur content and consequent precipitation of a wide range of sulfides and sulfosalts along with continuation of silicification, tourmalinization and sericitization. Petrographic and ore microscopic data suggest that most of hydrothermal pyrite, chalcopyrite, arsenopyrite, sulfosalts and associated minerals, were produced during this main stage.

In this assemblage at first arsenopyrite, pyrrhotite, pyrite and sulfosalts were precipitated. With the increase of sulfur fugacity, the copper absorbed the main amount of sulfur and formed chalcopyrite. At the same time, the ions of Fe, Pb, and Zn have absorbed the rest of sulfur and formed primary galena and sphalerite in lesser amounts. This phase has produced the main amount of gold in the mineralization which can mainly be traced in arsenopyrite.

#### Weathering assemblage

Oxidation of sulfide minerals including pyrite, chalcopyrite, and arsenopyrite formed oxides of iron and arsenic which have created gossan patches on top of quartz-sulfide and sulfide veins and veinlets.

### **3.7 Metal associations and distribution at Deh Hosein**

43 samples were analyzed by NAA at Actlabs Canada for gold and other trace elements by the programs Au+48 and Au+34. 11 ore, 7 gossan, 4 mineralized host rock (impregnated and disseminated), 9 host rock and 12 quartz vein samples were parts of the selection of samples (Table 3.1).

The analyses revealed that gold (up to 13.3ppm), tin (up to 6.72%), copper (up to 10%), and arsenic (up to 23.4%) have the highest concentrations in the sulfide ore and gossan samples. Lead (less than 3.7%), zinc (up to 0.75%), bismuth (up to 1805ppm), tungsten (up to 2420ppm) and antimony (up to 1530ppm) indicate also rather high anomalies. In the gossan samples, probably due to leaching, the copper content is lower than the sulfide ore. The rather high silver content in the ore is correlated with copper and/or lead (Figure 3.7).

The high content of tin at Deh Hosein is significant, whereas the high content of copper and other base metals (lead and zinc) due to vein type of the mineralization is not of economic value. So far, only very few tin occurrences or deposits have been reported from Iran. The presence of tin in high concentrations at Deh Hosein is of great significance from an economical and an archaeological points of view.



Sample No.	Description	Location	As ppm	Au ppb	Ag ppm	Cu %	Pb ppm	Zn ppm	S %	Sn %	W ppm	Bi ppm	Sb ppm	Se ppm	Mo ppm	Fe %	Ni ppm	Co ppm	Ba ppm	Th ppm	U ppm	La ppm	Ce ppm	Sc ppm	Al %	Na %	K %	Ca %
<b>Ore Samples</b>																												
DHN-1A	Chalcopyrite, bi-minerals, pyrite, Fe-oxides	N33° 45.406', E049° 18.993', Digging east of the prospect	44.7	31	19.2	6.0393	2117	228	0.641	<0.02	17	1252	98.9	29	<	4.11	60	16	<50	<0.2	2.7	0.7	<3	0.3	0.23	0.03	0.03	<
DHN-1B	Chalcopyrite, galena, pyrite, Fe-oxides	N33° 45.406', E049° 18.993', Digging east of the prospect	17.1	22	59.6	0.0306	37694	31	0.713	<0.02	18	3	223	<3	<	0.47	3	3	<50	1.9	<0.5	9.7	10	0.8	1.01	0.12	0.04	<
DHN-5	Chalcopyrite, pyrite, Fe-Cu-oxides	Ancient settlement	378	47	14	3.492	52	459	0.037	<0.02	6	5	6	<3	<	5.16	41	29	460	6.4	3.7	22.4	43	10.1	7.99	0.2	1.56	<
DHN-7A	Pyrite, chalcopyrite, cassiterite, pyrochlore, galena, stannite	398 0343347, UTM 3737263, Ghana Ghouli	2450	161	49.7	3.9638	2591	1245	0.658	<0.01	57	50	1530	<3	<	29.5	44	48	120	4.2	<0.5	18.1	26	7.1	3.26	0.09	1.04	<
DHN-10A	Chalcopyrite, pyrite, arsenopyrite	398 0342443, UTM 3737013, Ahmad Jigi I	4100	135	21.8	3.6908	37	156	0.023	<0.02	<	<2	35.4	6	<	3.02	20	11	<50	1.8	1.6	1.8	<3	2.1	1.86	0.09	0.03	<
DHN-10B	Chalcopyrite, pyrite, delafite	398 0342443, UTM 3737013, Ahmad Jigi I	3350	53	26.7	5.0685	98	186	0.708	<0.02	<	<2	28.1	<3	<	2.51	21	7	<50	4.8	<0.5	13	21	6.7	7.21	0.22	0.11	<
DHN-34	Native copper, pyrite, arsenopyrite	398 0342443, UTM 3737013, Ahmad Jigi I	19600	206	103.3	10	54	266	2.076	<0.02	<	73	107	<3	<	10.2	54	28	<50	4	<0.5	20.4	38	5.8	2.5	0.24	0.09	<
DHN-38	Arsenopyrite, pyrite, chalcopyrite, Bi-minerals	398 0342546, UTM 3736831, Ahmad Jigi II	214000	5359	6.5	0.722	234	20	3.777	<0.02	<	1686	1277	66	<	19.4	12	28	<50	<0.2	<0.5	<0.5	<3	0.8	0.17	0.02	0.02	<
DHN-42	Chalcopyrite, pyrite, cassiterite, Fe-oxides, etc.	398 0343347, UTM 3737263, Ghana Ghouli	1660	109	27	2.9301	279	625	0.58	0.42	32	800	137	<3	<	15.6	60	12	<50	<0.2	<0.5	1.5	<3	0.6	0.18	0.03	0.02	<
DHN-47	Chalcopyrite, arsenopyrite, gold, cassiterite, ferberite, Fe-oxides	N33° 46.61', E049° 19.99', Grandolite	541	845	19	4.4777	541	106	1.391	<0.02	2420	1805	10.8	30	42	8.23	51	38	<50	14.7	22.6	25.6	56	3.4	0.99	0.11	0.09	<
DHN-93	Arsenopyrite, Bi-minerals	398 0342443, UTM 3737013, Ahmad Jigi I	239000	13300	<5	N.A.	N.A.	<50	N.A.	<0.05	<20	N.A.	428	75	<20	20.6	<50	913	<100	<	<1.5	<	<5	0.9	N.A.	<	N.A.	<
<b>Gossan</b>																												
DHN-2	Pyrochlore + Fe-oxides	398 0341207, UTM 3738556, Jafar Khan	278	34	<0.3	0.2039	1064	413	0.071	<0.02	<	<2	36	4	<	41.2	92	46	<50	1	2.5	1.9	7	2.5	0.93	0.05	0.05	2
DHN-4	Fe-oxides + pyrite	398 0341626, UTM 3737312, North of Deh Hosein village	2150	28	1.1	0.0861	202	48	0.029	<0.02	1	115	33.3	<3	<	25.8	32	28	<50	2.7	5.2	10.2	21	3.6	1.11	0.02	0.2	<
DHN-15B	Fe-oxides + pyrite, chalcopyrite	398 0340895, UTM 3738846, Ghaidan	1600	50	1	0.249	209	662	0.008	<0.02	7	44	23.3	<3	<	22.5	67	35	<50	2.5	4.1	2.3	4	4.3	1.89	0.17	<0.01	<
DHN-16B	Fe-oxides + pyrite	398 0340182, UTM 3739756, Ghaidan	1380	372	26.9	0.2112	9793	7544	0.228	<0.03	<	43	65.6	15	<3	51	249	219	<50	<0.2	2.5	1.8	<3	2.8	0.67	0.02	0.08	<
DHN-43	Fe-oxides + pyrite, cassiterite, sphalerite	398 0342446, UTM 3737047, Close to the ancient settlement	16000	1101	98.4	0.4383	3930	2010	0.087	6.72	150	916	1353	<3	<	39.5	79	61	<50	<0.2	<0.5	6.3	<3	4.4	0.43	0.06	0.13	<
DHN-60	Fe-oxides + pyrite, arsenopyrite	N33° 46.083', E049° 18.992', Northeast of the prospect	4340	314	130	N.A.	N.A.	897	N.A.	<0.01	<	N.A.	178	29	<	17.8	<20	9	<50	1.9	<0.7	2.4	<3	3.4	N.A.	0.76	N.A.	<
DHN-71	Fe-oxides + pyrite, chalcopyrite	N33° 45.337', E049° 18.406', Beside the dirt road	9270	<2	<6	N.A.	N.A.	<50	N.A.	<0.01	<	N.A.	<	<3	<	33.9	<25	3	<50	5.1	<1.3	17.5	28	1.9	N.A.	0.98	N.A.	<
<b>Host Rock with Impregnation or Dissemination</b>																												
DHN-7B	Spotted slate	398 0343347, UTM 3737263, Ghana Ghouli	487	<2	4.1	1.4662	2168	661	0.052	<0.02	107	2	67.6	<3	<	7.32	31	19	520	11.9	2.1	45.6	89	15.2	9.5	0.18	3.39	<
DHN-33	Meta sandstone	398 0341207, UTM 3738556, Jafar Khan	313	34	1.1	0.1484	77	300	0.024	<0.01	19	12	8.6	<3	11	20.8	48	23	<50	12	4.8	4.2	<3	10.1	3.52	0.32	0.03	<
DHN-40	Silicified phyllite + cassiterite	398 0342546, UTM 3736831, Ahmad Jigi II	35400	107	17.2	4.2297	15	35	1.026	<0.02	<	32	9	<3	<	5.05	9	<3	<50	9.3	<0.5	12.2	29	8.1	2.45	0.23	0.38	<
DHN-51	Meta sandstone	N33° 45.930', E049° 20.457', Luzar Mount	572	121	44	10	222	2542	0.121	<0.01	43	19	8.7	15	<	3.78	62	12	230	8.1	3.8	25.5	49	7.8	3.54	0.23	0.76	<

**Table 3.1** Chemical analyses of host, mineralized and altered rocks from the Deh Hosein deposit, measured by NAA. Detection limits: Au (2 ppb), As (0.5 ppm), Ag (0.3 ppm), Bi (2 ppm), Sb (0.1 ppm), W (1 ppm), Sn (0.01 %), Ni (0.1 %), Na (0.1 %), K (0.1 %), Ca (0.1 %).

Sample No.	Description	Location	As ppm	Au ppb	Ag ppm	Cu %	Pb ppm	Zn ppm	S %	Sn %	W ppm	Bi ppm	Sb ppm	Se ppm	Mo ppm	Fe %	Ni ppm	Co ppm	Ba ppm	Th ppm	U ppm	La ppm	Ce ppm	Sc ppm	Al %	Na %	K %	Ca %	
<b>Host Rock</b>																													
DHN-8	Spotted slate	39s 0343347, UTM 3737263, Ghana Ghouli	940	8	0.8	0.0487	41	48	0.009	<0.02	5	2	17.3	<3	<1	5.37	22	4	620	15.6	1.5	46.8	92	19.3	11.92	0.14	4.21	<1	
DHN-11	Phyllite	39s 0342443, UTM 3737013, Ahmad Jigi I	90.8	<2	0.9	0.088	64	1210	0.001	<0.02	25	<2	4.9	<3	5	5.37	80	6	480	11.6	2.8	41.7	76	16.7	10	0.17	3.46	<1	
DHN-48	Granodiorite	N33° 46.611', E049° 19.99', Granodiorite	92.1	<2	<0.3	0.0217	53	34	<0.001	<0.01	<1	3	0.2	<3	<1	1.93	17	9	363	18.3	4.3	31.2	57	8.1	4.54	1.94	4.25	<1	
DHN-56	Spotted slate	N33° 46.188', E049° 18.553', Spotted slate	63.2	3	<5	N.A.	N.A.	147	N.A.	<0.01	<1	N.A.	2	<3	4	4.96	102	11	570	15.1	3	44.4	92	15.7	N.A.	0.41	N.A.	<1	
DHN-61	Meta sandstone	N33° 46.083', E049° 18.992', Northeast of the prospect	62	<2	<5	N.A.	N.A.	280	N.A.	<0.01	6	N.A.	3.2	<3	2	5.61	<20	7	430	12.4	3.7	36.5	76	13.4	N.A.	0.14	N.A.	<1	
DHN-64	Meta sandstone	N33° 45.819', E049° 18.525', Ghana Ghouli	51.6	<2	<5	N.A.	N.A.	87	N.A.	<0.01	<1	N.A.	2	<3	<1	6.61	<20	8	240	95	2.2	29.5	58	10.7	N.A.	0.2	N.A.	<1	
DHN-70	Silicified spotted slate	N33° 45.337', E049° 18.406', Beside the dirt road	111	<2	<5	N.A.	N.A.	83	N.A.	<0.01	4	N.A.	3	<3	<1	5.22	<25	7	570	16.6	5.3	50	100	20.9	N.A.	0.2	N.A.	<1	
DHN-74	Meta sandstone	N33° 45.406', E049° 18.993', Digging east of the prospect	34.7	<2	<5	N.A.	N.A.	73	N.A.	<0.01	12	N.A.	3.8	<3	<1	2.67	<20	4	160	5.1	0.8	15.3	30	3.9	N.A.	0.09	N.A.	<1	
DHN-82	Tourmaline of tourmaline granite	N33° 46.770', E049° 19.848', Tourmaline granite	36.2	<2	<5	N.A.	N.A.	<50	N.A.	<0.01	<1	N.A.	<0.1	<3	<1	1.18	49	5	<50	4.4	1.4	5.9	13	6.6	N.A.	1	N.A.	<1	
<b>Quartz Veins</b>																													
DHN-6	Qz + Fe-oxides	Quartz vein	84.8	<2	<0.3	0.0264	20	34	0.004	<0.01	<1	<2	9.7	<3	<1	3.81	20	5	<50	<0.2	<0.5	2.3	<3	2.2	1.8	0.1	0.09	<1	
DHN-9	Qz + Pyrite	39s 0343497, UTM 3737946, Spotted Slate	1060	44	2.3	0.0299	500	65	0.031	<0.02	<1	22	14.1	<3	<1	3.77	16	10	<50	<0.2	<0.5	4.1	9	1.8	0.9	0.05	0.09	<1	
DHN-12A	Quartz, pyrite, chalcopyrite	39s 0342546, UTM 3736831, Ahmad Jigi II	2990	<2	1.2	0.3897	157	99	0.005	<0.02	<1	69	102	<3	<1	1.23	9	7	<50	<0.3	<0.5	1	<3	4.7	3.8	0.16	0.03	<1	
DHN-12B	Quartz, kobeinite, Bi-minerals	39s 0342533, UTM 3736838, Ahmad Jigi II	399	9	3.6	0.0279	535	19	0.023	<0.02	<1	486	107	<3	<1	0.26	<1	<1	<50	<0.2	1.4	0.9	<3	0.5	0.34	0.03	0.01	<1	
DHN-12C	Black Quartz	39s 0342546, UTM 3736831, Ahmad Jigi II	186	7	<0.3	0.0406	187	43	0.003	<0.02	<1	23	116	<3	<1	1.15	1	4	<50	2.9	<0.5	40.2	73	5.3	4.46	0.15	0.02	<1	
DHN-14	Qz + Fe-oxides, enasiterite	39s 0342946, UTM 3737407, Center of the prospect	120	<2	0.5	0.0193	52	110	0.001	<0.02	8	2	3	<3	<1	1.92	8	9	<50	1.1	<0.5	3.4	7	1.8	1.26	0.04	0.1	<1	
DHN-15A	Qz + Fe-oxides	39s 0340895, UTM 3738846, Chaidan	56	4	2.1	0.0042	56	1704	0.003	<0.01	3	<2	4.2	<3	<1	2.43	42	6	<50	1.4	0.6	17.9	31	1.3	0.78	0.05	0.02	<1	
DHN-16A	Qz + Fe-oxides	39s 0340182, UTM 3739756, Chaidan	12.6	6	3.8	0.0033	207	42	0.003	<0.01	2	4	6	<3	<1	0.38	3	1	<50	<0.2	0.5	2.6	5	0.5	0.15	0.03	0.02	<1	
DHN-30	Qz + Fe-oxides	N33° 46.711', E049° 17.1077', Top of Cheshmeh Jafir Khan	108	17	0.8	0.019	123	118	0.076	<0.01	<1	<2	6.6	<3	<1	3.35	60	6	<50	3.5	1.8	11.1	23	4.2	1.66	0.14	0.4	<1	
DHN-37	Qz + Fe-Cu-oxides	39s 0342330, UTM 3736818, Behind Ahmad Jigi I	6370	27	16.5	4.474	67	113	0.095	<0.02	<1	26	41.2	25	<1	4.81	27	7	<50	<0.2	<0.5	2.7	<3	1.7	0.44	0.05	0.06	<1	
DHN-45	Qz + Fe-Mn-Cu oxides	N33° 46.718', E049° 20.138, Quartz vein in granodiorite	109	7	<0.3	0.1851	25	36	0.013	<0.01	<1	16	3.1	<3	<1	0.78	10	2	<50	<0.2	<0.5	7	16	1	0.39	0.05	0.13	<1	
DHN-57	Qz + Cu-oxides	N33° 46.188', E049° 18.553', Spotted slate	61.2	30	<5	N.A.	N.A.	540	<0.01	<1	N.A.	5.3	<3	<1	1.12	<20	5	<50	0.7	<0.5	1.8	3	0.6	N.A.	0.05	N.A.	<1		

Table 3.1 (continued)



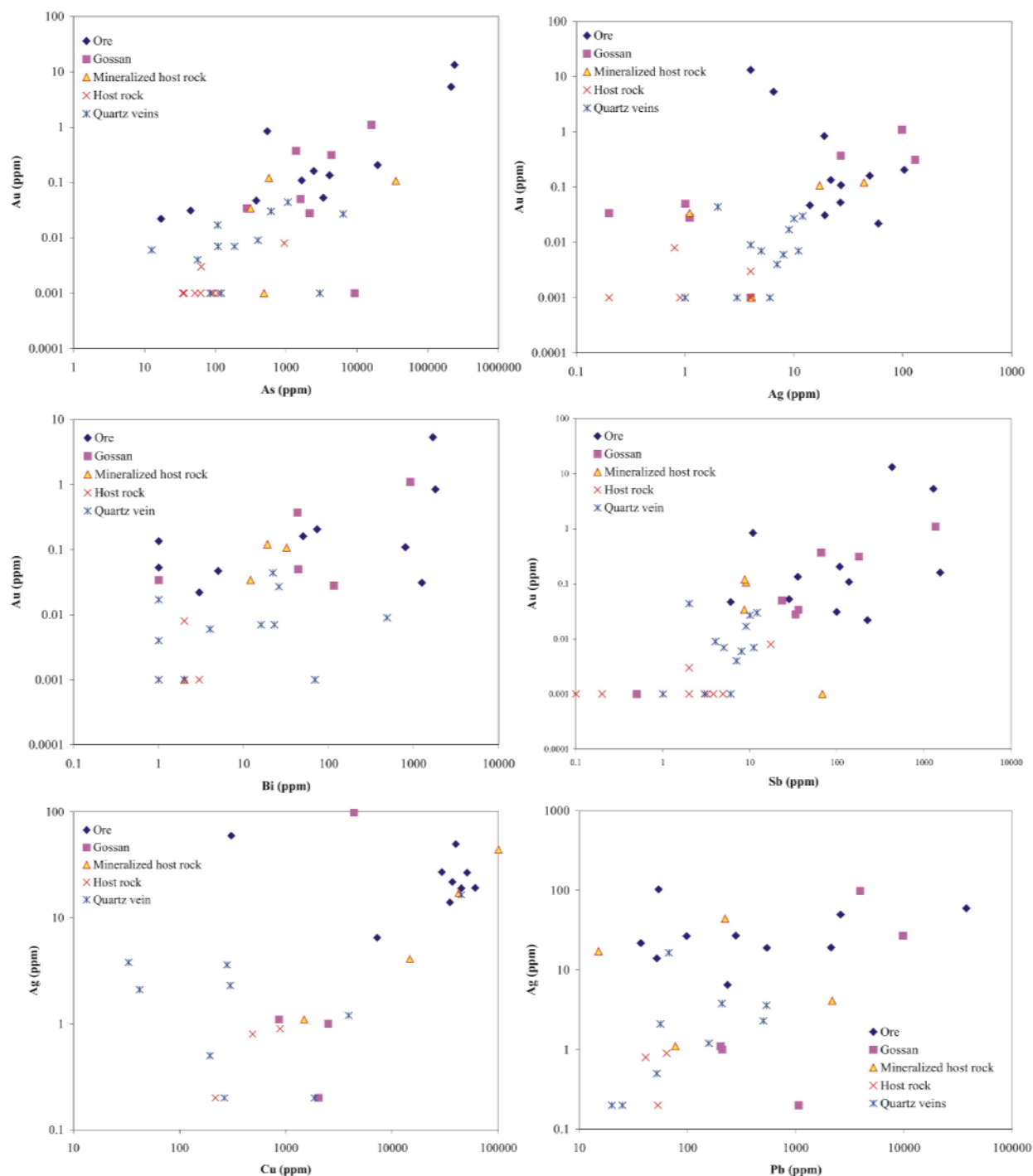


**Figure 3.7** Scatter diagrams (logarithmic axes) for Au-As, Au-Ag, Au-Bi, Au-Sb, Ag-Cu and Ag-Pb at Deh Hosein, based on analyses of 43 samples by NAA.

A comparison of the gold and arsenic contents of the meta-sandstone of the area with the average values of these elements in the metamorphic rocks worldwide (Wedepohl et al. 1978) indicates a significant enrichment of arsenic and a moderate depletion of gold. The low gold content of the altered meta-sandstone in the periphery of the mineralization suggests that the hot hydrothermal solutions may have leached gold and some other metals out of these rocks.

Field observations along with analytical and electron microprobe results reveal that the gold occurrence at Deh Hosein is not restricted to a certain formation or rock unit. The highest gold

concentrations are primarily found in the massive arsenopyrite veins, whereas the sulfide and gossan veins and to a lesser extent the mineralized host rocks are also enriched in gold (Table 3.1). The gold content of plain quartz and the host rocks is generally low.

According to both bulk chemical analyses and electron microprobe investigations, the gold concentration is positively correlated with arsenic, bismuth, selenium, tellurium, and antimony (Tables 3.1 and 3.2, Figure 3.7). It has no significant correlation with other elements.

The electron microprobe analyses revealed that arsenopyrite, pyrite, chalcopyrite, native bismuth, bismuthinite and Pb-Bi-sulfosalts are the main gold-bearing minerals in the prospect (Table 3.2). Due to its abundance and typically high gold content, arsenopyrite is the most important gold-bearing mineral at Deh Hosein. It contains up to 1900 ppm gold which shows a positive correlation with bismuth, antimony, and selenium. Pyrite, which is also an abundant mineral in the area, shows high contents of gold, especially in its arsenic rich parts. Native bismuth grains enclosed by arsenopyrite contain some amounts of arsenic (up to 9.3%) and display the highest amounts of gold (4000 ppm), whereas bismuthinite with lesser amounts of arsenic shows lesser contents of gold (up to 200 ppm). The results of electron microprobe analyses of these minerals for trace gold are summarized in Table 3.2.

Mineral / Phase	Sample No.	n	Au (ppm)	As (%)	Bi (%)	Te (%)	Sb (%)	Se (%)	Observations / Remarks
<b>Native bismuth</b>	DHN-38	3	<b>200-4000</b>	<b>1.5-9.3</b>	<b>80.7-86.9</b>	N.A.	<b>0.29-3.11</b>	<u>0.04-0.1</u>	Bismuth inclusions in arsenopyrite. Few percents of Pb, Fe and S are present too
<b>Arsenopyrite</b>	DHN-38 DHN-93	130	<b>0-1900</b>	45-46	0-1	0-0.05	<b>0-1.61</b>	<u>0.46-0.52</u>	High gold concentration especially around Bi inclusions
<b>Pyrite</b>	DHN-7A,43,47	16	<b>0-1200</b>	0-0.25	0	0-0.04	0-0.02	<u>0-0.31</u>	Remarkable correlation between amount of gold and arsenic
<b>Kobellite</b>	DHN-12B	3	<b>260-1000</b>	0.02	<b>39</b>	0	<b>8.3</b>	0.02-0.05	Associated with quartz vein and arsenopyrite
<b>Szrokayite</b>	DHN-12B	1	<b>900</b>	0	<b>74.6</b>	<b>21.96</b>	<u>0.626</u>	<u>0.17</u>	-----
<b>Chalcopyrite</b>	DHN-1, 7,43,47	11	<b>25-700</b>	0	0-0.004	<b>1.46-1.5</b>	0	0-0.02	-----
<b>Krupkaite</b>	DHN -1A	4	<b>100-450</b>	0-0.01	<b>58</b>	<u>0.27-0.38</u>	<u>0.28-0.35</u>	<u>0.4-0.44</u>	Associated with quartz vein, pyrite and chalcopyrite
<b>Bismuthinite</b>	DHN-93	4	<b>0-200</b>	<u>0.15-1.4</u>	<b>71.5-77.5</b>	<u>0-0.59</u>	<b>0-1.88</b>	<u>0.1-0.65</u>	Remarkable correlation between amount of gold and arsenic
<b>Cerussite</b>	DHN-60	95	<b>0-150</b>	0-0.031	0	0-0.10	0-0.06	0-0.03	-----
<b>Scordite</b>	DHN-93	7	<b>40-100</b>	26.6-29	0.08-0.4	0-0.05	0.01-0.18	0.11-0.16	Associated with Fe-oxides
<b>Beaverite</b>	DHN-60	13	<b>0-100</b>	<u>0.20-1.64</u>	0-0.02	0-0.05	0-0.03	0.01-0.2	Associated with Fe-oxides and cerussite

**Table 3.2** Ranges of concentrations of gold, arsenic, bismuth, tellurium, antimony and selenium in ore minerals examined by electron microprobe analyses.

## *Chapter 4*

### **Petrography, mineralogy and geochemistry of the Astaneh occurrence**

#### **4.1 Introduction**

The Astaneh occurrence is located 4km west-southwest of the town of Astaneh ( $33^{\circ} 50' - 33^{\circ} 52' N$ , and  $49^{\circ} 17' - 49^{\circ} 20' W$ ), in west central Iran. The mineralization occurs in the northern part of the Astaneh intrusion and is mainly hosted by the Shirmazd granodioritic stock and its surrounding intrusive bodies (Figure 4.1).

The presence of placer gold in the alluvia adjacent to the Shirmazd stock has been known to the local people for centuries. The rare tracks of old mining in the hard rock can only be traced in the copper-quartz vein of Molla Yahya hill as small open pits. In the early 1960s some exploration work was conducted by individuals in the hard rock in order to find the source of the gold of alluvia. Some trenches and small tunnels were dug as a result. During the last three decades some geological and mineralogical investigations were performed by the Geological Survey of Iran, the Samim Resources and some Iranian universities in the Astaneh area and specifically on the Shirmazd stock.

In order to complete the previous studies, in addition to field observations, a suite of 20 representative ore and rock samples was collected from the occurrence for analytical and mineralogical investigations. Results of these investigations and the previous researches are presented in the current chapter.

## 4.2 Geology of the prospect and petrography of the host rocks

The NW-SE trending Astaneh intrusive body that hosts the gold mineralization is mainly composed of biotite granite, which is locally accompanied by granodiorite, tourmaline granite, and quartz diorite. These rock units are locally altered and/or intersected by microgranodiorite dykes, and quartz or aplitic veins. The northeastern part of the Astaneh intrusion has been intersected by the Shirmazd granodioritic stock. This stock is about 400m in diameter and has likewise been intersected by NE-trending microgranodiorite dykes (Figure 4.1).

The main trend of the faults, fractures and other structural features of the area is NW-SE, which corresponds with the main trend of the Sanandaj-Sirjan zone and the Zagros chain. In the following the main petrographical characteristics of the exposed rocks of the area will be briefly described.

*Biotite granite* comprises the major portion of the Astaneh intrusive body. Masoudi 1997 has determined the age of this unit for  $98.9 \pm 1.0$  Ma by Rb/Sr method. In field scale, this rock unit is characterized by considerable amounts of biotite and different types of xenoliths (Figure 4.2a). The xenoliths are several centimeters to one meter in size. Biotite granite also contains andalusite which in some cases (southeast of the Shirmazd mount) forms a considerable amount of the rock volume.

Biotite granite with mainly granular and sporadically poikilitic, and perthitic textures contains mainly quartz (20-30%), orthoclase (30-35%), plagioclase (20-30%), biotite and amphibole (20-25%). Apatite, zircon, rutile, esphene and some opaque minerals are among the accessory minerals of the rock (Hashemi 2002). Biotite has been altered to chlorite, calcite, opaque minerals and muscovite while plagioclase and orthoclase were altered to sericite and clay minerals. According to Hashemi (2002) and Masoudi (1997) the xenoliths of the rock are of various types, but dominantly of quartz dioritic and granodioritic compositions. Xenoliths of andalusite schist and micro-textural magmatic rocks have been reported as well.

In the mineralization area at the southern end of Parmeh Valley the unit of biotite granite is characterized by intensive alteration and moderate mineralization at *Tappeh Khileh* and *Tappeh Dor* (Figure 4.1 and 4.2a). The alteration on the field scale is recognized by the brown surface of these hills due to chloritization and the iron oxide varnish. The microscopic characteristics of these units are in general the same as biotite granite with the difference of intensive alteration of biotite and amphibole into chlorite and iron oxides as well as sericitic and argillic alteration of plagioclase and orthoclase. These units lack xenoliths which are often seen in the usual biotite granite of the area.

*Granodiorite* in the study area occurs in two localities: The Shirmazd stock (Figure 4.2c and d), which is the most mineralized unit in the study area, and southwest of Shirmazd as a NE-SW trending band which rarely hosts any mineralization.

Shirmazd mount appears as a dome shaped stock with a radius of 400-600m and 2450m height (the peak is about 250m above the valley bed). This stock has an apophysis in its northeastern part.

Under the microscope (Figure 4.2e), the sections of the rock show granular and porphyroid textures which consist of quartz (20-30%), mainly euhedral plagioclase (35-40%), orthoclase (20-25%), and biotite (10-15%). In the case of porphyroid textures plagioclase and biotite comprise the porphyroblasts. Zircon, apatite, rutile, esphene and opaque minerals (including chalcopyrite, pyrite and Fe-oxides) are among accessory minerals. Plagioclase has been altered into sericite (Figure 4.2h) and sporadically chlorite and clay minerals. Orthoclase has been altered into chlorite and calcite while biotite into, muscovite and Fe-oxides.

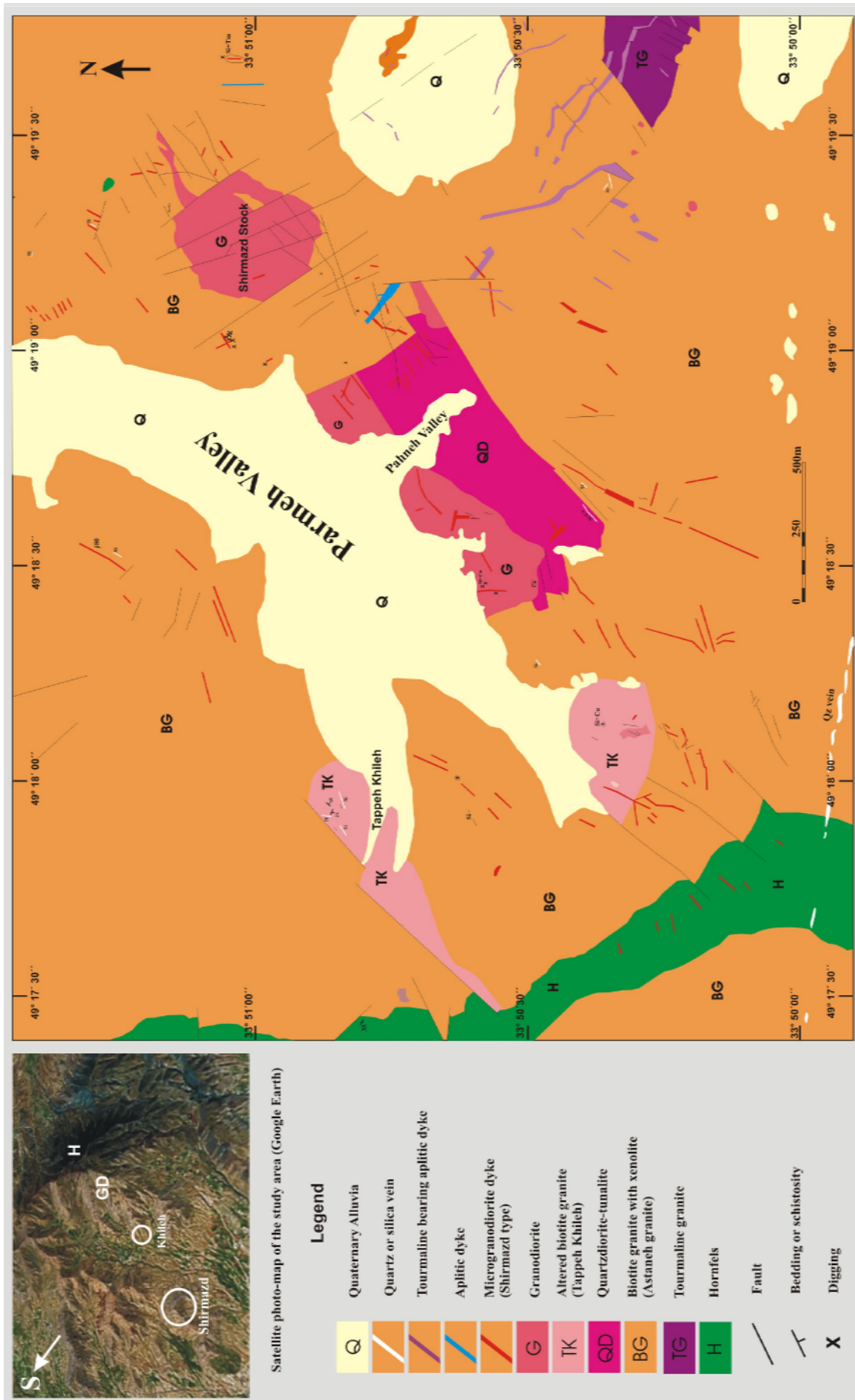


Figure 4.1 Geological map of the Astaneh gold prospect. Modified after Ojaghi et al. 2000 (Samim Resources).

Both Rb/Sr and Pb-Pb ages of zircon (see Chapter 6) suggest an Eocene age for the Shirmazd stock. The Shirmazd mount is frequently intersected by several NE-SW (N45E to N60E) trending vertical micro-granodioritic dykes that should be younger than the one at Shirmazd. The dykes are from several centimeters to several decimeters wide and several meters long. In some cases these dykes are intersected by small veinlets of quartz and quartz-sulfide or accompanying by parallel arsenopyrite veins. The micro-granodioritic dykes (Figure 4.2f and g) show almost the same microscopic characteristics as Shirmazd granodiorite with the difference of micro scale size of the grains (1-5 $\mu$ m, micro granular texture), a little less quartz, lack of zircon, and more intensive alteration.

Dissemination of chalcopyrite and pyrite occurs often in the dykes. Although these micro-granodioritic dykes reach their highest abundance in the Shirmazd mount, but they are also observed in other parts of the area including southern parts of Shirmazd mount.

The granodiorite southwest of the Shirmazd mount is a 0.3 x 1 km NE-SW trending band. According to Hashemi (2002), the microscopic characteristics of this unit resemble the ones from granodiorite xenoliths of biotite granite, although the proportion of mineral components is similar to the Shirmazd granodiorite. This rock comprises of quartz (20-25%), plagioclase (30-35%), alkali-feldspar (20-25%), and biotite (15-20%). Apatite, zircon, and opaque minerals are among the accessory minerals.

The *quartzdiorite-tonalite* unit is seen as a NE-SW trending lens parallel to southwestern band of granodiorite and no mineralization has been observed in it. According to Hashemi (2002), this rock is composed of quartz (15-25%), plagioclase (50-55%), biotite and actinolite (25-30%) with granular to porphyroid texture. Orthoclase, apatite, esphene, zircon and opaque minerals are among the accessory minerals.

*Tourmaline granite* is a rather common rock unit in different parts of the Astaneh intrusive body. In the area of Astaneh gold prospect, it exposes mainly in the southeast of Shirmazd mount at the end of Darreh Boleh valley. This rock unit is characterized by existence of numerous round and ellipsoidal grains of tourmaline which reach up to 10cm diameter (Figure 4. 3a). This rock is similar to biotite granite in the field scale but lacks xenolith. The rock shows a granular texture with feldspar, quartz and biotite grains as major minerals. Many spheroid grains of tourmaline in the rock are surrounded by a light-colored halo which is devoid of dark minerals. No copper mineralization has been observed or reported in relation to tourmaline granite unit. The tourmaline granite unit has been intersected by younger tourmaline granite dykes especially in the southeastern part of the Shirmazd mount. Both tourmaline granite bodies and dykes have been intersected by microgranodiorite dykes of Shirmazd type. Single zircon evaporation and Rb/Sr dating methods of a similar tourmaline granite unit in the southern part of Astaneh intrusive body (see Chapter 6) indicate a Middle Jurassic age (177 $\pm$ 8 Ma) by the zircon evaporation method and Late Cretaceous (Campanian; 77 $\pm$ 33 Ma) age by the Rb/Sr method for this unit.

*Hornfels* has surrounded the Astaneh intrusive body in its southern, western and to some extent northern parts. Hornfels covers the western part of the Astaneh prospect area. It shows a rather sharp contact with the biotite granite (Figure 4.3b). According to field and microscopic investigations (Hashemi 2002), an original clay-sandstone has been converted into hornfels due to contact metamorphism. Some small highly altered granitic patches are seen in the hornfels unit, especially close to its contact with the Astaneh intrusive body.



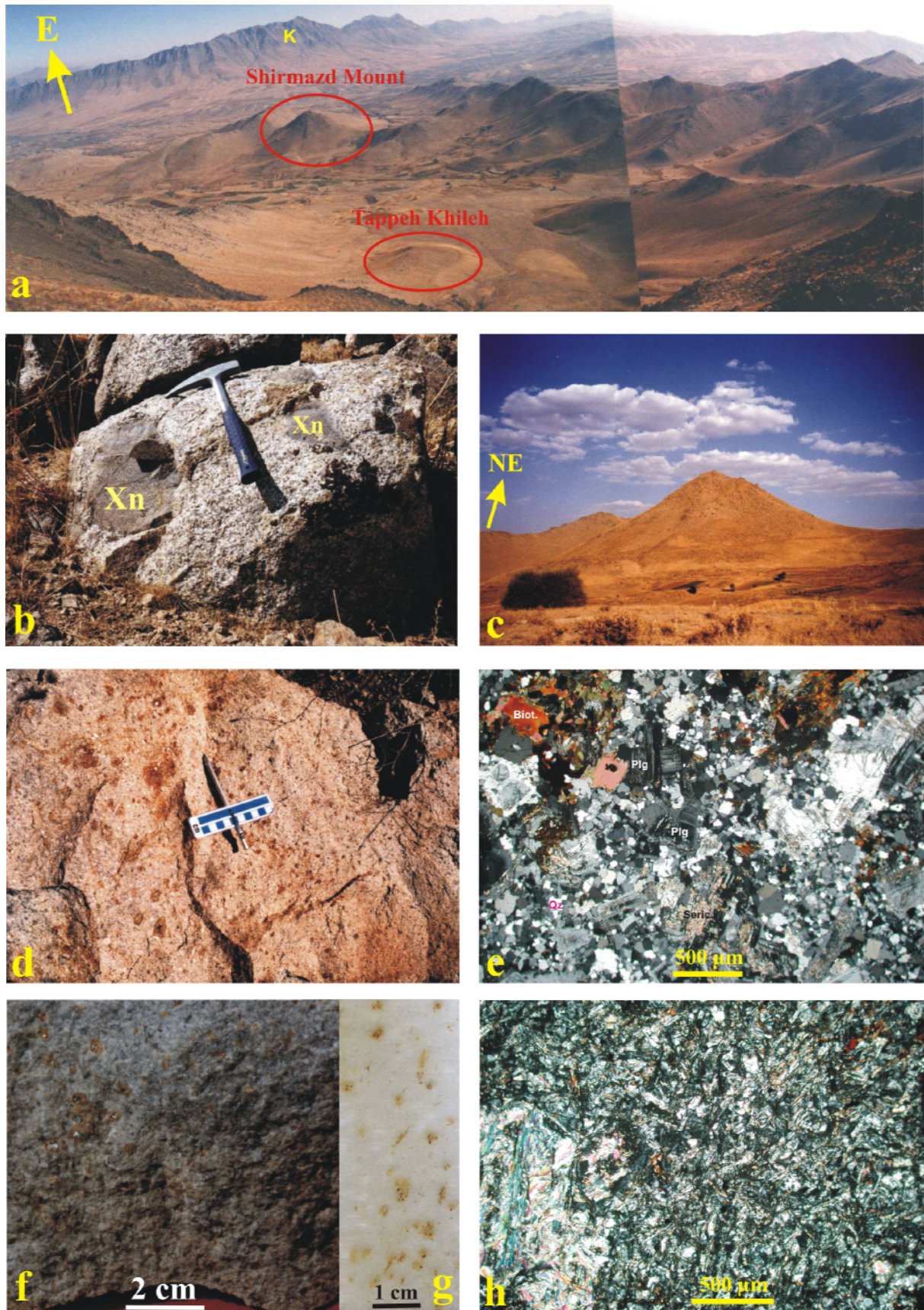


**Figure 4.2** a) An Overview of the Astaneh gold occurrence, b) The biotite granite of the area with its xenoliths, c) An overview of the Shirmazd stock, d) Disseminated granodiorite of Shirmazd, e) Microscopic photograph of the Shirmazd granodiorite, f and g) Disseminated microgranodiorite dyke of the Kolah Morghoun locality, h) Alteration of plagioclase of the granodiorite into sericite.

### 4.3 Alteration

The alteration zones of the area are not pervasive or extensive and are mainly restricted to highly mineralized areas namely Shirmazd mount, Tappeh Dor and Tappeh Khileh with the same general trend as the mineralization (NE-SW). The most important mineralization-related alterations in the area are sericitization, chloritization, and silicification, although argillic alteration can be seen as small patches as well.

*Sericitization* is the most widespread alteration in the study area. Conversion of plagioclase into sericite is the main cause responsible for this alteration, although alkali-feldspar in lesser amounts has also been altered into sericite. Albeit the sericitization is observed in most of the rock units of the study area, it is most intensive in the units adjacent to mineralized patches and veins including Shirmazd stock and its intersecting microgranodiorite dykes. This alteration is occasionally accompanied with chlorite alteration.

*Chloritization* is rather widespread and mainly observed along with sericitization due to alteration of mainly mafic minerals namely biotite and amphibole. Biotite, amphibole and in some cases plagioclase of the rocks at Tappeh Khileh, Tappeh Dor and Shirmazd have been altered into chlorite and calcite. Some small veinlets of chlorite are seen along with mineralization zones.

*Silicification* which is recognizable as small veins and veinlets of quartz (texture of open space filling) and also small quartz crystals along with disseminated balls of sulfide minerals in the rocks, demonstrates a good correlation with the mineralization.

*Calcite* is observed usually together with chlorite and in the mineralized zones occurs as small veinlets. In the rocks calcite has mainly been altered from biotite and to some extent from plagioclase.

*Argillic* alteration which is a result of conversion of K-feldspar and plagioclase into clay minerals is seen as small patches in Shirmazd mount and Tappeh Khileh.

### 4.4 Mineralization

The mineralization at Astaneh occurs mainly as dissemination and NE-trending veins and veinlets of quartz, quartz-sulfide and arsenopyrite in the Shirmazd stock, the intersecting microgranodioritic dykes, and in the nearby Tappeh Khileh and Tappeh Dor (Figures 4.2d, f, g and 4.3 c, d). The dissemination is best exposed in the Shirmazd stock and microgranodiorite dykes while less frequent in Tappeh Khileh and Tappeh Dor. The disseminated mineralization is mainly composed of chalcopyrite and pyrite which have mostly been replaced by goethite and other Fe-oxides. Arsenopyrite veins are adjacent and parallel to microgranodiorite dykes. Quartz and quartz-sulfide veins are of 5-50 cm wide and 2-3 m long while arsenopyrite veins are up to 25cm thick and 2-3m long. Overall, the mineralization at Astaneh is rather weak and highly oxidized on the surface.

Some 20 ore minerals have now been identified at Astaneh, of which chalcopyrite, pyrite and arsenopyrite are the most abundant ones and are easily visible in hand specimen. The minerals recognized by Khoii (1982) and Hashemi (2002) along with those now identified for the first time, are described below:

*Arsenopyrite* has so far been observed as small veins in Kolah Morghun mount, Tappeh Khileh, 1km north of Shirmazd mount (east of Parmeh valley), north of Tappeh Khileh (west of Parmeh valley), and south of Tappeh Khileh (Ataii trench). Hashemi (2002) has observed scattered pieces of arsenopyrite at Tappeh Dor as well. Arsenopyrite is mainly restricted to the mentioned locations and has been rarely observed in other localities including the Shirmazd mount. In the veins arsenopyrite has a massive and highly fractured (cataclastic) texture



(Figure 4.3e) which is due to its early crystallization and its brittleness (Rahmdor 1980). In some cases euhedral big rhombic crystals of arsenopyrite have been observed (Figure 4.3f).

The arsenopyrite is replaced by scorodite from its rims and fractures. Chalcopyrite, pyrite, quartz and sporadically galena have filled fractures of arsenopyrite. Inclusions of native bismuth, bismuth oxides, rooseveltite (BiAsO<sub>4</sub>), and Bi-As-oxides (< 35µm) are scattered in the massive arsenopyrite (Figure 4.3i, l).

*Chalcopyrite* is the most abundant sulfide mineral and occurs as both vein type and disseminated in the study area. Disseminated chalcopyrite is especially seen at the Shirmazd stock and microgranodiorite dykes (Figure 4.3g, h). The Shirmazd mount contains disseminated small balls (< 2 cm) of chalcopyrite-pyrite which are on the surface converting into malachite and Fe-oxides from their rims (Figure 4.2d).

Chalcopyrite occurs as subhedral to anhedral scattered or aggregated grains as well as fracture fillings. It is seen along with primary pyrite, pyrrhotite, arsenopyrite, and bornite. Tiny inclusions of chalcopyrite have been observed in pyrite and bornite. Chalcopyrite sporadically contains exsolved sphalerite “stars” (Figure 4.3i, j), which suggests formation temperatures above about 400°C (Hutchison and Scott 1981). Chalcopyrite has often been altered into covellite, malachite, and Fe-oxides.

*Pyrite* has occurred in two generations in the area. The primary pyrite occurs as euhedral (mainly) to subhedral grains. They are small in size (<150µm) and usually along with chalcopyrite and sporadically with pyrrhotite. It occurs in both quartz and sulfide veins.

The secondary pyrite has a fracture filling texture and occurs as subhedral to anhedral grains or as veinlets in arsenopyrite or quartz. Pyrite is converting to Fe-oxides.

*Pyrrhotite* is less abundant than chalcopyrite and pyrite and is observed along with these minerals. It is more frequent with secondary pyrite, which is possibly a product of pyrrhotite conversion. Pyrrhotite occurs as anhedral and in some cases subhedral grains and fills open spaces of the rock. Inclusions of pyrrhotite have been observed in chalcopyrite. In some cases chalcopyrite has filled the fractures of pyrrhotite. Hashemi (2002) has reported anhedral grains of pyrrhotite in the contact hornfels.

*Sphalerite* is a rare mineral in the area and has been observed as small (<20µm) anhedral or star shaped inclusions on chalcopyrite (Figure 4.3i, j).

*Bismuth minerals* occur as several anhedral to subhedral inclusions of arsenic bearing native bismuth, bismuth oxides, rooseveltite (BiAsO<sub>4</sub>), Bi-sulfide and Bi-As-oxides (<35µm) in arsenopyrite.

*Gold* occurs in both visible and invisible forms at Astaneh. Hashemi (2001) has reported very fine grained scattered particles of visible gold (<15 µm) in chalcopyrite and the goethite produced from its oxidation, and in sericitized plagioclase. Careful microscopic and electron microprobe investigations of arsenopyrite samples which show the highest contents of gold revealed no visible grain of gold in them. This suggests the occurrence of gold in invisible form in arsenopyrite. Probably gold is present as very fine grains also in quartz.

*Bornite* is rare and has only been observed as scattered grains and open space filler in the north of Shirmazd along with chalcopyrite.

*Galena* is a rare mineral in the area. Hashemi has reported galena in the south of Tappeh Dor (Sib Talkh mount) in a quartz-sulfide vein and in west Parmeh valley (1km northwest of Tappeh Khileh) in an arsenopyrite vein in which it fills the open spaces of arsenopyrite.

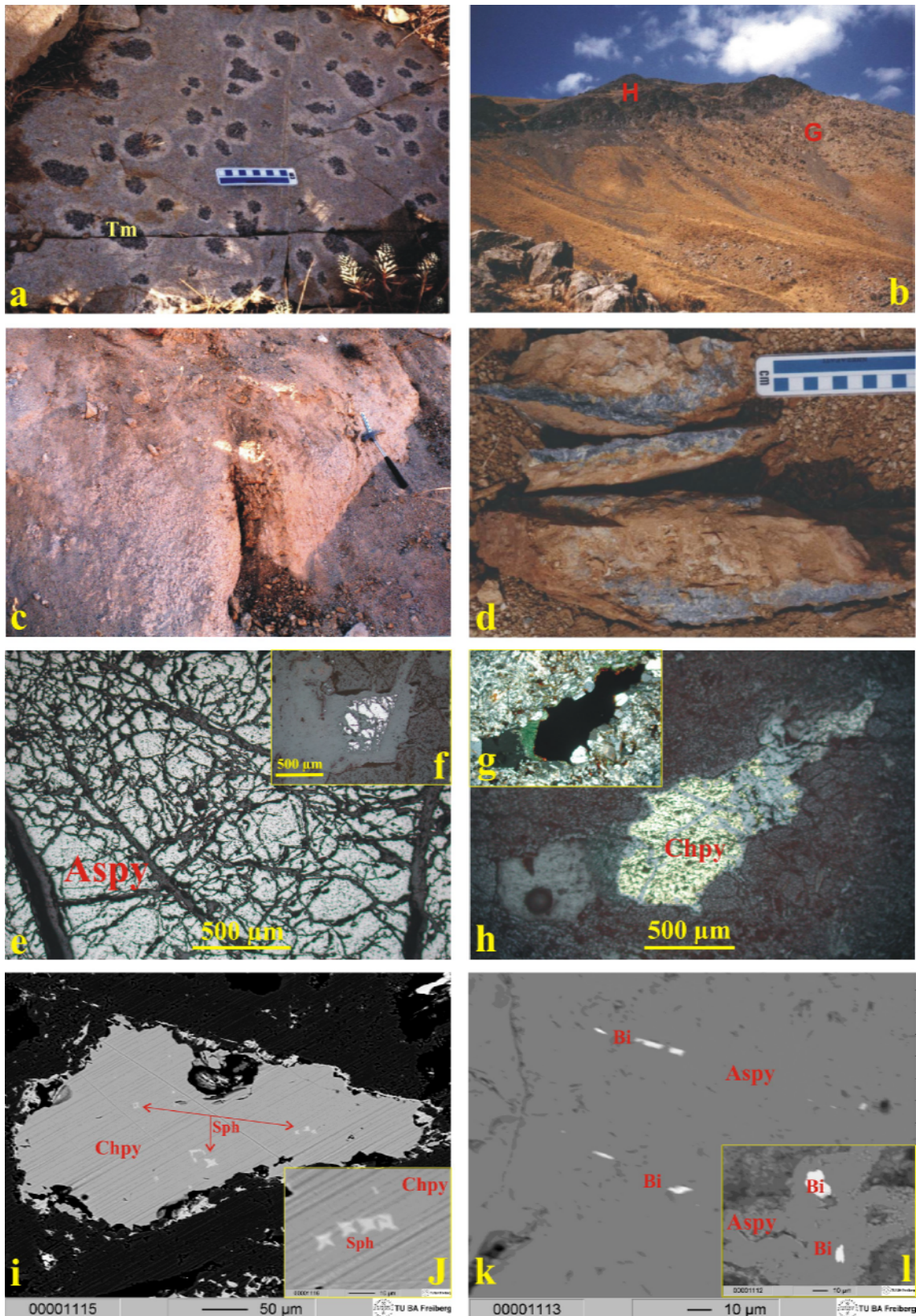


**Figure 4.3** a) Tourmaline granite of the area, b) The contact between biotite granite and hornfels in the west of study area, c) A small quartz-sulfide vein in the altered granodiorite of Shirmazd stock, d) Part of an arsenopyrite vein in the Kolah Morghoun locality, e) Massive arsenopyrite of a vein with cataclastic texture, f) A euhedral arsenopyrite grain which has been altered into Fe-oxides and scorodite from its rims and fractures, g and h) issemimentation of chalcopyrite in a microgranodiorite dyke. Back scattered electron micrographs of i and j) Stars of sphalerite in chalcopyrite, and k and l) Inclusions of native bismuth in arsenopyrite.

*Scheelite* is the only tungsten mineral found in the Astaneh prospect and occurs as rare anhedral to subhedral grains along with molybdenite and illmenite. It is obtained also by panning in which case it shows greenish white color under a UV lamp. No direct relationship has been observed between scheelite and gold mineralization in the prospect.

*Ilmenite* occurs as anhedral to euhedral crystals (mostly anhedral) and has sporadically chipped and skeleton texture. There are sometimes grains of rutile around it.

*Rutile* needles are visible in highly sericitized areas and also in biotite and plagioclase. Part of rutile needles have occurred due to replacement of illmenite.

*Molybdenite* grains with open space filling texture have been reported by Hashemi (2002) from the Tappeh Dor altered granite and the arsenopyrite vein of Tappeh Khileh. It has been observed as aggregates of fine grains.

*Marcasite* occurs as fine euhedral crystals along with secondary pyrite. Apparently it is a product of alteration and decomposition of pyrrhotite. Marcasite has been intensively altered into Fe-oxides.

Primary *chalcocite* has been reported by Hashemi (2002) which has been altered to tenorite along its cleavages.

#### *Weathering products*

Covellite, malachite, Fe-oxides (goethite, hematite), scorodite, and tenorite are among the minerals which have been produced due to conversion of sulfide minerals of the area. Box work texture is also visible in goethite.

### **4.5 Paragenetic sequence**

The mineral assemblages at Astaneh include four different origins; early hydrothermal assemblage, main hydrothermal assemblage, late hydrothermal assemblage and secondary minerals resulting from weathering of hydrothermal minerals. These mineral assemblages demonstrate a rather high temperature mineralizing fluid.

#### Early hydrothermal assemblage

This assemblage comprises high temperature minerals of ilmenite and rutile which have occurred along with quartz. Probably scheelite and molybdenite have occurred also at this stage in minor amounts.

#### Main hydrothermal assemblage

This assemblage is marked by the precipitation of a range of sulfides and the continuation of silicification and sericitization in the quartz-sulfide veins and Shirmazd mount as well as Tappeh Dor and Tappeh Khileh. The hydrothermal quartz forms mainly in this stage. The pioneer fluids which had a low fugacity of sulfur precipitated arsenopyrite, pyrrhotite and native bismuth whilst the copper absorbed the main amount of sulfur and formed chalcopyrite and a little bornite. At the same time, the ions of Fe, Pb, and Zn have absorbed the rest of sulfur and formed primary pyrite, galena and sphalerite in minor amounts.

#### Late hydrothermal assemblage

This stage is characterized by presence of marcasite and secondary pyrite which have been formed by the late hydrothermal fluids.

#### Weathering assemblage

Iron oxides and hydroxides, scorodite, covellite, tenorite and cerrusite formed due to oxidation of sulfide minerals.

#### 4.6 Metal associations and distributions at Astaneh

In order to study the mineralization of gold in the hard rock, 13 ore and host rock samples were analyzed by NAA at Actlabs Canada for gold and trace elements by programs Au+48 and Au+34 (Table 4.1).

The field observations show a low sulfide content of the ore. Bulk Au, Cu, Ag, Sn, W and S contents of veins ranged up to 7.32 ppm, 0.97%, 52 ppm, 0.05%, 100 ppm, and 0.006%, respectively (Table 4.1). These results indicate that gold is the only economically valuable metal in the occurrence, albeit copper, silver, and arsenic show high anomalies.

At Astaneh gold can be well observed in heavy mineral concentrates by panning of the sediments and alluvia from the surrounding valleys of the Shirmazd mount including Darreh Boleh and Darreh Parmeh. The grain size reaches 1000 microns, whereas the average size is 50-200 microns.

In the hard rock, according to geochemical investigations and field observations, gold is mostly found in Shirmazd mount, Tappeh Khileh and Tappeh Dor as dissemination in the rocks (especially in Shirmazd and its intersecting dykes), and as quartz, quartz-sulfide and arsenopyrite veins and veinlets. Samim Resources (2002) has reported a good correlation between gold and arsenic with up to 9.5 ppm gold content in the ore.

The geochemical investigations of this study demonstrate the highest gold contents in arsenopyrite veins, quartz-sulfide veins, quartz veins, and disseminated host rock, respectively. The gold content reaches 7.32 ppm in the arsenopyrite vein of Kolah Morghun locality while it remains less than 2 ppm in quartz-sulfide and quartz veins and less than half a ppm in disseminated host rock. Although some quartz veins and microgranodiorite samples show rather high contents of gold but there are also some such samples with low to very low amounts of gold.

According to chemical analyses and electron microprobe investigations, gold shows a positive correlation with arsenic, bismuth, silver, selenium and weak positive correlations with tellurium and antimony. The uncorrelated trace elements were found to be W, Sn, and Mo (Tables 4.1 and 4.2). The arsenopyrite contains inclusions of bismuth and bismuth oxides. These inclusions contain the highest concentrations of gold in the minerals of the area (<3400 ppm).

An analysis of tourmaline grains in the tourmaline granite of the area (southeast of Shirmazd, in Darreh Boleh) showed only 11 ppb gold. Nevertheless, Samim Resources has reported fine gold grains from panning of a crushed and grinded sample of this rock unit.

Also analyses of a quartz sample from a quartz vein at Tappeh Dor did not reveal much gold in it (17 ppb), while Hashemi (2002) has reported presence of gold in this part.

Samim Resources (2000) have estimated 36 tons of gold for the Shirmazd stock (120,000m<sup>3</sup> x 300m x 2.5m<sup>3</sup>/ton) with an average gold of 0.4 ppm.

Mineral / Phase	Sample No.	n	Au (ppm)	As (%)	Bi (%)	Te (%)	Sb (%)	Se (%)	Ag (%)	Observations / Remarks
Arsenopyrite	ASN-31-38-40	85	0-130	41-44.5	0-2.25	0-0.097	0-0.082	0-0.2	0-0.072	-----
Bismuth, Bi-oxide Bi-sulfide	ASN-40	3	0-3400	3.1-4.6	62-81	0.008-0.098	0.03-0.16	0.017-0.067	0.1-0.67	Bismuth-sulfide inclusions in arsenopyrite

**Table 4.2** Ranges of concentrations of gold, arsenic, bismuth, tellurium, antimony, selenium, and silver in arsenopyrite and bismuth minerals in the samples examined by electron microprobe analysis.



Sample No.	Description	Location	As ppm	Au ppb	Ag ppm	Cu %	Pb ppm	Zn ppm	S %	Sn %	W ppm	Bi ppm	Sb ppm	Se ppm	Mo ppm	Fe %	Ni ppm	Co ppm	Ba ppm	Th ppm	U ppm	La ppm	Ce ppm	Sc ppm
ASN-16	Au bearing quartz-hematite veinlet	N33° 51.112', E049° 19.272', Shurmazd	9140	1920	1.6	0.124	53	40	<0.001	<0.01	100	103	13	<3	<1	5.71	9	9	470	9.1	<0.5	29.6	29	5
ASN-17	Disseminated granodiorite	N33° 51.112', E049° 19.272', Shurmazd	44.8	243	0.9	0.099	6	42	<0.001	<0.01	3	5	<0.1	<3	2	2.19	9	8	450	8.4	1.8	21.3	39	6.3
ASN-18	Disseminated granodiorite	N33° 51.112', E049° 19.272', Shurmazd	567	463	4.9	0.968	14	119	0.006	<0.01	5	3	1.9	<3	19	3.45	10	14	300	18.2	10.8	88.8	149	5.7
ASN-20	Altered micro granodiorite	N33° 51.019', E049° 19.254', Shurmazd	38.4	<2	0.4	0.041	6	34	0.001	<0.01	26	7	5.5	<3	<1	1.72	14	5	370	14.3	3	72.2	128	5.9
ASN-25	Quartz vein (Tunnel 1)	N33° 50.879', E049° 19.149', southwest of Shurmazd	84.2	1150	1.4	0.028	70	18	0.005	<0.01	9	138	2.1	<3	1	0.41	9	1	<50	0.6	<0.5	4.6	9	0.6
ASN-26	Quartz vein (Tunnel 2)	N33° 51.036', E049° 18.989', southwest of Shurmazd	50.1	3	<0.3	0.012	<3	14	0.001	<0.01	1	8	0.3	<3	<1	0.30	5	<1	<50	-0.2	<0.5	<0.5	<3	0.2
ASN-28	Quartz vein with well-grown crystals	N33° 51.661', E049° 20.472', Molla Yahya hill	454	24	<5	N.A.	N.A.	86	N.A.	<0.01	<1	N.A.	2.5	<3	<1	2.1	79	30	<50	0.4	<0.5	24.2	48	4.9
ASN-31	Arsenopyrite vein	N33° 51.205', E049° 19.359', Kolah Morghoun	212000	7320	<5	N.A.	N.A.	<50	N.A.	<0.04	<20	N.A.	546	<5	<20	19.1	<20	3	<100	-0.9	<0.5	<0.9	<4	0.5
ASN-32	Micro granodiorite with disseminated chalcopyrite and pyrite	N33° 51.205', E049° 19.359', Kolah Morghoun	3620	418	<5	N.A.	N.A.	196	N.A.	<0.04	<1	N.A.	24.8	<3	<3	4.62	<70	25	540	8.8	<0.7	25.8	42	18.7
ASN-34	Tourmaline from tourmaline granite	N33° 50.707', E049° 19.182', Darreh Boleh	357	11	<5	N.A.	N.A.	<50	N.A.	<0.01	<1	N.A.	1.9	<3	<1	1.46	<20	1	<50	5.3	1.5	7.1	15	7.7
ASN-37	Quartz with oxidized pyrite	N33° 50.366', E049° 18.096', Tappeh Dor	284	17	<5	N.A.	N.A.	<50	N.A.	<0.01	3	N.A.	2.7	<3	<1	1.83	<20	10	<50	0.5	<0.5	0.8	<3	1
ASN-38	Arsenopyrite vein	N33° 50.633', E049° 18.006', A'tai digging	269000	2620	52	N.A.	N.A.	<50	N.A.	<0.05	<1	N.A.	294	122	<20	24.5	<50	10	<100	-0.9	<0.5	<0.5	<3	1.4
ASN-40	Arsenopyrite vein	N33° 50.876', E049° 17.905', Tappeh Khaleh	268000	494	<5	N.A.	N.A.	<50	N.A.	<0.05	<1	N.A.	278	<5	<20	24.5	<50	268	<100	-0.9	<1.6	<0.9	<3	0.3

Table 4.1 Trace element analysis of representative ore at Astaneh.

## *Chapter 5*

# **Petrography, mineralogy and geochemistry of the Nezam Abad occurrence**

### **5.1 Introduction**

The Nezam Abad mineralization is composed of five close localities 24km southwest of Astaneh and in the vicinity of Nezam Abad village. The mainly vein type mineralization is generally hosted by Eocene quartz diorite which has intruded into older intrusive rocks and Jurassic schist. In the area, relics of ancient mining activities have been followed by modern exploration and small scale exploitation activities.

Although the Nezam Abad area has been long recognized as a copper-tungsten-bearing region, the current investigations (this study) have revealed considerable contents of gold in the prospect.

In order to integrate the previous geological, mineralogical and geochemical investigations on the Nezam Abad prospect, a suite of 20 representative ore and rock samples was collected from the occurrence for analytical and mineralogical investigations. The isotopic characteristics of the samples are discussed in chapter 6.

### **5.2 Geology of the prospect and petrography of the host rocks**

At Nezam Abad the quartz diorite unit is the major host of the mineralization and is surrounded by hornfels and schist in the south as well as granite and granodiorite in the north, east and west (Figures 5.1 and 5.2a). In the following a petrographic description of the major rock units of the area is presented based on the original investigations and the data presented by Farhadian (1992) and Shamanian (1994). Shamanian (1994) has suggested an I-type, calcalkaline and peraluminous origin for the plutonic rocks of the area, according to geochemical and mineralogical investigations.

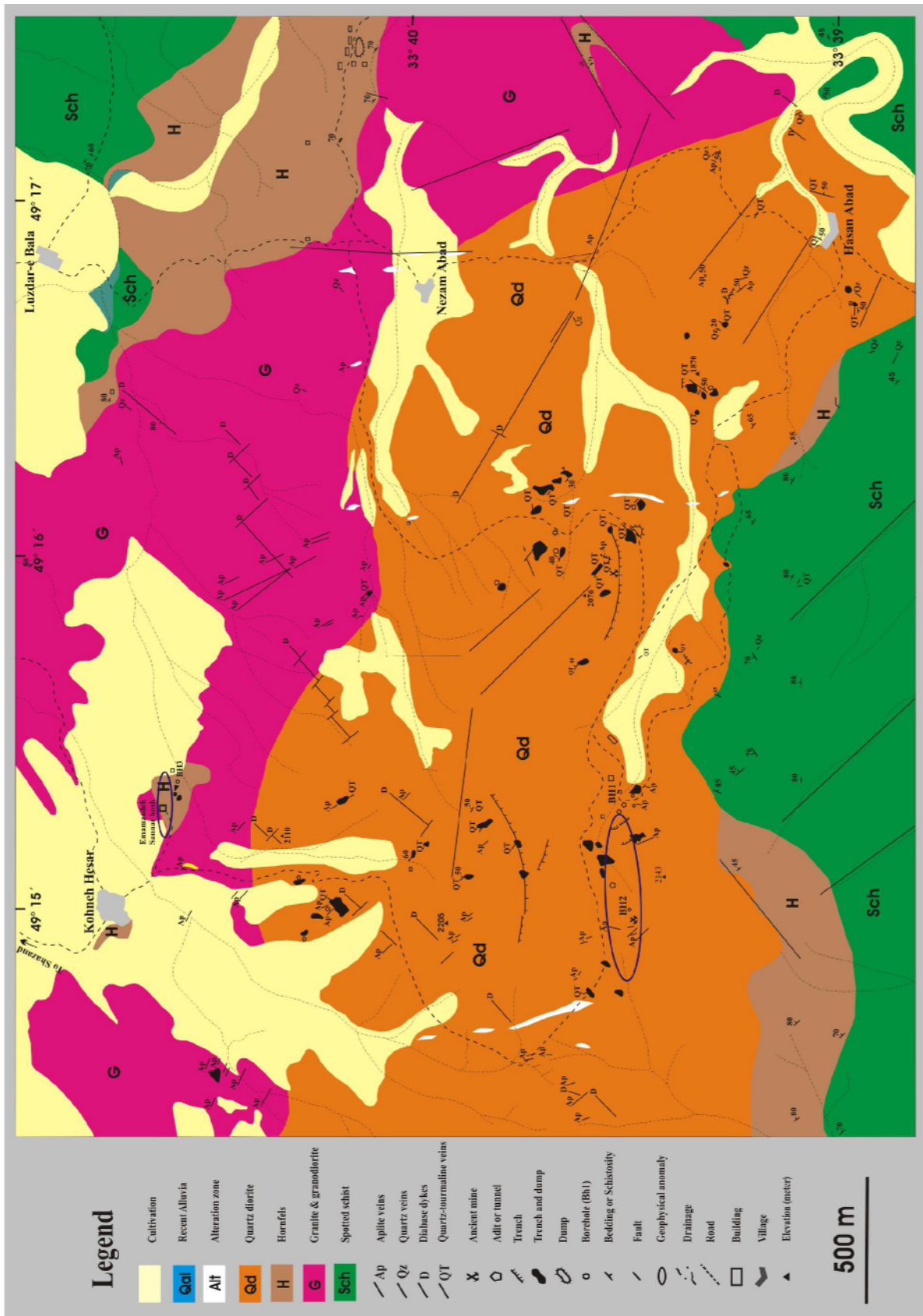


Figure 5.1 Geological map of the Nezam Abad prospect. Modified after Farhadian (1992) and Shamanian (1994).

*Quartz diorite* generally exhibits a granular texture and is comprised of 15-25% quartz, 40-65% plagioclase (oligoclase and andesine), 10-25% mafic minerals including biotite (8-10%) and amphibole (5-15%), and some minor minerals including opaque (Fe-oxides), apatite, zircon, titanite, garnet, and tourmaline. The composition of this unit occasionally tends to be tonalitic. Quartz forms subhedral to anhedral grains which sporadically show undulatory extinction, stretching or cataclastic texture. Plagioclase forms euhedral to subhedral large grains (up to 3mm). Sericite is the main alteration product of plagioclase, but clay minerals and epidote have been produced too. Although the amphibole is mainly hornblende but tremolite and actinolite are present as well. The amphibole grains are mainly anhedral but some euhedral rhombic grains are visible too. The amphibole has been replaced by biotite, chlorite, and occasionally by epidote and prehnite. The primary biotite composes large crystals and lamellas with occasional folding and stretching. Biotite has been altered into chlorite, and in cases epidote and muscovite. The rare alkali feldspar of the rock has been altered into kaolinite and sericite. Tourmaline is normally associated with the veins of quartz-tourmaline and tourmaline and has seemingly occurred due to hydrothermal fluids (Figure 5.2d). The K-Ar dating of this rock unit for biotite and hornblende (by Hasani Pak) has shown 39.54-51.75 Ma age (Early-middle Eocene, Farhadian 1992).

The *granodiorite-granite* rock unit has mainly a granular texture and consists of plagioclase (30-40%), alkali feldspar (orthose), quartz (10-15%), and mafic minerals (10-15%) including biotite and amphibole. Plagioclase forms large euhedral to anhedral crystals which have been altered into sericite and partly into chlorite, clay minerals, and epidote. Orthoclase comprises massive crystals which have been replaced by plagioclase and clay minerals from its rims. Quartz with subhedral to anhedral crystals occasionally shows re-crystallization. Biotite also forms large lamellae partly altered into chlorite, Fe-oxides, epidote or muscovite. Amphibole is mainly composed of hornblende and altered into biotite, epidote and chlorite. Opaque minerals, apatite, zircon, sphene and tourmaline are among the minor minerals of the rock and are mainly seen as inclusions in biotite. Alteration and secondary minerals include sericite (5-15%), clay minerals (5-15%), chlorite (5-20%), and calcite (25-30%). The K-Ar dating of this rock unit (by Hasani Pak) has shown 100.91 Ma age (Albian, Lower Cretaceous, Farhadian 1992).

*Aplitic veins and dykes* are 0.2 to 1 m thick and intersect granodiorite (more frequently) and quartz diorite in different directions (Figure 5.2b). These veins mostly consist of quartz and feldspar, although altered plagioclase (sericite and clay minerals) and scattered altered fine grained biotite (chlorite) are visible as well. The aplitic veins have usually the same trend as the tourmaline veins of the area. Hasani Pak has dated this unit to 25 Ma (Oligocene) by K-Ar (Farhadian 1992).

Some *Diabasic dykes* have intersected quartz diorite and aplitic veins of the area with N 40 and N120 trends. These rocks have doleritic (interstitial) texture and consist mainly of plagioclase grains. The intervals of plagioclase grains are filled with chlorite, epidote, sericite and some amphibole and pyroxene.

### 5.3 Alteration

The alteration in the mining area is not widespread and is mainly vein and fracture controlled. It has its highest intensity in the vicinity of and adjacent to mineralized veins.

The main mineralization-related alteration products in the quartz diorite unit are sericite, clay minerals (kaolinite), chlorite and sporadically calcite and epidote. Also tourmalinization is manifested as very frequent veinlets and patches in the host rock, especially adjacent to quartz-



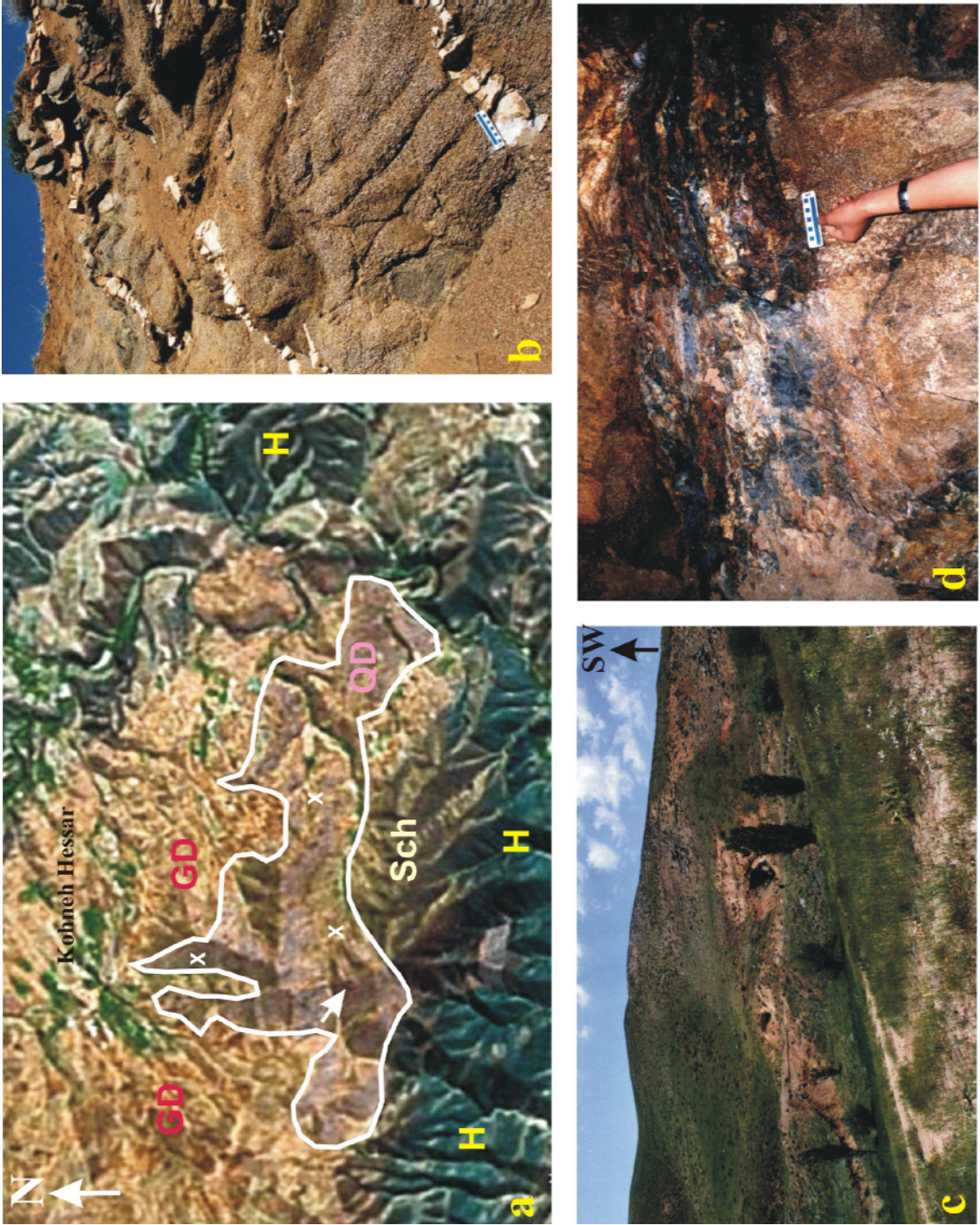


**Figure 5.2** a) Satellite photo-map of the study area (from Google Earth), the quartz diorite unit is easily recognizable, b) The host rock at Jafar Abad locality which has been intersected by aplitic veins, c) An overview of the Nezam Abad tunnels No.1 and No. 2 at the end of Gorg Darreh Valley, d) A mineralized quartz-tourmaline vein in the tunnel No.1.

tourmaline and tourmaline veins. Sericite has mainly formed by plagioclase alteration and composes 5-35% of the rock volume. Plagioclase has altered into clay minerals (5-15%) and epidote (<5%) as well. Chlorite is a product of the alteration of mafic minerals and composes up to 5% of the rock volume. Calcite has been observed in minor amounts (<2%). The tectonic activities which have caused a rather extensive system of fractures in the rock have strengthened the alteration effect.

## 5.4 Mineralization

Mineralization at Nezam Abad is exposed in a moderate topography and has occurred in the form of quartz-tourmaline, quartz-tourmaline-sulfide and quartz-sulfide veins and veinlets in a rather large area (4.5 x 5.5 km<sup>2</sup>) mainly in the north and west of the valley of Gorg Darreh as well as localities of Jafar Abad, Fizuneh, Hasan Abad and Revesht (Figures 5.2c and 5.2d). The basically vertical mineralized veins are fracture-controlled and show mainly N140 and sporadically N40 and N70 trends. Some of veins show 40-60 SE dip. The veins are 0.5 to 2m thick and several meters long. Dissemination, impregnation and networks of thin quartz veinlets and veins are visible in the vein selvages and adjacent parts. There are also some barren quartz-tourmaline and quartz veins and veinlets in the prospect which are generally thinner than fertile ones. The barren veins have, in some places, intersected the mineralized veins. The main visible sulfide minerals of the veins in hand specimen scale are arsenopyrite, chalcopyrite and pyrite which have often been thoroughly oxidized. The sulfide content of the ore in quartz and quartz-tourmaline veins is generally less than 2-3 volume percent. Also small grains of scheelite are traceable by UV light in the field. Panning of the soil in the valleys and streams of the prospect area reveals a considerable amount of scheelite.

In the following is a brief description of mining relics, according to field observations and Farhadian's report (1992), and is followed by a list of the observed minerals.

### 5.4.1 Ancient mining relics

The ancient diggings at Nezam Abad are mainly located at the end of the Gorg Darreh valley, on the Kalagh Zee heights and on the top of tunnel No.1. These diggings are in the form of conical depressions, similar to the diggings at Deh Hosein, and are up to 50 m in diameter and 10 m deep and have a general E-W trend. Scattered unglazed pottery shards have been observed, in the dump of these diggings. It is possible that the ancient miners have exploited this area for copper and perhaps tin. There are also remains of a collapsed tunnel in the north of Gorg Darreh in Agh Gineh height. Possibly the (modern) tunnel No.1 of Nezam Abad is a result of widening the ancient workings.

### 5.4.2 Modern mining and exploration

The modern mining relics, which mainly belong to the early 20<sup>th</sup> century, include three tunnels at the end of Gorg Darreh, and the tunnels of Jafar Abad, Hasan Abad, Fizuneh, and Revesht. Several smaller tunnels (Seyyed Ali in NE of Gorg Darreh, end of Ghouzlar valley, and Kahlik Boulaghi valley), soundings, trenches, and boreholes have also been dug during the last decades (Figure 5.1). A brief description of the modern mining relics is presented in the following.

#### *Gorg Darreh tunnels*

*Tunnel No. 1* or the main tunnel (N33° 39' 15.5'', E 49° 15' 43'', entrance) has N60 trend and cuts the mineralized veins perpendicularly. It has six adits from which the first one cuts a 1.5 m quartz-tourmaline vein (Figure 5.2c).

*Tunnel No. 2* is parallel to the tunnel No. 1 and has several adits to its north. It connects to the tunnel No.1 via its second adit. The first adit is connected to the first and third tunnels via a vertical shaft.

*Tunnel No. 3* is located 18 m lower than the above mentioned tunnels and has three adits, each several meters long. These three tunnels have been exploiting tunnels.

#### *Jafar Abad tunnel*

Jafar Abad hill (N33° 39' 56'', E49° 15' 22'') is located in the southwest of Kohneh Hesar village. It contains three exploration-exploitation tunnels. One of them on the top of the hill has N-S trend and follows a quartz-tourmaline vein to the north. Two other tunnels are small, one contains some veinlets and the other one which has been dug in the alluvia does not show any trace of mineralization.

#### *Hasan Abad tunnel*

In the north of Hasan Abad village there is one two-part tunnel. One part is 7 m long and goes to the north and the other part with 20 m length goes to the east. The mineralized vein has N40E trend with 30 NW dip. There is a dump of mining at the entrance of this tunnel. There is also a 2m exploration tunnel along the mineralized vein to the north in the west of Hasan Abad village.

#### *Fizuneh tunnel*

Fizuneh tunnel (N33° 40' 43'', E49° 15' 03'') is located in the north of Kohneh Hesar village. There are two small exploration tunnels in this area with considerable amount of dump.

#### *Revesht tunnel*

Revesht tunnel (N33° 41' 55'', E49° 10' 32'') is located about 7 km northwest of Gorg Darreh tunnels. There are several 5-10m tunnels in this locality. The quartz-tourmaline veins are up to 70cm wide and show the following trends and dips N30, 40SE and N70, 55NW.

#### *Trenches and boreholes*

Several exploration trenches and soundings have been dug in the north and west of Gorg Darreh, and north of Hasan Abad village.

During 1990-1991, three boreholes have been dug by the Geological Survey of Iran in an area of geophysical anomalies (Farhadian 1992). Unfortunately, no core of these boreholes was available to the author.

Borehole No.1 (BH1), which was dug in 1990, is located in front of the tunnel No.1 with 45° dip and 209 m depth. This is almost perpendicular to the veins with N140, 80NE trend.

BH2, 1991 is located in Kalagh Zee height (west of Gorg Darreh), 450m west of BH1 and has 60°SW dip and 255 m depth.

BH3, 1991 is located beside the Sannar Kosh shrine with 60°N dip and 205 m depth.

### **5.4.3 Geophysical investigations**

In 1983 the Geological Survey of Iran (Nicolaus et al. 1983) has carried out an induced polarization (IP) investigation in an area of 3 km<sup>2</sup>. In the course of this study, two major anomalies were revealed; 1- west of Gorg Darreh 2- Beside the Sannar Kosh shrine. According to the borehole results the latter anomaly was mainly due to the presence of graphite in lower layers although some veinlets of scheelite were observed as well. Some minor anomalies have been also reported on different parts of quartz diorite.

#### 5.4.4 Ore minerals

Some 20 ore minerals have been identified at Nezam Abad by this study (by optical microscopy and electron microprobe investigations). Those and the ones found by Farhadian (1992, 1999) and Shamanian (1994) are described below.

*Scheelite* ( $\text{CaWO}_4$ ) is the only recognized tungsten mineral in the Nezam Abad mining area. It normally occurs as scattered anhedral grains and small patches in quartz-tourmaline veins and veinlets separate from sulfide minerals assemblage. The abundance of scheelite grains in quartz is more than in tourmaline (Farhadian 1992). Farhadian (1992) has reported also rare cases in which chalcopyrite occurs beside scheelite. Probably the scheelite has occurred simultaneously with quartz and tourmaline in the first stage of the mineralization. It seems that the required Ca for the formation of scheelite has been derived from plagioclase due to remobilization of Ca during alteration. In hand specimen scale it is difficult to recognize scheelite in Nezam Abad. It is normally similar to quartz, small in size (normally  $<1$  cm) and light blue in color under the light of UV lamp.

*Cassiterite* has been reported by Farhadian (1992) from the borehole BH1 samples of 35m depth. It has been observed as subhedral inclusions in chalcopyrite. Karimi-Bafghi and Khoii (1365) have also reported cassiterite and stannite from some samples.

*Arsenopyrite* is a common mineral in the mineralization. It occurs either as individual euhedral to subhedral grains ( $<200$   $\mu\text{m}$ ) or as massive grains with cataclastic texture (Figures 5.3a, b and 5.4c). Arsenopyrite has been altered into scorodite from its rims and fractures. Arsenopyrite contains inclusions of pyrrhotite ( $<50\mu\text{m}$ ), native bismuth ( $<50\mu\text{m}$ ), and maldonite ( $<25\mu\text{m}$ ). Fractures of arsenopyrite have often been filled by chalcopyrite while in some cases by sphalerite. Also inclusions of euhedral arsenopyrite ( $<25\mu\text{m}$ ) is observed in chalcopyrite (Figure 5.3d). A minor portion of arsenopyrite also occurs as small veinlets crosscutting other minerals or with open space filling texture. This type of arsenopyrite is probably a secondary one which possibly has occurred at the final phase of mineralization by remobilization of primary ones. In one case a euhedral grain of arsenopyrite has been replaced by covellite from its rims (Figure 5.3b). In this case, according to electron microprobe investigations, both arsenopyrite and covellite show high contents of gold.

*Chalcopyrite* is a widespread mineral at Nezam Abad and occurs as massive, individual anhedral scattered grains (disseminated), open space filling or as intersecting lean veinlets. It contains inclusions of pyrrhotite ( $<120\mu\text{m}$ ), arsenopyrite ( $<25$   $\mu\text{m}$ ), euhedral to subhedral native bismuth ( $<15$   $\mu\text{m}$ ), marcasite, pyrite and sphalerite (Figures 5.3c, d, e). In cases arsenopyrite veinlets fill the fractures of chalcopyrite or pyrrhotite. The massive chalcopyrite has cataclastic textures with jagged rims and has been altered into covellite and Fe-oxides. Farhadian (1992) has reported also bird's eye texture in chalcopyrite.

*Pyrite* occurs in two generations; primary and secondary. The primary pyrite has occurred in the early phases of mineralization in minor amounts. It usually occurs as euhedral inclusions in pyrrhotite or chalcopyrite and is sporadically along with arsenopyrite. Pyrite has been altered into Fe oxides and marcasite. Inclusions of this pyrite ( $<100\mu\text{m}$ ) are present in chalcopyrite.

The secondary pyrite has derived from pyrrhotite. It is anhedral and shows reactive rims with pyrrhotite. Pyrrhotite has filled its fractures. Figure 5.3e shows a veinlet of pyrite II in chalcopyrite. According to electron micro probe investigations pyrite is occasionally arsenic-bearing.

*Pyrrhotite* is widespread in the occurrence. It occurs as subhedral to anhedral grains which together form larger aggregations. Pyrrhotite is observed along with chalcopyrite and pyrite and is present as inclusions in chalcopyrite ( $<120\mu\text{m}$ ) and arsenopyrite ( $<50\mu\text{m}$ ). It also fills open spaces which occur as small veinlets in other minerals including arsenopyrite.



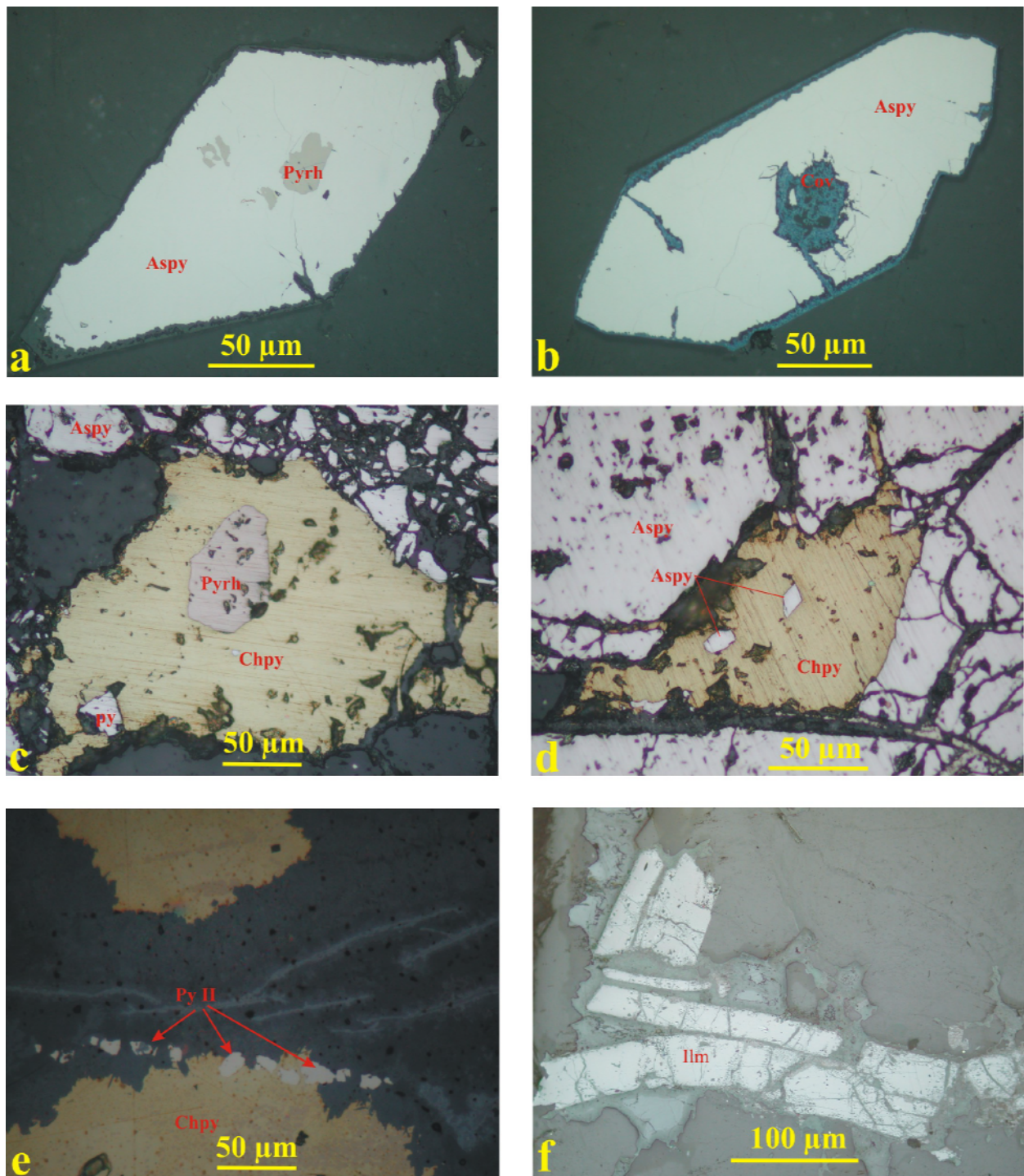


**Figure 5.3** **a)** Inclusion of pyrrhotite in a euhedral arsenopyrite grain, **b)** A euhedral arsenopyrite grain which is replacing by covellite from its rims and fractures, **c)** Inclusions of pyrrhotite and pyrite in chalcopyrite, **d)** Inclusions of arsenopyrite in chalcopyrite, **e)** A veinlet of secondary pyrite in chalcopyrite, **f)** Illmenite subhedral grain in quartz.

Pyrrhotite occasionally has been altered into secondary pyrite and marcasite, the latter is visible as small inclusions in pyrrhotite. Shamanian (1994) has reported corrugated lamellae textures which imply the impact of tectonic movements after mineralization.

*Sphalerite* is a scarce mineral in the occurrence. The anhedral grains of sphalerite have usually occurred as inclusions in chalcopyrite (sporadically along with native bismuth, Figure 5.4a). It is also observed with open space filling texture in chalcopyrite.

*Antimonite* has been reported by Farhadian (1999) as very rare anhedral grains in fractures of arsenopyrite and pyrite.

*Bismuth minerals* show a rather vast compositional variety in the mineralization. The recognized Bi-bearing minerals include native bismuth, rooseveltite ( $\text{BiAsO}_4$ ), maldonite ( $\text{Au}_2\text{Bi}$ ), bismuthinite ( $\text{Bi}_2\text{S}_3$ ), joseite [ $\text{Bi}_4(\text{S},\text{Te})_3$ ], makovickyite ( $\text{Ag}_{1.5}\text{Bi}_{5.5}\text{S}_9$ ), baksanite ( $\text{Bi}_6\text{Te}_2\text{S}_3$ ), and some unidentified Bi-As and Bi oxides. The primary bismuth minerals normally occur as fine grained inclusions in other minerals, especially arsenopyrite (Figures 5.4b, c, d), while Bi-As and Bi oxides often fill the open spaces and fractures of the other minerals (Figures 5.4e, f). Native bismuth occurs as euhedral to subhedral disseminated grains ( $<30\mu\text{m}$ ) in arsenopyrite but it is also present as inclusions in chalcopyrite and quartz. Also bismuthinite occurs as euhedral crystals in arsenopyrite. Small inclusions of maldonite have been observed in arsenopyrite too. Baksanite has been observed as inclusions ( $<120\mu\text{m}$ ) in pyrite, arsenopyrite and/or quartz. Presence of maldonite, joseite, bismuthinite and other bismuth minerals which typically occur in high temperature hydrothermal auriferous quartz veins worldwide (extracted after Rahmdor 1980), suggests a high temperature mineralizing fluid for the Nezam Abad mineralization.

*Gold* occurs in invisible form at Nezam Abad. Despite high contents of gold revealed by geochemistry, examination of several thin polished and polished sections of the ore samples by means of high-resolution optical microscopy and electron microprobe failed to reveal any native gold. The scarcity of visible gold, coupled with the high concentrations of gold in the mineralized rocks at Nezam Abad, suggests the occurrence of “invisible gold” (see section 5.6).

*Marcasite* is visible as orthorhombic grains in pyrrhotite and sometimes in pyrite due to alteration of pyrrhotite and pyrite. It is also present as scattered euhedral to subhedral grains which are intersecting chalcopyrite veinlets or as inclusions in chalcopyrite. Marcasite has been replaced by Fe-oxides.

*Ilmenite* is present as euhedral grains which have been altered into rutile from their rims (Figure 5.3f). It is also present as small subhedral grains. Ilmenite may fill fractures of the rock forming small veinlets.

The euhedral *rutile* grains are rare and usually occur as inclusions in quartz and tourmaline.

*Schneiderhöhnite* ( $\text{Fe}^{++}\text{Fe}^{+++}3\text{As}^{+++}5\text{O}_{13}$ ), *pitticite* ( $\text{Fe},\text{AsO}_4,\text{SO}_4, \text{H}_2\text{O}$ ), and *wurtzite* [ $(\text{Zn}, \text{Fe})\text{S}$ ] are the minerals which occur in minor amounts at Nezam Abad and have only been detected by electron microprobe investigations.

*Supergene minerals* of covellite, scorodite, and goethite are a result of supergene alteration of chalcopyrite, arsenopyrite, and pyrite and pyrrhotite, respectively. Also malachite, azurite, and calcite are among the minerals of the occurrence.

Farhadian (1999) has also reported rare grains of chalcopyrrhotite (cubanite) normally as inclusions in chalcopyrite. Shamanian (1994) has reported melnikovite as porous aggregates and sometimes with colloform texture. It has occurred by hypogene alteration of pyrrhotite due to increase in S fugacity. Melnikovite occurs in low temperatures and is usually with marcasite. It has recognizable reactive rims with pyrrhotite.

### 5.5 Paragenetic sequence

The mineralization at Nezam Abad has an open space filling nature. The fertile hydrothermal fluids have filled faults and fractures of the host rock which occurred due to tectonic movements.

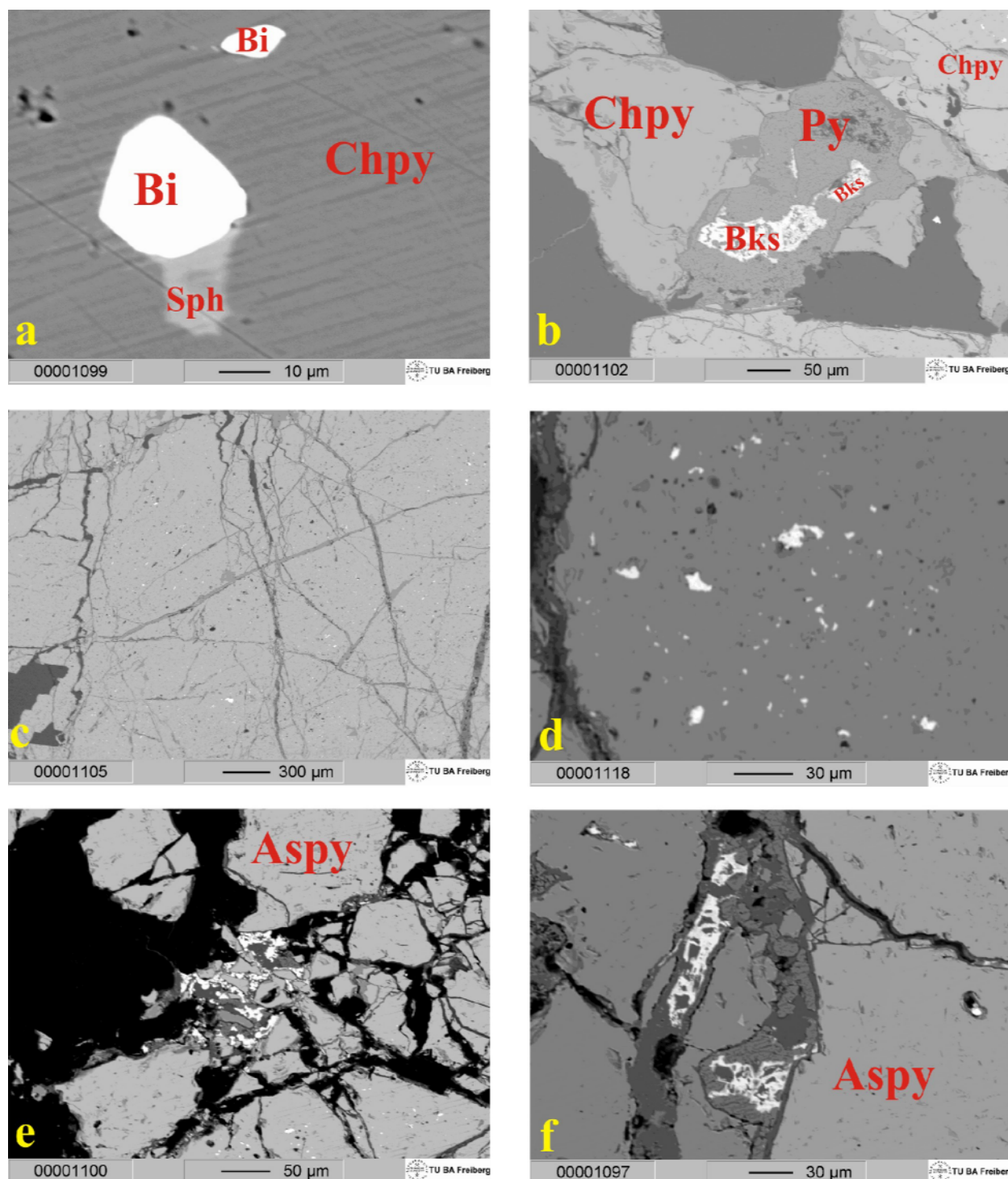


**Figure 5.4** Back scattered electron micrographs of **a)** Inclusions of native bismuth and sphalerite in chalcopyrite, **b)** Inclusions of baksanite in pyrite, and pyrite in chalcopyrite, **c)** Cataclastic texture of massive arsenopyrite with numerous inclusions of native bismuth and bismuth minerals, **d)** Inclusions of maldonite in arsenopyrite, **e** and **f)** Veinlets of bismuth oxides which have filled the fractures of arsenopyrite.



Three major mineralization phases (early, main, and late) have been recognized in the Nezam Abad occurrence.

#### Early hydrothermal assemblage

This assemblage comprises of quartz, tourmaline (according to XRD result performed by Farhadian (1992), *dravite*:  $\text{NaMg}_3(\text{Al, Fe})(\text{Si}_6\text{O}_{18})(\text{BO}_3)_3(\text{OH, F})_4$ ), scheelite and cassiterite. The fluid of this stage is characterized by a low sulfur fugacity and high magnesium-boron content. Probably tourmaline and quartz were the earliest minerals which were accompanied with scheelite and cassiterite.

#### Main hydrothermal assemblage

This assemblage is marked by high temperature, abundance of metallic ions and low to intermediate sulfur fugacity which has followed by precipitation of a rather wide range of sulfides and sulfosalts including arsenopyrite, pyrrhotite, pyrite, bismuth minerals and chalcopyrite. Quartz precipitation has continued in this stage while tourmaline deposition has been reduced. The major amount of gold in the mineralization has occurred in this assemblage along with arsenopyrite and other sulfides and sulfosalts. An important part of alteration of the host rock has occurred during this stage.

#### Late hydrothermal assemblage

This stage is characterized by an increase in sulfur fugacity along with decrease of temperature and the volume of metallic ions. The additional sulfur of the fluid has stormed the previous minerals and resulted in secondary sulfide minerals such as arsenopyrite II, Pyrite II and marcasite.

#### Weathering assemblage

Oxidation of sulfide minerals including pyrite, chalcopyrite, and arsenopyrite formed oxides of iron and arsenic and has created malachite, azurite, and Fe-oxides.

### **5.6 Metal associations and distributions at Nezam Abad**

According to geochemical investigations performed on the ore by Farhadian (1992, 1999) the highest contents of tungsten, tin, arsenic, gold, silver, Bismuth and copper in the prospect of Nezam Abad reach up to 3.37%, 0.87%, 2.9%, 0.3 ppm, 22 ppm, 548 ppm and 4.72%, respectively. These results have been obtained from the core samples of different depths and have been analyzed at the Geological Survey of Iran and the Northwest Geological Research Institute of China (the analyzing method has not been specified). Farhadian has reported that the W/Sn ratio increases with depth.

Also Jahangiri (1999) has reported up to 0.44% tungsten, 11903 ppm tin, 900 ppb gold and 2% copper from the samples taken from tunnel No. 1 based on the analyses results conducted at the Geological Survey of Iran by means of atomic emission spectrometry and atomic absorption analyses. He has also reported 1900 ppb gold from the Revesht locality.

According to Jahangiri (1999) the average grade of tungsten in different adits of tunnel No.1 ranges from 30 to 1467 ppm while this average grade differs from 559 to 750 ppm for tin. Jahangiri (1999) and Haj Zein Ali (1992) have estimated 8000 tons of 0.22% grade tungsten ore for the mineralization of Nezam Abad (only for the Gorg Darreh tunnels).

Mallak Pour et al. (1993) analyzed 145 host rock (quartz diorite) samples of the mineralization by the AA method. These samples were taken from the surface (95 samples) and tunnel No.1 (50 samples). Their investigations revealed the following values for some trace elements in the

Sample No.	Description	Location	As ppm	Au ppb	Ag ppm	Cu %	Pb ppm	Zn ppm	S %	Sn %	V ppm	Bi ppm	Sb ppm	Mo ppm	Fe %	Ni ppm	Co ppm	Ba ppm	Th ppm	U ppm	La ppm	Ce ppm	Sc ppm	Al %	Na %	K %	Ca %
<b>NNZ-3</b>	Ore (arsenopyrite, chalcopyrite, pyrite), quartz-tourmaline vein	N33° 39' 56.6", E49° 15' 22", Jafar Abad	3280	1243	56.8	10	113	273	0.443	<0.01	45	226	28.5	<3	11.5	61	11	<50	9.0	42.0	7.5	<3	19.4	2.20	0.52	-0.01	0.36
<b>NNZ-9</b>	Ore (arsenopyrite, chalcopyrite, pyrite), quartz-tourmaline vein	N33° 41' 55.3", E49° 10' 32.7", Revesht	125	425	24	1.79	23	134	0.398	<0.01	2	70	4.4	6	12	17.1	205	<50	<0.2	15	1.5	3	0.7	0.60	0.02	0.03	0.19
<b>NNZ-12</b>	Ore (chalcopyrite, pyrite), quartz-tourmaline vein	N33° 39.261', E49° 15.476", ancient digging of Nezam Abad	3540	66	9.2	4.49	<3	17	0.026	<0.01	849	128	18	<3	4.22	<20	7	<50	4.1	6.8	4.1	<3	15.0	3.86	0.66	0.01	0.36
<b>NNZ-16</b>	Ore, quartz-tourmaline vein	Tunnel No.1 of Nezam Abad	2447	94	2.9	0.242	6	63	0.1	<0.01	3257	416	13.4	<3	6.35	<21	11	<50	<0.2	<0.5	1.7	<3	14.0	3.70	0.46	0.06	0.49
<b>NNZ-21</b>	Ore, quartz-tourmaline vein	Tunnel No.1 of Nezam Abad	19100	<2	5.9	0.056	<3	51	0.307	<0.01	78	68	11.3	<3	5.22	37	34	<50	<0.2	<0.5	-0.5	<3	14.9	3.91	0.74	-0.01	0.38
<b>NNZ-27</b>	Ore (arsenopyrite, pyrite), quartz vein	N33° 40.722', E 049° 15.045' Firuzeh	278000	36200	<20	N.A.	N.A.	<100	N.A.	0.01	720	N.A.	270	<10	24.6	<1000	5740	<200	<15	<0.5	-1.7	<5	0.6	N.A.	<1.38	N.A.	<5
<b>NNZ-30</b>	Quartz-tourmaline vein	Tunnel No.1 of Nezam Abad	282	10	<5	N.A.	N.A.	<50	N.A.	<0.01	<1	N.A.	<0.1	<3	0.06	<20	2	<50	<0.2	<0.5	-0.5	<3	<0.1	N.A.	<0.01	N.A.	<1
<b>PA-30</b>	Pegmatite vein (arsenopyrite)	N33° 48' 02", E49° 07' 41", north of Deh Moulā	419000	<100	<5	N.A.	N.A.	<50	N.A.	<0.03	<20	N.A.	184	<3	25.2	<20	1	<50	<0.4	<0.5	<1	<3	<0.1	0.13	<0.03	0.02	<1

Table 5.1 Trace element analysis of representative ore at Nezam Abad (N.A.=Not Analyzed).

host rock; 0.7 to 6.5 ppb gold (average 1.38 ppb), 1.3 to 33 ppm tungsten (average 5.38 ppm), 0.1 to 13 ppm bismuth (average 1.31 ppm), 1.7 to 346 arsenic (average 64.73ppm), 0.04 to 0.41 silver (average 0.09 ppm), and 10 to 790 copper (average 118.25 ppm). A comparison of the aforementioned values with the average values of the elements in the quartz diorite and other intermediate igneous rocks worldwide (Wedepohl et al. 1978) indicates a significant enrichment of arsenic and tin, a moderate enrichment of bismuth and tungsten and a moderate depletion of gold in the quartz diorite of the Nezam Abad prospect.

During this study, 7 ore samples were analyzed by NAA at Actlabs Canada for gold and trace elements by programs Au+48 and Au+34 from which 3 show high contents of gold. The Au, Cu, W and, As amounts of veins are as much as 36.2ppm, 10%, 3257ppm, and 27.8% for Nezam Abad (Table 5.1). Tin does not show high contents (<0.1%) in the measured samples. The highest gold concentrations at Nezam Abad were found in samples containing visible arsenopyrite and pyrite.

The electron microprobe analyses revealed that arsenopyrite, pyrrhotite, covellite, native bismuth, bismuthinite, schneiderhöhnite and maldonite are the main gold-bearing minerals in the prospect (Table 5.2). Due to its abundance and typically high gold content, arsenopyrite is the most important gold-bearing mineral at Nezam Abad. It contains up to 580 ppm gold which shows a positive correlation with bismuth, selenium, nickel and cobalt. Pyrrhotite, which is a widespread mineral in the area, shows high contents of gold as well (800 ppm). Covellite that in some cases forms a rim around the euhedral arsenopyrite grains indicates up to 450 ppm gold. Native bismuth and other bismuth-bearing minerals enclosed by arsenopyrite contain some amounts of arsenic (up to 3%) and display high contents of gold (340 ppm). The rare schneiderhöhnite shows the highest contents of gold (1360 ppm) after maldonite. The results of electron microprobe analyses of these minerals for trace gold are summarized in Table 5.3. The above mentioned results corroborate the importance of the already reported gold contents (Farhadian 1992, 1999 and Jahangiri 1999) of the ore at Nezam Abad occurrence.

Mineral / Phase	Sample No.	n	Au ppm	Ag %	As %	Bi %	Te %	Sb %	Se %	Ni %	Co %
Arsenopyrite	NNZ-21-27	18	0-580	0-0.04	45-49	0-2	0-0.0567	0.03-0.07	0.55	0-1.28	0.05-1.4
Covellite	NNZ-21	2	22-460	0	0.3-0.5	0	0-2.85	0-0.02	0-0.01	0.02	---
Pyrrhotite	NNZ-21	1	800	0	0	0	0.024	0	0	0.01	---
Schneiderhöhnite	NNZ-27	1	1360	0.04	43.2	0.04	0	0	0.23	0.05	0.87
Bismuth minerals	NNZ-27	3	10-340	0-0.2	0.7-3	69-100	0-0.64	0-0.09	0-0.13	0-0.45	0-0.4

**Table 5.2** Ranges of concentrations of gold, silver, arsenic, bismuth, tellurium, antimony, selenium, nickel and cobalt in arsenopyrite, covellite, pyrrhotite, schneiderhöhnite and bismuth minerals in the samples examined by electron microprobe analysis.

According to both bulk chemical analyses and electron microprobe investigations, gold shows a strong positive correlation with arsenic, bismuth, selenium and a weakly positive correlation with tellurium, nickel, cobalt, silver and tungsten (Tables 5.1 and 5.2). Silver and copper indicate a rather good correlation with each other. Apart from gold, copper, tungsten and perhaps tin show to some extent economic value at Nezam Abad.

## 5.7 Mineralization in pegmatite

So far no direct relationship was observed between pegmatite veins of the Astaneh-Sarband area and the Deh Hosein, Astaneh and Nezam Abad occurrences. The pegmatite veins with general NW-SE trend are mainly located in the western part of the study area. These veins are commonly composed of large crystals of quartz, muscovite, feldspar and tourmaline with occasional occurrence of garnet and some ore minerals including arsenopyrite, pyrite and hematite.

In order to examine the possible occurrence of gold in such pegmatite veins, a sample of arsenopyrite from a pegmatite vein situated in north of Deh Moula village ( $33^{\circ} 48' 02''$ ,  $49^{\circ} 07' 41''$ ) was analyzed by NAA. Contrary to all of the arsenopyrite samples of the studied prospects which show high contents of gold, this sample has only a low content ( $<100\text{ppb}$ ) of gold (Table 5.1).

## *Chapter 6*

# **Isotope studies and geothermometry**

### **6.1 Introduction**

Stable isotopes have become an integral part of studies of ore deposits. The determination of the light isotopes H, C, O, and S can provide information about the various origins of ore fluids, about temperatures of mineralization, and about the physico-chemical conditions of mineral deposition (Hoefs 2004).

Several ore and rock samples from the occurrences in the Astaneh-Sarband area (Deh Hosein, Astaneh and Nezam Abad) were analyzed for stable (oxygen, sulphur, and lead) and radiogenic (Rb-Sr) isotope values, in order to better understand the nature and origin of the mineralizing fluids, the formation conditions, the age of host rocks and eventually the mineralizations, and to detect any possible relationship between the mineralizing fluids of the occurrences. In the following chapter the analytical techniques and the results are discussed.

### **6.2 Sulfur isotope analysis**

Sulfur is widely distributed in the lithosphere, biosphere, hydrosphere, and atmosphere of the Earth. Sulfur also occurs in the reduced form as sulfide in metallic mineral deposits associated with igneous, sedimentary, and metamorphic rocks. For this reason, the isotopic composition of S is especially useful in the study of sulfide ore deposits (Faure and Mensing 2005).

Sulfur ( $Z=16$ ) has four stable isotopes whose approximate abundances and masses are  $^{32}\text{S}$  95.02%, 31.972070 amu (atomic mass unit),  $^{33}\text{S}$  0.75%, 32.971456 amu,  $^{34}\text{S}$  4.21%, 33.967866 amu, and  $^{36}\text{S}$  0.02%, 35.967080 amu. The mass of  $^{34}\text{S}$  is 6.2% greater than that of  $^{32}\text{S}$ , which is sufficient to cause extensive mass-dependent isotope fractionation (Faure and Mensing 2005). The isotopic composition of a hydrothermal sulfide is determined by a number of factors such as: (1) temperature of deposition, (2) isotopic composition of the hydrothermal fluid from which the mineral is deposited, (3) chemical composition of the dissolved element species

including pH and  $fO_2$  at the time of mineralization, and (4) relative amount of the mineral deposited from the fluid (Hoefs 2004).

The sulfur isotopic composition of 10 bulk representative samples and mineral separates from the occurrences of Deh Hosein, Astaneh and Nezam Abad has been determined in order to characterize the sulfur source in the hydrothermal fluids responsible for the mineralization. These isotopic ratios were determined for the most abundant sulfide minerals of the area including chalcopyrite, galena, arsenopyrite, and pyrite.

### 6.2.1 Method

The isotope composition of S is commonly measured as  $SO_2$  with a gas mass spectrometer equipped with double collectors. Sulfides are converted to  $SO_2$  by reactions with  $CuO$ ,  $V_2O_5$ , or  $O_2$  at temperatures of up to  $1000^\circ C$  (Faure and Mensing 2005).

The sulfide minerals of the study area were handpicked and were then crushed and powdered to  $<63 \mu m$  in an agate mortar.  $\delta^{34}S$  analyses of sulfides were performed by means of combustion with mass spectrometry (C-IRMS) using a Carlo Erba EA 1110 elemental analyzer connected to a Finnigan MAT Delta plus mass spectrometer via a Finnigan MAT Conflo II split interface (Gieseemann et al. 1994) at the isotope laboratory of the Institute of Mineralogy in Freiberg. The reproducibility of the  $\delta^{34}S$  analysis is better than  $\pm 0.2 \text{ ‰}$ . All samples were double analyzed. For routine measurements an internal standard ( $SO_2$ ) was used, which is calibrated against the international IAEA-standard NBS-127 (barium sulfate). Isotope values are reported to the international standard V-CDT.

### 6.2.2 Results

The average  $\delta^{34}S$  concentration of duplicate measurements for all analyses is given in Table 6.1 together with a short petrographic description of the samples.  $\delta^{34}S$  in samples from the Deh Hosein vary between  $-5.6$  and  $0 \text{ ‰}$  (avg.  $-2.36 \text{ ‰}$ ,  $n = 5$ ) for bulk galena, pyrite, chalcopyrite, and arsenopyrite. The values from the Astaneh prospect have a little higher isotope ratios, between  $-0.5$  and  $+1.8 \text{ ‰}$  (avg.  $+0.9 \text{ ‰}$ ,  $n = 3$ ) for bulk arsenopyrite. At Nezam Abad the  $\delta^{34}S$  values have the highest ratios in the area and range between  $+1.2$  and  $+4 \text{ ‰}$  (avg.  $+2.6 \text{ ‰}$ ,  $n = 2$ ).

The  $\delta^{34}S$  values of the mineral occurrences show a rather narrow range (from  $-5.6$  to  $4$  with an average of  $-0.93 \text{ ‰}$ ) and therefore a fairly specific origin for them which match the magmatic sulfur values. A comparison of the  $\delta^{34}S$  values of the sulfide ores of the Astaneh-Sarband area with the same values for sulfur-bearing minerals in some hydrothermal deposits is presented in Figure 6.1a. These values are compatible with a magmatic hydrothermal source, especially because the majority of  $\delta^{34}S$ -values of sulfide minerals in magmatic hydrothermal deposits fall between  $-3$  and  $1 \text{ ‰}$  (Field and Gustafson 1976; Shelton and Rye 1982; Hoefs 2004). These values are also comparable with values reported from intrusion related gold deposits in Alaska and other deposits of this type around the world (Boundtzen and Miller 1997; McCoy et al. 1997; Rombach and Newberry 2001).

Calculated sulfate-sulfide temperatures of magmatic hydrothermal deposits, for conditions of complete isotope equilibrium, are typically between  $450$  and  $600^\circ C$  (Ohmoto and Rye 1979) and agree well with temperatures estimated from other methods. Thus, the sulfur isotope data and temperatures support a magmatic origin of the sulfur in magmatic hydrothermal deposits (Hoefs 2004). It should be mentioned that using these criteria to determine the source of S in sulfide deposits and distinguish ore deposits of different origins is not always effective because of extensive overlap of  $\delta^{34}S$  values of different types of deposits. Also the  $\delta^{34}S$  values of



individual minerals do not necessarily reflect the isotopic composition of S in the fluid from which they formed because they may also be controlled by the pH and the oxygen fugacity (Faure and Mensing 2005).

Sample No.	Location	Description	$\delta^{34}\text{S}\text{‰}$ CDT
DHN-1B	N33° 45.406', E049° 18.993', Digging east of the prospect	Galena	-5.6
DHN-7A	39s 0343430, UTM 3737939, Ghara Ghouii	Pyrite + Chalcopyrite	-2
DHN-10B	39s 0342443, UTM 3737013, Ahmad Jigi I	Chalcopyrite + Pyrite	-3.8
DHN-38	39s 0342546, UTM 3736831, Ahmad Jigi II	Arsenopyrite	0
DHN-47	N33° 46.611', E049° 19.991', Contact granite	Chalcopyrite	-0.4
ASN-31	N33° 51.205', E049° 19.359' Kolah Morghoun	Arsenopyrite	-0.5
ASN-38	N33° 50.633', E049° 18.006' Ataii digging	Arsenopyrite	1.8
ASN-40	N33° 50.876', E049° 17.905' Tappeh Khileh	Arsenopyrite	-0.4
NNZ-21	Tunnel No.1	Arsenopyrite	4
NNZ-27	N33° 40.722', E 049° 15.045', Fizuneh	Arsenopyrite + Pyrite	1.2

**Table 6.1** Sulfur isotopic data ( $\delta^{34}\text{S}\text{‰}$  CDT) for sulfides from Deh Hosein (DHN), Astaneh (ASN) and Nezam Abad (NNZ) prospects in the Astaneh-Sarband Area. Measuring and preparation error  $< +0.2 \text{‰}$  (in case of DHN-1B and DHN-10B  $< +0.3 \text{‰}$ ).

### 6.3 Oxygen isotope analyses

Oxygen is the most abundant element on Earth. It occurs in gaseous, liquid, and solid compounds, most of which are thermally stable over large temperature ranges. These facts make oxygen one of the most interesting elements in isotope geochemistry (Hoefs 2004). Oxygen has three stable isotopes with the following abundances:  $^{16}\text{O}$ : 99.763%,  $^{17}\text{O}$ : 0.0375%,  $^{18}\text{O}$ : 0.1995% (Galick 1969). Because of the higher abundance and the greater mass difference, the  $^{18}\text{O}/^{16}\text{O}$  ratio is normally determined, which may vary in natural samples by about 10% or in absolute numbers from about 1:475 to 1:525 (Hoefs 2004).  $\delta^{18}\text{O}$  values vary in nature by about 100 ‰, about half of this range occurring in meteoric water (Figure 6.1). The mantle has a  $\delta^{18}\text{O}$  value of  $5.7 \pm 0.3 \text{‰}$  and this seems to have been constant through time for the earth and the moon (Taylor 1980; Rollinson 1993). Most granites, metamorphic rocks and sediments are enriched in  $\delta^{18}\text{O}$  relative to the mantle value, whereas seawater and meteoric waters are depleted, thus forming complementary  $\delta^{18}\text{O}$  reservoirs (Rollinson 1993). According to Hoefs (2004) and Rollinson (1993) the isotopic composition of present-day seawater is close to zero, while meteoric and magmatic water show values of  $< 5.7\text{‰}$ , and 6 to 10‰, respectively. In the

case of hydrothermal ore deposits, the  $\delta^{18}\text{O}$  value of the hydrothermal fluid may be estimated from the measured  $\delta^{18}\text{O}$  values of gangue minerals (e.g. feldspar, quartz, calcite) in order to find the possible source of fluid.

17 quartz samples from mineralized quartz and quartz-sulfide veins and veinlets of Deh Hosein, Astaneh, and Nezam Abad occurrences were analyzed for their oxygen isotope compositions, in order to realize the nature and source of mineralizing hydrothermal fluids.

### 6.3.1 Methods

$\delta^{18}\text{O}$  isotope analyses were performed at the Isotope Laboratory of the TU Bergakademie Freiberg. The oxygen isotope composition was determined following the procedure of Borthwick & Harmon (1982) using  $\text{ClF}_3$  as oxidizing reagent and measured by a mass spectrometer (Finnigan Delta plus). The reproducibility of analyses is better than  $\pm 0.2\%$ . All measurements have been corrected based on analyses of the standard NBS-28 (accepted value  $\delta^{18}\text{O}_{\text{V-SMOW}} = 9.6\%$ ). All oxygen isotopic data are reported in standard delta notation, relative to V-SMOW.

### 6.3.2 Results

The average  $\delta^{18}\text{O}$  values of duplicate measurements for all analyzed quartz samples of the Astaneh-Sarband area is given in Table 6.2. The  $\delta^{18}\text{O}$  values range from 11.6 to 19.2 with an average of  $14.5\ \delta^{18}\text{O}$ .

$\delta^{18}\text{O}$  in quartz samples from Deh Hosein has the highest values among the occurrences of the study area and vary between 13.6 and 19.2 ‰ (avg.  $16.4\%$ ,  $n = 7$ ). The values from the Astaneh prospect have a little lower but more homogeneous isotope compositions, between 11.5 and 13.7 ‰ (avg.  $13\%$ ,  $n = 4$ ) for quartz of the mineralized quartz veins. At Nezam Abad the  $\delta^{18}\text{O}$  values for quartz and tourmaline range between 11.6 and 15 ‰ (avg.  $13.3\%$ ,  $n = 6$ ).

A comparison of the oxygen isotope values of the mineralized veins of the Astaneh-Sarband area with the known data of the natural oxygen isotope reservoirs from Taylor (1974), Onuma et al. (1972), Sheppard (1977), Graham and Harmon (1983), Hoefs (1987), and Rollinson (1993), excludes seawater or meteoric water as sources for the quartz-sulfide veins and suggests a metamorphic or magmatic-metamorphic origin for them (Figure 6.1b).

Metamorphic water is defined as water associated with metamorphic rocks during metamorphism. Thus, it is a descriptive, nongenetic term and may include waters of different ultimate origins. In a narrower sense, metamorphic water refers to the fluids generated by dehydration of minerals during metamorphism. The isotopic composition of metamorphic water may be highly variable, depending on the respective rock types and their history of fluid-rock interaction. A wide range of  $\delta^{18}\text{O}$  values (5 to 25‰) is generally attributed to metamorphic waters (Taylor 1974; Hoefs 2004). On the other hand, magmatic fluids may change their isotopic composition during cooling through isotope exchange with country rocks and mixing with fluids entrained within the country rocks (Hoefs 2004).

In the interaction of water with crystalline rocks at high temperatures the  $\delta^{18}\text{O}$  of water is generally shifted towards higher values (Taylor 1997). It is thus possible that in the area the essentially magmatic mineralizing fluid (with 6 to 10‰  $\delta^{18}\text{O}$  values) has been isotopically modified through water-rock reactions with the vast metamorphic rocks of the area (with 5-25‰  $\delta^{18}\text{O}$  values). This can be attested by higher  $\delta^{18}\text{O}$  values of the metamorphic-hosted prospect of Deh Hosein (avg.  $16.4\%$ ) compared to the intrusion-hosted Nezam Abad (avg.  $13.3\%$ ) and Astaneh (avg.  $13\%$ ) prospects. Anyhow, the metamorphic contribution to the isotopic signature has been dominant.

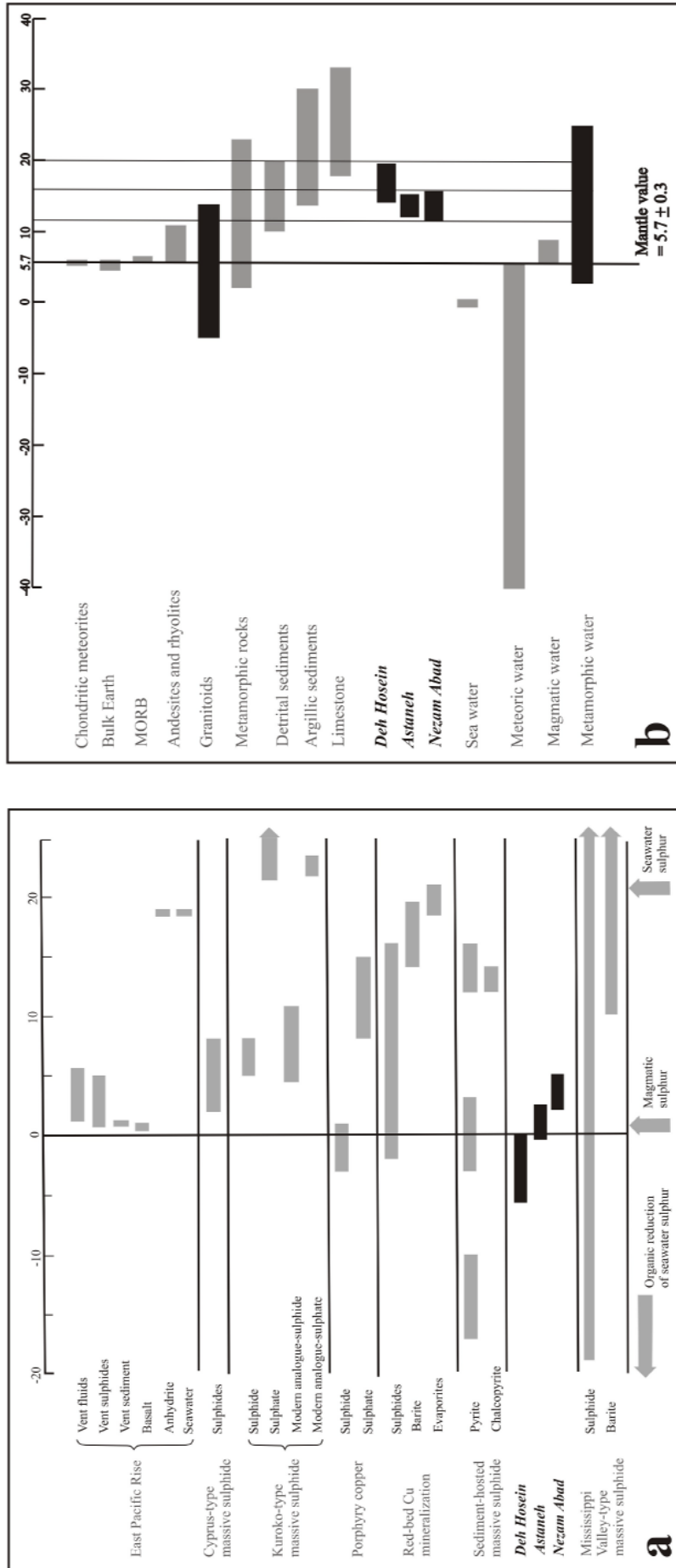


**Figure 6.1** a) Comparison of  $\delta^{34}\text{S}$  values of sulfur-bearing minerals in Astaneh-Sarband occurrences and hydrothermal deposits. Data from Kerridge et al. 1988, Ohmoto and Rye 1979, Halbach et al. 1989, Naylor et al. 1989, Eldridge et al. 1988, and Rollinson 1993. b) Comparison of  $\delta^{34}\text{S}$  values from Astaneh-Sarband occurrences and natural oxygen isotope reservoirs. Data from: Taylor (1974), Onuma et al. (1972), Sheppard (1977), Graham and Harmon (1983), Hoefs (1987), and Rollinson (1993).

Sample No.	Location	Description	$\delta^{18}\text{O}_{\text{V-SMOW}} \text{‰}$
DHN-1A	N33° 45.406', E049° 18.993', Digging east of the prospect	Quartz + Chalcopyrite	13.6
DHN-1B	N33° 45.406', E049° 18.993', Digging east of the prospect	Quartz + Galena	16.7
DHN-6	Quartz vein, east of the prospect	Quartz	17.0
DHN-15A	39s 0340895, UTM 3738846, Near Ghaidan	Quartz + Fe oxides	19.2
DHN-16A	39s 0340182, UTM 3739756, Near Ghaidan	Quartz + Fe oxides	17.2
DHN-39	39s 0342546, UTM 3736831, Ahmad Jigi II	Quartz + Arsenopyrite	17.4
DHN-45	N33° 46.718', E049° 20.138', Vein in the contact granite	Quartz + Cu-Fe oxides	14.0
ASN-16	N33° 51.112', E049° 19.272', Shirmazd	Quartz + Fe oxides	13.3
ASN-25	N33° 50.879', E049° 19.149', Shirmazd, Tunnel I	Quartz	13.5
ASN-28	N33° 51.661', E049° 20.472' Molla Yahya hill	Quartz	13.7
ASN-37	N33° 50.366', E049° 18.096' Tappeh Dor	Quartz + Fe oxides	11.5
NNZ-9	N33° 41' 55.3'', E049° 10' 32.7'', Revesht	Quartz + tourmaline + ore (arsenopyrite, chalcopyrite, pyrite)	14.2
NNZ-11	N33° 39.261'', E049° 15.476'', Nezam Abad main tunnel	Quartz + tourmaline + Cu-Fe oxides	11.6
NNZ-25	N33° 40.722', E 049° 15.045', Fizuneh	Quartz + malachite	12.7
NNZ-28	N33° 39.953', E049° 15.362', Jafar Abad	Quartz	13.9
NNZ-31	Qz-Tm vein in the main tunnel of Nezam Abad	Quartz	15.0
NNZ-34	N33° 41' 55.3'', E049° 10' 32.7'', Revesht	Quartz	12.5

**Table 6.2** Oxygen isotopic data ( $\delta^{18}\text{O}_{\text{V-SMOW}} \text{‰}$ ) for samples from Deh Hosein (DHN), Astaneh (ASN) and Nezam Abad (NNZ) deposits at the Astaneh-Sarband Area. Measuring and preparation error:  $< \pm 0.2 \text{‰}$ .

## 6.4 Lead isotope studies

The study of lead isotope ratios has nowadays consolidated its status in geosciences including mineral exploration as well as scientific archaeology and greatly contributed to the present picture of the Earth's development, ore forming processes and provenance studies (Bielicki and Tischendorf 1991; Pernicka et al. 1984).

The present study on lead isotopes follows two major aims;

- Investigation of the source of mineralizing fluids, tectonic setting of the mineralization environment, relationship between the ore and the host rocks and comparison of the occurrences of the Astaneh-Sarband area from this point of view.

- Comparison of the lead isotope ratio of the ore of Deh Hosein with ancient bronze artifacts from Luristan, Mesopotamia, Asia Minor and Western Asia which will be discussed in chapter 7.

#### 6.4.1 Methodology and analytical procedure

70 ore and host rock samples from Deh Hosein, Astaneh and Nezam Abad occurrences were analyzed by multi collector ICP-Mass spectrometer Axiom of the VG Elemental Company in the Institute of Archaeometry of the TU Bergakademie Freiberg.

With using the above mentioned instrument chemical separation of lead is not strictly necessary. Since good signal intensity can be achieved with solutions containing on the order of 100ng ml<sup>-1</sup> of lead, solid samples with more than 0.1% of lead could be measured directly after dissolution. Most samples were first analyzed by NAA to determine if the lead concentration was sufficiently high, and were then prepared and measured by following the procedure of Niederschlag et al. 2003 as follows:

The samples were broken into chips of several milligrams and an appropriate amount of them (usually 60-80mg) was rinsed with dilute HNO<sub>3</sub> and afterwards dissolved in half-concentrated HNO<sub>3</sub> (Merck Suprapur) in an ultrasonic bath at 70°C for several hours. The insoluble residue was removed from the solution by decantation. The solution was then diluted with high-purity deionized water. The final solution had a lead concentration of 200 ppb within 2% HNO<sub>3</sub>. All measured solutions were doped with 50 ppb thallium. The standard material SRM-981 was also dissolved in HNO<sub>3</sub>, diluted to a concentration of 200ppb Pb and doped with 50 ppb thallium (Niederschlag et al. 2003).

The <sup>205</sup>Tl/<sup>203</sup>Tl ratio was measured simultaneously with the lead isotope ratios and compared to the value of <sup>205</sup>Tl/<sup>203</sup>Tl=2.3871 (Dunstan *et al.* 1980). The deviation of the measured value from the true value was used to correct for the mass discrimination of the lead isotopes, using an exponential relationship. The technique of thallium doping for correction of the mass discrimination of lead has been tested on several occasions and can now be considered as the standard procedure for the measurement of lead isotope ratios by ICP-MS (Walder and Furuta 1993; Walder 1997; White *et al.* 2000).

The sample solutions were analyzed in runs of 20 single measurements, each with an integration time of 15s Background measurements of 20s duration were performed before and after each run. The data reported in Table 6.3 were generally calculated as the mean of four runs. Data points of each run that exceeded a 2σ error limit were rejected and the mean calculated again. This cyclic rejection routine was applied to a maximum rejection of 15% of the measurements. The in-run precision of the reported lead isotope measurements was in the range of 0.002–0.023% (2σ), depending on the lead isotope ratio considered.

All measurements were accompanied by control measurements of the NIST standard SRM-981 to ensure the reproducibility and accuracy of the data. SRM-981 was analyzed in the same way as the samples, except for the four repetitions of each measurement. The evaluation of these 70 measurements results in a relative standard deviation (2σ) of 0.09% for the <sup>206</sup>Pb/<sup>204</sup>Pb ratio, of 0.04% for the <sup>208</sup>Pb/<sup>206</sup>Pb ratio and of 0.02% for the <sup>207</sup>Pb/<sup>206</sup>Pb ratio.

#### 6.4.2 Results

The Pb isotope data for mineral separates and whole rock samples are presented in Table 6.3. At Deh Hosein Pb isotope ratios from 21 sulfide samples are very similar and plot within a narrow range between 18.415 and 18.547 for <sup>206</sup>Pb/<sup>204</sup>Pb (avg. 18.463), 15.641 to 15.667 for <sup>207</sup>Pb/<sup>204</sup>Pb (avg. 15.651) and 38.571 to 38.833 for <sup>208</sup>Pb/<sup>204</sup>Pb (avg. 38.650). In this respect, the



Pb signatures of the dominant metamorphic-hosted ore and the minor intrusion-hosted ore are consistent.

Among 14 whole-rock samples of different host rock types of the mineralization area, meta-sandstone and hornfels (which has probably been originated from sandstone) yielded Pb values in the range of the ore lead signatures while the other types of host rock show divergent lead isotope signatures (Table 6.3, and Figure 6.2). Especially Pb values from tourmaline granite differ markedly from all other analyzed samples by having higher proportions of uranium and thorogenic Pb. The tourmaline balls of this granite show, in contrary, much lower Pb values than the ore and the rock itself. Although Pb values of spotted slate and phyllite differ from meta-sandstone and ore values but their variation is not significant.

At Astaneh Pb isotope ratios from six ore samples, including arsenopyrite and quartz-sulfide, are very similar and range from 18.54 to 18.59 for  $^{206}\text{Pb}/^{204}\text{Pb}$ , 15.615 to 15.638 for  $^{207}\text{Pb}/^{204}\text{Pb}$  and 38.672 to 38.688 for  $^{208}\text{Pb}/^{204}\text{Pb}$ . Pb values of two micro granodiorite dykes and four Shirmazd granodiorite samples are in a rather good agreement with the same values of the ore although they show a little higher signatures, especially in case of two Shirmazd samples. The lead signatures of two microgranodiorite dykes, the tourmaline granite and its tourmaline and one quartz-sulfide vein differ significantly from the ore and Shirmazd signatures, although they have very close and similar values among themselves (Table 6.3, and Figure 6.2).

At Nezam Abad, the lead isotope values of different ores and rock units are similar but do not match as good as the values of the ores and rocks of the two previously discussed prospects. Nevertheless, the Pb signatures of the ores of Nezam Abad, Fizuneh, Jafar Abad, and Revesht are in a rather good agreement with quartz diorite of Nezam Abad (Figure 6.2). The lead values of diabasic dykes which have intersected the quartz diorite differ significantly from the latter sections. In one case a tourmaline quartz vein shows very close value with the diabasic values. This could imply that a later barren magmatic activity has affected the area and has caused the intersecting diabasic dykes and some tourmaline quartz veins. The occurrence of the aplitic veins which have, likewise, intersected the quartz diorite and have been dated to Oligocene (25 Ma, Farhadian 1992) could support this statement.

A comparison of the lead isotope signatures of the ore in three prospects of Deh Hosein, Astaneh, and Nezam Abad indicates that although each prospect has a distinct cluster of values in smaller scale, the general Pb values are similar in a larger scale and range from 18.41 to 19.00 for  $^{206}\text{Pb}/^{204}\text{Pb}$ , 15.61 to 15.7 for  $^{207}\text{Pb}/^{204}\text{Pb}$  and 38.55 to 39.00 for  $^{208}\text{Pb}/^{204}\text{Pb}$ . The lead signatures of Deh Hosein and Astaneh show closer values while Nezam Abad ore shows rather higher signatures.

According to the above mentioned results, it seems that the hydrothermal fluids responsible for the mineralizations in the Astaneh-Sarband area have had similar magmatic sources and have been clearly influenced by the characteristics of their host rocks.

According to the plumbotectonics model of Doe and Zartman (1981), the lead in the ores has a Lower Crustal Pb component for all three prospects (Figure 6.3). Doe and Zartman (1979) and Zartman and Doe (1981) introduced the plumbotectonics model to account for variations in average lead isotopic composition among different tectonic settings. Originally used to explain the distinct lead isotopic provinces in western United States (Doe, 1967; Zartman 1974), the approach has proven applicable worldwide (Zartman and Haines 1988).

Since the application of single stage model ages has been proven to be meaningless in terms of dating young mineral deposits (Haack 1993), this method has not been applied to the samples.

Sample No.	Location	Description	$^{206}\text{Pb}/^{204}\text{Pb}$	$^{207}\text{Pb}/^{204}\text{Pb}$	$^{208}\text{Pb}/^{204}\text{Pb}$
DHN-1A	N33° 45.406', E049° 18.993', Digging east of the prospect	Polymetallic ore	18.439	15.652	38.608
DHN-1B	N33° 45.406', E049° 18.993', Digging east of the prospect	Quartz, galena	18.415	15.643	38.578
DHN-7A	39s 0343430, UTM 3737939, Ghara Ghouii	Polymetallic ore	18.445	15.650	38.595
DHN-7B	39s 0343430, UTM 3737939, Ghara Ghouii	Quartz + Cu-Fe oxide	18.446	15.655	38.604
DHN-8	39s 0343347, UTM 3737263, Ghara Ghouii	Spotted slate with disseminated monazite)	18.462	15.651	38.72
DHN-10A	39s 0342443, UTM 3737013, Ahmad Jigi I	Quartz, Cu-As minerals, malachite	18.437	15.649	38.625
DHN-10B	39s 0342443, UTM 3737013, Ahmad Jigi I	Polymetallic ore: quartz, chalcopryrite, malachite, iron oxides	18.528	15.661	38.833
DHN-11	39s 0342443, UTM 3737013, Ahmad Jigi I	Phyllite	18.411	15.618	38.569
DHN-12A	39s 0342533, UTM 3736838, Ahmad Jigi II	Chalcopryrite, pyrite	18.453	15.652	38.615
DHN-15B	39s 0340895, UTM 3738846, Near Ghaaidan	Fe oxides + Quartz	18.461	15.662	38.646
DHN-16B	39s 0340182, UTM 3739756, Near Ghaaidan	Fe-Mn oxides + Quartz	18.429	15.641	38.58
DHN-33	39s 0341207, UTM 3738556, Jafar Khan	Chip sampling from altered sandstone (Fe oxides and Quartz)	18.473	15.660	38.664
DHN-34	39s 0342443, UTM 3737013, Ahmad Jigi I	Copper ore (native copper), pyrite, arsenopyrite	18.487	15.655	38.703
DHN-38	39s 0342546, UTM 3736831, Ahmad Jigi II	Arsenopyrite, Scordite and Quartz	18.446	15.651	38.604
DHN-40	39s 0342546, UTM 3736831, Ahmad Jigi II	Meta Sandstone, chalcopryrite, malachite, quartz, Fe oxides	18.531	15.655	38.818
DHN-42	39s 0343430, UTM 3737939, Ghara Ghouii	Quartz, chalcopryrite, malachite, Fe oxides	18.444	15.649	38.588
DHN-43	39s 0344246, UTM 3737047, North of the deposit	Oxidized ore (chalcopryrite, pyrite, sphalerite, cassiterite)	18.422	15.641	38.571
DHN-45	N33° 46.718', E049° 20.138', Vein in the contact granite	Quartz, malachite, Fe-Mn oxides	18.547	15.65	38.684
DHN-47	N33° 46.611', E049° 19.991', Contact granite	Chalcopryrite, malachite, quartz, Fe oxides	18.517	15.652	38.703
DHN-48	N33° 46.611', E049° 19.991', Contact granite	Granite with disseminated Cu-Fe oxides	18.865	15.656	38.913
DHN-51	N33° 45.930', E049° 20.457', Metasandstone	Meta Sandstone	18.433	15.645	38.607
DHN-56	N33° 46.188', E049° 18.553', Spotted slate digging	Spotted slate	18.424	15.609	38.66
DHN-60	N33° 46.083', E049° 18.992', North of the deposit	Pyrite, arsenopyrite, sphalerite	18.434	15.644	38.593
DHN-61	N33° 46.083', E049° 18.992', Spotted slate-Meta sandstone contact	Meta sand stone	18.424	15.641	38.591
DHN-62	N33° 46.045', E049° 18.956', Spotted slate-Meta sandstone contact	Spotted slate	18.421	15.637	38.564
DHN-64	N33° 45.819', E049° 18.525', Ghara Ghoii	Meta sand stone	18.452	15.657	38.667
DHN-70	N33° 45.337', E049° 18.406', beside the dirt road	Silicified phyllite	18.687	15.660	39.572
DHN-71	N33° 45.337', E049° 18.406', beside the dirt road	Gossan	18.686	15.667	38.939
DHN-74	N33° 45.406', E049° 18.993', Digging east of the prospect	Meta sand stone	18.43	15.654	38.606
DHN-75	N33° 45.453', E049° 19.029', Digging east of the prospect	Phyllite	18.404	15.628	38.549
DHN-76	N33° 45.727', E049° 19.144', Close to the castle	Oxidized ore (chalcopryrite, galena, pyrite)	18.447	15.655	38.604
DHN-82	N33° 46.770', E049° 19.848', Contact granite	Tourmaline of the tourmaline granite	17.303	15.514	36.920
DHN-83	N33° 46.754', E049° 19.883', Contact granite	Tourmaline granite	21.939	15.873	39.504
DHN-84	N33° 46.754', E049° 19.883', Contact granite	Tourmaline granite with malachite stain	19.141	15.68	38.713
DHN-87	N 33° 46.621', E049° 19.175', Luzdar	Hornfels	18.507	15.658	38.905
DHN-91	39s 0342443, UTM 3737013, Ahmad Jigi I	Meta sandstone	18.463	15.650	38.647
DHN-93	39s 0342443, UTM 3737013, Ahmad Jigi I	Arsenopyrite	18.509	15.656	38.777

**Table 6.3** Lead isotope signatures of ore and whole rocks from the occurrences of Deh Hosein (DHN), Astaneh (ASN), and Nezam Abad (NNZ) in the Astaneh-Sarband area.

Sample No.	Location	Description	$^{206}\text{Pb}/^{204}\text{Pb}$	$^{207}\text{Pb}/^{204}\text{Pb}$	$^{208}\text{Pb}/^{204}\text{Pb}$
ASN-16	N33 51.112 , E049 19.272, Shirmazd	Au bearing quartz-hematite veinlet	18.565	15.63	38.679
ASN-17	N33 51.112 , E049 19.272, Shirmazd	Disseminated granodiorite	18.978	15.662	39.685
ASN-18	N33° 51.112', E049° 19.272', Shirmazd	Disseminated granodiorite	18.557	15.616	38.628
ASN-20	N33° 51.019' , E049° 19.254', Shirmazd	Altered micro granodiorite	18.8	15.657	39.037
ASN-21	N33° 51.019', E049° 19.254'	Quartz-malachite veinlet	18.590	15.615	38.672
ASN-25	N33° 50.879', E049° 19.149', southwest of Shirmazd	Quartz vein (Tunnel 1)	18.572	15.631	38.688
ASN-30	N33° 50.988', E049° 19.220', Shirmazd	Granodiorite	18.724	15.698	38.98
ASN-31	N33° 51.205' , E049° 19.359', Kolah Morghoun	Arsenopyrite vein	18.559	15.637	38.688
ASN-32	N33° 51.205' , E049° 19.359', Kolah Morghoun	Micro granodiorite with disseminated chalcopyrite and pyrite	18.663	15.645	38.945
ASN-34	N33° 50.707', E049° 19.182', Darreh Boleh	Tourmaline from tourmaline granite	16.937	15.489	36.687
ASN-35	N33° 50.707', E049° 19.182', Darreh Boleh	Tourmaline granite	16.939	15.490	36.693
ASN-36	N33° 50.310' , E049° 18.095', Shirmazd	Altered granodiorite	18.723	15.624	38.923
ASN-37	N33° 50.366' , E049° 18.096', Tappeh Dor	Quartz with oxidized pyrite	16.937	15.488	36.686
ASN-38	N33° 50.633' , E049 18.006, Ataii digging	Arsenopyrite vein	18.555	15.637	38.684
ASN-39	N33° 50.633' , E049 18.006, Ataii digging	Micro granodiorite with diss. Fe-Oxides	16.937	15.487	36.686
ASN-40	N33° 50.876' , E049° 17.905', Tappeh Khileh	Arsenopyrite vein	18.540	15.638	38.683
ASN-42	N33° 50.876' , E049° 17.905', Tappeh Khileh	Altered microgranodiorite	16.942	15.493	36.699
NNZ-3	N33° 39' 56.6'', E49° 15' 22'', Jafar Abad	Ore (arsenopyrite, chalcopyrite, pyrite) , quartz-tourmaline vein	18.943	15.678	39.047
NNZ-4B	N33° 39' 56.6'', E049° 15' 22'', Nezam Abad	Diabasic dyke	16.937	15.489	36.687
NNZ-5	N33° 39' 17'', , E049° 16' 22.4'', Nezam Abad	Tourmaline-quartz vein + Cu-Fe oxides	16.934	15.484	36.676
NNZ-6B	N33° 39' 15.5'', E049° 15' 42.8'', Nezam Abad	Quartz diorite (host rock)	18.806	15.670	38.938
NNZ-6C	N33° 39' 15.5'', E049° 15' 42.8'', Nezam Abad	Diabasic dyke	19.828	15.710	38.894
NNZ-9	N33° 41' 55.3'', E49° 10' 32.7'', Revesht	Ore (arsenopyrite, chalcopyrite, pyrite) , quartz-tourmaline vein	18.826	15.670	38.945
NNZ-12	N33° 39.261' , E49° 15.476'', ancient digging of Nezam Abad	Ore (arsenopyrite, chalcopyrite, pyrite) , quartz-tourmaline vein	19.138	15.725	39.108
NNZ-16	Tunnel No. 1, Nezam Abad	Ore, quartz-tourmaline vein	18.716	15.673	38.922
NNZ-18	Nezam Abad	Quartz + malachite	18.748	15.66	38.932
NNZ-19	Nezam Abad	Tourmaline-quartz vein + Cu-Fe oxides	18.979	15.675	39.071
NNZ-21	Nezam Abad mine	Ore, quartz-tourmaline vein	19.059	15.702	39.245
NNZ-25	N33° 40.722' , E 049° 15.045', Fizuneh	Quartz + malachite	18.699	15.666	38.812
NNZ-27	N33° 40.722' , E 049° 15.045', Fizuneh	Ore (arsenopyrite, pyrite), quartz vein	18.679	15.664	38.732
NNZ-28	N33° 39.953' , E049° 15.362', Jafar Abad	Quartz vein	18.995	15.681	38.967
NNZ-29	N33° 39.953' , E049° 15.362', Jafar Abad	Tourmaline vein	18.840	15.675	38.922
NNZ-30	Tunnel No. 1, Nezam Abad	Quartz-tourmaline vein	18.536	15.659	38.641
NNZ-31	Tunnel No. 1, Nezam Abad	Quartz-tourmaline vein	18.700	15.661	38.796

Table 6.3 (continued)

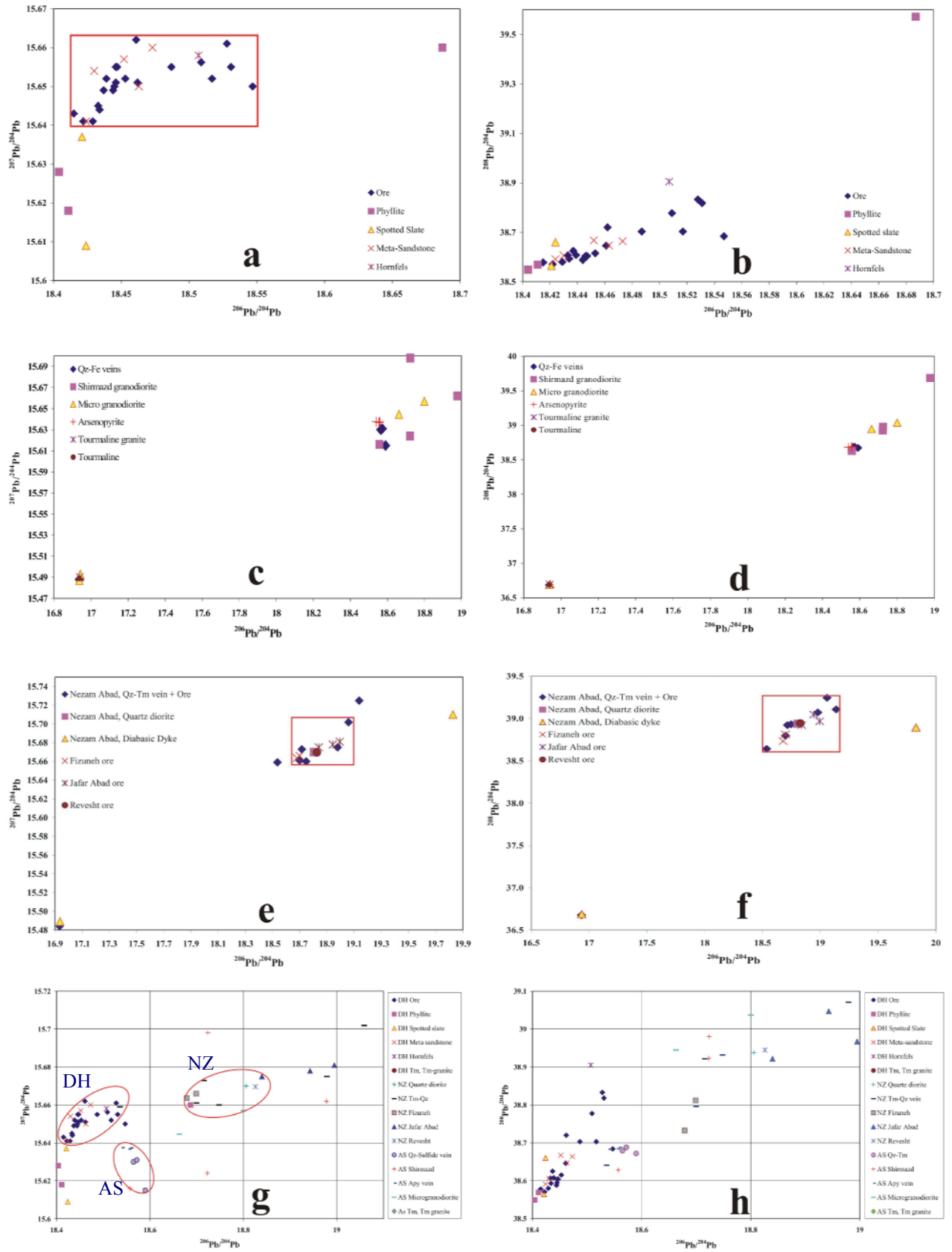
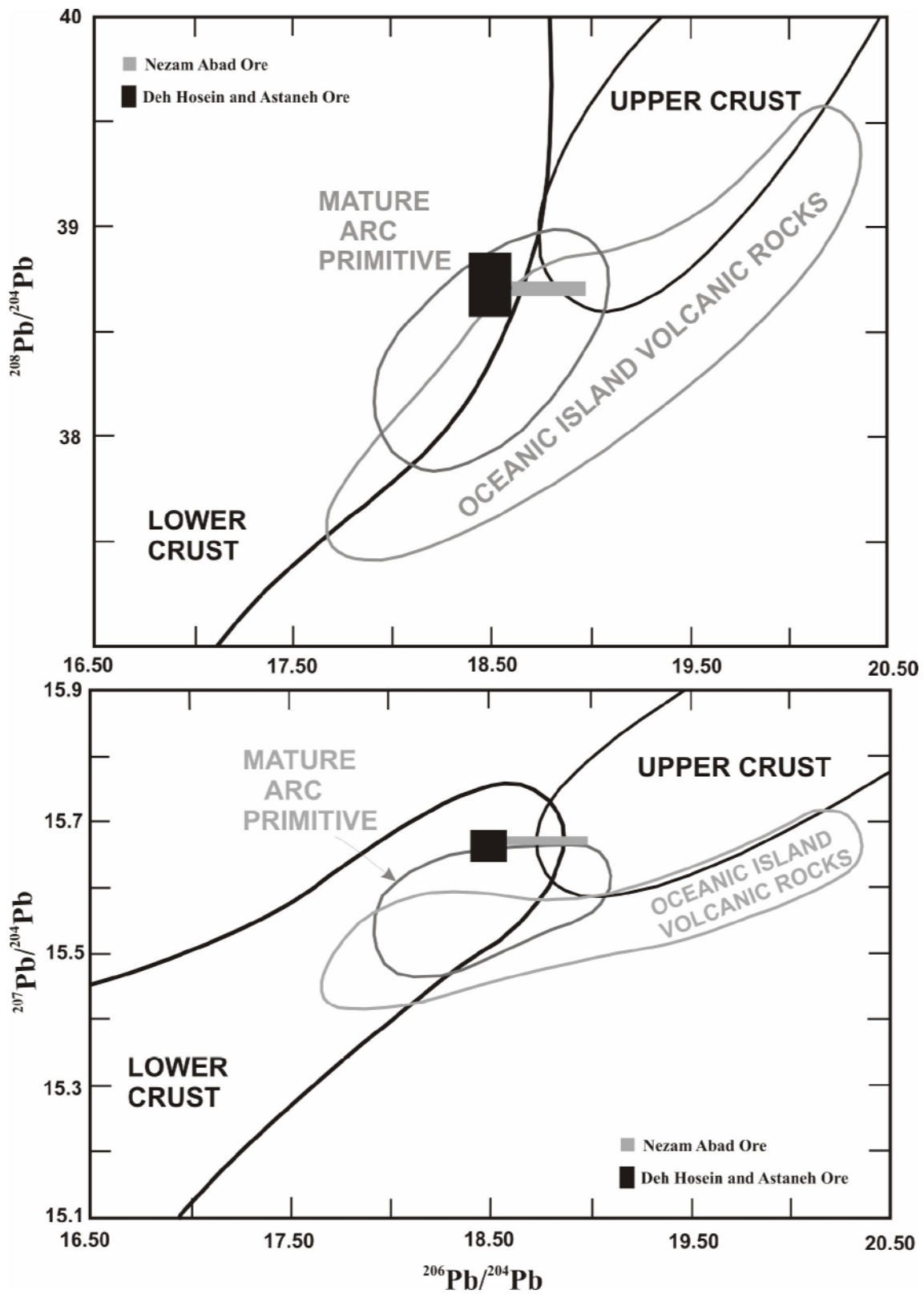


Figure 6.2 Three isotope plot of lead in ore and host rock samples from Deh Hosein (a and b), Astaneh (b and c), and Nezam Abad (e and f) together with a comparison of the lead signatures of all three occurrences (g and h).



**Figure 6.3** Location of the lead isotope compositions from the occurrences of the Astaneh-Sarband area in the "Plumbotectonics Model" of Doe and Zartman (1981).

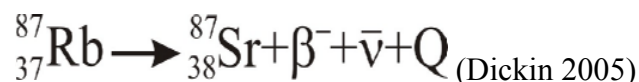


## 6.5 Age determination studies

In order to better conceive the nature of host rocks of the mineralization, the environment in which the mineralization has occurred, and the spatial relationship between host rocks and mineralization three samples of granodiorite, tourmaline granite, and hornfels were analyzed by Rb-Sr and single zircon evaporation methods. The analyses results of these samples have been presented in the following.

### 6.5.1 Rb-Sr method

The Rb-Sr method has largely been superseded as a means for dating igneous rocks (Dickin 2005). Rubidium has two naturally occurring isotopes,  $^{85}\text{Rb}$  and  $^{87}\text{Rb}$  whose abundances are 72.17% and 27.83%, respectively. These figures yield an atomic abundance ratio of  $^{85}\text{Rb}/^{87}\text{Rb}=2.593$  (Catanzaro et al. 1969), which is a constant throughout the Earth, Moon and most meteorites due to isotopic homogenization in the solar nebula (Dickin 2005).  $^{87}\text{Rb}$  is radioactive, and decays to the stable isotope  $^{87}\text{Sr}$  by emission of a  $\beta$  particle and anti-neutrino ( $\bar{\nu}$ ). The decay energy (Q) is shared as kinetic energy by these two particles:



Three relatively fresh samples from granodiorite of Shirmazd stock, tourmaline granite at the contact of the Deh Hosein prospect, and hornfels of the Deh Hosein were chosen to be analyzed by Rb-Sr method. Each sample weighed 5 kg. The samples were crushed by an adjustable jaw crusher and periodically sieved to obtain the meshes of 30-60 (approx. 250-500  $\mu\text{m}$ ), 60-90 (approx. 165-250  $\mu\text{m}$ ), and 90-120 (approx. 100-165  $\mu\text{m}$ ). Mineral separates including white mica, plagioclase, biotite, and quartz were thoroughly hand-picked to ensure purity for them. A whole rock sample also was chosen after crushing.

Rb and Sr concentrations were determined by isotope dilution. Precision is estimated at about  $\pm 1\%$ . Isotopic measurements were carried out on a Finnigan MAT-262 mass spectrometer. Over the course of this study the NBS-987 standard (accepted value = 0.71025) yielded  $^{87}\text{Sr}/^{86}\text{Sr} = 0.71031 \pm 4$  ( $2\sigma$ ,  $n = 50$ ).

#### 6.5.1.1 Results

The Rb/Sr results are presented in Table 6.4 and Figure 6.3. The Rb/Sr analysis of four mineral separates of quartz, plagioclase, muscovite, biotite in addition to whole rock for the granodiorite of the Shirmazd stock yields an age of  $35.05 \pm 0.92$  Ma. This suggests a formation age of Late Eocene (Priabonian) for this rock which hosts the main ore body of the gold mineralization at Astaneh. According to  $^{87}\text{Sr}/^{86}\text{Sr}$  ratio which, in the case of this sample, is essentially less than 0.706 the Shirmazd stock is possibly of I-type magmatic origin.

The Rb/Sr analyses of the quartz, plagioclase, muscovite, tourmaline and whole rock of the tourmaline granite of the southern part of the Astaneh intrusion (north of the Deh Hosein prospect) revealed  $77 \pm 33$  Ma age which within the large error corresponds to the Late Cretaceous (Companionian). As a matter of fact, this age is in rather good agreement with the result presented by Masoudi (1997) which suggests an age of  $98.9 \pm 1.0$  Ma (Late Cretaceous, Albian) for biotite granite of the area by the same method. Since the  $^{87}\text{Sr}/^{86}\text{Sr}$  ratio in the tourmaline granite is essentially higher than 0.706, the rock is possibly of S-type magmatic origin.

Because of difficulties with mineral separation in the case of hornfels due to the very fine grain size of the minerals, the determination of a reasonable age was not possible.

Sample	Rb (ppm)	<sup>87</sup> Rb [nmol/g]	Sr (ppm)	<sup>86</sup> Sr [nmol/g]	<sup>87</sup> Rb/ <sup>86</sup> Sr	<sup>87</sup> Sr/ <sup>86</sup> Sr	± σ %	Age (Ma)	Age
<b>Shirmazd intrusion, Granodiorite, ASN-30</b>									
Quartz	69.71	227.04	231.17	260.27	0.872	0.70516	0.01		
Plagioclase	81.88	266.67	555.97	625.98	0.426	0.7049	0.01		
Muscovite	21.71	70.7	36.24	40.8	1.733	0.70623	0.01		
Biotite	189.92	618.51	26.6	29.92	20.672	0.71502	0.01		
Whole Rock	139.32	453.71	290.35	326.9	1.388	0.70549 0.70546	0.01	<b>35.05±0.92</b>	<b>Priabonian (Late Eocene)</b>
<b>Astaneh intrusion, Tourmaline Granite, DHN-83</b>									
Quartz	7.79	25.38	14.88	16.73	1.517	0.71472	0.01		
Plagioclase	25.57	83.27	130	146.26	0.569	0.71301	0.01		
Muscovite	41.1	133.85	10.52	11.82	11.324	0.72571	0.01		
Tourmaline	7.95	25.9	35.6	40.06	0.647	0.71182	0.02		
Whole Rock	30.48	99.27	93.15	104.79	0.947	0.71451	0.02	<b>77±33</b>	<b>Campanian (Late Cretaceous)</b>
<b>Hornfels, Metasandstone, DHN-87</b>									
Quartz	124.86	406.65	40.12	45.03	9.031	0.73764	0.01		
Whole Rock	150.16	489.03	54.72	61.41	7.964	0.73833	0.02	<b>-46±24</b>	-----

**Table 6.4** The Rb/Sr measurements of three samples from the Astaneh-Sarband area. Measurement error for <sup>87</sup>Rb/<sup>86</sup>Sr [s]: 1%.

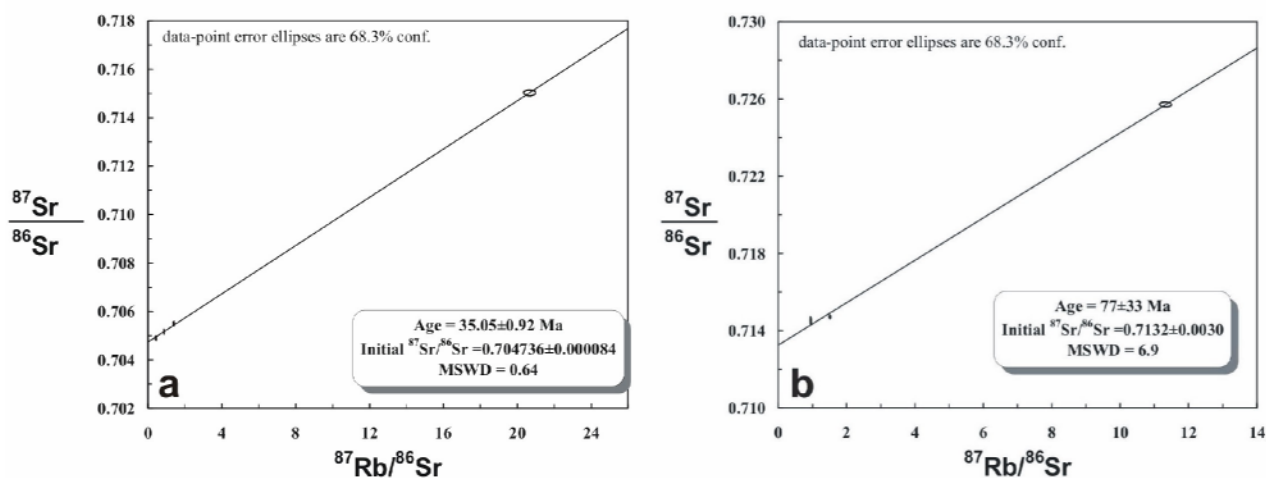


**Figure 6.4** Rb-Sr isochron diagrams for the Shirmazd granodiorite (a) and the tourmaline granite of Astaneh (b).

### 6.5.2 Single zircon evaporation method

In order to examine the accuracy and precision of the results obtained by Rb/Sr method, the same samples (ASN-30, DHN-83, and DHN-87) were also measured by single zircon evaporation method. In the case of sample DHN-87 (hornfels) no sufficient zircon grains were obtained for a reliable measurement.

### 6.5.2.1 Sample preparation, zircon morphology and methodology

Zircons have been extracted by the usual procedure (crushing, Wifely table, Frantz magnetic separator, heavy liquids, final handpicking). More than 20 grains per sample were selected for characterization by optical microscopy.

The zircon population in sample ASN-30 consists predominantly of clear, long-prismatic grains with only slightly rounded terminations. The average length/wide ratio of the zircons is 2.78 with maximum size of 420/150 $\mu\text{m}$  (L/W) and minimum size of 170/70 $\mu\text{m}$ .

In sample DHN-83, the zircon population consists also predominantly of clear, long-prismatic grains with only slightly rounded terminations. The average length/wide ratio of the zircons is 2.9 with maximum size of 490/113 $\mu\text{m}$  (L/W) and minimum size of 125/50 $\mu\text{m}$ .

The single zircon evaporation method involves evaporation deposition of Pb and other elements on a second filament, and subsequent measurement of Pb isotope ratios in a mass-spectrometer (Kober 1987). Measurements were carried out in the Isotope Laboratory in TU Bergakademie Freiberg on a Finnigan-MAT 262 mass spectrometer equipped with an ion counter. Corrections for mass fractionation (0.0036 amu) deduced from NBS-981 and two zircon standards (zircon 91500 reported in Wiedenbeck et al. 1995 and zircon S-2-87, Wenham Monzonite, US Geological Survey) have been applied. The obtained  $^{207}\text{Pb}/^{206}\text{Pb}$ -ages of standard zircons 91500 (accepted value: 1065.4  $\pm$  0.4 Ma) and S-2-87 (accepted value: 381.5  $\pm$  4 Ma) yield 1065.5  $\pm$  1.7 Ma (2 $\sigma$  mean, n=39) and 380.8  $\pm$  1.8 Ma (2 $\sigma$  mean, n=42), respectively. The calculated  $^{207}\text{Pb}/^{206}\text{Pb}$ -age of one measurement and its 2 sigma error of the mean is based on the mean of all measured scans (usually 90) of isotope ratios with those omitted lying outside the 95% confidence level. For dating with the evaporation technique a mean age of several zircons from one sample has to be determined. The statistical error (2 $\sigma$  calculated with the number of dated zircons) is used for error estimation by measuring several zircons from one sample.

### 6.5.2.2 Results

The zircon ages of this study suggest two distinct ages for two different intrusives of the Astaneh Intrusion (Table 6.5, and Figure 6.5).

The Shirmazd stock (ASN-30) shows an age of 44 $\pm$ 13 Ma which within error corresponds to the Eocene. This age is in a good agreement with the age determined by the Rb/Sr method, although it is slightly older. The younger age indicated by Rb/Sr can be due to the effect of younger intrusions (for instance microgranodiorite into the Shirmazd Stock) or hydrothermal fluids and consequently the slight change in the Rb/Sr ratio. The Eocene age for the granodiorite of Shirmazd, which has been confirmed by both Rb/Sr and single zircon evaporation methods, is in a good agreement with the K-Ar age for the quartz diorite of Nezam Abad. Both of these rocks host similar mineralizations.

The tourmaline granite at the northern contact of the Deh Hosein prospect indicates an age of 177 $\pm$ 8 Ma which correlates with Middle Jurassic. This age is much older than the age obtained by the Rb/Sr method (Late Cretaceous); the latter may imply the reheating of the rock by different phase of magmatism of the area. In fact the age obtained by means of zircon evaporation method introduces the oldest magmatic stage in the whole area. This result is consistent with the geochronological data for the granitoids of Borujerd magmatic complex (west-northwest of the study area) obtained by U-Pb zircon method (169-172 Ma, Ghaderi et al. 2004). Until now, the oldest magmatic activities of the area (before this study) which have been manifested as granitoids and pegmatites have revealed ages not older than Early Cretaceous (Masoudi 1997).

Zircon	$^{207}\text{Pb}/^{206}\text{Pb} \pm 2\sigma$	$^{204}\text{Pb}/^{206}\text{Pb} \pm 2\sigma$	Age (Ma) $\pm 2\sigma$	Scan
<b>ASN-30, granodiorite</b>				
1	0.051638 $\pm$ 0.00056	0.000485 $\pm$ 5.2E-05	269.4 $\pm$ 24.9	63
3	0.049051 $\pm$ 0.00149	0.00039 $\pm$ 0.00012	150.2 $\pm$ 71.0	18
8	0.047999 $\pm$ 0.000667	0.000656 $\pm$ 8.27E-05	99.2 $\pm$ 32.9	90
9	0.04757 $\pm$ 0.0011	0.00128 $\pm$ 0.000151	77.9 $\pm$ 54.8	18
10	0.049001 $\pm$ 0.000385	0.000324 $\pm$ 2.57E-05	147.8 $\pm$ 18.4	90
11	0.046946 $\pm$ 0.000117	0.000573 $\pm$ 1.95E-05	46.4 $\pm$ 6.0	90
14	0.046878 $\pm$ 0.000147	0.00118 $\pm$ 3.59E-05	42.9 $\pm$ 7.5	90
16	0.044639 $\pm$ 0.000306	0.000638 $\pm$ 1.61E-05	-11.1	90
18	0.046483 $\pm$ 0.000302	0.000342 $\pm$ 1.94E-05	22.7 $\pm$ 15.6	90
19	0.047201 $\pm$ 0.00071	0.000548 $\pm$ 4.83E-05	59.3 $\pm$ 35.8	41
19	0.047456 $\pm$ 0.000738	0.000535 $\pm$ 5.81E-05	72.2 $\pm$ 37.0	45
20	0.047174 $\pm$ 0.00037	0.000517 $\pm$ 2.89E-05	58.0 $\pm$ 18.7	90
21	0.046781 $\pm$ 0.000341	0.00084 $\pm$ 2.76E-05	38.0 $\pm$ 17.5	90
			<b>44 <math>\pm</math> 13</b>	
<b>DHN-83, Tourmaline granite</b>				
1	0.043786 $\pm$ 0.000788	0.000493 $\pm$ 6.35E-05	-11.1	90
1	0.047036 $\pm$ 0.000245	0.000244 $\pm$ 1.83E-05	51.0 $\pm$ 12.5	45
2	0.049843 $\pm$ 0.000184	5.69E-05 $\pm$ 5.16E-06	187.6 $\pm$ 8.6	90
3	0.049556 $\pm$ 8.65E-05	5.96E-05 $\pm$ 2.7E-06	174.1 $\pm$ 4.0	90
4	0.049095 $\pm$ 8.39E-05	0.000146 $\pm$ 6.2E-06	152.3 $\pm$ 4.0	90
5	0.048208 $\pm$ 0.000161	0.000158 $\pm$ 1.18E-05	109.5 $\pm$ 7.9	90
5	0.049713 $\pm$ 0.000688	6.58E-05 $\pm$ 5.42E-06	181.6 $\pm$ 32.2	90
5	0.049604 $\pm$ 4.21E-05	5.69E-05 $\pm$ 2.15E-06	176.4 $\pm$ 1.9	71
5	0.049624 $\pm$ 4.16E-05	0.0000472 $\pm$ 2.15E-06	177.4 $\pm$ 1.9	63
7	0.047935 $\pm$ 0.000246	0.000184 $\pm$ 1.91E-05	96.0 $\pm$ 12.1	90
7	0.049423 $\pm$ 0.000143	5.79E-05 $\pm$ 1.01E-05	167.9 $\pm$ 6.7	90
7	0.049539 $\pm$ 0.000126	4.49E-05 $\pm$ 5.41E-06	173.4 $\pm$ 6.0	80
8	0.049137 $\pm$ 8.22E-05	7.88E-05 $\pm$ 2.79E-06	154.3 $\pm$ 3.9	90
9	0.040909 $\pm$ 0.000601	0.00068 $\pm$ 5.29E-05	-11.1	90
10	0.05996 $\pm$ 4.44E-05	4.72E-05 $\pm$ 2.01E-06	602.1 $\pm$ 1.6	90
11	0.049633 $\pm$ 5.29E-05	3.72E-05 $\pm$ 1.93E-06	177.8 $\pm$ 2.5	88
12	0.050714 $\pm$ 3.75E-05	5.13E-05 $\pm$ 9.46E-07	227.8 $\pm$ 1.7	90
			<b>177 <math>\pm</math> 8</b>	

**Table 6.5** Zircon single-crystal evaporation Pb isotopic data and the estimated age for the Shirmazd granodiorite and the tourmaline granite of Astaneh.

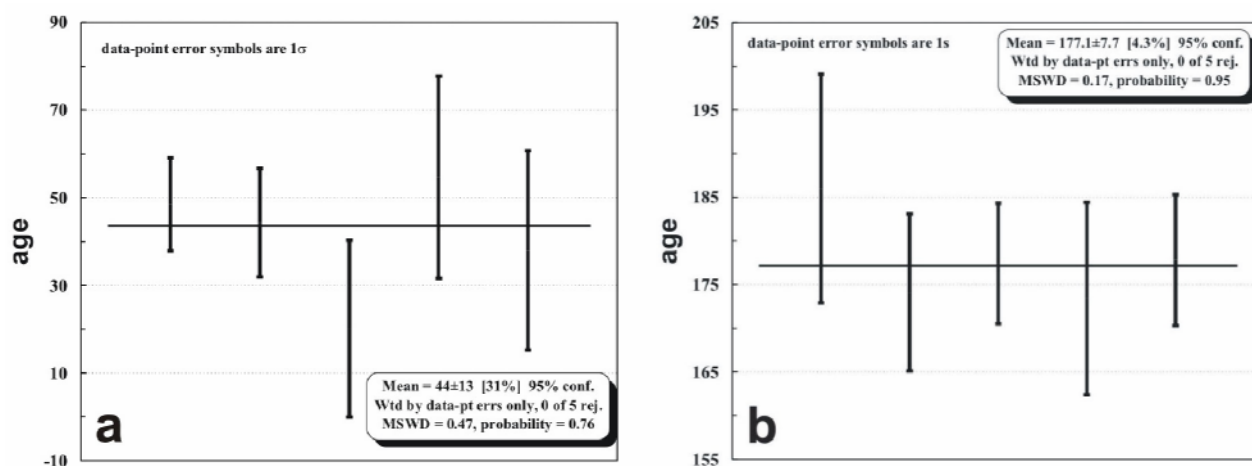


**Figure 6.5** Age versus evaporation steps diagram for zircon crystals from the Shirmazd granodiorite (a) and the tourmaline granite of Astaneh (b).

## 6.6 Arsenopyrite Geothermometry

Arsenopyrite which is the most refractory of the common sulfides (Kretschmar and Scott 1976) has been applied successfully for reliable estimations of either sulfur activity ( $a_{S_2}$ ) or temperature. Many hydrothermal vein deposits and, particularly, the mineral mounds and chimneys presently forming from hot springs on the deep ocean floor at various sites along the East Pacific Rise satisfy this constraint (Scott 1983). Since arsenopyrite is one of the most abundant ore minerals in the occurrences of the Astaneh-Sarband area, the arsenopyrite geothermometry method was utilized in order to estimate the temperature and sulfur activity during the formation of ore and associated minerals.

### 6.6.1 Method

Most sulfides easily undergo retrograde reactions and consequently change their compositions and therefore only the most refractory minerals including arsenopyrite and sphalerite can provide reliable information for high P and T. Equilibrium compositions of these two minerals are usually preserved from hydrothermal vein deposits which cool relatively rapidly. However, equilibrium may not always be preserved, particularly for sphalerite, from regionally metamorphosed sulfides which can cool very slowly (Scott 1983). Since the composition of arsenopyrite (Fe-As-S) is a function of sulfur fugacity and temperature, it is possible to estimate these conditions at formation utilizing the local Fe-As-S mineral assemblage and the atomic percent of arsenic in arsenopyrite (Barton 1969; Kretschmar and Scott 1976; Scott 1983; Sharp et al. 1985).

The weight percent of arsenic for several arsenopyrite grains of different locations in the occurrences of Deh Hosein, Astaneh, and Nezam Abad were obtained by microprobe analyses. Atomic percent of arsenic was later calculated.

### 6.6.2 Results

The microprobe analyses revealed arsenopyrites from Deh Hosein, Astaneh and Nezam Abad contain 32.3 to 34.3, 30.7 to 31.4, and 33.6 to 35.6 atomic percent of arsenic, respectively. Average compositions, with consideration of the sulfide assemblage (Table 6.6), lead to the conclusion that the mineralizations occurred at temperatures of  $\sim 460^\circ\text{C}$  for Deh Hosein, 380 to 410  $^\circ\text{C}$  for Astaneh and 510 to 565 $^\circ\text{C}$  for Nezam Abad (Table 6.6 and Figure 6.6). These indicate the formation temperature of arsenopyrite which has occurred during the main phase of mineralization for all three occurrences. Interestingly, the measured temperatures for different samples of each occurrence lay in a narrow range. The obtained temperatures are consistent with the results and evidence obtained from mineralogical investigations which likewise attest to high temperature conditions. Also these temperatures are consistent with early mineralization in intrusion-related systems in Alaska and elsewhere, where high temperatures are derived from both fluid-inclusion and arsenopyrite geothermometry (McCoy et al. 1997; Smith et al. 1999; Rombach and Newberry 2001).

The initial parts of sulfide mineralization at Nezam Abad have taken place at relatively high sulfur activities ( $<10^{-4}$ ), while the main sulfide mineralization has occurred at significantly lower sulfur activity at Deh Hosein ( $<10^{-8}$ - $10^{-7}$ ) and Astaneh ( $<10^{-7}$ - $10^{-6}$ , Figure 6).

Sample	Sulfide assemblage	<i>n</i>	As (at%)	Standard deviation	T (°C)
<b>Deh Hosein</b>					
DHN-38	Arsenopyrite + Pyrite + Chalcopyrite	9	32.29	0.44	460°C
DHN-78	Arsenopyrite + Loellingite	4	34.28	0.32	460°C
DHN-93	Arsenopyrite + Loellingite + Chalcopyrite	28	34.31	1.1	460°C
<b>Astaneh</b>					
ASN-31	Arsenopyrite	13	31.4	0.54	410°C
ASN-38	Arsenopyrite + Pyrite + Chalcopyrite	21	30.74	0.37	390°C
ASN-40	Arsenopyrite	23	30.66	0.29	380°C
<b>Nezam Abad</b>					
NNZ-21	Arsenopyrite + Pyrrhotite	5	33.65	0.98	510°C
NNZ-27	Arsenopyrite + Chalcopyrite + Pyrrhotite	8	35	0.41	565°C

**Table 6.6** Arsenopyrite compositions and derived formation temperatures (analyzed by microprobe) for Deh Hosein (DHN), Astaneh (ASN) and Nezam Abad (NNZ) occurrences. *n* number of analyses. T calculated using Kretschmar and Scott (1976) and Scott (1983).

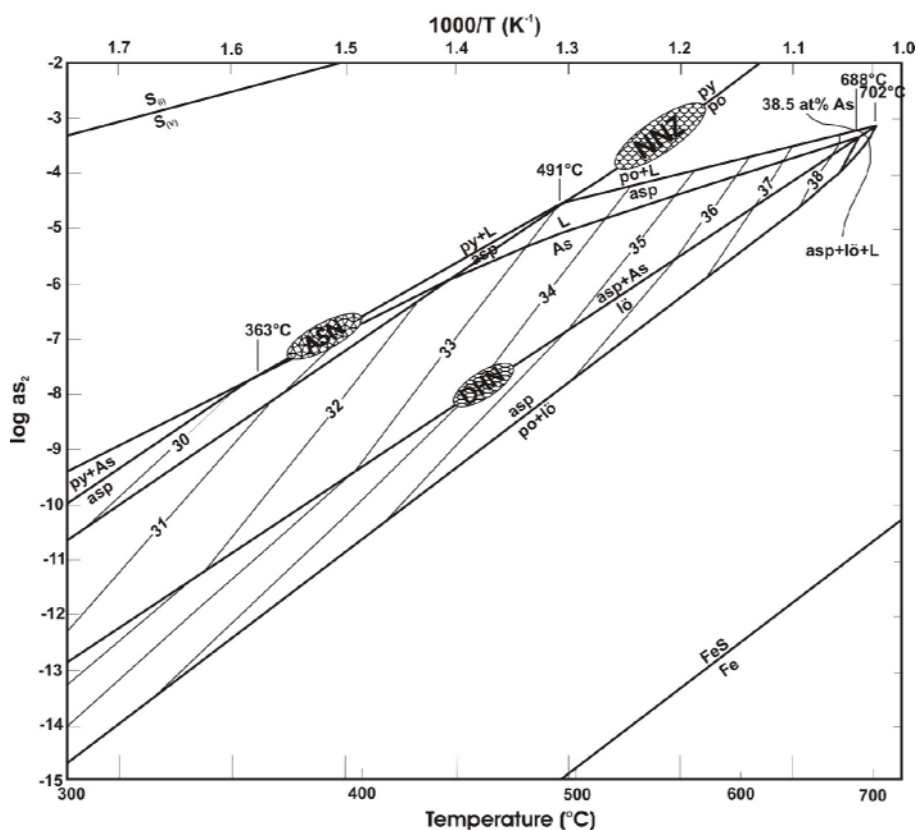


**Figure 6.6** Phase relations for the Fe-As-S system in equilibrium with vapor. Isopleths are Atomic % As in arsenopyrite. Abbreviations: asp, arsenopyrite; L, As-S, liquid; lö, löllingite; po, pyrrhotite; py, pyrite; S<sub>l</sub>, liquid sulfur; S<sub>v</sub>, sulfur vapor. After Kretschmar and Scott 1976; Scott 1983.



## *Chapter 7*

# **Archaeometrical investigations on the Deh Hosein ore and the ancient bronze artefacts**

### **7.1 Introduction**

In spite of rather extensive archaeological and geological investigations in Western Asia during the past decades, the source of tin for the huge bronze production in the ancient Near- and Middle-East has long remained enigmatic. Recently, by discovery of an ancient tin-copper mine at Deh Hosein in West Central Iran (Momenzadeh et al. 2002) on the eastern rim of the Zagros Mountains; it seems that a pivotal clue for solving this old riddle has emerged. In this chapter, following an introduction to the tin issue in antiquity, the ancient mine at Deh Hosein will be introduced and described. Lead isotope as well as compositional analyses of ores from Deh Hosein are compared with results of Early Bronze and Iron Age bronze artifacts from Luristan and Western Asia. As will be seen, much geological, analytical, archaeological, textual, chronological and geographical evidence attests that the Deh Hosein mine has been a major ore supplier for bronze in prehistoric times.

### **7.2 Review of the riddle of tin in antiquity**

In order to conceive the problem of tin source in antiquity, we first need to know the places in which tin-bronze alloy has foremost appeared and massively utilized. Therefore in the following the occurrence of tin-bronze in two regions will be briefly reviewed; the Bronze Age in Southwestern Asia and the eastern Mediterranean as well as the Bronze and Iron Age in Luristan (western Iran).

### **7.3 Early tin bronzes**

The first bronze objects appeared in Mesopotamia and southwest Iran (Susa) in the late fourth millennium and the beginning of the 3rd millennium BCE, although the extensive consumption of tin and tin-bronze in Mesopotamia emerges at mid third millennium and in Iran

even later. Since Mesopotamia and the Khuzestan plain lack metallic resources, the ancient artisans were dependent on their adjacent mineral-rich neighbors namely the Iranian plateau and Anatolia or even farther lands in order to supply their raw materials. Despite the wealth of the Iranian plateau and Anatolia in base and precious metal resources (at least from the ancient consumers' point of view), the known tin resources are rare in these lands. It has long been discussed where the source(s) of tin for this huge amount of bronze production in a long period of time from mid Bronze Age to the end of Iron Age could be.

It should be taken into consideration that the earliest tin mines might have probably been copper mines as well. It is possible that the first inventors of the alloy of bronze gained it fortuitously. Probably at first a tin bearing copper ore or arsenic-copper ore had been smelted for production of metallic copper or arsenical bronze, but then because of the presence of tin in the ore, bronze has been involuntarily produced. The final product of such a process was recognizable by its golden color, its hardness and better casting properties. The hardness may have been recognized by honing some naturally produced bronze tools. Also it is possible that in the very beginning the early smelters did not recognize cassiterite (or stannite) as a mineral. They just knew that the ore of some specific mines result in better quality products. Maybe soon after, the ancient mineralogist due to market demand, tried to find the secret of the high-quality of this kind of ore and finally found cassiterite as a by-product. This hypothesis is supported by the evidence that the earliest surviving textual references distinguish only between copper and bronze and do not refer to tin (Limet 1960; Waetzoldt & Bachmann 1984; Muhly 1985).

Intentional alloying of copper with tin is usually considered to be indicative by a tin content of more than 1% or in some cases more than 5 percent tin, but in terms of provenance investigations, even half a percent tin in artifacts can be significant, because most of the known ancient copper mines in the region do not contain any significant concentrations of tin.

## 7.4 Archaeological evidence

The earliest tin-bronze artifacts in the early to mid third millennium BCE have emerged in the following ancient sites in the near and middle east (Figure 7.1):

### *Iran*

- The earliest tin-bronze artifacts (isolated) have been found in contexts A, B, C of Susa from later fourth-early third millennium BCE (Cleuziou and Berthoud 1982; Moorey 1982; Stech & Pigott 1986) but tin-bronze appears more frequently in the Susa IVA2 period (equal to EDIII B in southern Mesopotamia, Malfoy and Menu 1987; Potts 1994; Weeks 2004). Also high lead-bronzes are among the early Near Eastern metal objects as indicated by a pin from the late Uruk period layer at Susa which contains 14.3% lead and shows low silver and nickel contents (Tallon 1987; Müller-Karpe 1991).
- From the earliest burials at Kalleh Nissar (Luristan), area A-I, date to late 4<sup>th</sup> to early 3<sup>rd</sup> millennium BCE (equal to Jemdet Nasr/early dynastic I), 5 purposely alloyed tin-bronzes were unearthed and analyzed (Fleming et al. 2005). According to Fleming et al. (2005) these artifacts may well be the earliest group of excavated and well dated tin-bronzes currently known from the Iranian Plateau.



Figure 7.1 Approximate location of some of the Bronze and Iron Age sites and mines in Western Asia.

- One arsenical tin-bronze artifact from period IV at Tappeh Giyan (mid-third 3<sup>rd</sup> millennium BCE).
- A tin bronze needle from Tappeh Sialk III-5 (Ghirshman 1938).
- An arsenical low tin bronze from Tappeh Yahya IV C/B (Heskel and Lamberg-Karlovsky 1980).

### *Mesopotamia*

- Level VIII (early third millennium BCE) of Tepe Gawra (only one object, a pin with 5.62% Sn, out of 13) in the north Mesopotamia (Speiser 1935; Stech and Pigott 1986).
- Y cemetery at Kish, Early Dynastic I period (ED I, ca. 2990-2700 BCE), 8 of 23 analyzed copper-base objects contain one percent or more tin (Moorey and Schweizer 1972; Stech 1999; Muhly 1995; Müller-Karpe 1991).
- Royal Cemetery at Ur (ED III period, ca. 2600-2350 BCE) with a significant percentage of the copper-based objects (Stech 1999; Müller-Karpe 1991; Muhly 1985).

Except for the mentioned sites the use of tin-bronze remains uncommon till the Akkadian-post Akkadian period (2600-2400 BCE) (Moorey 1994; Muhly 1987; Stech 1999).

### *Northwestern Syria*

6 human figurines have been reported from level G at Tell Judeidah (ca. 3000 BCE, Braidwood and Braidwood 1960; Stech & Pigott 1986).

### *South and Central Anatolia*

The sites of Tarsus, Ahlatlibel, Mahmatlar, Alaca Höyük and Horoztepe (Esin 1969; Muhly 1993; Yener & Vandiver 1993) have been reported to contain some bronze artifacts.

***Northwestern Turkey***

Some bronze artifacts have been reported from Troia and Besiktepe (Pernicka et al. 1984; de Jesus 1980), and a number of nearby Aegean settlements such as Poliochni on Lemnos in the Aegean (Pernicka et al. 1990), Thermi on Lesbos (Begemann et al. 1992, 1995; Stos-Gale 1992) and Kastri on Syros (Stos-Gale et al. 1984).

***Southern Persian Gulf (UAE)***

Several tin-bronze objects at Al Sufouh, Unar 1, Unar 2 and Tell Abraç, from second half of the third millennium BCE (Weeks 1999, 2004).

***Afghanistan***

- An axe head (5% Sn) from Mundigak III6, which is roughly contemporary with the earliest tin-bronzes in Mesopotamia (Shaffer 1978; Cleuziou and Berthoud 1982; Berthoud et al. 1982).
- Three bronze artifacts found at Ghar-e Mar (Snake Cave) sixth millennium (Shaffer 1978). Even if this surprisingly early date for tin bronze production is correct (which it probably is not; Moorey 1982), there is no indication that this alloy passed into common use after its first appearance (Stech and Pigott 1986).

***Egypt and Palestine***

Except for a few artifacts (Lucas 1934; Eaton and Mc Kerrell 1976; Maddin et al. 1980; Cowell 1987; Muhly 1993) tin-bronze is absent before the fifteenth century BCE (Schiegl 1994; El Goresy et al. 1995).

Although tin-bronze first appears in later fourth-early third millennium BCE in the ancient world, but only at the end of the 3<sup>rd</sup> millennium the use of bronze becomes much more widespread, and the 2nd millennium sees the development of a true bronze metallurgy in most areas of ancient Western Asia (Weeks 2004). In Mesopotamia, a dramatic increase in tin consumption occurs in ED III (2700-2334 BCE) in southern part of it (Chárvat 1982; Stech and Pigott 1986). It is noteworthy that the earliest example of metallic tin, a bangle, has been found from Level IV at Thermi (3<sup>rd</sup> millennium BCE, Begemann et al. 1992).

**7.5 Texts referring to the Bronze Age tin trade**

The earliest surviving textual (cuneiform) references that refer to bronze (and subsequently tin) in Mesopotamia come from the early-mid 3rd millennium BCE, from which the earliest ones distinguish only between copper and bronze (Limet 1960; Waetzoldt & Bachmann 1984; Muhly 1985; Weeks 1999, 2004). These texts along with the early second millennium BCE texts from Mari (on the Euphrates) and from Kültepe (ancient Kanesh, central Anatolia) indicate that all the major sources of tin used in the region in the Early Bronze Age were located east of Mesopotamia (Muhly 1973; Larsen 1976, 1987; Moorey 1994; Weeks 1999, 2004).

The Kanesh texts refer to tin coming overland through the Zagros Mountains to Mesopotamia from northwestern Iran (Muhly 1973), while Mari seems to have obtained its tin almost exclusively through gift exchange with Susa, the tin having reached Susa from some unknown point further to the east (Joannes 1991; Moorey 1994; Weeks 1999, 2004).

Several sources have been mentioned in the ancient texts whose real location is equivocal or unknown today. Among the names which have been mentioned in literary, lexical, administrative and royal texts and inscriptions the followings are notable (T.F.Potts 1994, Table 4.2):

Arrata and near Arrata (*Ela*), Magan (*Hymn to Ninurta*, Cohen 1975), mines behind Ebih (Hamrin) (*Innana and Ebih*, Muhly 1973), Zarshur (*Hh XXII*, Leemans 1960), [Za]rha (*Lipshur, ibid*), BAR-gungunnu (*Lipshur; Hh, ibid*), Dilmun (*MEE*, Pettinato 1983, Waetzoldt 1981, *UR III*, Leemans 1960), Shimashki/Zabshali (*Shu-Sin*, Kutscher 1989), and Anshan (*Shulgi*, Davidovic' 1984). Although some of the place-names mentioned in the texts can refer only to way-stations along the trade routes (Weeks 1999, 2004), at least two of them seem to be noteworthy; Zarshur and some mines behind Ebih (Hamrin). In today Iran there is an ancient mine of gold and arsenic (and copper) near Takab whose name is Zarshuran, although no trace of tin has been found in it. The Hamrin or Jabal Hamrin is an area in central Iraq slightly above the 34° 00' meridian, opposite which the Deh Hosein ancient mine is located on the other side of the Zagros Mountains slightly below the same meridian.

Geological research has proven that tin deposits do not exist on the eastern Saudi Arabian coast and Bahrain which is an area that is supposed to be ancient Dilmun (T.F.Potts 1994; Weeks 1999, 2004), therefore it seems that Dilmun has also been a trade station.

Although the frequent reference of the 3rd-millennium Mesopotamian texts to lapis lazuli and carnelian in association with tin which are known to have come from the east (Herrmann 1968; T.F. Potts 1994), implies the importance of these materials and possibly the same center which controlled their trade in the east, but is no sign of the same origin for them. From the reign of Gudea of Lagash (c. 2150-2100 BCE) we have one text which mentions that, in addition to lapis lazuli and carnelian, tin was also traded to Mesopotamia from the land of Meluhha (Muhly 1973). Meluhha, is now known to be the region of the Indus Valley, and would have reached Mesopotamia via the Persian Gulf (Muhly 1973). Geological research has proven that tin deposits do not exist in the Indus Valley. The tin deposits of India have been suggested as a potential source for the tin used in the Indus Valley (Hegde 1978), however there is limited evidence for their early exploitation (Stech & Pigott 1986; Moorey 1994).

Concerning Turkey and Anatolia, it is not until the second half of the second millennium BCE that texts, from Hittite and from Middle Assyrian towns, name parts of Turkey, Nairi (eastern Turkey), and Kizzuwadna (Cilicia) as sources of tin, though with no certain indication that the metal itself was then mined there (Moorey 1994).

## 7.6 Geological aspects

From the geological point of view, among the regions that are close to ancient western Iran and Mesopotamia, the geological features in Iran and Turkey favor the occurrence of tin or tin bearing deposits, but until recently no authentic deposit or mine had been reported from these areas.

Lately some tin deposits have been discovered in different regions of western and central Asia including; Turkey (*Kestel/Göltepe*, Yener & Özbal 1987; Yener et al. 1989; Yener & Goodway 1992; Willies 1990, 1992; Yener & Vandiver 1993), the western Arabian Peninsula in both Saudi Arabia and Yemen (*Jabal Silsilah* and *Kutam*, Stacey et al. 1980; Du Bray 1985; Du Bray et al. 1988; Kamilli & Criss 1996; Overstreet et al. 1988), Eastern Desert of Egypt (Wertime 1978; Muhly 1978,1993), Afghanistan (Shareq et al. 1977; Berthoud 1979; Stech and Pigott 1986), Central Asia (Masson and Sarianidi 1972; Wertime 1973, 1978; Crawford 1974; Ruzanov 1979; Alimov et al. 1998; Boroffka et al. 2002), India and finally Iran (*Deh Hosein*, Momenzadeh et al. 2002; Nezafati et al. 2006) which could be considered as suppliers of the ancient tin needs. A list of known areas and deposits has been summarized in the Table 7.1.

Based upon the recent lead isotope studies accomplished by Weeks (1999, 2004), along with archaeological evidence (Garenne-Marot 1984; Muhly 1973; Glanzman 1987; Fleming and

IRAN						
Deposit	Location	Type of country rock	Form and type of deposit	Ore mineralization	Metal content	Mine workings
<b>Deh Hosein ancient mine</b>	West central Iran (eastern Zagros)	Mainly Jurassic meta-sedimentary rocks	Hydrothermal, veins, veinlets, and dissemination	Native copper, copper sulfide minerals, cassiterite, arsenopyrite, ferberite	Cu: 0.05-10%, Sn: 0.05-6.72%, Au: 0.05-13.3 ppm	Numerous diggings along veins, C <sup>14</sup> dating: 1775-1522 BCE, pottery shards: early first millennium BCE
<b>Chah Palang</b>	South of Anarak area	Triassic-Jurassic weakly metamorphosed sandy-clay rocks	Hydrothermal, veins, veinlets, and dissemination	Gold-tungsten, copper, copper-nickel, copper-bismuth and tin (?) mineral associations	Cu: 0.002-5%, Ni: 0.005-0.08%, Co: 0.004-0.01%, W: 203; < 0.002%	Several adits and galleries, Ore bodies worked out near the surface have up to 30m extension and 1.7m thickness
AFGHANISTAN						
Deposit	Location	Type of country rock	Form and type of deposit	Ore mineralization	Metal content	Mine workings
<b>Mesgaran</b>	South of Herat	.....	Veins and nests, gossan	Copper, magnetite, tin and disseminated pyrite and chalcopyrite, lead-zinc sulphides, cassiterite	Sn: 0.01-6.61%, Pb: 0.06-15%	Signs of ancient working
Several tin bearing districts have been introduced by Shareq et al. (1977): A) 7 pegmatite districts with tin mineralization in Badakhshan, Maydan, Parwan and Oruzghan provinces, B) 3 tin mineral deposits in Herat province (Misgaran), Farah province and in Oruzghan province (Taghawlor), C) 44 mineral occurrences, D) 18 mineral showings, 2 non-commercial placers and 100 mechanical mineral halos, Berthoud (1978, 1979) could gain cassiterite by panning in the Sarkar Valley						
CENTRAL ASIA						
Deposit	Location	Type of country rock	Form and type of deposit	Ore mineralization	Metal content	Mine workings
<b>Kharnab</b>	Between Samarkand and Bukhara (Uzbekistan)	Contact of granite and Devonian limestone	Quartz vein	Arsenopyrite, pyrite, sphalerite, cassiterite	Sn: <1.3%, high sulfur	C <sup>14</sup> dating: 1700-800 BCE, Pottery shards: 2nd mill. BCE
<b>Mushiston</b>	South of Zarafshan valley, NW Tajikistan	Devonian dolomitized limestone and schist	Vein type	Stannite, cassiterite, arsenopyrite, pyrite, chalcopyrite, tetraehedrite, Varlamoffit (Sn <sub>2</sub> Fe <sub>2</sub> (OH) <sub>2</sub> ), Muschistonit (Cu <sub>2</sub> Zn <sub>2</sub> Fe <sub>2</sub> (OH) <sub>6</sub> )	Cu: up to 50%, Sn: up to 34%	C <sup>14</sup> dating: 2100 - 1000 BCE, pottery shards: middle of 2nd mill. BCE
Plus some other occurrences of tin between Bukhara and Dushanbe including Lapas and Cangai						
TURKEY (ANATOLIA)						
Deposit	Location	Type of country rock	Form and type of deposit	Ore mineralization	Metal content	Mine workings
<b>Kestel</b>	Taurus mountains, southeastern Turkey	.....	Vein type	Iron ore, cassiterite	Sn: 0.1-2.3%	From Chalcolithic to Byzantine times, > 15 km shafts and galleries used
Cassiterite has been recorded in southeastern Anatolia in the Kestel/Jelaller region (Yener et al. 1983, Kaptan 1995) and stannite is known from Suludjaderi/Bolkardag and Sogukpinar near Bursa (Yener and Özbal 1987, Kaptan 1995). Several minor occurrences of tin have also been recorded in Anatolia (Kaptan 1995, Weeks 2004)						
WESTERN ARABIAN PENINSULA						
Deposit	Location	Type of country rock	Form of deposit	Ore mineralization	Metal content	Mine workings
<b>Jabal Sifsilah</b>	Central Saudi Arabia	Granite (Fawarrah pluton)	Dissemination, elliptical pods (greisen), high temperature hydrothermal veins	Cassiterite, W minerals	Sn: 0.1% to several percent, in cassiterite-rich greisen 60-90%	Last century workings for tin, No trace of ancient workings prior to 1st mill. BCE
Several granite-hosted and alluvial cassiterite bearing deposits have been reported including Abu Dabbab, Nuweibi, Iqla, El Muellha, Homr Akarem (Rapp et al. 1993, Werthe 1978, Muhlly 1978, 1993)						
EASTERN DESERT OF EGYPT						

Table 7.1 General characteristics of the known tin bearing areas and tin deposits in the Western and middle Asia.



Pigott 1987; Wertime 1978; Weeks 1999, 2004), many of these deposits including deposits of Egypt and the Arabian Peninsula as well as Anatolia (Kestel) have been withdrawn as possible sources of tin for the early Bronze Age.

## 7.7 The Luristan Bronzes

Luristan is a region in west central Iran which embraces the central part of the Zagros Mountain chain (Figure 7.2). Its landscape is dominated by rugged NW-SE aligned mountain ranges that separate valleys and small plains from one another. In modern terms this includes the provinces of Ilam and Luristan as well as parts of provinces of Hamadan and Kermanshah.

In the context of Iranian archaeology, the issue of “Luristan Bronzes” is one of the most enigmatic subjects in various aspects such as a very distinctive style of bronze artifacts, reserving this style almost exclusively to the Luristan region, the source of tin for the huge bronze production in the region, and the population who created these artifacts, their way of subsistence, beliefs or political structure. Unfortunately, contrary to ancient Mesopotamia, the ancient Luristan region lacks textual records which could help to locate the source(s) of tin.

Although according to the excavated tombs built with stone structures (Overlaet 2004), the graveyards belong to different periods, ranging from the second half of the 5<sup>th</sup>- first half of the 4<sup>th</sup> millennium BCE (Middle Chalcolithic era) to ca. 650 BCE (end of Iranian Iron Age), the characteristic “Luristan style” objects all belong to a period ranging from 1300/1250 to 650 BCE (Iranian Iron Age) (Haerinck and Overlaet 2002, Overlaet 2003, 2005). During the Bronze Age (ca. 3000/2900-1300/1250 BCE), the bronze objects are related to those of neighboring regions in Mesopotamia and on the Iranian plateau (Table 7.2)

There are a wide range of tools (utensils, dishes, decorative horse bits), decorative and ceremonial objects with fabulous motifs (idol, standards, figurines, finials and adzes), ornaments (pins and disc headed pins, bracelet, jewelry), and weapons (mace-head, dagger, shield, axe and, adze heads) among the objects known as Luristan Bronze artifacts. These are occasionally accompanied with the decorated iron swords, bracelets and pins. These metal objects are decorated in a very distinctive style with animals, humans and fantastic creatures, combining human as well as animal traits (Figure 7.3). This decorative style culminates in the “master of animals finials”, in which two confronted felines and a central human figure, often with several Janus-heads on top of each other, are fused into one (Figure 7.3c, Overlaet 2004).

Except for two finds, so far no other site in Iran or the Near East has yielded a single example of a Luristan bronze (Muscarella 1988). These two important finds which have occurred outside Luristan are: the upper portion of a standard with master of animals that was excavated in the temple of Hera on the Aegean island of Samos, and an openwork pendant of possible Luristan workmanship which was found at Fortetsa on Crete (Muscarella 1977). How and why these two objects traveled west remain intriguing questions. The simple, unembellished standard from Samos mentioned above is also dated by its context to the late 8th or 7th century B.C. (Jantzen 1972; Muscarella 1988, 2004; Overlaet 2003).

According to excavations of the Belgian Archaeological Mission in Iran (BAMI) on Iron Age Luristan tombs, among the burial-goods occur pottery shapes and objects which indicate that the population had contacts with Kassite Mesopotamia. Good chronological markers are imported decorated shell fingerings and faience buckets which are known from Kassite burials in the nearby Hamrin region (Jabal Hamrin in central Iraq) and from elsewhere in Mesopotamia (Beyer 1982; Boehmer 1982; Boehmer and Dämmer 1985; Clayden 1998; Overlaet 2003). At the same time, the first objects in canonical Luristan style are present (Overlaet 2004).

Around the middle of the 12th century BCE came an end to the presence of Mesopotamian objects among the burial-goods. This can be explained by the destruction of the nearby Kassite settlements in the Hamrin by the Elamite army of Shutruk-Nahhunte around 1160 BCE (Overlaet 2004).



Figure 7.2 Approximate location of the ancient sites in the Luristan area and Mesopotamia.



**Figure 7.3** Some characteristic “Luristan style” objects, **a**) Standard showing two confronted predators and a central woman figure, height 14 cm, **b**) Standard showing two confronted felines, height 12.6 cm, 1000-900 BCE **c**) Standard showing two Janus-heads on top of each other confronting felines, height 18.8 cm, 800-700 BCE, **d**) and **e**) Disc-headed pins, d: 1300-1100 BCE, diameter: 13 cm, e: height 24.6, diameter 11.8 cm, **f**) Different Luristan bronze objects as well as some pottery presented in the Pergamon Museum Berlin, **g**) Ornamented knob-beaker, height 13 cm, 1000-900 BCE, **h**) Laurel-dagger, 25.2 cm, 3000 BCE, **i**) Horse-pendant 8.7cm, early 1000 BCE, **j**) Quasi-ax, 22cm, 1200-1000 BCE, **k**) Snaffle toggle, 11cm, 800-700 BCE. Photos b, c, g, h, i, j, and k after Zahlhaas 2002, photos a and e after Rickenbach 1992 and photo d after Ayazi 2004.

BCE	Periods	Known tombs in Luristan	Artefacts	Mesopotamian and Susian periods	BCE	Comments	
3000	Early Bronze Age I			Mesilim period, Susa III	3000		
2900				Fara Period	2900		
2800				Susa III	2800		
2700				Meskelamdug Period, Susa III	2700		
2600				Ur I period, Susa III	2600		
2500	Early Bronze Age II	Bani Surmah, Kalleh Nissar, Dar Tanha, Tappeh Gigan IV A	Laurel-Dagger, Macehead Axe, az blade, Hoe, Pick	Akkade Period	2500	Oldest Bronzes from "Amlash" - No.3 Lullubians and Akkadians in Zagros	
2400				Susa IV and V	2400		
2300	Early Bronze Age III	Mir Khair, Kalleh Nissar A II, Gululal-e Galbi, Kazhab, Darwand A, Sardant	Vessels (beaked-pot)	Ur III / Isin Period	2300	Lullubian and Kassites in Zagros	
2200					2200		
2100					2100		
2000					Old Babylonian/ Assyrian and Elamide Epoch		2000
1900	Middle Bronze Age	Tappeh Gigan III, Baba Djan IV	Dagger blade, Axe, Hoe, Pick Spearhead, Statuette (seldom)		1900		
1800					1800		
1700					1700		
1600					1600		
1500	Late Bronze Age 3600 till 3300/3250	Tawarsa, Tappe Sarab Bagh		Kassite Period 1557-1158	1500	Kassites in Gilan / Mazandaran	
1400					1400		
1300					1300		
1200	Iron Age I 1300/1250 till 1000/900	Bard-e Bal, Pa-ge Kal, Kutal-e Gulgul, Shurabah, Awazha, Durugah, Karkhai	Fan-handle Dagger, daggers with different types of handle, spearhead, spearshoe, sword, macehead, quasi-az, halberd, necklace, bracelet, earring, needle, stamp, vessels (cup, mug)	Isin II Period 1157- Ca. 1000	1200	Babylonian influence in Zagros, Oldest Iron weapons from Luristan Assyrian influence, buffer states in Zagros	
1100					1100		
1000					New Babylonian		1000
900					Assyrian and Elamide Epoch		900
800	Iron Age II 1000/900 till 800/750	Bard-e Bal, Pa-ge Kal, Kutal-e Gulgul, Shurabah-Payravand, Awazha, Durugah, Karkhai	Spearhead, quiver plate, snaffle, harness, whetstone handle, belt-buckle, anklet, bracelet, needle, disc headed needle, couple needle pendant, fingerring, standard, standard support, sickle, figurine, bell, climp, plates of unknown use, vessels (situla, pot)		800		
700					700		
700	Iron Age III	War Kabud Chavar, Chamzi-Mumah,	Sword, Mace head, az, snaffle, necklace, stamp, standard, standard support, sickle, tube idol, adornment plates,	Late Babylonian Period / Median Kingdom	700	Scythian invasion to West Iran	
600		Djub-e Gauhar, Tadjarian, Sar Kabud, Gul Khanan Murdah	vessels (beaked-pot, cup, bucket, bowl)		600		

Table 7.2 Chronology of the Luristan Bronze artifacts and tombs in comparison with Mesopotamian and Susian periods, based on the data from Calmeyer & Schaefer 1964; Meier-Arendt 1984; and Zahlhaas 2002.

## 7.8 Ancient workings and relics at Deh Hosein ancient mine

The Deh Hosein ancient mine, in the northeastern rim of the Luristan area and eastern part of the central Zagros Mountains (33°.40'-33°.50' N, 49°.08'-49°.20' W) is located in the northern part of the Sanandaj-Sirjan tectonic unit. Geological, mineralogical and geochemical characteristics of the Deh Hosein mine and the specifications of its ore were discussed in chapter 3.

The ancient workings at Deh Hosein occur as numerous (more than 75) big ellipsoidal open depressions, along the mineralized horizons, in an area of 4.5 x 6 km<sup>2</sup> (Figures 7.4a and 3.1). The old workings are up to 70 by 50 by 15 meters in size which array along rows up to 500m long (Figure 7.4b). All the visible ore bearing zones on the surface have been worked out by ancient miners and the ore is visible as weak mineralized selvages of the diggings or as scattered pieces in the dumps. It is possible that underground workings extend underneath each depression and the adits are blocked by debris. Huge waste dumps are piled up at the periphery of each depression.





**Figure 7.4** a) An overview of the Deh Hosein ancient mine with part of its ancient diggings, b) The Ghara Ghouii ancient linear diggings at Deh Hosein, c) The Ahmad Jigi ancient digging with a large mining dump, d) A hammer stone of silicified phyllite found in the Ghara Ghouii digging, e) A hammer stone of granite found in the Ghara Ghouii digging, f) Granitic grinding stones found in the greater ancient settlement, g) Pottery shards and granitic grinding stone (top: a piece of depicted pottery shard).

Several hammer stones of two different materials, namely silicified phyllite and granite (which are common rocks in the area) and pottery shards have been found in the open cast mines (Figures 7.4 d, e). Beside the diggings there are two rather small settlements or workshops in the mining area on which presence of pieces of ore relates them to the mining site. Several grinding stones, hammer stones and pottery shards are visible on the surface of these sites. The bigger site is a rectangular (50 x 30m<sup>2</sup>) structure on a hill, on the northeastern side of the mining area which overlooks all mining sites. A rather big rectangular grinding stone (70 x 35 cm<sup>2</sup>) and several pieces of smaller ones of granitoidic material (Figure 7.4.f), a carved stone with an unknown sign, plenty of pottery shards (Figure 7.4.g) and pieces of copper ore were found on the surface of the site. The grinding stones are of two types, concave and convex with smooth surfaces. The pottery shards are variable in color and thickness and are sporadically depicted with a black material which according to preliminary inspection by archaeologists, date to the early first millennium BCE (Figure 7.4.g).

During a mining exploration campaign accomplished by Zaryaban Exploration Company, pieces of charcoal were found in one of the diggings in a depth about 2 m. Radiocarbon measurement of this charcoal yielded a date of 3380±55 BP, which on calibration results in an interval of 1775-1522 BCE at the 2-sigma confidence level (95% probability). It has to be noted that this date relates to an intermediate layer of the mine; the earliest mining activity can be even older.

No evidence for ancient smelting has been found in the vicinity of the mine. It seems that the ore exploited has been transported to the settlements and smelted outside the area.

Also no sign of medieval or modern mining has been observed in the area of ancient mining. In addition, heavy mineral prospection in the streams of the ancient mining area by Zaryaban Exploration revealed nuggets of cassiterite.

Beside the high content of tin, the high amounts of arsenic and copper in the Deh Hosein ore is noteworthy, especially when we consider this fact that the co-occurrence of arsenic and tin is characteristic of Early Bronze Age metallurgy in Mesopotamia (Fleming et al. 2005).

## 7.9 Compositional analyses from Luristan Bronzes

29 Luristan Bronze artifacts from Iranian National Museum, Tehran Money Museum and a private collection were analyzed for trace elements using energy dispersive X-ray fluorescence (EDXRF). The EDXRF analysis is a widely used technique for the analysis of ancient metal objects (Hackens et al. 1977). The principle advantages are non-destructive and multi-element analysis of a wide range of elements combined with short analysis time and accordingly high sample throughput. Its relatively low sensitivity and dependence on surface alternations are usually considered as main limitations (Lutz and Pernicka 1996).

The samples were taken from different types of finished artifacts including bracelets, dishes, swords, belts, idol supports, pins and disc headed pins, one adze, an oil lamp, a sickle and two statuettes. These artifacts were partly from the BAMI excavations (Belgian Archaeological Mission in Iran, 1965-1979, directed by Van Den Berghe) and partly from unknown places in Luristan or from non-scientific excavations. They range chronologically from the early second to the first millennium BCE. The results of the EDXRF analyses and characteristics of the samples are presented in Table 7.3.



Sample No.	Museum	Location	Museum No.	Description	Cu	Sn	As	Pb	Zn	Ag	Au	Fe	Co	Ni	Sb	Se	Bi	Age
LAN-1	Private collection	Zarrin Chogha (Luristan)	.....	Bracelet	89.918	9.70	0.127	0.125	0.09	0.061	0.09	0.04	0.008	0.031	0.029	0.004	0.004	?
LAN-3	Ir.Nat. Museum	Luristan (?)	.....	Sword	85.00	13.00	0.004	1.820	0.09	0.077	0.020	0.230	0.006	0.009	0.013	0.004	0.009	?
LAN-4	Ir.Nat. Museum	Luristan (?)	28 DK	Sickle	90.00	8.80	0.004	1.020	0.09	0.034	0.009	0.080	0.004	0.009	0.004	0.004	0.004	?
LAN-5	Ir.Nat. Museum	Luristan (?)	115 DK	Lamp?	92.00	6.10	0.450	0.230	0.09	0.025	0.009	0.120	0.033	0.400	0.040	0.009	0.004	?
LAN-6	Ir.Nat. Museum	Luristan (?)	161 DK	Idol pile?	84.00	15.40	0.135	0.010	0.09	0.011	0.009	0.520	0.011	0.012	0.017	0.022	0.004	?
LAN-7	Ir.Nat. Museum	Luristan (?)	192 HR	half round plate	92.00	7.70	0.178	0.350	0.09	0.032	0.009	0.070	< 0.005	0.020	0.040	0.004	0.004	?
LAN-8	Ir.Nat. Museum	Luristan (?)	117 DK	Small Dagger	92.00	7.10	0.450	0.420	0.09	0.013	0.009	0.080	0.014	0.162	0.100	0.008	0.004	?
LAN-9	Ir.Nat. Museum	Luristan (?)	117 DK 2	Medium Dagger	91.00	7.30	0.530	0.270	0.09	0.013	0.009	0.140	0.049	0.460	0.169	0.016	0.004	?
LAN-10	Ir.Nat. Museum	Luristan (?)	191 DK	corroded plate	86.00	13.50	0.017	0.120	0.09	0.039	0.009	0.160	0.004	0.026	0.008	0.004	0.004	?
LAN-11	Ir.Nat. Museum	Luristan (?)	.....	Belt	92.00	6.60	0.600	0.460	0.09	0.067	0.009	0.070	0.008	0.017	0.085	0.004	0.019	?
LAN-12	Ir.Nat. Museum	Luristan (?)	121 DK	Bottom of a plate	89.00	9.80	0.287	0.040	0.09	0.023	0.010	0.180	0.004	0.012	0.048	0.013	0.004	?
LAN-13	Ir.Nat. Museum	War Kabud (Ilam), Van den Berghen excavation	316/16100	A small corroded bowl	89.00	9.90	0.490	0.090	0.09	0.009	0.009	0.160	0.011	0.011	0.084	0.004	0.029	First millennium BCE
LAN-14	Ir.Nat. Museum	Luristan	15620/2673 DK	A small patterned bowl	95.00	3.90	0.020	0.790	0.09	0.030	0.009	0.080	0.004	0.084	0.010	0.004	0.006	First Millennium BCE
LAN-15	Ir.Nat. Museum	Luristan	3004/15943	Plate	87.00	11.50	0.242	0.320	0.09	0.075	0.009	0.180	0.013	0.068	0.104	0.004	0.004	?
LAN-16	Ir.Nat. Museum	Luristan-Kermanshah	2786/15725	A small bowl without bottom	90.00	9.00	0.228	0.230	0.09	0.099	0.009	0.070	0.014	0.129	0.026	0.008	0.004	?
LAN-17	Ir.Nat. Museum	Luristan-Kermanshah	15801/2862 RK	Bowl with 15cm diameter	89.00	10.10	0.490	0.100	0.09	0.020	0.009	0.140	0.022	0.036	0.042	0.004	0.004	?
LAN-18	Ir.Nat. Museum	Kermanshah	15416/2468 DK	Part of a plate	89.00	9.90	0.440	0.170	0.09	0.049	0.009	0.180	0.020	0.196	0.106	0.004	0.004	Early 2nd Millennium BCE
LAN-19	Money Museum	Luristan (?)	.....	Standard head with three deers	92.00	0.48	0.093	0.490	0.300	0.114	0.020	6.100	0.004	0.026	0.016	0.004	0.004	?
LAN-20	Money Museum	Luristan (?)	.....	Small Gilgamesh statue	91.00	0.90	0.004	4.400	0.09	0.013	0.009	3.200	0.004	0.022	0.009	0.004	0.004	?
LAN-21	Money Museum	Luristan (?)	.....	Axe head with an animal statue	90.00	0.95	0.077	2.570	2.600	0.104	0.120	2.930	0.004	0.107	0.030	0.009	0.004	?
LAN-23	Ir.Nat. Museum	Luristan (?)	LM 76.1	Bronze pin	96.00	2.56	0.277	0.100	0.09	0.014	0.009	0.640	0.008	0.037	0.026	0.006	0.004	?
LAN-24	Ir.Nat. Museum	Luristan (?)	LM 76.3	Bronze pin	93.00	3.50	0.185	0.340	0.09	0.008	0.009	2.800	0.008	0.044	0.017	0.004	0.004	?
LAN-25	Ir.Nat. Museum	Luristan (?)	LM 76.4	Bronze pin	96.00	0.75	0.082	0.380	0.09	0.004	0.009	2.330	0.004	0.030	0.039	0.004	0.004	?
LAN-26	Ir.Nat. Museum	Luristan (?)	LM 76.5	Bronze pin	92.00	4.70	0.266	0.280	0.09	0.069	0.030	2.800	0.012	0.033	0.127	0.004	0.004	?
LAN-27	Ir.Nat. Museum	Luristan (?)	LM 76.7	Bronze pin	93.00	1.92	0.069	0.210	0.200	0.009	0.020	4.600	0.018	0.080	0.021	0.004	0.004	2nd Millennium BCE
LAN-28	Ir.Nat. Museum	Luristan (?)	LM 76.8	Bronze pin	86.00	10.30	0.420	0.210	0.09	0.045	0.320	2.040	0.004	0.083	0.201	0.004	0.004	2nd Millennium BCE
LAN-29	Ir.Nat. Museum	Luristan (?)	LM 76.9	Bronze pin	91.00	7.70	0.242	0.450	0.09	0.004	0.020	0.410	0.014	0.009	0.011	0.007	0.007	2nd Millennium BCE
LAN-30	Ir.Nat. Museum	Luristan (?)	LM 76.10	Bronze pin	89.00	3.30	0.035	0.180	6.800	0.069	0.110	0.510	0.004	0.009	0.024	0.014	0.004	2nd Millennium BCE
LAN-31	Ir.Nat. Museum	Luristan (?)	LM 76.11	Bronze pin	96.00	2.06	0.271	0.460	0.100	0.009	0.010	0.980	0.016	0.077	0.017	0.004	0.004	2nd Millennium BCE

Table 7.3 EDXRF results of some Luristan bronze artifacts.

The EDXRF analyses indicate that most of the artifacts are mainly composed of copper (84-96%) and tin (0.48-15.4 %) with lesser amounts of iron (max. 6.1%), lead (max. 4.4%), arsenic (max. 0.6%), zinc (max. 6.8%), silver (max.0.114%), nickel (max. 0.46%) and in a few samples antimony (max. 0.2%). The iron, lead and zinc contents are highest, significantly in less tin-bearing samples. In case of lead, most of the samples and in case of arsenic many of them show at least 0.1% of these metals. Two bronze pins and one adze show rather high content of gold (max. 0.32%).

Eight samples analyzed by Rickenbach (1992) by the same method show 69.4-93.3% Cu, 5.9-26.7% Sn and maximum 3.2% Pb. The content of some other elements are: As (max. 0.36%), Fe (0.22%), Ni (0.29%), and Sb (0.13%).

The comprehensive analytical research on Luristan bronzes of different periods performed by Fleming et al. (2005) show high arsenic contents in the early artifacts which clearly becomes lower with time and technological improvements in the Iron Age. As a result of this fact arsenic is no longer an important alloying ingredient in the Iron Age. According to this study (Fleming et al. 2005), it has also been realized that there was usually no technical control on the percentage of tin in the final products (either weapons or ornaments) and the admixture has occurred randomly. This variation in Sn-contents in finished artifacts may imply that they have simply used a naturally mixed source of copper and tin which can be Deh Hosein ore.

Comparison of the analytical results of the ore from Deh Hosein and with the results of Luristan bronzes accomplished in the course of this study as well as previous researches (Rickenbach 1992 and Fleming et al. 2005) implies that the Deh Hosein ore, with up to 6.72% Sn and up to 10% Cu (see chapter 3), can well be the source of many of these artifacts. In addition to copper and tin, other elements like arsenic, iron, lead, and zinc show high contents in many samples of both sides. Gold, silver, nickel and antimony which indicate traces in the artifacts also show anomalies in the ore.

### 7.10 Lead isotope analysis (LIA)

Lead isotope analysis (LIA) has nowadays reached a reasonable position in the provenance studies of archaeological investigations. Although in some aspects application of LIA is still controversial. Since the isotope composition of lead is more or less constant within an ore body and is not changed at all by chemical reactions during smelting or corrosion (Hezarkhani and Pernicka 2000), it is possible to utilize the lead isotope ratios as fingerprints of individual ore deposits whose ores have been used for production of certain finished artifacts. It is true as long as the ore of two or more deposits of different lead isotope ratios have not been mixed for production of artifacts. In case of admixture of ores of different sources, the lead isotope ratios would be homogenized and the results differ from each individual deposit (Begemann, personal communication).

The application of lead isotope ratios provides, strictly speaking, conclusive evidence only in the negative sense, i.e. a specific ore deposit can be conclusively excluded as a possible source of raw metal when its isotope fingerprints do not match the artifact under study (Hezarkhani and Pernicka 2000).

18 ore samples from Deh Hosein along with 25 metal samples of Luristan Bronze artifacts (the samples which were used for compositional analyses) were examined with a multi-collector inductivity coupled plasma mass spectrometer, VG Axiom MC, for lead isotope ratios (Table 7.4, see also chapter 6, section 6.4). All 2- $\sigma$  (95% confidence level) errors are less than 0.05% for the  $^{207}\text{Pb}/^{206}\text{Pb}$  and  $^{208}\text{Pb}/^{206}\text{Pb}$  ratios. All experiments were performed at the Institute of Archaeometry at the TU Bergakademie Freiberg.

Sample No.	Location	Description	$^{206}\text{Pb}/^{204}\text{Pb}$	$^{207}\text{Pb}/^{206}\text{Pb}$	$^{208}\text{Pb}/^{206}\text{Pb}$	Reference
<b>Deh Hosein Ore</b>						
DHN-1A	East of the deposit	Copper ore	18.439	0.8488	2.0938	This work
DHN-1B	East of the deposit	Galena	18.415	0.8494	2.0949	This work
DHN-7A	Ghara Ghoii digging	Copper ore, cassiterite, parite, galena	18.445	0.8484	2.0924	This work
DHN-7B	Ghara Ghoii digging	Oxidized copper ore	18.446	0.8487	2.0928	This work
DHN-10A	Ahmad Jigi I	Copper ore, arsenopyrite	18.437	0.8488	2.095	This work
DHN-10B	Ahmad Jigi I	Copper ore, pyrite	18.528	0.8452	2.0959	This work
DHN-12A	Ahmad Jigi II	Chalcopyrite, pyrite	18.453	0.8482	2.0926	This work
DHN-15B	Ghaiidan	Copper ore, pyrite	18.461	0.84838	2.0933	This work
DHN-16B	Ghaiidan	Oxidized ore	18.429	0.84868	2.0933	This work
DHN-34	Ahmad Jigi I	Copper ore (native copper), pyrite, arsenopyrite	18.487	0.8468	2.0935	This work
DHN-38	Ahmad Jigi II	Arsenopyrite, chalcopyrite, pyrite	18.446	0.8485	2.0928	This work
DHN-42	Ghara Ghoii digging	Quartz, chalcopyrite, malachite, azurite, Fe oxides	18.444	0.8484	2.0922	This work
DHN-43	North of the deposit	Oxidized ore (chalcopyrite, pyrite, sphalerite, cassiterite)	18.422	0.849	2.0937	This work
DHN-45	veinlet in the northern granite	Oxidized copper ore	18.547	0.8438	2.0857	This work
DHN-47	mineralization in the northern granite	Oxidized ore (chalcopyrite, arsenopyrite, ferberite)	18.517	0.8453	2.0901	This work
DHN-60	North of the deposit	Pyrite, arsenopyrite, sphalerite	18.434	0.8486	2.0935	This work
DHN-76	East of the deposit	Oxidized ore (chalcopyrite, galena, pyrite)	18.447	0.8486	2.0927	This work
DHN-93	Ahmad Jigi I	Arsenopyrite	18.509	0.8458	2.0950	This work
<b>Luristan Bronze</b>						
LAN-1	Zarrin Chogha	Bracelet	18.504	0.84516	2.0854	This work
LAN-3	Luristan (?)	Sword	18.219	0.85989	2.1017	This work
LAN-4	Luristan (?)	Sickle	18.204	0.85978	2.1013	This work
LAN-5	Luristan (?)	Lamp?	18.831	0.83316	2.0683	This work
LAN-6	Luristan (?)	Idol pile?	18.513	0.84353	2.081	This work
LAN-7	Luristan (?)	half round plate	18.525	0.84409	2.0856	This work
LAN-8	Luristan (?)	Small Dagger	18.351	0.85311	2.0934	This work
LAN-13	War Kabud (Ilam)	A small corroded bowl	18.285	0.85403	2.0961	This work
LAN-14	Luristan	A small patterned bowl	18.462	0.84812	2.0914	This work
LAN-15	Luristan	Plate	18.445	0.84755	2.0893	This work
LAN-16	Luristan-Kermanshah	A small bowl without bottom	18.703	0.83884	2.0752	This work
LAN-17	Lorestan-Kermanshah	Bowl with 15cm diameter	18.566	0.84352	2.0812	This work
LAN-18	Kermanshah	Part of a plate	18.561	0.84406	2.0831	This work
LAN-19	Luristan (?)	Standard head with three deers	18.278	0.85497	2.095	This work
LAN-20	Luristan (?)	Small Gilgamesh statue	18.516	0.84511	2.0869	This work
LAN-21	Luristan (?)	Axe head with an animal statue	18.446	0.84836	2.0884	This work
LM-76.1	Luristan (?)	Bronze pin	18.557	0.84384	2.0837	This work
LM-76.3	Luristan (?)	Bronze pin	18.567	0.8445	2.086	This work
LM-76.4	Luristan (?)	Bronze pin	18.547	0.84341	2.084	This work
LM-76.5	Luristan (?)	Bronze pin	18.458	0.84854	2.0924	This work
LM-76.7	Luristan (?)	Bronze pin	18.542	0.84448	2.0819	This work
LM-76.8	Luristan (?)	Bronze pin	18.64	0.84164	2.0808	This work
LM-76.9	Luristan (?)	Bronze pin	18.741	0.83636	2.0706	This work
LM-76.10	Luristan (?)	Bronze pin	18.711	0.83769	2.0738	This work
LM-76.11	Luristan (?)	Bronze pin	18.847	0.83247	2.0658	This work

**Table 7.4** Lead isotope ratios and sample description of the ore samples from Deh Hosein as well as bronze artifacts from Luristan, UAE, Mesopotamia, the Aegean, and Bulgaria.

Sample No.	Location	Description	$^{206}\text{Pb}/^{204}\text{Pb}$	$^{207}\text{Pb}/^{206}\text{Pb}$	$^{208}\text{Pb}/^{206}\text{Pb}$	Reference
<b>Luristan Bronze</b>						
HDM 356	Luristan	Bronze artifact	18.474	0.8464	2.0901	Begemann & Schmitt-Strecker 2006
HDM 349	Luristan	Bronze artifact	18.3823	0.8495	2.091	Begemann & Schmitt-Strecker 2006
HDM 352	Luristan	Bronze artifact	18.4706	0.8486	2.0912	Begemann & Schmitt-Strecker 2006
HDM 338	Luristan	Bronze artifact	18.3823	0.8497	2.0913	Begemann & Schmitt-Strecker 2006
HDM 343	Luristan	Bronze artifact	18.4433	0.8488	2.092	Begemann & Schmitt-Strecker 2006
LU 39(17888)	Luristan	Bronze artifact	18.4433	0.8497	2.092	Begemann & Schmitt-Strecker 2006
LUI7850	Luristan	Bronze artifact	18.423	0.8486	2.0922	Begemann & Schmitt-Strecker 2006
HDM 339	Luristan	Bronze artifact	18.4331	0.8494	2.0927	Begemann & Schmitt-Strecker 2006
HDM 348	Luristan	Bronze artifact	18.4536	0.8488	2.0928	Begemann & Schmitt-Strecker 2006
LUI7907	Luristan	Bronze artifact	18.4501	0.8486	2.093	Begemann & Schmitt-Strecker 2006
HDM 347	Luristan	Bronze artifact	18.4638	0.8482	2.0932	Begemann & Schmitt-Strecker 2006
HDM 336	Luristan	Bronze artifact	18.4162	0.8503	2.0945	Begemann & Schmitt-Strecker 2006
LUI7866	Luristan	Bronze artifact	18.4399	0.8491	2.0948	Begemann & Schmitt-Strecker 2006
HDM 358	Luristan	Bronze artifact	18.4331	0.8494	2.0953	Begemann & Schmitt-Strecker 2006
<b>Persian Gulf</b>						
ASI-3	Al Sufouh	flat fragment Cu-As-Ni-Co-Sn(low)	18.247	0.8540	2.10518	Weeks (1999, 2004)
ASTomb 1d	Al Sufouh	flat fragment Cu-Sn(low)-As-Ni	18.485	0.8508	2.09485	Weeks (1999, 2004)
M10-7	Unar 1	flat fragment Cu-Sn(low)	18.451	0.8501	2.09589	Weeks (1999, 2004)
M10-13v	Unar 1	flat fragment Cu-Sn	18.461	0.8487	2.09475	Weeks (1999, 2004)
M10-19	Unar 1	ring Cu-Sn(low)	18.299	0.8554	2.10341	Weeks (1999, 2004)
M10-22r	Unar 1	ring Cu-Sn-Fe	18.330	0.8525	2.10149	Weeks (1999, 2004)
M10-39	Unar 1	flat fragment Cu-Sn-Fe	18.372	0.8492	2.09712	Weeks (1999, 2004)
1014.76000	Unar 2	ring Cu-Sn-Fe	18.167	0.8630	2.11168	Weeks (1999, 2004)
1014.15800	Unar 2	ring Cu-Sn-As	18.055	0.8683	2.11632	Weeks (1999, 2004)
1018-3.99	Unar 2	flat fragment Cu-Sn-As-(Ni)	18.615	0.8440	2.09053	Weeks (1999, 2004)
1019-5.71	Unar 2	ring Cu-Sn-As	18.655	0.8428	2.08447	Weeks (1999, 2004)
1023-4.10	Unar 2	ring Cu-Sn-(Fe)	18.404	0.8543	2.09453	Weeks (1999, 2004)
1019-3.105	Unar 2	flat fragment Cu-Sn-As-Fe	18.028	0.8731	2.10920	Weeks (1999, 2004)
TA1217	Tell Abraq	flat fragment Cu-Sn	18.831	0.8342	2.07250	Weeks (1999, 2004)
TA1231	Tell Abraq	spearhead Cu-Sn(low)	18.061	0.8707	2.12420	Weeks (1999, 2004)
TA1286	Tell Abraq	flat fragment Cu-Sn	18.792	0.8350	2.07430	Weeks (1999, 2004)
TA1306	Tell Abraq	flat fragment Cu-Sn	18.807	0.8354	2.07620	Weeks (1999, 2004)
TA1428	Tell Abraq	pin/awl Cu-Sn(low)-Fe	18.515	0.8471	2.08580	Weeks (1999, 2004)
TA1459	Tell Abraq	pin/awl Cu-Sn	18.531	0.8462	2.09190	Weeks (1999, 2004)
TA1648	Tell Abraq	spearhead Cu-Sn	17.919	0.8743	2.12170	Weeks (1999, 2004)
TA2918	Tell Abraq	ring Sn-As ring	18.454	0.8490	2.09443	Weeks (1999, 2004)
<b>Near East</b>						
MASC 22	Kish, Mesopotamia	Bronze artifact	18.6289	0.8442	2.0914	Begemann & Schmitt-Strecker 2006
JD- 36/1	Zeiraqun, Jordan	Bronze artifact	18.5014	0.8471	2.0905	Begemann & Schmitt-Strecker 2006
<b>Aegean</b>						
HDM 251	Troia, Turkey	Bronze artifact	18.3688	0.8497	2.0909	Pernicka et al. 1984
HDM 809	Thermi III	Cu (Sn:4.2%)	18.546	0.8448	2.0809	Begemann et al. 1992
HDM 993	Thermi, Potter's Pool	Cu (Sn: 6.2%)	18.4877	0.8493	2.0917	Begemann et al. 1992
HDM 809	Thermi III	Cu (Sn)	18.546	0.8448	2.0809	Begemann et al. 1992
HDM 805	Thermi V	Cu (Sn)	17.9985	0.8682	2.1142	Begemann et al. 1992
HDM 855	Thermi V	Cu (Sn)	18.843	0.8318	2.0618	Begemann et al. 1992
HDM 854	Thermi, Potter's Pool	Cu (Sn)	18.1488	0.8635	2.1065	Begemann et al. 1992
HDM 860	Thermi, Potter's Pool	Cu (Sn)	18.6428	0.8403	2.0781	Begemann et al. 1992
HDM 868/989	Thermi, Potter's Pool	Cu (Sn)	18.688	0.8405	2.0805	Begemann et al. 1992
HDM 870/991	Thermi, Potter's Pool	Cu (Sn)	18.6811	0.8388	2.0747	Begemann et al. 1992
HDM 993	Thermi, Potter's Pool	Cu (Sn)	18.4877	0.8493	2.0917	Begemann et al. 1992
HDM 856	Late Bronze Age	Cu (Sn)	18.7441	0.8342	2.0739	Begemann et al. 1992
HDM 863/994	Thermi IV	Sn (76.3%) + Fe (22.7%)	17.4794	0.8903	2.142	Begemann et al. 1992
<b>Bulgaria</b>						
HDM 1957	Durankulak	Bronze artifact	18.5014	0.8474	2.0915	Pernicka et al. 1997

Table 7.4 (continued)

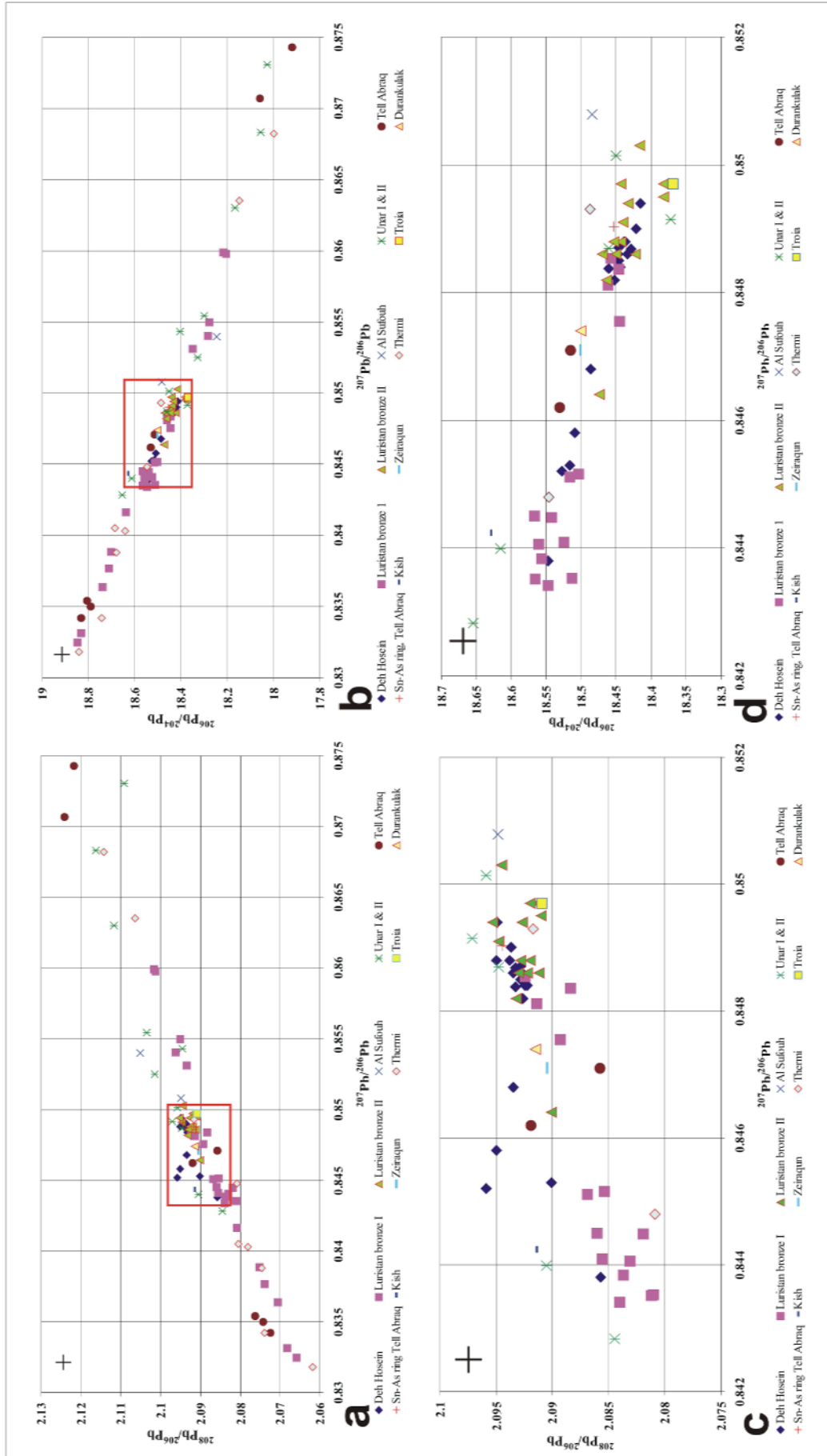


**Figure 7.5** Isotope plot of lead in ore samples from Deh Hosein in comparison with bronze artefacts from Luristan, UAE, Mesopotamia, the Aegean, and Bulgaria (figures a and b). The error bars show the  $2\sigma$  uncertainty. Luristan Bronze I refers to the 1st and 2nd millennium BCE artifacts analyzed during this study, while Luristan Bronze II refers to the 3rd millennium BCE samples analyzed by Begemann & Schmitt-Strecker. In the figures c & d the scale of the diagrams are greatly expanded.



The lead isotope data of bronze artifacts of different periods and locations published by Weeks (Southern Persian Gulf including Al Sufouh, Tell Abraaq, Unar 1 and Unar 2, 1999, 2004), Pernicka et al. 1997, Begemann et al. (Thermi in Aegean, 1992) as well as unpublished data from Begemann & Schmitt-Strecker (3<sup>rd</sup> millennium Luristan, Troia, Mesopotamia and, Jordan) have been used in order to compare the results and have more accurate conclusion.

The samples, their description and isotopic concentrations are shown in Table 7.4. By comparison of the lead isotope ratios of the Deh Hosein ancient mine with bronze artifacts from Luristan, southern Persian Gulf, Mesopotamia, Aegean and Bulgaria (Figures 1, 2, and 3) the following conclusions can be drawn:

- The Deh Hosein deposit shows a rather small variation of lead isotope ratios disregarding if the ratio is from copper minerals, galena, arsenopyrite, copper and tin minerals or bulk samples which contain different range of minerals.
- The metal used in a number of the bronze artifacts is isotopically compatible with the Deh Hosein deposit. These include most of the 3<sup>rd</sup> millennium BCE Luristan artifacts, half of the 1<sup>st</sup> and 2<sup>nd</sup> millennium BCE Luristan objects, some southern Persian Gulf artifacts, two samples from Thermi, one artifact from Kish (Mesopotamia), Zeiraqun (Jordan) and Durankulak (Bulgaria). This indicates that the Deh Hosein ancient mine could have been a major supplier of the tin which was used in the contexts of a wide area from western Turkey (and even farther to Bulgaria) to southern Persian Gulf in a rather wide period of time from third millennium to the first millennium BCE.
- Although a sample from Kish, two samples from Tell Abraaq, two samples from Unar 2, the sample from Zeiraqun, and a sample from Thermi do not match exactly the samples from Deh Hosein, they plot in the same area as the Deh Hosein samples.
- Interestingly, the lead isotope ratio of a tin-arsenic bangle from the site Tell Abraaq reported by Weeks (1999, 2004) matches very well with the isotope ratio of the ore at Deh Hosein.
- The rather numerous outliers to the main distribution which are from the sites of Tell Abraaq, Unar 1, Unar 2, Al Sufouh, Thermi and some 1<sup>st</sup> and 2<sup>nd</sup> millennium BCE Luristan artifacts indicate that either another source of tin has been used for them or their metal derives from a mixture of Deh Hosein ore with some copper ore with a different lead isotope ratio.
- Although a positive assignment is not possible out of principle the very small variation of lead isotope ratios in the Deh Hosein deposit and the almost identical lead isotope ratios in ores from there and in bronze samples from Luristan, Southern Persian Gulf, Western Turkey and Mesopotamia strongly suggest that the ore from Deh Hosein have already been known and exploited as early as the third millennium BCE. It is also reasonable because the Deh Hosein ancient mine is the only so far known copper-tin deposit which is located in the vicinity of ancient cultures and its lead isotope ratios matches the ones from ancient artifacts. In the other hand, if tin sources are very scarce, one or a very limited number of sources could have supplied a very large area, and such isotopic matches could be a reflection of shared provenance (Weeks 2004).

## 7.11 Summary and conclusions

The recent discovery of the Deh Hosein tin-copper occurrence together with ancient mining along with new analytical results of bronze artifacts from Iran and the United Arab Emirates, provide a pivotal clue to find an answer for the old archaeological question in terms of tin. The following evidence attest that the Deh Hosein ancient mine has been a major supplier of tin for



ancient civilizations of ancient Iran and Mesopotamia and even perhaps further localities to its west:

### ***The mineralogical and analytical evidence***

The simultaneous occurrence of tin and copper minerals within one mineralization, the strong correspondence of lead isotope ratios as well as good correlation between trace elements of the Deh Hosein ancient mine and the ancient artifacts including high tin, copper and arsenic contents attest to the role of this mine in supplying copper-tin ore of the ancient workshops.

### ***The chronological evidence***

According to  $^{14}\text{C}$  dating and archaeological evidence, the Deh Hosein ancient mine has been in operation at least from early second millennium till first millennium BCE.

### ***The ancient textual records (repeated textual reference)***

In the ancient cuneiform texts, it has been several times mentioned that copper, bronze and tin come from the east. Among these texts, the text from Kanesh which refers to tin coming overland through the Zagros Mountains to Mesopotamia from northwestern Iran (Muhly 1973), and the text referring to mines behind Jabal Hamrin (Ebih) (*Innana and Ebih*, Muhly 1973) may have mentioned Deh Hosein Mine.

### ***The geographical evidence***

The recently discovered Deh Hosein ancient mine is the only known tin (-copper) bearing source in close distance to the eastward Mesopotamia and Luristan area.

### ***The statistical evidence***

The abundance of bronze artifacts from the mid Bronze Age to the end of Iron Age in the whole Mesopotamia and western Iran attests to a rich source of ore in the vicinity of these areas, especially when it would be taken into consideration that this abundance has emerged mainly in these areas and not to adjacent areas.

### ***The denomination evidence***

The Greek word for tin,  $\kappa\alpha\sigma\sigma\iota\tau\epsilon\rho\zeta$  (Kassiteros), can be interpreted as metal “coming from the country of the Kassites” (Ghirshman 1954), and the Kassites lived in central and west central Iran. Also the characteristic Luristan Bronze artifacts appear under the reign of the Kassites in west central Iran and Mesopotamia. Finding two canonical artifacts of Luristan Bronze on Samos and Crete islands may confirm the influence of Kassites (or Luristani people) and the export of their wares to ancient Greek territories in the late 8th or 7th century BCE.

Although the huge amount of bronze finds in the ancient sites of Western Asia implies that the Deh Hosein ancient mine could not have been the only source of copper-tin ore in antiquity, but the geological and economic geological evidence indicate that the whole northern part of Sanandaj-Sirjan belt which favors the occurrence of such ore deposits or perhaps ancient mines should be considered for prospecting of the possible undiscovered ancient mines. The Nezam Abad prospect with up to 1.19 % tin and 10% copper (see chapters 5 and 6) which contains some ancient workings and shows similar lead isotope ratios to the Deh Hosein ore can be an indication for this hypothesis, although at this occurrence the amount of ancient diggings and the content of tin are less than in Deh Hosein.

It should also be taken into consideration that the Deh Hosein ancient mine has only recently been discovered (2000) and therefore it is possible that further ancient tin mines may have remained undiscovered in the northern part of the Sanandaj-Sirjan zone.

## *Chapter 8*

### **Conclusions**

Considering the geological, mineralogical, and geochemical results presented in chapters 1 to 7, the following conclusions can be extracted for the nature and age of the mineralizations in the three occurrences of the Astaneh-Sarband area.

At *Deh Hosein* the field investigations show a good association between the meta-sandstone intercalations and the mineralization. This can be confirmed by the good correlation of the lead isotope signatures in the ore and the meta-sandstone. The oxygen isotope studies suggest a metamorphic or a mixed metamorphic-magmatic source (due to rock-fluid interactions) of hydrothermal fluids while sulfur isotope values imply a magmatic source for sulfur. Also according to geochemical investigations, some metal contents, including gold and silver, have been depleted in the meta-sandstone while arsenic still shows positive anomalies. These results lead to the conclusion that some of the metals including gold, arsenic and silver have perhaps been mobilized from the meta-sandstone of the region by hot hydrothermal solutions. It is possible that the meta-sandstone intercalations, because of their better permeability, have also played a role as a channel or passage for the hot mineralized fluids. The temperature of the fluids of the main mineralizing phase was about 460°C. Fluid mixing and reactions with host rocks were important processes during the evolution of the hydrothermal system at Deh Hosein. Fluid-rock reaction caused alteration of the host rocks, leading to gold deposition.

Although the mineralization continues in the northern intrusive body of Deh Hosein, including tourmaline granite, according to lead isotope studies this intrusive body can not genetically be related to the mineralization and only some of their fractures have been filled with the younger mineralization. The intrusive body responsible for generating the mineralization has not been found. It is possible that some covered stocks underneath the occurrence or farther intrusive bodies to the north of the occurrence, which probably are of lower crustal origin, have caused the mineralization.

A direct age determination for the mineralization of Deh Hosein was not possible. Dating of the northern intrusive body (tourmaline granite) of the mineralization has shown a Middle

Jurassic age, but as already mentioned this rock is not genetically related to the mineralization. Close similarities of the Deh Hosein occurrence with two other gold and tungsten mineralizations in the area (Farhadian 1991; Nezafati et al. 2005) indicate that the event of mineralization at Deh Hosein has probably occurred in Eocene as well.

At *Astaneh*, field observations, along with mineralogical, geochemical and isotopic studies suggest a magmatic source for the mineralization. The fertile (I-type) Eocene and post-Eocene magmatism in the area produced the Shirmazd stock and some younger dykes and probably caused the hydrothermal mineralization with fluid temperatures of about 380-410°C. According to lead isotope studies this magma has been also of lower crustal origin. The mineralization probably occurred during the final stages of the cooling of the Shirmazd stock and intrusion of microgranodiorite dykes in it. This has been controlled by NE-trending faults in the area.

At *Nezam Abad*, the gold-tungsten mineralization is more or less restricted to the fertile quartz diorite unit which has occurred in Eocene and hosts the mineralization. According to field observations along with mineralogical and lead and sulfur isotope studies, the quartz diorite has played an essential genetic role in the generation of the ore, for its heat, fluid and metal sources. A high temperature (510-565°C) mineralizing fluid, originated from this intrusion, has perhaps been affected by already present metamorphic rocks or fluids of the area and has caused the mineralization. Small-scale magmatism not related to ore formation has influenced the Nezam Abad occurrence during the Oligocene. Aplitic and diabasic dykes as well as some non-mineralized quartz-tourmaline veins indicate traces of this magmatism in the area.

Overall, it appears that a wave of simultaneous, basically I-type, fertile intrusions during Pyrenean Orogeny (Eocene-Oligocene) in the Astaneh-Sarband area has been responsible for a rather extensive Au-Sn-W-Cu mineralization. The occurrences have probably formed from magmatic hydrothermal fluids which were tapped by deep-seated crustal structures.

Increase in pH, wall-rock interaction, mixing of magmatic and metamorphic fluids, and finally simple cooling (temperature reduction) are among the viable mechanisms responsible for the decrease in the solubility of metals and consequently for the deposition of ore minerals in the occurrences of the study area. The simultaneous tectonic movements have facilitated the deposition by creating fractures and open spaces.

The age determinations of this study together with the results from Farhadian (1992), Masoudi (1997), and Ghaderi et al. (2004) on the rocks of the area suggest four distinct periods of granitoid magmatism in the Astaneh-Sarband area and northern part of Sanandaj-Sirjan zone. This magmatism starts in Middle Jurassic with tourmaline granite, and continues in (Early-Late) Cretaceous-Early Paleocene with granitoid and pegmatitic intrusion. The fertile magmatism of Eocene manifests as granodiorite and quartz diorite. Finally a rather weak and basically barren magmatism has caused aplitic and diabasic dykes in Oligocene.

### **Comparison of the prospects in the Astaneh-Sarband area with each other**

A comparison of petrological, mineralogical and geochemical characteristics of the three occurrences of the Astaneh-Sarband area shows considerable similarities. In order to compare and contrast Deh Hosein, Astaneh and Nezam Abad, their most similarities and differences are presented as follows:

- The Nezam Abad and Astaneh prospects are intrusion-hosted while Deh Hosein is essentially hosted in metamorphic rocks. The investigated mineralization-related intrusions are basically of I-type and calc-alkaline nature. Also the alkalinity values suggest a “peraluminous field” and imply the formation of intrusive bodies during collision (Masoudi 1997).

- Sericitization, chloritization and silicification are the most important and abundant ore-related alterations in all occurrences. Tourmalinization is present at both Deh Hosein and Nezam Abad, while it is absent at Astaneh. Monazite alteration has been observed only at Deh Hosein.
- Quartz and quartz-sulfide veining as well as dissemination and impregnation along the veins are common forms of mineralization in the occurrences. The veins and mineralization-related structures essentially show NE-trends, although NW and E-W trends have been observed as well (especially at Nezam Abad). Sheeted forms of veins are sporadically observed especially at Deh Hosein.
- The Mineral assemblages are dominated by arsenopyrite, chalcopyrite and pyrite as major sulfides. The presence of pyrrhotite, absence of magnetite and lack of molybdenum are common for all three occurrences as well. However, variations in mineralogy are present from one occurrence to another. Deh Hosein shows the most diverse assemblage of minerals among the three prospects. Anglesite, native copper, cuprite, some sulfosalts (including kobellite, krupkaite, beaverite, sulphotsumoite, and sztokavite), löllingite, monazite, and pyrolusite are among the minerals which have only been observed at the mineralization of Deh Hosein. Additionally galena is abundant at Deh Hosein. A major difference among the mineralizations is in relation to their tungsten mineral which is solely scheelite in the Nezam Abad and Astaneh prospects, while ferberite in Deh Hosein, in both of its metamorphic and magmatic host rocks. The occurrence of ferberite at Deh Hosein may hint to a higher oxygen fugacity of the mineralizing fluids (Foster et al. 1975 and Gallagher 1989). Cassiterite is most abundant at Deh Hosein, while it has not been observed in the Astaneh prospect.
- In the first stage of mineralization scheelite, ferberite and cassiterite have formed. This stage was followed by the main phase of sulfide-gold mineralization in which arsenopyrite, bismuth minerals, different sulfide minerals and gold have been precipitated.
- Invisible gold in arsenopyrite is the main form of gold occurrence in the prospects of the area. In this regard, inclusions of native bismuth and bismuth minerals are common in the arsenopyrite of all mineralizations which likewise demonstrate high contents of gold.
- According to the field and trace element investigations, the ore of the occurrences is characterized by low sulfur content (generally less than 3%), high gold contents, and high anomalies of copper, tin, tungsten, bismuth, silver, and arsenic. Gold is strongly correlated with bismuth, arsenic, silver and selenium. The Nezam Abad prospect indicates the highest content of gold (at locality Fizuneh) among the three prospects, while the Deh Hosein has the second rank. At Deh Hosein, tin and to some extent copper can be of economic value beside the gold; tungsten may be a valuable by-product at Nezam Abad. At Astaneh, except gold no other metal shows economic value.
- All three occurrences show similar oxygen and sulfur isotope values which indicate a metamorphic and/or metamorphic-magmatic source for the hydrothermal fluid, and a magmatic source for the sulfur. Nevertheless, as sulfur isotope values increase from Deh Hosein to Nezam Abad (Deh Hosein>Astaneh>Nezam Abad) the oxygen isotope ratios decrease. On the other hand, the O and S values show a negative correlation.
- Although the lead isotope signature of each occurrence is individual all three occurrences indicate generally similar signatures especially in the case of Astaneh and Deh Hosein.
- Arsenopyrite geothermometry and mineral assemblage demonstrate high temperatures (380°C to 565°C) for the mineralizing fluids in all prospects.
- According to age determination studies accomplished by this study and Farhadian (1992) the age of the mineralizations of Astaneh and Nezam Abad can be, with great confidence,

considered Eocene and post-Eocene. In case of Deh Hosein, the significant similarities of the occurrence with the Astaneh and Nezam Abad occurrences suggest the same age range.

### Comparison of the occurrences with known deposits

The above mentioned characteristics of the occurrences of the Astaneh-Sarband area clearly show their resemblance with the recently defined intrusion-related gold systems (Newberry et al. 1995; McCoy et al. 1997; Thompson et al. 1999; Lang et al. 2000; Lang and Baker 2001; Baker 2002). The deposits of this type have previously been called “porphyry gold deposits” (Hollister 1992; Bakke 1995), “intrusion-related stockwork-disseminated deposits” (Sillitoe 1991), “plutonic-related gold deposits” (Newberry et al. 1988; McCoy et al. 1997) and “intrusion-related gold deposits” (Thompson et al. 1999). The term “intrusion-related gold systems” has been finally proposed by Lang et al. (2000), because it reflects a tendency common to all magmatic-hydrothermal environments to form ores that manifest multiple styles, metal assemblages, and spatial associations with their related intrusive centers (Lang and Baker 2001).

The most common similarities of the intrusion-related gold systems are as follows: (1) Phanerozoic age, (2) a tectonic setting well inboard of inferred or recognized convergent plate boundaries, where continental magmatism commonly contains coeval intrusions of alkalic, metaluminous calc-alkalic, and peraluminous compositions, (3) location in magmatic provinces with tungsten and/or tin deposits, (4) granitic to granodioritic intrusions emplaced into meta-sedimentary rocks, (5) metaluminous to slightly peraluminous subalkalic intrusions of intermediate to felsic composition that lie near the boundary between ilmenite and magnetite series, (6) a reduced ore mineral assemblage that typically comprises arsenopyrite, pyrrhotite, pyrite and lacks magnetite and hematite, (7) areally restricted, commonly weak hydrothermal alteration (interpreted to result from low fluid volumes), (8) a low-sulfide (<5 vol. %) ore assemblage, (9) geochemical enrichment in gold, bismuth, arsenic, tungsten, tellurium, and/or antimony, (10) strong correlation of gold and bismuth, (11) occurrence of gold commonly in sheeted quartz veins, (12) fluid temperatures of 300°C to 600°C range (mainly over 300°C), and (13) dominance of magmatic and metamorphic fluids together with paucity or absence of meteoric fluids (McCoy et al. 1997; Thompson et al. 1999; Baker and Lang 1999; Goldfarb et al. 2000; Lang and Baker 2001; Baker 2002). Also as Goldfarb et al. (2000) assert placer deposits of gold, and more rarely tungsten or tin, are commonly derived from intrusion-related gold systems. Table 8.1 presents general characteristics of some of the known intrusion-related gold systems worldwide.

The significant differences between the occurrences of the Astaneh-Sarband area and the majority of the intrusion related gold systems are the age of mineralization and the rather high contents of base metals (especially copper) in the Astaneh-Sarband area. The age of mineralization of most of the intrusion-related gold systems ranges from the Proterozoic to the end of the Cretaceous, while it is Eocene in the Astaneh-Sarband area. Also base metals are relatively low (typically <500 ppm of combined copper, zinc and lead) in the majority of such systems. However, in zoned systems like Kidston, base metals are more abundant and occur with gold above the molybdenum-tungsten zone (Thompson et al. 1999).

Hart et al. (2000) proposed a model with three-categories for the intrusion-related gold systems based on their spatial relationship to intrusions and their metal content (Figure 8.1). According to this model, auriferous, mostly sheeted and lesser stockwork vein deposits that are characterized by a metal assemblage of Au-Bi<sup>+</sup>Te<sup>+</sup>As<sup>+</sup>Mo<sup>+</sup>W fit to the category of “*intrusion-hosted deposits*”. “*Proximal deposits*” are located in host rocks adjacent to the intrusions, or slightly removed from them, but within the metamorphic aureole. Common deposit types are W<sup>+</sup>Cu<sup>+</sup>Au and Cu-Bi-Au<sup>+</sup>W skarns, high to low sulfide replacements of calcareous rocks, tin-



bearing and copper-rich breccias and diatremes, and veins and disseminated deposits in meta-sedimentary host rocks. “*Distal deposits*” are located beyond the outer limit of hornfels. The intrusion-hosted and proximal settings contain the deposits most characteristic of intrusion-related gold systems (Lang and Baker 2001). According to the above mentioned model, the Astaneh and Nezam Abad occurrences can be considered in the category of intrusion-hosted deposits, while the Deh Hosein occurrence matches well the category of proximal deposits.

Concerning the deposits similar to Deh Hosein, the deposits of Brewery Creek in the Yukon (Poulsen 1996) and True North in the Fairbanks district (Harrison and Gorton 1998) which are distal to intrusions ( $1 \pm 3$  km) and formed beyond their contact aureoles as well as the Muruntau giant gold deposit (Wilde and Gilbert 2000) and some of the Au-Sn-W deposits in southern Finland (Luukkonen 1994) including Kutemajärvi (Au, Sn), Tammijärvi (Au, Sn, W, Cu), and Ahvenlammi (Au, Sn, W) show several similar characteristics (Table 8.1).

### **Recommendations for future researches**

The limited sub-surface information in the area hampered our knowledge about the depth and strength of the mineralizations. Numerous similarities between the occurrences of the area and some large world-class deposits, rather high content of gold along with tin and tungsten (and copper), and the moderate topography and climate of the area introduce a promising region for further exploration activities. Drilling some boreholes and soundings by digging are recommended, especially at Deh Hosein and Astaneh, in order to investigate the continuity and grade of gold mineralization in depth.

Because of the restricted nature of the alterations, especially in metamorphic terrains, application of remote sensing does not appear very useful for further prospecting in the area. A glimpse at the geological map of west central Iran (Figure 8.2) reveals the high potential of the area for occurrence of more intrusion-related Au-W-Sn-Cu mineralizations. In west central Iran, in the northern part of Sanandaj-Sirjan zone, several intrusive bodies are present in Triassic-Jurassic low grade metamorphic rocks. These intrusive bodies with a NW-SE trend form a small belt from southeast of Sanandaj in the north to the north of Golpaygan in the south.

These intrusive bodies have occurred in different magmatic phases from Middle Jurassic to Eocene-Oligocene, from which the intrusions of Eocene age can be very likely fertile for similar types of mineralization. Detail investigation and dating of these intrusive bodies, detailed geochemical exploration of the area and finally paying more attention to possible traces of ancient mining relics can be among the strategies for a further exploration program.

It should be emphasized that since intrusion-related gold deposits represent an economically important exploration objective, such targets, like the Astaneh-Sarband area and the northern Sanandaj-Sirjan zone, should not be ignored.

Deposit and country	Subsidiary metals	Ore minerals	Alteration	Type of country rock	Age (Ma)	Temperature of fluid (°C)	Deposit type	Genetically related intrusion	Reference
Fort Knox Alaska, USA	Bi, Te, Mo, As, Sb, W	Apy, Py, Sn, Sch, Po, Lo, Mol, Bim	Ab, Qz, Ser, Carb	Mica-quartz schist	92	300-480	Sheeted veins	Porphyritic granite	Bakke (1995), Thompson et al. (1999), Baker (2002)
Donlin Creek, Alaska	Ag, As, Sb, Hg	Py, Apy, Sn	Qz, Ser, Carb, Clay	Rhyolite sills/dikes	Late Cretaceous	>550	Veins, veinlets	I-type	Ebert et al. (2000), Baker (2002)
Shotgun, Alaska	Bi, Te, Mo, As, Cu	Apy, Po, Lo, Py, Cep, Sch	Ab, Ser, Qz, Carb	Granite stock	~ 70	350-650	Stockwork and breccia	I-type	Rombach and Nevobery (2001), Baker (2002)
Pogo, Alaska	Bi, Te, As, Ag, Cu, Pb	Apy, Py, Po, Lo, Bim	Bi, Qz, Ser, Carb	Granite, aplites	~ 104	300-600	Flat lenses	I-type	Smith et al. (1999), Baker (2002)
Brewery Creek, Yukon	As, Sb, (Hg)	Py, Po, Apy, Sn	Qz, Ser, Carb, Clay	Monzonite sills	Cretaceous	>450	Disseminated and veinlets	I > M	Diment (1996), Dunne (1995), Baker (2002)
Dublin Gulch, Yukon	Bi, Te, Mo, As, Sb, W, Pb, Cu	Py, Po, Apy, Bim, Sch, Gal, Pb-Bi-Te-S	Ksp>Ab, Qz, Ser, Carb	Granodiorite pluton	92.8 +/- 0.5	250-350	Sheeted	I-type	Malcoof et al. (2001), Baker (2002)
Timbarra, NSW, Australia	Bi, Mo, Sb, As, Ag	Mol, Bim, Py, Apy	Ab, Qz, Ser, Carb	Siliclastic metasedimentary rocks	245-238	200-400	Disseminated	Granite	Simmons et al. (1996), Thompson et al. (1999), Baker (2002)
Kidston, Queensland, Australia	Zn, Cu, Mo, W, Pb, As, Bi, Te, Sn	Py, Po, Apy, Bim, Ccp, Sph, Mol, Gal	Qz, Ser, Carb	Metamorphic rocks, granodiorite	332	400-540	Breccia-hosted	Rhyolite porphyry stock, I>M	Baker and Tullemans (1990), Thompson et al. (1999), Baker (2002)
Mokrovo, Czech Republic	As, Bi, Te, Mo, W, Sb, Cu	Py, Po, Apy, Mol, W, Sb	Ab, Amp, Bi, Qz	Mafic and felsic flows and tuffs	349 + 12	330±20	Sheeted veins	Granodiorite	Bouon et al. (1995), Thompson et al. (1999), Baker (2002)
Salave, Spain	As, Sb, Mo, W, Zn, Cu	Py, Po, Apy, Bim, Mol, Sph	Ab, Ser, Carb	Quartzite, slate, gabbro	285	-----	Disseminated (greisen)	Granodiorite	Harris (1980), Thompson et al. (1999), Baker (2002)
Vasilkovskoe, Kazakhstan	As, Sb, W, Pb, Cu, Bi, Te	Py, Po, Bim, Ccp, Sph, Gal, Mol, Sn, Sch	Ab, Qz, Ser, Carb	Metasedimentary rocks	443	280-370	Sheeted veins	Granodiorite	Bushlein (1996), Thompson et al. (1999), Baker (2002)
Jilau, Tajikistan	Bi, Te, W, As, Cu	Bim, Sch, Cpy, Py, Apy	Qz, Fsp, Carb, Ser	Granodiorite pluton	Late Paleozoic	300-450	Sheeted	I	Cole et al. (2000), Baker (2002)
Kori Kollo, Bolivia	Ag, As, Sb, Sn, Bi, Cu, Zn, Pb, W	Py, Apy, Ccp, Gal, Bim, Sn, Sph	Argillic	Quartzite, siltstone, shale	15.7	>300	Sheeted veins and veinlets	Dacite porphyry	Long et al. (1992), Thompson et al. (1999), Baker (2002)
Kutmajärvi, Finland	Sn	Py, Po, Cp, Apy, Cs, Gal, boulangerite, allanite, bessite, Te, Pb, Cu, Sb, Au	Silic, Ser	Sericit-quartz schist	Proterozoic	<350	Quartz veins, impregnation	Porphyritic tonalite and granite	Luukkonen (1994)
Tammijärvi, Finland	Sn, W, Cu	Apy, Sch, Po, Cp, Sph, St, Cs, herzenbergite, Bi, Ag, electrum, bessite, claushalite	Silic, Ser	Turbiditic metasedimentary rocks	Proterozoic	<450	Quartz veins, impregnation	Granodiorite	Luukkonen (1994)
Ahvenlammi, Finland	Sn, W	Sch, Apy, Cp, Py, Sph, St, Cs, Ilm, Ru, Bi, herzenbergite	-----	Turbiditic metasedimentary rocks	Proterozoic	350	Quartz veins, impregnation	Granodiorite, granite	Luukkonen (1994)
Muruntau, Uzbekistan	W	Py, Apy, Sch, Po, Cp, Sph, Mol, tetrahedrite, etc	Silic, Ab, Ser, biotite	Metasedimentary rocks	Pennan-Triassic	230-400	Quartz & quartz-sulfide veins	Felsic intrusive rocks	Wilde & Gilbert (2000), Graupner et al. (2005)

**Table 8.1** General characteristics of major, recognized intrusion-related gold systems as well as Muruntau giant deposit and three deposits in southern Finland.

Ab: albite, abs: no bismuth reported, Apy: arsenopyrite, Bim: bismuthinite, Bi: biotite, Carb: carbonate, Ccp: chalcocopyrite, Cs: Cassiterite, Fsp: feldspar,

Gal: galena, I: ilmenite series, I>M: ilmenite series more abundant than magnetite series, Ksp: K feldspar, Lo: lollingite, M: magnetite series,

Mol: molybdenite, Po: pyrrothite, Py: pyrite, Qz: quartz, Sbn: stibnite, Sch: scheelite, Ser: sericite, Sph: sphalerite, St: Stannite

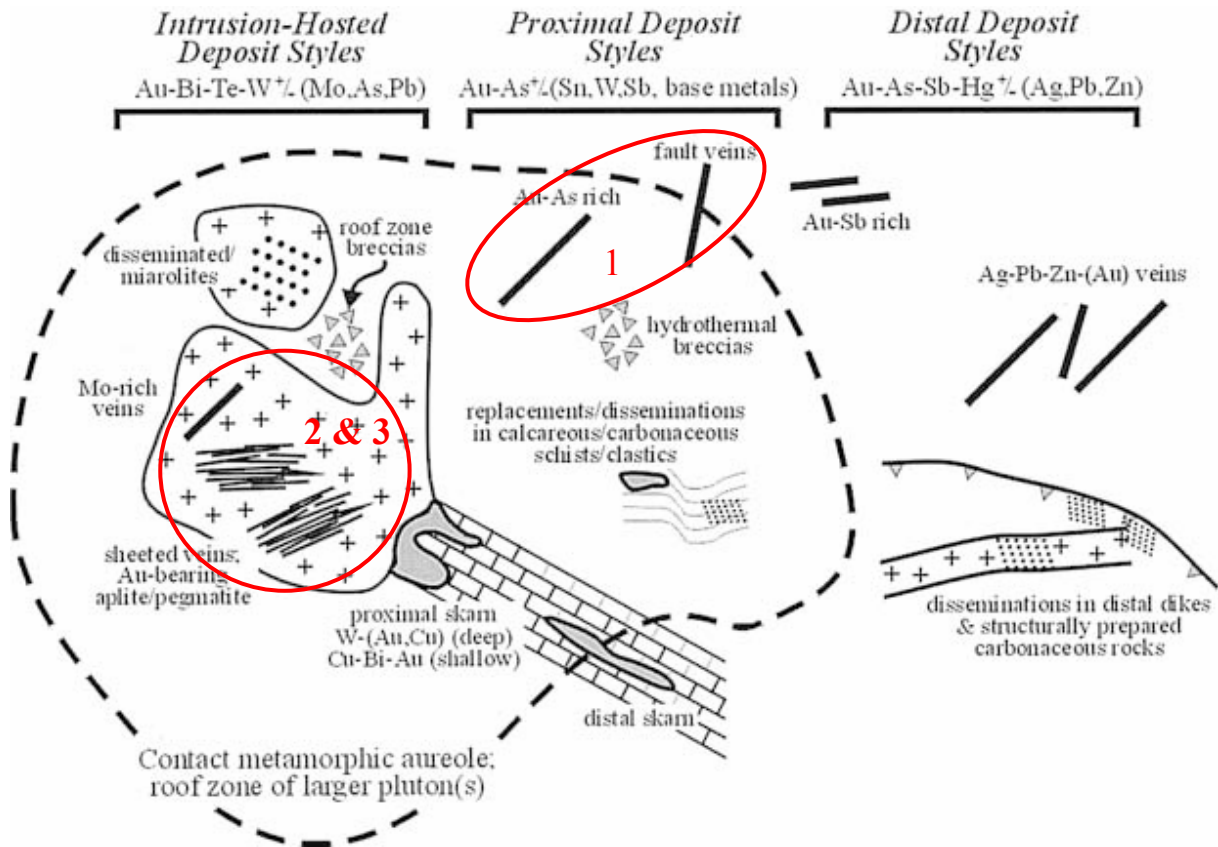


**Figure 8.1** Schematic geological and exploration model for intrusion-related gold systems illustrating the variation in styles from intrusion hosted to proximal and distal deposits (After Lang et al. 2001). The approximate location of Deh Hosein (1), Astaneh (2) and Nezam Abad (3) occurrences in this model has been highlighted.

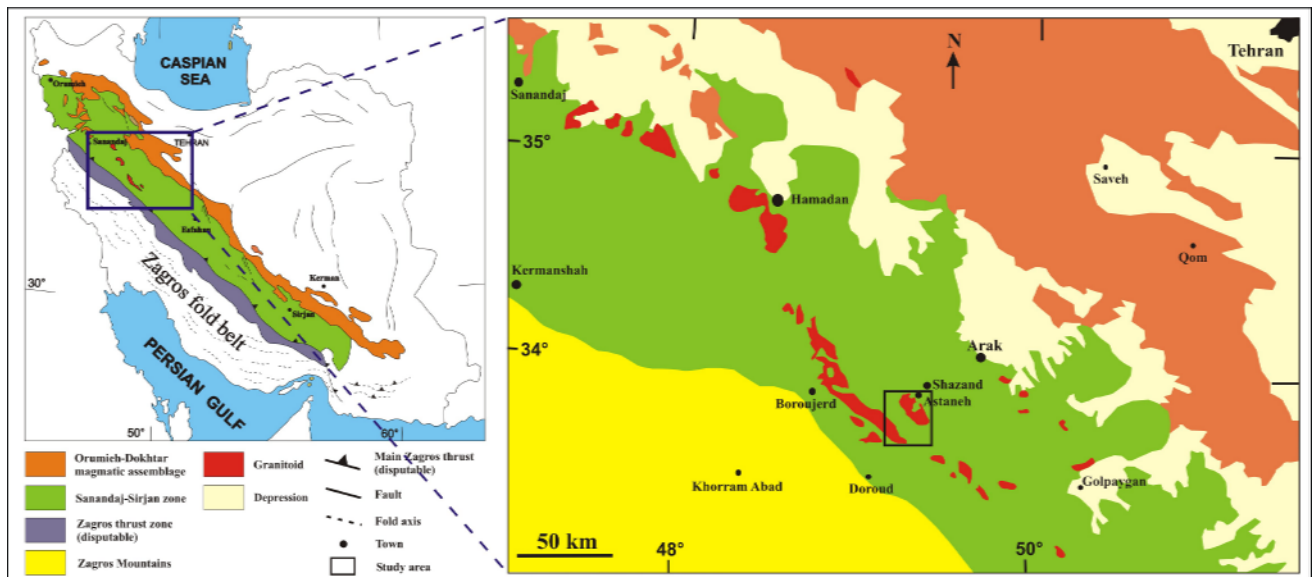


**Figure 8.2** Location of the intrusive bodies of the northern Sanandaj-Sirjan zone and the study area.

## References

- Alavi M. 1980. Tectonostratigraphic evolution of the Zagrosides of Iran, *Geology*, 8:144-149.
- Alavi M. 1994. Tectonics of the Zagros Orogenic belt of Iran: new data and interpretations, *Tectonophysics*, 229:211–238.
- Alimov K., Boroffka N., Bubnova N.M., Burjakov J., Cierny J., Jakubov J., Lutz J., Parzinger H., Pernicka E., Radililovskiy V., Ruzanov V., Sirinov T., and Wesigerber G. 1998. Prähistorischer Zinnbergbau in Mittelasian, Vorbericht der ersten Kampagne 1997, *Eurasia Antiqua*, 4:137-199.
- Amidi S.M. 1975. Contribution à l'étude stratigraphique, pétrologique et pétrographique des roches magmatiques de la région Natanz-Nain-Surk (Iran central), Thèse, Univ. Grenoble France.
- Asadi Haroni H. 2000. The Zarshuran gold deposit model applied in a mineral exploration GIS in Iran, PhD Thesis, Delft University of Technology and Institute for Aerospace Survey and Earth Sciences, the Netherlands, ITC Dissertation Number 78.
- Ayazi S. 2004. Luristan disc-headed bronze pins, in: Stöllner T., Slotta R. and Vatandoust A. (eds) *Persias Ancient Splendour (Persiens Antike Pracht) Mining, Handicraft and Archaeology*, Deutsches Bergbau-Museum, Bochum, pp 340-348.
- Azizpour Maghvan M. 2000. Geochemistry, mineralogy and genesis of the occurrences of Bamsar and Revesht, with a comparison with Nezam Abad tungsten deposit, Shazand, Arak.
- Baker E.M., Tullemans F.J. 1990. Kidstone gold deposit, in: Hughes F.E. (ed) *Geology of the mineral deposits of Australia and Papua New Guinea 2*, Australas Inst Mining Metall Mon 14, pp 1461-1465.
- Baker T. and Lang J.R. 2001. Fluid inclusion characteristics of intrusion-related gold mineralization, Tombstone-Tungsten magmatic belt, Yukon Territory, Canada, *Mineralium Deposita*, 36:563–582.
- Baker, T. 2002. Emplacement depth and carbon dioxide-rich fluid inclusions in intrusion-related gold deposits, *Economic Geology*, 97:1111-1117.
- Bakke A.A. 1995. The Fort Knox “porphyry” gold deposit-Structurally controlled stockwork and shear quartz-vein, sulphide-poor mineralization hosted by a Late Cretaceous pluton, east-central Alaska, in: Schroeter T.G. (ed) *Porphyry deposits of the northwestern Cordillera of North America*, Canadian Institute of Mining Metallurgy, Special Volume 46:795–802.
- Bariand P. 1963. Contribution à la minéralogie de l'Iran. *Bull. Soc. Franc. Miner. Crist.*, 76:17-64.
- Barnes H. L. 1997. *Geochemistry of hydrothermal ore deposits*, third edition, John Willey & Sons, Inc.
- Barton P.B. Jr. 1969. Thermochemical study of the system Fe-As-S, *Geochim. Cosmochim. Acta*, 33:841-857.
- Begemann F., Schmitt-Strecker S., and Pernicka E. 1992. The metal finds from Thermi III-V: a chemical and lead-isotope study. *Studia Troica* 2: 219-239.
- Begemann F., Pernicka E., and Schmitt-Strecker S. 1995. Thermi on Lesbos: A case study of changing trade patterns, *Oxford Journal of Archaeology*, 14:123-135.

- Begemann F. and Schmitt-strecker S. in preparation, 2006. Materialanalysen, Untersuchungen zur Herkunft der Rohstoffe. In: Die Metallindustrie Mesopotamiens von den Anfängen bis zum 2. Jahrtausend v. Chr., (eds.) H. Hauptmann & E. Pernicka, Orient-Archäologie, Rahden/Westfahlen.
- Bellon H. and Braud J. 1975. Données nouvelles le domaine métamorphique du Zagros (Zone de Sanandaj-Sirjan) au niveau de Kermanshah-Hamadan (Iran); Nature, âge et interprétation des séries métamorphiques et des intrusion, évolution structural: Fac, Sci. d'orsay, Paris 14 pp.
- Ben Yaghub A. 1999. Investigation on Astaneh gold mineralization, Arak, Iran, Unpublished MSc thesis (in Persian), Islamic Azad University, Tehran, Iran.
- Berberian M. and King G.C. 1981. Towards a palaeogeography and tectonics evolution of Iran, Canadian Journal of Earth Sciences, 18:210–265.
- Berberian F., and Berberian M. 1981. Tectono-plutonic episodes in Iran, in: Gupta H.K. and Delany F.M. (Eds.) Zagros, Hindu Kush, Himalaya, Geodynamic Evolution, American Geophysical Union, Geodynamics Series, 3:5–32.
- Berberian F., Muir I.D., Pankhurst R.J., Berberian M. 1982. Late Cretaceous and early Miocene Andean-type plutonic activity in northern Makran and Central Iran, Journal of the Geological Society of London, 139:605–614.
- Berthoud T. 1979. Etude par l'Analyse de Traces et la Modélisation de la Filiation Entre Minerais de Cuivre et Objets Archéologiques du Moyen Orient, PhD, University of Paris VI.
- Berthoud T., Cleuziou S., Hurtel L. P., Menu M., and Volfovsky C. 1982. Cuivres et Alliages en Iran, Afghanistan, Oman au Cours des IV<sup>e</sup> et III<sup>e</sup> Millénaires. Paléorient 8:39-54.
- Beyer D. 1982. Du Moyen-Euphrate au Luristan: Bagues-Cachets de la Fin du Deuxième Millénaire, in: Mari - Annales de Recherches Interdisciplinaires 1, Paris, 169-189.
- Bielicki K.H. and Tischendorf G. 1991. Lead isotope and Pb-Pb model age determinations of ores from Central Europe and their metallogenic interpretation, Contributions to Mineralogy and Petrology, 106:404-461.
- Boehmer R. M. 1982. Ringe aus kassitischen Gräbern. Baghdader Mitteilungen, 13: 31-49.
- Boehmer R. M. and Dämmer H. W. 1985. Tell Imlihiye, Tell Zubeidi, Tell Abbas. Baghdader Forschungen 7, Mainz am Rhein.
- Boiron M.C., Barakat A., Cathelineau M., Durisová J., and Morávek P. 1995. Microfissural ore fluid migration: The example of a granodiorite-hosted gold deposit (Mokrsko, Bohemia), in: Pasava J., Kribek B., Zák K. (eds) Mineral deposits: From their origin to their environmental impacts, 3rd Biennial SGA Meeting, 3rd Biennial SGA Meeting, A.A. Balkema, Rotterdam Brookfield, Prague, 1995, Proceedings, pp 97–100.
- Boroffka N., Cierny J., Lutz J., Parzinger H., Pernicka E., and Weisgerber G. 2002. Bronze Age tin from Central Asia, in Ancient Interactions: East and West, in: Eurasia (eds) Boyle K., Renfrew, C. and Levine M., pp.135-159. McDonald Institute Monographs, McDonald Institute for Archaeological Research, Cambridge.
- Borthwick J. and Harmon R. S. 1982. A note regarding ClF<sub>3</sub> as an alternative to BrF<sub>5</sub> for oxygen isotope analysis, Geochim. Cosmochim. Acta. 46:1665-1668.
- Braidwood R. J. and Braidwood L. S. 1960. Excavations in the Plain of Antioch 1, The Earlier Assemblages Phases A-J, Oriental Institute Publications Volume LXI, University of Chicago Press, Chicago.
- Bundtzen T.K. and Miller M.L. 1997. Precious metals associated with Late Cretaceous-Early Tertiary igneous rocks of southwestern Alaska, in: Goldfarb R.J. and Miller L.D (eds) Mineral deposits of Alaska, Economic Geology Monograph 9: 242-286.

- Burshtein E.F. 1996. Genetic types of granite-related mineral deposits and regular patterns of their distribution in central Kazakhstan, in: Shatov V., Seltmann R., Kremenetsky A., Lehmann B., Popov V. (eds) Granite-related ore deposits of central Kazakhstan and adjacent areas, Glagol Publishing House, St. Petersburg, pp 83-91.
- Cabri L.J., Newville M., Gordon R.A., Crozier E.D., Sutton S., McMahon G. and Jiang D.T. 2000. Chemical Speciation of Gold in Arsenopyrites, *The Canadian Mineralogist*, 38:1265-1281.
- Calmeyer P. and Schaefer H. 1964. Altiranische Bronzen der Sammlung Bröckelschen, Staatliche Museen, Museum für Vor- und Frühgeschichte, Berlin.
- Catanzaro E.J., Murphy T.J., Garner E.L. and Shields W.R. 1969. Absolute isotopic abundance ratio and atomic weight of terrestrial rubidium, *J. Res. Natl. Bur. Std. Phys. and Chem.*, 73A: 511-516.
- Charvát P. 1982. Early Ur-war chiefs and kings of Early Dynastic III, *Altorientalische Forschungen*, 9: 43-59.
- Chevreton V.B. 1986. Tethys-marginal sedimentary basins in western Iran. *Geological Society of American Bulletin*, 97:516-522.
- Clayden T. 1998. Faience Buckets. *Baghdader Mitteilungen*, 29: 47-72.
- Cleuziou S. and Berthoud T. 1982. Early tin in the Near East: a reassessment in the light of new evidence from western Afghanistan, *Expedition* 25: 14-19.
- Cohen M. E. 1975. UR.SAG..ME.SHAR.HR4. A Sirmam-Shuhha of Ninurta. *Die Welt des Orients*, 8:22-36.
- Cole A., Wilkinson J.J., Halls C. and Serenko T.J. 2000. Geological characteristics, tectonic setting, and preliminary interpretations of the Jilau gold-quartz vein deposit, Tajikistan: *Mineralium Deposita*, 35:600–618.
- Cowell R. M. 1987. Scientific appendix I. Chemical analysis, In *Catalogue of Egyptian Antiquities in the British Museum VII, Tools and Weapons I, Axes*, by W. V. Davies, pp 96-118. British Museum, London.
- Crawford A.R. 1972. Iran, continental drift and plate tectonics. 24th international congress, Montreal, section 3, pp 106-112.
- Crawford H. E. W. 1974. The problem of tin in Mesopotamian bronzes, *World Archaeology* 6:242-246.
- Darvishzadeh A. 1991. *Geology of Iran (in Persian)*, Danesh-e Emrouz press, Tehran.
- Davidovic' V. 1984. Testi di Ur III concernenti bottino di Guerra? *Annali Istituto Universario Orientale*, 44:177-205.
- Davoudzadeh M. 1997. Iran. in (eds) Moores E. M., and Fairbridge R. W., *Encyclopedia of European and Asian Regional Geology*, Encyclopedia of earth sciences series, Chapman and Hall.
- de Jesus P.S. 1980. The Development of Prehistoric Mining and Metallurgy in Anatolia, Parts i and ii. BAR International Series 74, British Archaeological Reports, Oxford.
- Dercourt J., Zonenshain L., Ricou L.E., Kasmin G., LePichon X., Knipper A.L., Grandjacquet C., Sbertshikov I.M., Geysant J., Lepvrier C., Pechersky D.H., Boulin J., Bazhenov M.L., Lauer J.P. and Biju-Duval B. 1986. Geological evolution of the Tethys Belt from the Atlantic to Pamirs since the Lias, *Tectonophysics*, 123:241-315.
- Dewey J.F., Pitman W., Ryan W. And Bonin J. 1973. Plate tectonics and the evolution of the Alpine system. *Geol. Soc. Am. Bull.*, 84:3137-3180.
- Dickin A.P. 1997. *Radiogenic isotope geology*, Cambridge University Press.
- Diment R. 1996. Brewery Creek gold deposit, in: Yukon exploration and geology: Field work report for 1995, Whitehorse, Yukon, Indian, and Northern Affairs Canada, Exploration and Geological Services Division, pp 89–97.



- Doe B.R. 1967. Bearing of lead isotopes on source granitic magma, *Journal of Petrology*, 8(1): 51-83.
- Doe, B.R., Zartman, R.E. 1979. Plumbotectonics. The Phanerozoic. in: Barnes H.L. (ed) *Geochemistry of hydrothermal ore deposits*, 2<sup>nd</sup> edition Interscience, New York.
- Du Bray E. A. 1985. Geology of the Silsilah ring complex, and associated tin mineralization, Kingdom of Saudi Arabia-a synopsis, *American Mineralogist*, 70:1075-1086.
- Du Bray E. A., Elliot J. E. and Stuckless J. S. 1988. Proterozoic peraluminous granites and associated Sn-W deposits, Kingdom of Saudi Arabia, in: Taylor R.P. and Strong D.K. (eds) *Recent Advances in the Geology of Granite-Related Mineral Deposits*, pp 142-156. Canadian Institute of Mining and Metallurgy Special Volume 39, Canadian Institute of Mining and Metallurgy, Montreal.
- Dunne K.P.E. 1995. Brewery Creek: Preliminary fluid inclusion study: Unpublished consultant report to Yukon Geology Program and Viceroy Mining Pty., Vancouver, B.C., Viceroy Mining Pty., 6 p.
- Dunstan L. P., Gramlich J.W., Barnes I. L. and Purdy W. C. 1980. The absolute isotopic bundance and the atomic weight of a reference sample of thallium, *Journal of Research of the National Bureau of Standards*, 85:1-10.
- Eaton E. R. and McKerrell H. 1976. Near eastern alloying and some textual evidence for the early use of arsenical copper, *World Archaeology*, 8:169-191, Economic and Social Commission for Asia and the Pacific.
- Ebert S., Miller L., Petsel S., Dodd S. and Kowalczyk P. 2000. Geology, mineralization, and exploration at the Donlin Creek project, southwest Alaska, in: Tucker, T.L. and Smith M.T. (eds) *The Tintina gold belt: Concepts, exploration, and discoveries*, British Columbia and Yukon Chamber of Mines, Cordilleran Roundup 2000, pp 99-114.
- El Goresy A., Schiegl S. and Weiner K. L. 1995. A chronological scheme for the technological evolution of copper in ancient Egypt. In: *Proceedings of the First International Conference on Ancient Egyptian Mining and Metallurgy and Conservation of Metallic Artifacts*, (ed.) F. A. Esmael, 215-234. Egyptian Antiquities Organization Press, Cairo.
- Emami M.H. 1981. *Geologie de la region de Qom-Aran (Iran). Contribution á l'étude dynamique et geochemique du volcanisme Tertiaire de l'Iran central*. Thèse, Sciences Naturalles, Univ. Sci. Et Medicale de Grenoble. 489 pp.
- Esin, U. 1969. *Kuantitatif Spektral Analiz Yardimiyla Anadolu'da Baslangicindan Asur Kolonileri Cagina Kadar Bakir ve Tunc Madenciligi*, Tas Matbaasi, Istanbul.
- Farhadian M.B. 1992. *Geochemical and mineralogical investigation on Nezam Abad tungsten deposit, Arak, Iran*, Equivalent MSc thesis (in Persian), Tehran University, Iran.
- Farhadian, M.B. 1999. *List of analysis results of Tungsten exploration program at Nezam Abad*, Internal report (in Persian), Geological Survey of Iran, Tehran.
- Faulkner E.L. 1992. *Introduction to Prospecting*, Geological Survey Branch, Canada, Mineral Resources Division, Paper 1986-4.
- Faure G. and Mensing T.M. 2005. *Isotopes: Principles and Applications*. Third edition. John Wiley & sons, Inc.
- Field C.W. and Gustafson L.B. 1976. Sulfur isotopes in the porphyry copper deposit at El Salvador, Chile, *Economic Geology*, 71:1533-1548.
- Fleming S. J. and Pigott V. C. 1987. *Archaeometallurgy*, in *Site Reconnaissance in the Yemen Arab Republic, 1984*: in Glanzman W.D. and Ghaleb A.O. (eds) *The Stratigraphic Probe at Hajar Ar-Rayhami*, pp. 171-181, *The Wadi Al-Jubah Archaeological Project Volume 3*, American Foundation for the Study of Man, Washington, D.C.

- Fleming S.J., Pigott V.C., Swann C.P. and Nash S.K. 2005. Bronze in Luristan: Preliminary analytical evidence from copper/bronze artifacts excavated by the Belgian mission in Iran, *Iranica Antiqua*, XL:35-64.
- Foster R.P., Mann A.G., Armin T. and Burmeister B.B. 1975. Richardson's Kop wolframite deposit: a geochemical model for the hydrothermal behaviour of tungsten, in: Verwoerd W.J. (ed) *Mineralization in metamorphic terranes*, Geol. Soc. S. Africa Spec. Pub., 4:107-128.
- Gallagher V. 1989. Geological and isotope studies of microtonalite-hosted W-Sn mineralization in SE Ireland, *Mineralium Deposita*, 24:19-28.
- Garenne-Marot L. 1984. Le cuivre en Égypte Pharaonique: sources et métallurgie, *Paléorient* 10:97-126.
- Garlick G.D. 1969. The stable isotopes of oxygen, in: Wedepohl K.H. (ed) *Handbook of geochemistry*, 8B. Springer, Berlin, Heidelberg, New York.
- Ghirshman R. 1938. Fouilles de Sialk, près de Kashan, 1933, 1934, 1937. Vol. I. Librairie Orientaliste Paul Geuthner, Paris.
- -Ghirshman, R. 1954. Iran: from the earliest times to the Islamic conquest, A volume in the Pelican archaeology series, Penguin books.
- Giesemann A., Jäger H.J., Norman A.L., Krouse H.R., Brand W.A. 1994. On-line sulfur isotope determination using an elemental analyser coupled to a mass spectrometer, *Analytical Chemistry*, 66:2816-2819.
- Glanzman W. D. 1987. Metallurgical debris, in Site Reconnaissance in the Yemen Arab Republic, 1984, in: Glanzman W.D. and Ghaleb A.O. (eds) *The Stratigraphic Probe at Hajar Ar-Rayhami*, pp 14S-148, The Wadi AI-Jubah Archaeological Project Volume 3, American Foundation for the Study of Man, Washington, D.C.
- Goldfarb R., Hart C., Miller M., Miller L., Farmer G.L., Groves D. 2000. The Tintina gold belt: a global perspective, in: Tucker T.L. and Smith M.T. (eds) *The Tintina gold belt: concepts, exploration and discoveries*, British Columbia and Yukon Chamber of Mines, Special Volume 2:5-34.
- Graham C.M. and Harmon R.S. 1983. Stable isotope evidence on the nature of crust-mantle interactions, in: Hawkesworth C.J. and Norry M.J. (eds) *Continental basalts and mantle xenoliths*, Shiva, Nantwich, pp 20-45.
- Graupner T., Kempe U., Klemd R., Schüssler U., Spooner E.T.C., Götze J. and Wolf D. 2005. Two stage model for the Muruntau (Uzbekistan) high grade ore structures based on characteristics of gold, host quartz and related fluids, *Neues Jahrbuch für Mineralogie - Abhandlungen*, 181(1):67-80(14).
- Gulson B. L. 1986. *Lead isotopes in mineral exploration*, Elsevier Science Publishing Company Inc.
- Haack U. 1993. Critical note on lead-lead model ages, *Monograph series on mineral deposits*, Berlin-Stuttgart, 30:115-116.
- Hackens T., McKerrel H. and Hours M. (eds). 1977, *X-ray microfluorescence analysis applied to archaeology*, PACT 1, Strasbourg.
- Haerinck E. and Overlaet B. 2002. The Chalcolithic and Early Bronze Age in Pusht-i Kuh, Luristan (West-Iran), *Chronology and Mesopotamian Contacts*, *Akkadica* 123, 2:163-181.
- Hajian H. 1977. Geological map of the Tafresh area, scale 1:100,000. Geological Survey of Iran, Tehran.
- Haj Zein Ali M.A. 1992. Geology and exploration at Nezam Abad tungsten deposit, Geological Survey of Iran, Internal report (in Persian).
- Hart C.J.R., Baker T. and Burke M. 2000. New exploration concepts for country-rock-hosted, intrusion-related gold systems: Tintina gold belt in Yukon, in: Tucker T.L. and

- Smith M.T. (eds) The Tintina gold belt: concepts, exploration and discoveries, British Columbia and Yukon Chamber of Mines, Special Volume 2:145-172.
- Harris, M. 1980. Hydrothermal alteration at Salave gold prospect, northwest Spain: Transactions of the Institute for Mining and Metallurgy, Applied Earth Sciences, B89, pp B5–B15.
  - Harrison R.H., Gorton R.K. 1998. The True North project, Alaska, In: Walton G., Jambor J. (eds) Pathways '98 Extended Abstr Vol BC and Yukon Chamber of Mines and Soc Econ Geol, pp 80-82.
  - Hashemi M. 2002. Gold mineralization associated with igneous body of Astaneh, Arak, Iran. Unpublished MSc thesis (in Persian), Teacher Training University of Tehran, Iran.
  - Haynes S.J. and McQuillan H. 1974. Evolution of the Zagros suture zone, southern Iran. Geol. Soc. Am. Bull., 85:739-744.
  - Herrmann G. 1968. Lapis lazuli: the early phases of its trade. Iraq, 30:21-57.
  - Hegde K. T. M. 1978. Sources of ancient tin in India. In: The Search for Ancient Tin, A. D. Franklin, J. S. Olin, and T. A. Wertime (eds.), 39-42, U.S. Government Printing Office, Washington, D.C.
  - Herzog P.M., Hannington M.D., Arribas A. Jr. 1998. Sulfur isotopic composition of hydrothermal precipitates from the Lau back-arc: implications for magmatic contributions to seafloor hydrothermal systems, Mineralium Deposita, 33:226-237.
  - Heskell D. and Lamberg-Karlovsky C. C. 1980. An alternative sequence for the development of metallurgy: Tepe Yahya, Iran, in: Wertime T.A. and Muhly J.D. (eds) The Coming of the Age of Iron, pp. 229-266. Yale University Press, New Haven.
  - Hezarkhani Z. and Pernicka E. 2000. Provenance studies on metal ores and artifacts. Archäologische Mitteilungen aus Iran und Turan, Sonderdruck 32:305-310. Dietrich Reimer Verlag, Berlin.
  - Hoefs J. 2004. Stable Isotope Geochemistry. Springer-Verlag, Berlin, Germany.
  - Hollister V.F. 1992. On a proposed plutonic porphyry gold deposit model, Nonrenewable Res., 1: 293-302.
  - Hutchison M.N. and Scott S.D. 1981. Sphalerite geobarometry in the Cu-Fe-Zn-S system, Economic Geology, 76:143-153.
  - Jahangiri H. 1999. Investigation into W-Sn anomalies in the areas of Nezam Abad and Bamsar, Internal report (in Persian), Geological Survey of Iran, Tehran.
  - Kaptan E. 1995. Tin and ancient tin mining in Turkey. Anatolica, 21:197-203.
  - Karimi-Bafghi M. R., and Khoii N. 1984. Investigation of some samples from Nezam Abad occurrences. Geological survey of Iran, Internal report (In Persian).
  - Khoii N. 1982. Formation of gold in the Astaneh granite, internal report (in Persian), Geological survey of Iran, Tehran.
  - Kober B. 1987. Single zircon evaporation combined with Pb + emitter-bedding for 207/206 age investigations using thermal mass spectrometry, and implications to zirconology, Contrib. Mineral. Petrol., 96:63-71.
  - Kretschmar U. And Scott S.D. 1976. Phase relations involving arsenopyrite in the system Fe-As-S and their application. Canadian Mineralogist, 14:364-386.
  - Kutscher R. 1989. Royal inscriptions, The Brockmon tablets at the University of Haifa, Haifa.
  - Jantzen U. 1972. Ägyptische und orientalische Bronzen aus dem Heraion von Samos, Samos VIII. Bonn.
  - Joannés F. 1991. L'Étain, de l'Élam à Mari. In: Meyer L.D. and Gasche H. (eds) Mésopotamie et Élam, pp 67-76. Mesopotamian History and Environment Occasional Publications 1. Mesopotamian History and Environment, Ghent.

- Kamilli R. J. and Criss R. E. 1996. Genesis of the Silsilah tin deposit, Kingdom of Saudi Arabia. *Economic Geology*, 91: 1414-1434.
- Lang J.R., Baker T., Hart C.J.R., Mortensen J.K. 2000. An exploration model for intrusion-related gold systems, *SEG Newsletter*, 40(1):7-15.
- Lang J.R., Baker T. 2001. Intrusion related gold systems: the present level of understanding, *Mineralium Deposita*, 36: 477-489.
- Larsen M. T. 1976. *The Old Assyrian City-State and its Colonies*, Akademisk Forlag, Copenhagen.
- Larsen M. T. 1987. Commercial networks in the ancient Near East, in Centre and Periphery, in: Rowlands M., Larsen M.T., and K. Kristiansen K. (eds) *The Ancient World*, pp 47-56. *New Directions in Archaeology*, Cambridge University Press, Cambridge.
- Leemans W. F. 1960. *Foreign Trade in the Old Babylonian Period*, E. J. Brill, Leiden.
- Limet H. 1960. *Le travail du métal au pays de Sumer au temps de la IIIe dynastic d'Ur*, Les Belles Lettres, Paris.
- Long K., Ludington S., du Bray E., Andrè-Ramos O. and McKee E.H. 1992. Geology and mineral deposits of the La Joya district, Bolivia. *SEG Newsletter*, 10: (1):13-16.
- Lucas A. 1934. *Ancient Egyptian Materials and Industries*, Second edition, Edward Arnold, London.
- Luscuyer J.L. and Rio R. 1976. *Geologie de la region de Mianeh (Azarbaijan), contribution à l'étude du volcanisme Tertiaire de l'Iran*, Thèses, Univ. Grenoble, France.
- Lutz J. and Pernicka E. 1996. Energy dispersive X-ray fluorescence analysis of ancient copper alloys: empirical values for precision and accuracy, *Archaeometry*, 38(2):313-323.
- Luukkonen, A. 1994. Main geological features, metallogeny and hydrothermal alteration phenomena of certain gold and gold-tin-tungsten prospects in southern Finland, *Geological Survey of Finland, Bulletin 377*, Helsinki.
- Maddin R., Muhly J. D. and Stech-Wheeler T. 1980. Research at the center for ancient metallurgy, *Paheorient*, 6:111-119.
- Maddox L.M., Bancroft G.M., Scaini M.J., Lorimer J.W. 1998. Invisible gold: Comparison of Au deposition on pyrite and arsenopyrite. *American Geologist*. 83: 1240-1245.
- Malfoy J.M. and Menu M. 1987. La Metallurgie du cuivre à Susa aux IVe et IIIe milleénaires: analyses en laboratoire, in: Tallon F. (ed) *Métallurgie Susienne*, pp 355-373. *Notes et Documents des Musées de France 15*, Louvre Museum, Department of Oriental Antiquities, Paris.
- Mallak Pour M.A., Hasani Pak A.A. and Farhadian M.B. 1993. Interpretation of geochemical data at Nezam Abad, (in Persian), University of Tehran, Mining Faculty.
- Maloof T.L., Baker T. and Thompson J.F.H. 2001. The Dublin Gulch intrusion-hosted gold deposit, Tombstone plutonic suite, Yukon Territory, Canada *Mineralium Deposita*, 36: 583-593.
- Masoudi F. 1997. Contact metamorphism and pegmatite development in the region SW of Arak, Iran, PhD thesis, The University of Leeds, UK.
- Masoudi F., Yardley B.W.D. and Cliff R.A. 2002. Rb-Sr Geochronology of Pegmatites, Plutonic Rocks and a Hornfels in the Region South-West of Arak, Iran, *Journal of Sciences, Islamic Republic of Iran*, 13(3).
- Masson V. M. and Sarianidi V. I. 1972. *Central Asia: Turkmenia before the Achaemenids*, Praeger, New York.
- McCoy D., Newberry R.J., Layer P., DiMarchi J.J., Bakke A., Masterman S. and Minehane D.L. 1997. Plutonic-related gold deposits of Interior Alaska, in: Goldfarb R.J. and Miller L.D. (eds) *Mineral deposits of Alaska*, *Economic Geology Monograph 9*:191-241.

- Meier-Arendt W. 1984. Bronzen and Keramik aus Luristan und anderen Gebieten Irans im Museum für Vor- and Frühgeschichte, Frankfurt am Main.
- Mohajjel M., Fergusson B.C.L. and Sahandi M.R. 2003. Cretaceous–Tertiary convergence and continental collision, Sanandaj–Sirjan Zone, western Iran, *Journal of Asian Earth Sciences*, 21:397-412.
- Momenzadeh M., Nezafati N. and Pernicka E. 2002. First indication of tin at the ancient mining site near Deh Hosein, West-Central Iran: a possible source for Luristan bronze? *Proceedings of the 33rd international symposium on Archaeometry, 2002*, Amsterdam, The Netherlands, 116-117.
- Moorey P.R.S. 1974. *Ancient bronzes from Luristan*, British Museum. London.
- Moorey P. R. S. 1982. Archaeology and pre-Achaemenid metalworking in Iran: a fifteen year retrospective, *Iran*, 20:81-101.
- Moorey P. R. S. 1994. *Ancient Mesopotamian Materials and Industries: the Archaeological Evidence*, Clarendon Press, Oxford.
- Moorey P. R. S. and Schweizer F. 1972. Copper and copper alloys in ancient Iraq, Syria and Palestine and new analyses, *Archaeometry*, 14:177-198.
- Muhly J. D. 1973. Copper and tin transactions, *The Connecticut Academy of Arts and Sciences*, 43:155-535.
- Muhly J. D. 1978. New evidence for sources of and trade in Bronze Age tin, in: Franklin A.D., Olin J.S. and Wertime T.A. (eds) *The Search for Ancient Tin*, pp 43-48, U.S. Government Printing Office, Washington, D.C.
- Muhly J. D. 1985. Sources of tin and the beginnings of bronze metallurgy, *American Journal of Archaeology*, 89: 275-291.
- -Muhly J. D. 1987. Review of "Tin in Antiquity: its Mining and Trade throughout the Ancient World with Particular Reference to Cornwall", by Penhallurick, R.D., *Archeomaterials*, 2:99-107.
- Muhly J. D. 1993. Early Bronze Age tin and the Taurus, *American Journal of Archaeology* 97:239-253.
- Muhly J. D. 1995. Mining and metalwork in ancient Western Asia, in: Sasson J.M. (ed) *Civilizations of the Ancient Near East*, pp. 1501-1521, Vol. 3. Charles Scribner's Sons, New York.
- Müller-Karpe M. 1991. Aspects of early metallurgy in Mesopotamia, in: Pernicka E. and Wagner G.A. (eds) *Archaeometry '90*, pp. 105-116, Birkhauser Verlag, Basel.
- Muscarella O.W. 1977. The archaeological evidence for relations between Greece and Iran in the first millennium B.C., *The Journal of the Ancient Near Eastern Society of Columbia University*, 9:31-57.
- Muscarella O.W. 1988. The background to the Luristan Bronzes, in: Curtis J. (ed) *Bronzeworking Centres of Western Asia 1000-539 B.C.*, London, pp 177-92.
- Muscarella O.W. 2004. Bronzes of Luristan, in: Yarshater E. (ed) *Encyclopedia Iranica*, Columbia University, Center for Iranian studies, pp 478-483.
- Nabavi M.H. 1976. *An introduction to geology of Iran*. (in Persian), Geological Survey of Iran, Tehran.
- Newberry R.J., McCoy D.T. and Brew D.A. 1995. Plutonic-hosted gold ores in Alaska: Igneous vs. metamorphic origin, in: Ishihara S. and Czamanske G.k. (eds) *Proceedings of Sapporo International Conference on Mineral Resources of the NW Pacific Rim 1994*, *Resource Geology*, Special Issue 18:57-100.
- Newberry R.J. 1998. W- and Sn. skarn deposits: a 1998 status report, in: Lentz D.R. (ed) *Mineralized intrusion-related skarn systems*. Mineral Association Canada Short Course Series 26:289-336.

- Nezafati N., Herzig P.M., Pernicka E., Momenzadeh M. 2005. Intrusion-related gold occurrences in the Astaneh-Sarband area, west central Iran, in: Mao J. and Bierlein F.P. (eds) *Mineral deposit research: meeting the global challenge*, Springer, Heidelberg, 1: 445-448.
- Nezafati N., Pernicka E. and Momenzadeh M. 2006. Ancient tin: old question and a new answer. *Antiquity*, 80: 308. 4pp.
- Nicolaus H., Shahin E., Shahryari A. 1983. Exploration geophysical investigations in Khorram Abad quadrangle, south of Astaneh of Arak. Geological survey of Iran, Internal report (in Persian).
- Niederschlag E., Pernicka E., Seifert Th. and Bartelheim M. 2003. Determination of lead isotope ratios by multiple collector ICP–MS: a case study of Early Bronze Age artifacts and their possible relation with ore deposits of the Erzgebirge, *Archaeometry*, 45:61–100.
- Oberthur T., Weiser T. and Amanor S. L. 1997. Mineralogical setting and distribution of gold in quartz veins and sulphide ores of the Ashanti mine and other deposits in the Ashanti belt of Ghana: genetic implications, *Mineralium Deposita*, 32:2-15.
- Ohmoto H. and Rye R.O. 1979. Isotopes of sulfur and carbon, in: *Geochemistry of hydrothermal ore deposits*, 2<sup>nd</sup> edition. Holt Rinehart and Winston, New York.
- Ojaghi B., Shabani K. and Hashemi M. 2002. Geological map of the Astaneh prospect, scale: 1:10,000, Samim Resources, Internal report.
- Ojaghi B., Shabani K., Asfari S. and Nezafati N. 2001. Geological map of the Deh Hosein area, scale: 1:5000. Zaryaban Exploration, Internal report.
- Onuma N., Clayton R.N. and Mayeda T.K. 1972. Oxygen isotope cosmo thermometer. *Geochimica et Cosmochimica Acta*, 36:169-188.
- Overlaet B. 2003. The Early Iron Age in the Pusht-i Kuh, Luristan. *Luristan Excavation Documents IV, Acta Iranica* 40, Leuven.
- Overlaet B. 2004. Luristan Metalwork in the Iron Age, in: Stöllner T., Slotta R. and Vatandoust A. (eds) *Persias Ancient Splendour (Persiens Antike Pracht) Mining, Handicraft and Archaeology*, Deutsches Bergbau-Museum, Bochum, pp 328-338.
- Overlaet B. 2005. The Chronology of the Iron Age in the Pusht-i Kuh, Luristan, *Iranica Antiqua*, XL:1-33.
- Overstreet W. C., Detra D. E., Botinelly T., Grolier M. S., Stoesser D. B. and Schmidt D. L. 1988. Mineral resources of the al-Jubah quadrangle, Yemen Arab Republic, in: W. Overstreet W., Grolier M.J. and Toplyn M.R. (eds) *Geological and Archaeological Reconnaissance in the Yemen Arab Republic, 1985*, pp. 359-418, The Wadi Al-Jubah, Archaeological Project Volume 4, American Foundation for the Study of Man, Washington, D.C.
- Pernicka E., Seeliger T. C., Wagner G. A., Begemann F., Schmitt-Strecker S., Eibner C., Oztunali O. and Baranyi I. 1984. Archäometallurgische Untersuchungen in Nordwestanatolien. *Jahrbuch des Römisch-Germanischen Zentralmuseums*, Mainz 31:533-599.
- Pernicka E., Begemann F., Schmitt-Strecker S. and Grimianis A. P. 1990. On the composition and provenance of metal objects from Poliochni on Lemnos. *Oxford Journal of Archaeology*, 9:263-298.
- Pernicka E., Begemann, F., Schmitt-Strecker S., Todorova H., and Kuleff I. 1997. Prehistoric copper in Bulgaria, its composition and provenance. *Eurasia Antiqua. Sonderdruck Band 3*: 42-139.
- Pettinato G. 1983. Dilmun nella documentazione epigrafica di Ebla, in: Potts D.T. (ed) *Dilmun, New Studies in the Archaeology and Early History of Bahrain*, pp 75-82, *Berliner Beiträge zum Vorderen Orient* 2, Dietrich Reimer, Berlin.



- Poulsen K.H. 1996. Carlin-type gold deposits and their potential occurrence in the Canadian Cordillera, in: Current Research 1996-A, Geological Survey of Canada, pp 1-9.
- Potts T.F. 1994. Mesopotamia and the East, An Archaeological and Historical Study of Foreign Relations ca. 3400-2000 BC. Oxford Committee for Archaeology Monograph 37, Oxford Committee for Archaeology, Oxford.
- Radfar J. 1987. Petrology of granitic rocks from Astaneh area, Iran. MSc thesis (in Persian), Tehran University, Iran.
- Ramdohr P. 1980. The ore minerals and their intergrowths, Second edition, Akademie-Verlag Berlin.
- Rapp G., Rothe R. and Jing Z. 1999. Using neutron activation analysis to source ancient tin (cassiterite), in: Young S.M., Pollard A.M., Budd P., and Ixer R.A. (eds) Metals in Antiquity, pp 153-162, BAR International Series 792, Archaeopress, Oxford.
- Razavi M.H, Kashani F., Ghotbi H., Akrami M. 1983. Reconnaissance and semi-detailed exploration of Astaneh gold deposit, Arak. Internal report (in Persian), Geological survey of Iran
- Rollinson H. 1993. Using geochemical data: evaluation, presentation, interpretation, Langman Group UK Limited.
- Rombach C.S. and Newberry R.J. 2001. Genesis and mineralization of the Shotgun deposit, southwestern Alaska: Mineralium Deposita, 36:607–621.
- Ruzanov V. 1979. On general ancient tin ore sources on the territory of Uzbekistan, Material for the History of Uzbekistan, 15:98-104 (in Russian).
- Rickenbach J. 1992. Magier mit Feuer und Erz, Bronzekunst der frühen Bergvölker in Luristan, Iran, Museum Rietberg Zürich.
- Romanko E., Kokorin Y., Krivyakin B., Susov M., Morozov L. and Sharkovski M. 1984. Outline of metallogeny of Anarak area, Central Iran, Geological Survey of Iran, Report TechnoExport/No. 21.
- Sabzehie M. 1974. Les mélanges ophiolitiques de la région d’Esfandagheh (Iran méridional), Etude pétrologique et structurale Interprétation dans le cadre iranien, Thèse Univ. Grenoble, 306 pp.
- Sabzehi M. (compiler) 1992. Geologic map of the Neyriz quadrangle, scale 1:250:000, Geological Survey of Iran, Tehran.
- Samim Resources. 2002. Detail surface exploration At Astaneh gold prospect (Gold in hard rock), Internal report (in Persian), Tehran.
- Schandl E.S. and Michael P. Gorton M.P. 2004. A textural and geochemical guide to the identification of hydrothermal monazite: criteria for selection of samples for dating epigenetic hydrothermal ore deposits, Economic Geology, 99: 1027-1035.
- Schiegl S. 1994. Zusammensetzung und Provenienz von Blau- and Grünpigmenten in Altägyptischen Wandmalereien: Ein Beitrag zur exakten Chronologie der Bronzetechnologie in Altägypten-Resume, in Handwerk and Technologie im Alten Orient, R. B. Wartke (ed.), 95-96. Philip von Zabern, Mainz.
- Scott S.D. 1983. Chemical behavior of sphalerite and arsenopyrite in hydrothermal and metamorphic environments, Mineralogical magazine, 47:427-435.
- Sengör A.M.C. 1990. A new model for the late Paleozoic-Mesozoic tectonic evolution of Iran and implications for Oman, in: Robertson A.H.F., Searle M.P. and Ries A.C. (eds) The Geology and Tectonics of the Oman Region, Geol. Soc. London, Spec. Publ., 49:797-831.
- Shamanian Esfahani, G. 1994. Geochemical, mineralogical and fluid inclusion studies on Nezam Abad tungsten mine, Markazi province, Iran. Unpublished MSc thesis (in Persian), University of Shiraz.

- Sharp D., Essene J., Kelly C. 1985. A re-examination of the arsenopyrite geothermometer: pressure considerations and applications to natural assemblages. *Canadian Mineralogist*, 23:517-534.
- Shaffer J.G. 1978. "The Later Prehistory of Afghanistan", in: Hammond N. and Allchin F.R., (eds), *The Archaeology of Afghanistan*, London: Academic Press, pp 71-186.
- Shareq A., Chmyriov V. M., Stazhilo-Alexseev K. F., Dronov V. I., Gannon D. J., Lubemov, G. K., Kafarshiy A. Kh. and Malyarov E. P. 1977. *Mineral resources of Afghanistan*, Edition 2 Kabul: Ministry of Mines and Industries. Afghan Geological and Mines Survey, United Nations Development Support Project, AFG/74/012.
- Shelton K.L., Rye D.M. 1982. Sulfur isotopic compositions of ores from Mines Gaspe, Quebec: An example of sulfate-sulfide isotopic disequilibria in ore forming fluids with applications to other porphyry type deposits. *Economic Geology*, 77:1688-1709.
- Sheppard S.M.F. 1977. The Cornubian batholith, SW England: D/H and 18O/16O studies of kaolinite and other alteration minerals, *Journal of Geological Society*, 133:573-591.
- Sillitoe R.H. 1991. Intrusion-related gold deposits, in: Foster R.P. (ed) *Gold metallogeny and exploration*, Blackie, Glasgow, pp 165-209.
- Sillitoe R.H. 1996. Granites and metal deposits. *Episodes*, 19(4):126-133.
- Simmons H.W., Pollard P.J., Stewart J.L., Taylor L.A. and Taylor R.G. 1996. Granite-hosted, disseminated gold mineralisation at Timbarra, New South Wales. in: *Mesozoic geology of the eastern Australia plate Conference*, Brisbane, Queensland 1996, *Geol Soc Aust*, 43:507-509.
- Smith M.T., Thompson J.F.H., Bressler J., Layer P., Mortensen J.K., Abe I. and Takaoka H. 1999. Geology of the Leise zone, Pogo property, east central Alaska: *Society of Economic Geologists Newsletter*, Vol. 38, 10 p.
- Soheili M., Jafarian M.B., Abdollahe M.R. 1992. Geological map of the Aligudarz area 5956. 1:100,000, Geological Survey of Iran, Tehran.
- Soheili M, Sahandi M.R, et al. 1992. 1:250,000 geological map of Khorramabad, Geological Survey of Iran, Tehran.
- Speiser E. A. 1935. *Excavations at Tepe Gawra Vol.1: Levels I-VIII*. Philadelphia, University of Pennsylvania.
- Stacey J. S., Doe B. R., Roberts R. J., Delevaux M. H., and Gramlich J. W. 1980. A lead isotope study of mineralization in the Saudi Arabian Shield, *Contributions to Mineralogy and Petrology*, 74:175-188.
- Stech T. and Pigott V. C. 1986. The metals trade in southwest Asia in the third millennium BC. *Iraq*, 48:39-64.
- Stech T. 1999. Aspects of early metallurgy in Mesopotamia and Anatolia, in: Pigott V.C. (ed) *The Archaeometallurgy of the Asian Old World*, pp 59-71, University Museum Monograph 89, University of Pennsylvania Museum, Philadelphia.
- Stöcklin J. 1968. Structural history and tectonics of Iran; a review. *American Association of Petroleum Geologists Bulletin*, 52(7):1229-1258.
- Stöcklin J. 1977. Structural correlation of the Alpine ranges between Iran and central Asia. *Mem. Hors-serie Soc. Geol. Fr.*, 8:333-353.
- Stoneley R. 1975. On the origin and ophiolitic complexes in the southern Tethys region. *Tectonophysics*, 25:303-322.
- Stos-Gale Z. A., Gale N. H. and Gilmore G. R. 1984. Early Bronze Age Trojan metal sources and Anatolians in the Cyclades. *Oxford Journal of Archaeology* 3(3):23-37.
- Stos-Gale Z. A. 1992. The origin of metal objects from the Early Bronze Age site of Thermi on the island of Lesbos, *Oxford Journal of Archaeology* 11:155-177.

- Takin M. 1972. Iranian geology and continental drift in the Middle East. *Nature*, 235:147-150.
- Tallon F. 1987. *Métallurgie susienne I: De la foundations de Suse au XVIIIe siècle avant J.C.*, Notes et documents des Musées de France 15, Paris.
- Taylor H.P. 1974. The application of oxygen and hydrogen isotope studies to problems of hydrothermal alteration and ore deposition, *Economic Geology*, 69:843-883.
- Taylor H.P. 1980. The effects of assimilation of country rocks by magmas on  $^{18}\text{O}/^{16}\text{O}$  and  $^{87}\text{Sr}/^{86}\text{Sr}$  systematics in igneous rocks, *Earth Planetary Science Letters*, 47:243-254.
- Taylor H.P. Jr. 1997. Oxygen and hydrogen isotope relationships in hydrothermal mineral deposits, in: Barnes H.L. (ed.) *Geochemistry of Hydrothermal Ore Deposits* 3rd Ed. Wiley, New York, 229-302.
- Thiele O., Alavi-Naini M., Assefi R., Houshmandzadeh A., Seyed-Emami K. and Zahedi M., 1968. Explanatory text of the Golpaygan Quadrangle E7. 1:250 000, Geological Survey of Iran, Tehran, Iran, 24 pp.
- Thompson J.F.H., Sillitoe R.H., Baker T., Lang J.R. and Mortensen J.K. 1999. Intrusion-related gold deposits associated with tungsten-tin provinces, *Mineralium Deposita*, 34:323-334.
- Va,ezi pour M.J. and Eghlimi B. 1984. New data about Jurassic sediments in the Lakan area in Golpayegan quadrangle, Internal report (in Persian), Geological Survey of Iran.
- Valizadeh M.V. 1992. Granitoids and the problem of crustal transformation in west of Iran, in: *Experimental petrology and global tectonics*, Volume II, University of Tehran, 409-423 (in Persian).
- Waetzoldt H. 1981. Zur Terminologie der Metall in den Texten aus Ebla, in: Cagni L. (ed) *La Lingua di Ebla*, pp 363-378. Istituto Universitario Orientale, Seminario di Studi Asiatici, Naples.
- Waetzoldt H. and Bachmann H.G. 1984. Zinn- and Arsenbronzen in den Texten aus Ebla and aus dem Mesopotamien des 3. Jahrtausends. *Oriens Antiquus* 23.
- Walder A.J. 1997. Advanced isotope ratio mass spectrometry II: isotope ratio measurement by multiple collector inductively coupled plasma mass spectrometry, in: Platzner I.T. (ed) *Modern isotope mass spectrometry*, 83–108, John Wiley, Chichester.
- Walder A. J. and Furuta, N. 1993 High-precision lead isotope ratio measurement by inductively coupled plasma multiple collector mass spectrometry, *Analytical Sciences*, 9:675–80.
- Wedepohl, K. W., Correns C.W., Shaw D.M., Turekian K.K. and Zemann J. (eds) .1978. *Handbook of Geochemistry*, Vol. II/2-5. Springer Verlag, Heidelberg.
- Weeks L. R. 1999. Lead isotope analyses from Tell Abraq, United Arab Emirates: new data regarding the 'tin problem' in Western Asia, *Antiquity*, 73:49-64.
- Weeks L. 2004. *Early metallurgy of the Persian Gulf; Technology, trade and the Bronze Age World*, Brill Academic Publishers, Inc. Boston, Leiden.
- Wells A.J. 1969. The crush zone of the Iranian Zagros Mountains and its implications, *Geol. Mag.*, 106:385-394.
- Wertime T. A. 1973. The beginnings of metallurgy: a new look. *Science*, 182(4115):875-887.
- Wertime T. A. 1978. The search for ancient tin: the geographic and historic boundaries. in: Franklin A.D., Olin J.S. and Wertime T.A. (eds) *The Search for Ancient Tin*, pp. 1-6. U.S. Government Printing Office, Washington, D.C.
- White W. M., Albarède, F. and Télouk, P. 2000. High-precision analysis of Pb isotope ratios by multi-collector ICP-MS, *Chemical Geology*, 167:257–70.

- Wilde, A. and Gilbert, D. 2000. Setting of the giant Muruntau Gold Deposit: Implications for ore genesis. in: Lister, G. (ed) Geological research for the exploration industry, Journal of the Virtual Explorer, Electronic Edition, ISSN 1441-8142, Volume 01, Paper 1.
- Willies L. 1990. An Early Bronze Age tin mine in Anatolia, Turkey, Bulletin of the Peak District Mines Historical Society, 11(2):91-96.
- Willies L. 1992. Reply to Pernicka et al.: Comment on the discussion of ancient tin sources in Anatolia. Journal of Mediterranean Archaeology, 5:99-103.
- Yener K. A. and Özbal H. 1987. Tin in the Turkish Taurus mountains: the Bolkardag mining district, Antiquity, 61:220-226.
- Yener K. A., Özbal H., Kaptan E., Pehlivan A. N. and Goodway M. 1989. Kestel: an Early Bronze Age source of tin ore in the Taurus Mountains. Science, 244:200-203.
- Yener K. A. and Goodway M. 1992. Response to Mark E. Hall, and Sharon R. Steadman, 'Tin in Anatolia: another look', Journal of Mediterranean Archaeology, 5:91-98.
- Yener, K. A. and Vandiver P., Willies L. 1993. Reply to J.D. Muhly, "Early Bronze Age tin and the Taurus", American Journal of Archaeology, 97:255-262.
- Zahlhaas G. 2002. Luristan: Antike Bronzen aus dem Iran. Archäologische Staatssammlung München, Museum für Vor-und Frühgeschichte, München.
- Zartman R.E. 1974. Lead Isotopic provinces in the Cordillera of the Western United States and their Geologic Significance, Economic Geology, 69(6):792-803.
- Zartman R.E., Doe B.R. 1981. Plumbotectonics - The model. Tectonophysics, 75:135-162.
- Zartman, R. E. & Haines, S. M. 1988. The plumbotectonics model for Pb isotopic systematics among major terrestrial reservoirs—a case for bi-directional transport. Geochimica et Cosmochimica Acta, 52:1327–1339.

# CURRICULUM VITAE

## NIMA NEZAFATI

DATE OF BIRTH: April 1974 (Abadan, Iran)  
NATIONALITY: Iran  
FAMILY STATUS: Single  
E-MAIL ADDRESS: nnezafati@gmail.com

### EDUCATION

Jul. 2005-Nov. 2006 Ph.D student in economic geology at University of Tübingen, Germany, under the supervision of Prof. Dr. G. Markl, Prof.Dr.E.Pernicka, and Prof.Dr.M.Momenzadeh  
Topic of research:  
Mineralization of Au, W, Cu, and Sn in the Sarband-Astaneh area, west central Iran.

Oct. 2001-Jul. 2005 Ph.D. student in economic geology at TU Bergakademie Freiberg, Germany, under the supervision of Prof. Dr. P.M. Herzig, Prof. Dr. E. Pernicka, and Prof. Dr. M. Momenzadeh.

Sept. 1997-Sept. 2000 MSc. student in economic geology from the Research Institute for Earth Sciences (affiliated to the Geological Survey of Iran), Tehran, Iran, summa cum laude.  
Subject of thesis: Study on metallic minerals of Natanz area, Central Iran.  
Supervisors: Prof. Dr. Momenzadeh, Prof. Dr. Emami and Prof. Dr. Pernicka.

Sept. 1993-Aug. 1997 B.Sc. student in geology at the Faculty of Earth Sciences, Shahid Beheshti University,

1988-1992 High school in Tehran.

### WORK EXPERIENCE

Dec. 2000-Sept. 2001 Economic geologist at the Zaryaban Exploration Company  
1999-2001 Scientific cooperation with the Iranian-German project team "Arisman Project" on research of old mining and metallurgy in central Iran

Oct.2003-Present Supervisor of the survey of ancient mining and mineral potential of the Sialk Reconsideration Project, Iran

Jan. 2004-Present Permanent member of the Zarneh Research Group, Iran

### SCHOLARSHIPS AND AWARDS

- SEG travel grant to the SEG 2006 Conference, Keystone, Colorado, USA (May 2006)
- Quenstedt-Jahresfeier poster price, University of Tübingen (July 2005)
- SGA travel grant to the 8<sup>th</sup> SGA Meeting, Beijing, China (August 2005)
- Scholarship from the Curt-Engelhorn-Zentrum Archäometrie gGmbH, Mannheim (October 2004-October 2006)
- Scholarship from the DAAD including a German language course (June 2002-October 2004)
- Support from the PHD-program of the Freiberg University of Mining and Technology for studies at Freiberg and field work (October 2002- May 2005)
- Scholarship from the Volkswagen foundation (October 2001-April 2002)

## PUBLICATIONS

- **Nezafati N.** and Pernicka E. In Progress. Early Silver Production in Iran. *Applied Geochemistry*.
- **Nezafati N.** and Pernicka E. and Momenzadeh M. In progress. A major source of tin in the ancient world, *Archaeometry*.
- **Nezafati N.**, Pernicka E. and Momenzadeh M. 2006. Ancient tin: old question and a new answer. *Antiquity*. 80: 308. 4pp.
- Pernicka E., Adam K., Böhme M., Hezarkhani Z., **Nezafati N.**, Schreiner M., Winterholler B., Momenzadeh M. and Vatandoust A.R. In press. Archaeometallurgical Researches at Arisman in Central Iran. *Eurasia Antiqua*.
- **Nezafati N.** and Pernicka E. 2005. The Smelters of Sialk; outcomes of the first stage of archaeometallurgical researches at Tappeh Sialk, in: Malek Shahmirzadi S. (ed) *Sialk Reconsideration Project Monograph. No.4* (in English and Persian).
- **Nezafati N.**, Momenzadeh M., and Pernicka E. Submitted. 2007. The Iranian ore deposits and their role in the development of the ancient cultures. *Anatolian Metal IV. Der Anschnitt*. Deutsches Bergbau-Museum Bochum.
- **Nezafati N.** 2004. A tentative source of Chert for the central Iranian prehistoric sites, in: Malek Shahmirzadi, S. (ed.) *The Potters of Sialk. Sialk Reconsideration Project Monograph. No.3* (in English and Persian). pp 59-63. [ISBN: 964-421-002-6].
- **Nezafati N.** 2004. Preliminary prospect of copper resources used by the Sialk artisans, in: Malek Shahmirzadi, S. (ed.) *The Potters of Sialk. Sialk Reconsideration Project Monograph. No.3* (in English and Persian). pp 63-69. [ISBN: 964-421-002-6].
- Nokandeh J., **Nezafati N.** 2003. The Silversmiths of Sialk: evidence of the precious metals metallurgy at the southern mound of Sialk, in: Malek Shahmirzadi S. (ed) *The Silversmiths of Sialk, Sialk Reconsideration Project Monograph, No.2* (in Persian with an English abstract). pp 21-30. [ISBN: 964-7483-87-2].
- Momenzadeh M. and **Nezafati N.** 2000. Sources of ores and Minerals used in Arisman: A preliminary study, in: N.N. Chegini, M. Momenzadeh, H. Parzinger, E. Pernicka, T. Stoellner, R. Vatandoust, G. Weisgerber. Preliminary report on archaeometallurgical investigations around the prehistoric site of Arisman near Kashan, Western central Iran. *Archaeologische mitteilungen aus Iran and Turan*, Band 32, sonder druck, Dietrich Reimer Verlag GmbH. Berlin.

## EXTENDED ABSTRACTS

- **Nezafati N.**, Markl G., Pernicka E., Momenzadeh M. and Herzig P.M. 2006. The Deh Hosein prospect: a tin-gold hydrothermal occurrence in west central Iran. *Proceedings of the 12th IAGOD conference*, Understanding the genesis of ore deposits, 2006, Moscow, Russia. 4pp.
- **Nezafati N.**, Markl G., Pernicka E. and Momenzadeh M. 2006. Astaneh gold prospect; an intrusion-related gold system in west central Iran, *Proceedings of the SEG 2006 conference*, Wealth creation in the minerals industry, Keystone, Colorado, USA. pp 322-324.
- **Nezafati N.**, Herzig P.M., Pernicka E. and Momenzadeh M. 2005. Intrusion-related gold occurrences in the Astaneh-Sarband area, west central Iran, in: J. Mao and F. P. Bierlein (eds.) *Mineral deposit research: Meeting the global challenge*. Springer. pp 445-448.
- **Nezafati N.**, Momenzadeh M., Pernicka E. 2005. Darhand copper occurrence; an example of Michigan-type native copper deposits in central Iran, in: J. Mao and F. P. Bierlein (eds.) *Mineral deposit research: Meeting the global challenge*. Springer. pp 165-166.
- Momenzadeh M., **Nezafati N.** and Pernicka E. 2002. First indication of tin at the ancient mining site near Deh Hosein, West central Iran: a possible source for Luristan Bronze. *Proceedings of the 33rd international symposium on Archaeometry*, 22-26 April 2002 Amsterdam, The Netherlands. pp 116-117.
- **Nezafati N.** and Momenzadeh M. 2000. Sources of ores used in Arisman ancient metallurgy site: A preliminary study. *Proceeding of the 19th symposium on Geosciences*, Tehran, Iran, in Persian with an abstract in English.